

UNIVERSITÉ DU QUÉBEC À MONTRÉAL

ÉTUDE BIOPHYSIQUE DE LA FONCTION ET DU RÔLE DE SEGMENTS
INTRA- ET EXTRACELLULAIRES DU CANAL HERG DANS LE SYNDROME
DU QT LONG, ET DÉVELOPPEMENT DE NOUVELLES MEMBRANES
MODÈLES

THÈSE

PRÉSENTÉE

COMME EXIGENCE PARTIELLE

DU DOCTORAT EN BIOCHIMIE

PAR

ANDRÉE GRAVEL

OCTOBRE 2016

UNIVERSITÉ DU QUÉBEC À MONTRÉAL
Service des bibliothèques

Avertissement

La diffusion de cette thèse se fait dans le respect des droits de son auteur, qui a signé le formulaire *Autorisation de reproduire et de diffuser un travail de recherche de cycles supérieurs* (SDU-522 – Rév.07-2011). Cette autorisation stipule que «conformément à l'article 11 du Règlement no 8 des études de cycles supérieurs, [l'auteur] concède à l'Université du Québec à Montréal une licence non exclusive d'utilisation et de publication de la totalité ou d'une partie importante de [son] travail de recherche pour des fins pédagogiques et non commerciales. Plus précisément, [l'auteur] autorise l'Université du Québec à Montréal à reproduire, diffuser, prêter, distribuer ou vendre des copies de [son] travail de recherche à des fins non commerciales sur quelque support que ce soit, y compris l'Internet. Cette licence et cette autorisation n'entraînent pas une renonciation de [la] part [de l'auteur] à [ses] droits moraux ni à [ses] droits de propriété intellectuelle. Sauf entente contraire, [l'auteur] conserve la liberté de diffuser et de commercialiser ou non ce travail dont [il] possède un exemplaire.»

REMERCIEMENTS

Je m'approprie cette section pour remercier tous les gens qui m'ont aidé, scientifiquement ou personnellement, à réaliser cette thèse.

Premièrement, j'aimerais remercier ma directrice de recherche, Isabelle (WBB) Marcotte, qui a toujours été patiente, positive et très encourageante, même dans les moments difficiles. Merci de m'avoir encouragé à faire un stage en France et à participer à de nombreux congrès afin d'enrichir mon réseau et mes compétences de communication scientifique. Tu m'as toujours poussée à viser plus haut, et j'en suis très reconnaissante.

J'aimerais aussi remercier le groupe Marcotte, pour leur bonne humeur et avec qui j'ai pu avoir des discussions scientifiques stimulantes. J'ai bien apprécié les sorties et les activités de groupe qui ont fait de nous une petite famille. J'aimerais aussi remercier Alexandre (NMR Master) Arnold, pour ta confiance, ta patience et de m'avoir transmis ta passion pour la RMN.

Je remercie Érick J. Dufourc, mon superviseur de stage à Bordeaux, ainsi que les membres de son groupe de m'avoir accueilli si chaleureusement et avec qui j'ai eu des discussions stimulantes.

J'aimerais aussi remercier Dror pour ses conseils et discussions perspicaces.

Je remercie également le CRSNG, le *CIHR Training program in Chemical Biology* de l'Université McGill et le GRASP de l'Université McGill, le CQMF et la Fondation de l'UQAM pour leurs soutien financier.

J'aimerais spécialement remercier mes parents, Eveline et Paul, qui ont toujours cru en moi et qui ont su me soutenir, malgré tout, dans mes projets personnels et professionnels. Merci pour votre patience et votre compréhension même si les visites étaient trop espacées. Je n'oublie pas ma belle-mère, Suzanne, pour les longues discussions rassurantes et mon beau-père, Marcel, d'avoir été là quand j'avais besoin d'un coup de main.

Je remercie aussi ma sœur Anne, ma chère soeurette, avec qui j'ai passé tant de bons moments. Merci pour ton sens de l'humour, de m'accepter comme je suis et merci aussi d'avoir partagé les moments plus difficiles avec moi.

J'aimerais aussi remercier la famille à Julien de m'avoir toujours encouragée et de m'avoir accueillie dans votre famille comme si j'étais un des vôtres.

À mes amis, Gabrielle (Ginette), Anne-Frédérique, Katherine (cocotte) et Jason (J-Dawg), que malgré le fait qu'on n'habite plus dans la même ville, lorsqu'on se revoit c'est comme si on s'était vu hier. Merci pour toutes ces années d'amitié en espérant qu'il y en aura plusieurs à venir.

Et finalement, à ma petite famille, Julien, Florence et Alice. Julien, sans qui rien ne serait pareil, merci de ta patience et de ton soutien sans fin. Merci à Florence et à Alice, de me faire rire et sourire. J'ai bien hâte de vous voir grandir et devenir les femmes intelligentes et fortes que vous êtes.

TABLE DES MATIÈRES

LISTE DES FIGURES.....	IX
LISTE DES TABLEAUX.....	XIII
RÉSUMÉ	XXI
CHAPITRE I	
INTRODUCTION	1
1.1 Canal du <i>human ether-à-go-go-related gene</i> (hERG).....	2
1.1.1 Le syndrome du QT long (LQTS).....	4
1.1.2 Le syndrome du QT long acquis (ALQTS).....	5
1.1.3 La structure du hERG.....	7
1.1.4 Mécanisme d'ouverture et de fermeture du hERG.....	14
1.1.5 Environnement membranaire du hERG	16
1.2 Membranes modèles	17
1.2.1 Composition	18
1.2.2 Propriétés physiques et organisation des lipides	18
1.2.3 Choix du modèle membranaire	22
1.3 Problématique et objectifs spécifiques	28
CHAPITRE II	
ÉLÉMENTS THÉORIQUES DE LA SPECTROSCOPIE DE RMN APPLIQUÉE AUX SYSTÈMES BIOLOGIQUES	
2.1 Résonance magnétique nucléaire.....	31
2.2 Inhomogénéités naturelles et couplages	35
2.2.1 Déplacement chimique	36
2.2.2 Anisotropie du déplacement chimique (<i>chemical shift anisotropy</i> ; CSA)	37
2.2.3 Couplage scalaire (couplages J).....	38
2.2.4 Couplage dipolaire	40
2.2.5 Interaction quadripolaire	42

2.2.6 RMN en solution et RMN à l'état solide	42
2.3 RMN bidimensionnelle du proton pour la détermination de la structure des peptides	44
2.3.1 <i>Total Correlation Spectroscopy</i> (TOCSY)	45
2.3.2 <i>Nuclear Overhauser Effect Spectroscopy</i> (NOESY)	46
2.3.3 <i>Rotating-frame Overhauser Effect Spectroscopy</i> (ROESY)	48
2.4 Gradients de champs et saturation des résonances pour l'étude des interactions protéine-membrane	49
2.4.1 <i>Pulsed Field Gradient Spin-Echo</i> (PGSE)	49
2.4.2 <i>Saturation Transfer Difference</i> (STD)	51
2.5 RMN du phosphore-31 et du deutérium pour l'étude des systèmes membranaires	53
2.5.1 RMN du phosphore-31	53
2.5.2 RMN du deutérium (^2H)	55
2.5.3 Susceptibilité magnétique	57

CHAPITRE III

AN NMR INVESTIGATION OF THE STRUCTURE, FUNCTION AND ROLE OF THE HERG CHANNEL SELECTIVITY FILTER IN THE LONG QT SYNDROME

3.1 Résumé	59
3.2 Abstract	60
3.3 Introduction	61
3.4 Materials and Methods	65
3.4.1 Materials	65
3.4.2 Sample preparation	65
3.4.3 Solution and solid-state NMR	66
3.5 Results	70
3.5.1 Structure of the SF segment in aqueous environment	70
3.5.2 Interaction of the SF segment with the membrane	71
3.5.3 Interaction of the SF segment with hERG-active drugs	76
3.5.4 Role of the membrane in the long QT syndrome	77
3.6 Discussion	79

3.7	Conclusion	85
3.8	Acknowledgements.....	85

CHAPITRE IV

TYROSINE RESIDUES FROM THE S4-S5 LINKER OF KV11.1 CHANNELS ARE CRITICAL FOR SLOW DEACTIVATION

4.1	Résumé	89
4.2	Abstract.....	90
4.3	Introduction.....	90
4.4	Experimental procedures	92
4.4.1	NMR spectroscopy.....	92
4.4.2	Electrophysiology Methods.....	94
4.5	Results	98
4.6	Discussion.....	111
4.7	Complément au chapitre: <i>Saturation transfer difference</i> (STD) par RMN en solution.....	114
4.7.1	Matériel et méthode.....	114
4.7.2	Expériences de STD	115
4.7.3	Résultats et discussion.....	116

CHAPITRE V

CHARACTERIZATION OF MAGNETICALLY-ORIENTABLE TWEEN-BASED MODEL MEMBRANES FOR NMR APPLICATIONS

5.1	Résumé	119
5.2	Abstract.....	120
5.3	Introduction.....	120
5.4	Materials and Methods	124
5.4.1	Materials.....	124
5.4.2	Sample preparation.....	124
5.4.3	NMR experiments	124
5.4.4	³¹ P spectra fitting.....	126
5.4.5	Fourier transform infrared spectroscopy	127
5.5	Results	128
5.5.1	NMR characterization of PC/TW80 model membranes	128

5.5.2 Properties of phospholipids and TW80	137
5.6 Discussion	139
5.7 Conclusion	141
5.8 Acknowledgements	141
CHAPITRE VI	
CONCLUSIONS ET PERSPECTIVES	145
6.1 Résumé et conclusions du rôle et de la fonction du hERG	145
6.1.1 Étude de la structure, de la fonction et du rôle du filtre de sélectivité du hERG	145
6.1.2 Rôle du segment S4S5 dans le mécanisme d'ouverture et de fermeture du hERG	147
6.2 Vers de nouvelles membranes modèles pour les études de RMN – Résumé et conclusions.....	148
6.3 Perspectives pour l'étude du canal hERG et de la membrane par RMN	150
6.3.1 Raffiner le modèle structural et mieux comprendre la fonction du hERG	151
6.3.2 Développement de nouvelles membranes modèles avec d'autres détergents	155
6.3.3 Le hERG, une cible thérapeutique et son rôle dans le cancer	159
ANNEXE A	
POTENTIAL ROLE OF THE MEMBRANE IN HERG CHANNEL FUNCTIONING AND DRUG-INDUCED LONG QT SYNDROME.....	163
ANNEXE B	
CHOOSING MEMBRANE MIMETICS FOR NMR STRUCTURAL STUDIES OF TRANSMEMBRANE PROTEINS.....	177
RÉFÉRENCES	197

LISTE DES FIGURES

Figure	Page
1.1 Topologie des canaux ioniques dépendants du voltage Na_v , Ca_v et K_v . Image adaptée de Pringos <i>et al.</i> avec permission ⁶	2
1.2 Potentiel d'action cardiaque (haut) et tracé d'une unité de répétition d'un ECG (bas) de cardiomyocyte.....	3
1.3 Conformations du hERG adoptées selon le potentiel d'action de la membrane.....	4
1.4 Tracé d'un électrocardiogramme qui débute avec trois cycles cardiaques normaux suivi d'un épisode de torsade de pointes (TdP).....	5
1.5 Schéma de la vue latérale de la topologie du canal hERG stabilisé dans une bicouche lipidique (rectangle gris pâle).	9
1.6 Alignement des séquences du segment S5P de plusieurs canaux K_v	10
1.7 Simulation de dynamique moléculaire de la translocation d'ions K^+ (sphères mauves) et de molécules d'eau (sphères rouges et blanches) au travers la membrane par l'entremise du canal procaryote KirBac1.1.....	13
1.8 Mouvements des domaines du hERG suite à l'ouverture et la fermeture du canal.	15
1.9 La membrane des cardiomyocytes, appelée sarcolemme, est majoritairement faite de phospholipides.....	17
1.10 Formes moléculaires des lipides qui s'autoassemblent en solution sous forme de micelle (A), de bicouche (B) ou en phase hexagonale (C).	19
1.11 Schéma de divers modèles membranaires utilisés en RMN, telle que les micelles, les vésicules unilamellaires (SUV, LUV et GUV) et les vésicules multilamellaires (MLV).	24
1.12 Schéma A) de bicelles isotropes et B) orientées dans le champ magnétique. C) Les MLV perforées peuvent également s'orienter dans le champ magnétique (B_0).	26

2.1	Spin d'un noyau ayant un moment angulaire de spin (I) qui précesse autour d'un axe défini.	33
2.2	Niveaux d'énergie pour un spin $I = \frac{1}{2}$ avec et sans champ magnétique externe (B_0). En présence de B_0 , l'effet Zeeman lève la dégénérescence des niveaux d'énergie.	34
2.3	Mouvements de précession du spin d'un noyau ayant deux états de spin ($+\frac{1}{2}$ et $-\frac{1}{2}$) par rapport au champ magnétique B_0 défini selon l'axe y.	35
2.4	Spectres RMN du ^{31}P de phospholipides sans (A) et avec (B) mouvements de rotation axiale rapide selon l'axe z; les images sont obtenues de Smith et Ekiel avec permission ¹²⁴ . C : Axes principaux du tenseur de CSA d'un phosphore lipidique qui tourne selon l'axe z. D : Orientations possibles des phospholipides d'un liposome non orienté.	38
2.5	Structure secondaire des peptides et protéines.	40
2.6	Couplage dipolaire entre deux noyaux.	41
2.7	Spectre RMN du deutérium (^2H) d'un liposome.	42
2.8	Schéma de la rotation à l'angle magique où l'axe de l'échantillon, se trouvant dans un rotor (cylindre gris), tourne à un angle de 54.7° par rapport au champ magnétique externe (B_0).	43
2.9	Spectre de RMN du ^1H de <i>Total Correlation Spectroscopy</i> (TOCSY).	45
2.10	Séquence d'impulsions TOCSY.	46
2.11	Séquence d'impulsions NOESY.	47
2.12	Séquence d'impulsion ROESY.	48
2.13	Expérience PGSE.	50
2.14	Expérience de STD pour localiser les peptides et les PM dans une membrane tel que réalisée au chapitre III.	52
2.15	Comparaison des spectres RMN du ^{31}P de bicouches lipidiques non orientées et orientées.	54
2.16	Comparaison des spectres de RMN du ^2H des chaînes acyles deutérées de bicouches lipidiques non orientées et orientées.	56
3.1	A) Amino acid sequence and predicted topology of the hERG channel pore domain (S5–S6) ^{67, 155} . B) ^1H – ^1H contacts for hERG L622–K638 in water obtained by ROESY with a 300 ms mixing time.	62

3.2	^1H NMR spectra of the side chain region (top), amide and aromatic region (bottom) of SF (2 mM) in 10 % D_2O (black solid line), and with DMPC- d_{54} /DHPC ($q = 0.5$) bicelles (grey dashed line) at a lipid/peptide ratio of 50:1.....	71
3.3	Effect of the SF on the ^{31}P (left) and ^2H (right) SS-NMR spectra of DMPC MLVs, with and without KCl, at 37 °C, with a lipid/SF molar ratio of 100:1.....	74
3.4	Observed saturation transfer difference curves for A) SF Phe627 ring protons $\text{C}^{(2,6)}\text{H}$ (dashed line), $\text{C}^{(3,5)}\text{H}$ (dash-dotted line) and $\text{C}^{(4)}\text{H}$ (dotted line), and aromatic protons for B) bepridil, C) cetirizine, D) diphenhydramine, E) fluvoxamine and F) promethazine in DMPC/DHPC- d_{22} bicelles when choline (●), glycerol (■) or terminal methyl (▲) resonances of DMPC are saturated.	76
3.5	Effect of LQTS-active drugs on the ^{31}P (left) and ^2H (right) SS-NMR spectra of DMPC MLVs at 37 °C with a lipid/drug molar ratio of 180:1.	78
3.S1	^1H TOCSY spectra of the hERG L622-K638 in 10 % D_2O at 20 °C.....	88
4.1	Tyrosine residues are conserved among the KCNH family.	99
4.2	Tyrosine residues within the S4S5 linker of Kv11.1 are orientated towards the lipid membrane.....	100
4.3	Activation properties for S4S5 mutants.....	102
4.4	Kinetics of deactivation for S4S5 alanine mutants.....	104
4.5	Voltage dependence of the distribution between open and closed states for S4S5 mutants.....	106
4.6	Tyr545 (blue) is functionally different to Tyr542 (red).....	108
4.7	Double mutant cycle analysis of Tyr542 and Tyr545.....	110
4.S1	Courbes STD des protons aromatiques ($\text{C}^{(2,6)}\text{H}$ and $\text{C}^{(3,5)}\text{H}$) des Tyr542 and Tyr545 des peptides S4-S5 du hERG (Y542W, Y545W, S4S5) solubilisés dans des bicelles de DMPC/DPC- d_{38} $q=1$ à 25 °C lorsque les groupements choline (◆), glycérol (■), and méthyl terminaux (▲) de la DMPC sont saturés.....	117
5.1	Molecular structures of Tween 80 (A), dimyristoyl-PC (B) and dipalmitoyl-PC (C).	123

5.2	^{31}P NMR spectra of DMPC/TW80 (left) and DPPC/TW80 (right) at 37 °C and 57 °C, respectively, for different molar ratios (q).	129
5.3	^{31}P (first and third columns) and ^2H (second and last columns) NMR spectra of DMPC/TW80 (left) and DPPC/TW80 (right) with $q3$ at different temperatures.	131
5.4	Geometric model of an ellipsoid in a xyz plane where c and a are the major and minor axis, respectively, B_0 is the external magnetic field, and N the membrane normal.	132
5.5	^{31}P (left) and ^2H (right) NMR spectra of DMPC/TW80 $q3$ at 37 °C without (top) and with (bottom) lanthanide ions using a DMPC/Yb $^{3+}$ molar ratio of 105:1.....	134
5.6	^{31}P SS-NMR spectra fitting using Eq. (5.1).	135
5.7	Quality of orientation as a function of the magnetic field strength (A) and of the vesicle elasticity (B).	137
5.8	Temperature dependance of CD $_2$ symmetric stretching vibration ($\nu_s\text{CD}_2$) for PC/TW80 samples by FTIR spectroscopy.	138
5.S1	Molar ratio (q) and temperature influence the morphology of PC/TW80 aggregates.	142
5.S2	First derivative of the thermotropic curves for DMPC/TW80 and DPPC/TW80 at different molar ratios is plotted as a function of temperature to determine the temperature of phase transition (T_m).	142

LISTE DES TABLEAUX

Tableau	Page
1.1 Structures et classes pharmacologiques de médicaments qui ont la capacité de causer une prolongation de l'intervalle QT ou des torsades de pointe sur l'électrocardiogramme.	6
1.2 Composition lipidique du sarcolemme des cardiomyocytes exprimé en pourcentage par rapport à la quantité totale de phospholipides.	16
1.3 Concentration micellaire critique (CMC) de divers lipides et détergents communément employés pour les membranes modèles et pour la purification de protéines membranaires.	20
1.4 Nomenclature des chaînes acyles de divers phosphatidylcholine (PC) saturés et insaturés ainsi que leur température de transition (T_m).	22
2.1 Propriétés d'isotopes nucléaires utiles en RMN des systèmes biologiques.	32
3.1 Partition coefficients (log P), pharmacological classes and structures of studied LQTS-active drugs.	64
3.2 Calculated fraction of SF or drugs bound to the SF and to bicelles (with or without SF).	72
3.S1 Proton chemical shifts of the hERG L622-K638 segment in water at 25 °C, pH 4.5.	86
3.S2 Translational diffusion coefficients of bicelles ($q=0.5$), SF and drugs used to calculate the fraction of bound peptide and drugs.	87
4.1 Summary of the values for the 3 s isochronal deactivation $V_{0.5}$, rates of deactivation at -70 mV and -120 mV for S4S5 alanine mutants.	103
4.2 Summary of the values for the 3 s isochronal deactivation $V_{0.5}$, rates of deactivation at -70 mV and -120 mV for S4S5 alanine mutants.	105

4.3	Summary of the values for the $\Delta\Delta G^\circ$ (mean \pm S.E.M) and n denotes number of individual recordings.	111
5.S1	Summary of all ^{31}P NMR experiments of PC/TW80 model membranes at different molar ratios and temperatures (A).	143
5.S2	Phase transition temperatures (T_m) for DMPC and DPPC without and with TW80 at various molar ratios obtained by FTIR.	144
6.1	Propriétés moléculaires de détergents couramment utilisés dans les transférosomes et pour l'étude de protéines membranaires ^{90, 273}	157
A.S1	Proton chemical shifts of the hERG peptide in water at pH 5.5 and 25 °C and in bicelles DMPC/DHPC $q=1$ at pH 5.5 and 25 °C (grey color).	176

LISTE DES ABRÉVIATIONS, SIGLES ET ACRONYMES

ALQTS	<i>Acquired Long QT Syndrome</i>
C ₁₂ E ₈	Octaéthylèneglycol monododécyl éther
CD	Dichroïsme circulaire (<i>Circular Dichroism</i>)
CHAPS	3-[(3-cholamidopropyl)diméthylammonio]-1-propanesulfonate
CHAPSO	3-[(3-cholamidopropyl)diméthylammonio]-2-hydroxy-1-propanesulfonate
CMC	Concentration micellaire critique
CSA	Anisotropie du déplacement chimique (<i>Chemical Shift Anisotropy</i>)
D ₂ O	Oxyde de deutérium
DDM	Dodecyl-β-maltoside
DHPC	Dihexanoylphosphatidylcholine
DMPC	Dimyristoylphosphatidylcholine
DMPC-d ₅₄	Dimyristoylphosphatidylcholine avec chaînes acyles deutérées
DOPC	Dioléoylphosphocholine
DPC	Dodécylphosphocholine

DPC-d ₃₈	Dodécylphosphocholine avec chaînes acyles deutérées
DPPC	Dipalmitoylphosphatidylcholine
DPPC-d ₆₂	Dipalmitoylphosphatidylcholine avec chaînes acyles deutérées
D _s	Coefficient de diffusion
DSS	Acide 2,2-diméthyl-2-silapentane-5-sulfonique
DSV	Domaine sensible au voltage
ECG	Electrocardiogramme
GUV	Vésicules unilamellaires géantes (<i>giant unilamellar vesicles</i>)
hERG	<i>Human ether-a-go-go-related gene</i>
H _p	Hélice du pore (<i>pore helix</i>)
HSQC	<i>Heteronuclear Single Quantum Coherence Spectroscopy</i>
I	Nombre quantique de spin
\vec{I}	Moment angulaire de spin
K _v	Canaux potassiques dépendants du voltage
LUV	Grandes vésicules unilamellaires (<i>large unilamellar vesicles</i>)
MAS	Rotation à l'angle magique (<i>Magic Angle Spinning</i>)
MLV	Vésicules multilamellaires (<i>Multilamellar Vesicles</i>)
MPs	<i>Membrane proteins</i>

mg	Milligramme
NOE	<i>Nuclear Overhauser Effect</i>
NOESY	<i>Nuclear Overhauser Effect Spectroscopy</i>
PC	Phosphatidylcholine
PE	Phosphatidyléthanolamine
PFG	<i>Pulsed Field Gradient</i>
PGSE	<i>Pulsed Field Gradient Spin Echo</i>
PL	Phospholipides
PM	Protéine(s) membranaire(s)
q	Ratio molaire de la concentration des surfactants à chaînes longues par rapport à celle de ceux à chaînes courtes
RMN	Résonance magnétique nucléaire
ROESY	<i>Rotating frame nuclear Overhauser Effect Spectroscopy</i>
SDS	Dodécylsulfate de sodium
SF	Filtre de sélectivité (<i>Selectivity Filter</i>)
SQTLA	Syndrome du QT long acquis
SS-NMR	<i>Solid-State Nuclear Magnetic Resonance</i>
STD	<i>Saturation Transfer Difference</i>
SUV	Petites vésicules unilamellaires (<i>small unilamellar vesicles</i>)

TdP	Torsades de pointes
TOCSY	<i>Total COrrrelation SpectroscopY</i>
Triton X-100	Éther de polyéthylèneglycol
Tween 80	Monooléate sorbitane de polyéthylène 80
$\vec{\mu}$	Moment magnétique nucléaire
ν	Fréquence de résonance
γ	Ratio gyromagnétique

LISTE DES SYMBOLES ET DES UNITÉS

1D	Une dimension
2D	Deux dimensions
^1H	Proton
^2H	Deutérium
^{13}C	Carbone-13
^{31}P	Phosphore
Å	Angstrom (1×10^{-10} m)
B_0	Champ magnétique externe
I_{Kr}	Canaux rectifiants la composante rapide retardée du courant potassique (<i>Rapid delayed rectifier potassium current channels</i>)
kDa	Kilodalton
kHz	Kilohertz
$L\alpha$	Phase liquide cristalline
$L\beta$	Phase gel
MHz	Megahertz
mV	Millivolt
ms	Milliseconde
ppm	Déplacement chimique (δ) exprimé en parties par millions (RMN)
q	Ratio molaire des surfactants
s	Seconde

xx

S4S5	Segment S4-S5
S5P	Segment S5-P
τ_c	Temps de corrélation
T_m	Température de transition
TW80	Tween 80
$\Delta\delta$	Déplacement chimique
$\Delta\nu_Q$	Écart quadripolaire
μs	Microseconde
ω	Fréquence de Larmor
γ	Rapport gyromagnétique

RÉSUMÉ

Cette thèse porte principalement sur l'étude de la structure et de la fonction des segments intra- et extracellulaires du canal potassique *human ether-à-go-go-related gene* (hERG) ainsi que sur le développement de membranes modèles pour des applications RMN. Dans un premier temps, nous avons étudié la structure, la fonction et le rôle d'un segment renfermant le filtre de sélectivité (SF) du hERG qui serait impliqué dans le syndrome du QT long acquis (ALQTS) (chapitre II). Caractérisé par une prolongation de l'intervalle Q et T sur l'électrocardiogramme, l'ALQTS est un effet secondaire de médicaments ou de toxines qui résulte en un blocage du canal hERG, ce qui peut mener à des arythmies ou à l'arrêt cardiaque. Étant donné que les molécules cardiotoxiques ciblent majoritairement la région du pore, nous avons déterminé par RMN en solution et par dichroïsme circulaire que le SF est non structuré en solution, ce qui est cohérent avec la flexibilité qu'il requiert pour s'adapter aux différents états de conduction ionique. Par RMN en solution et de l'état solide, nous avons déterminé le rôle potentiel de la membrane dans le ALQTS, car les médicaments cardiotoxiques étudiés ont une haute affinité pour celle-ci et l'affinité du SF pour la membrane est affectée par la présence de ces médicaments. Ces résultats suggèrent que la membrane aurait un rôle potentiel dans le ALQTS en favorisant l'accès des molécules hERG-actives aux cibles du hERG ou en perturbant la synergie lipide-protéine.

Dans un deuxième temps, nous avons étudié le rôle du segment S4S5 du hERG dans le mécanisme d'ouverture et de fermeture de ce canal (chapitre III). Le hERG a un mécanisme d'ouverture et de fermeture particulier comparativement aux autres canaux K_v . Le segment S4S5, rejoignant le domaine sensible au voltage (DSV) à

celui du pore, est important pour le mécanisme de désactivation. Nous avons employé la spectroscopie de RMN pour identifier la surface du segment S4S5 qui se lie à la membrane, ainsi que pour démontrer que deux résidus tyrosine (Y542 et Y545), étant hautement conservés dans la famille KCNH, sont associés à la membrane. La mutagenèse dirigée et les analyses électrophysiologiques ont démontré que la Tyr542 interagit avec le domaine du pore et le DSV pour stabiliser la conformation active du canal, tandis que la Y545 contribue à la cinétique lente de désactivation, principalement en stabilisant l'état de transition entre les états actifs et fermés. Les deux résidus tyrosines du segment S4S5 jouent un rôle important, mais distinct dans la désactivation lente particulière du canal hERG.

Finalement, nous avons développé un nouveau modèle membranaire pour des applications en RMN (chapitre IV). Ce système lipidique est composé d'un mélange de détergent non ionique, le Tween 80 (TW80), et de phospholipides phosphatidylcholine (PC). Les membranes modèles PC/TW80 ont été caractérisées par RMN de l'état solide du ^{31}P et du ^2H ainsi que par spectroscopie infrarouge. Les bicouches de dimyristoylPC (DMPC) ou de dipalmitoylPC (DPPC) s'auto-assemblent avec le TW80 pour former des structures allongées qui s'orientent dans le champ magnétique. Ces structures maintiennent leur orientation sur une gamme étendue de ratios molaires et de températures. Le détergent TW80 pourrait être exploité afin d'extraire de manière efficace des protéines membranaires et d'améliorer l'orientation des membranes tout en évitant l'élimination du détergent.

Mots-clés : hERG, RMN, protéines membranaires, membranes modèles, ALQTS

CHAPITRE I

INTRODUCTION

L'étude des protéines membranaires (PM) est un domaine de recherche fondamental considérant leur rôle dans plusieurs processus biochimiques et leur importance en tant que cibles thérapeutiques. Les canaux ioniques sont une superfamille de protéines transmembranaires qui contrôlent le potentiel électrique de la membrane en activant le flux d'ions des environnements intra- et extracellulaires. Ils sont impliqués dans plusieurs processus physiologiques, tels que la relaxation musculaire et la régulation de la pression sanguine. Dans le génome humain, les canaux ioniques sont nombreux, car ils représentent 1 % des 20 000 gènes codants pour des protéines¹. Les canaux ioniques sont subdivisés en deux familles, la plus grande étant celle des canaux ioniques sensibles au voltage, et l'autre, des récepteurs ionotropes qui s'ouvrent en fonction de la présence d'un ligand.

Les canaux ioniques dépendants du voltage modulent leur ouverture et fermeture en fonction du changement de gradients de voltage de la membrane. Ces canaux comportent plusieurs classes, dont les canaux calciques (Ca_v), les canaux sodiques (Na_v), et la plus nombreuse étant celle des canaux potassiques (K_v). Leur topologie se ressemblent sauf que les quatres domaines des canaux Ca_v et Na_v sont formés d'une seule chaîne polypeptidique, tandis que les canaux K_v sont formés de quatre domaines indépendants (Fig. 1). En 1987, le premier gène d'un canal potassique à être cloné est celui du canal K_v *Shaker* de *Drosophila melanogaster*². Le nom de la famille « ether-à-go-go » a été employé pour la première fois par Kaplan et Trout en 1969 où il fait référence aux pattes des drosophiles, qui étaient anesthésiées avec de

l'éther, s'agitant de manière semblable aux danseurs à go-go des années 1960³. En 1994, le gène humain du *human ether-à-go-go-related gene* (hERG) a été isolé pour la première fois⁴. Un an plus tard, Sanguinetti *et al.* démontrent que la protéine humaine hERG est responsable de la composante rapide du courant potassique à rectification retardée (I_{Kr}) et que les médicaments antiarythmiques de classe III affectent ce courant potassique⁵. Depuis, plusieurs autres médicaments, appartenant à toutes les classes pharmacologiques, ont été divulgués, car eux aussi inhibaient les canaux I_{Kr} pour engendrer des arythmies cardiaques.

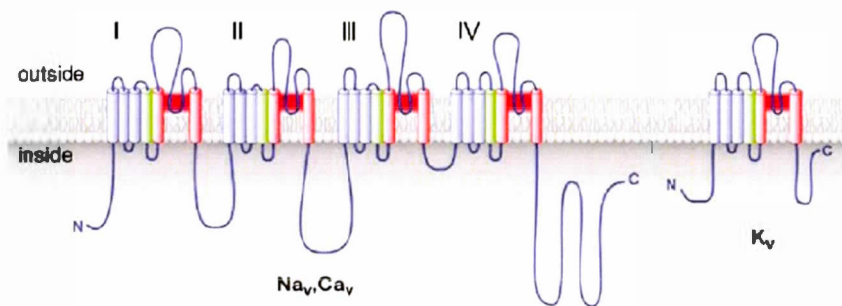


Figure 1.1 Topologie des canaux ioniques dépendants du voltage Na_v , Ca_v et K_v . Image adaptée de Pringos *et al.* avec permission⁶.

1.1 Canal du *human ether-à-go-go-related gene* (hERG)

Au sein du cœur, les cardiomyocytes sont des cellules qui modulent les contractions cardiaques par leur activité électrique, notamment grâce au flux d'ions de sodium (Na^+), de calcium (Ca^{2+}) et de potassium (K^+). Pour ce faire, plusieurs canaux ioniques dépendants du voltage sont présents dans les membranes afin de maintenir l'équilibre délicat des ions. L'activité de ces canaux déclenche le potentiel d'action des cellules (Fig. 1.2, haut) où l'activité électrique du cœur peut être suivie sur l'électrocardiogramme (ECG) (Fig. 1.2, bas). L'afflux des ions Na^+ et Ca^{2+} est responsable de l'excitation et la contraction des cellules cardiaques tandis que la sortie des ions K^+ sert à repolariser les cellules afin d'achever le potentiel d'action, ce

qui termine le tracé sur l'ECG. Toute modification au flux d'ions peut mener à des arythmies et même à la mort subite d'origine cardiaque⁷.

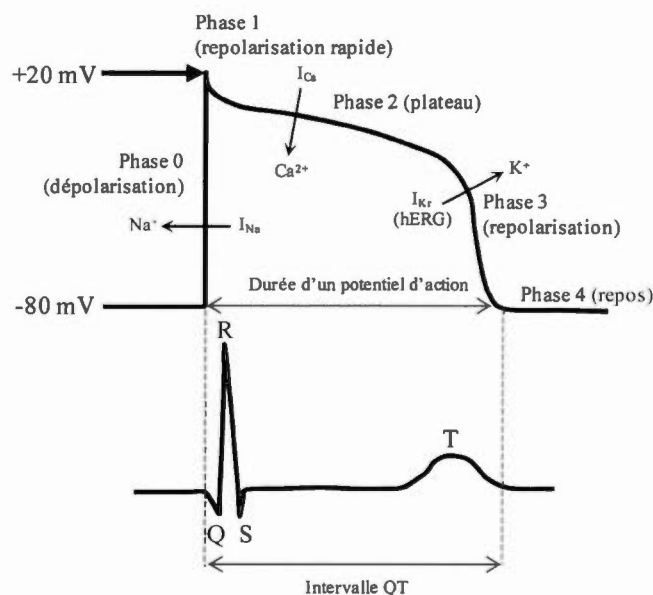


Figure 1.2 Potentiel d'action cardiaque (haut) et tracé d'une unité de répétition d'un ECG (bas) de cardiomyocyte. La phase initiale (phase 0) résulte de l'activation des canaux sodiques dépendants du voltage (I_{Na}) et est représentée par les intervalles QRS sur l'ECG. La forme du potentiel d'action est influencée par l'activité des canaux calciques dépendants du voltage, qui affectent surtout la phase initiale rapide de repolarisation (phase 1) et le plateau (repolarisation lente à la phase 2), ainsi que l'activité des canaux K_v qui affectent les dernières phases de repolarisation (phases 3 et 4). L'activité de ces canaux va aussi déterminer l'intervalle QT sur l'ECG.

Le canal potassique hERG, aussi appelé $Kv11.1$, est codé par le gène $KCNH2$ ⁸. Il appartient à la famille des canaux potassiques dépendants du voltage (K_v) car son ouverture et sa fermeture sont contrôlées par le potentiel de la membrane. Le rôle du hERG est de réguler les battements cardiaques, surtout au niveau de la repolarisation du potentiel de la membrane (Fig. 1.2, haut). Comparativement aux autres canaux

potassiques, le hERG a un mécanisme d'ouverture et de fermeture particulier qui fera l'objet de discussions au chapitre IV. Son activation et sa désactivation sont plus lentes, tandis que son inactivation est rapide. La désactivation lente du hERG permet l'échange suffisant d'ions afin d'assurer une contraction cardiaque efficace et dépourvue d'arythmies. Lorsque le potentiel de la membrane transite d'une valeur négative (-80 mV) à plus positive – ce qu'on appelle la dépolarisation – le hERG adopte une conformation ouverte (activation). Plus la membrane se dépolarise, plus le hERG transite vers une conformation inactive (Fig. 1.3). La transition des conformations du hERG est inversée lors de la repolarisation de la membrane. Elle débute par la réactivation (ouverture) des canaux où les K^+ diffusent vers l'extérieur de la cellule. Le hERG est surtout responsable de la composante rapide du courant potassique à rectification retardée (I_{Kr}) qui, vers la fin de la repolarisation, reconduit et maintient le potentiel de repos de la membrane (-80 mV) lorsque les canaux sont fermés.

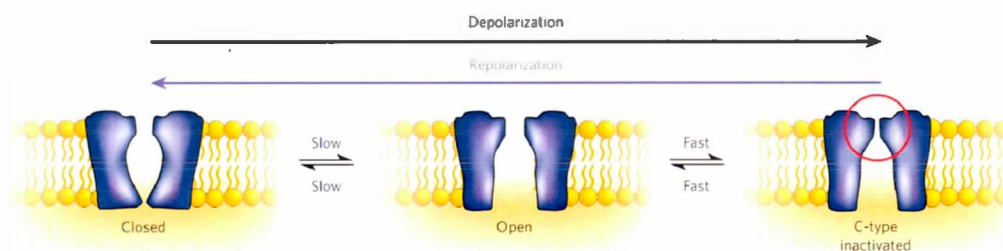


Figure 1.3 Conformations du hERG adoptées selon le potentiel d'action de la membrane. L'image a été obtenue de Sanguinetti *et al.* avec permission⁹.

1.1.1 Le syndrome du QT long (LQTS)

Le rôle fondamental du canal hERG a été mis en évidence en 1995 lorsque Curran *et al.* ont identifié des mutations héréditaires dans le gène *KCNH2*, qui seraient responsables de la perte de fonction des canaux $Kv11.1$ ¹⁰. Ce dysfonctionnement du

canal hERG est associé au LQTS. Il est caractérisé par une prolongation de l'intervalle entre les ondes cardiaques Q et T sur l'ECG (Fig. 1.2, bas), ce qui représente la durée du potentiel d'action – soit une dépolarisation suivie d'une repolarisation¹¹. La prolongation de l'intervalle QT peut engendrer des arythmies cardiaques, telles que les torsades de pointes (Fig. 1.4), qui sont potentiellement fatales¹². Aujourd'hui, plus de 319 mutations à effet putatif ont été découvertes sur le gène *KCNH2*^{13, 14}.

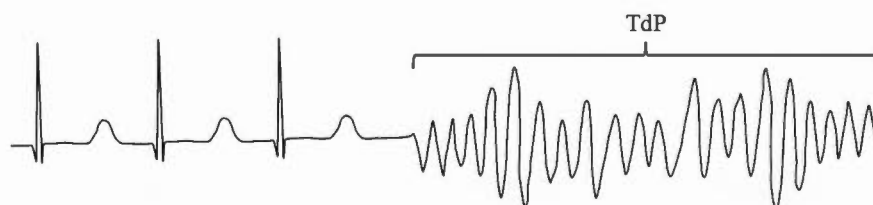


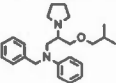
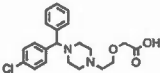
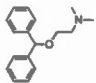
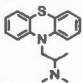
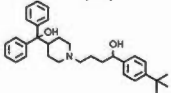
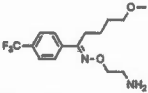
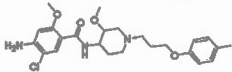
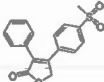
Figure 1.4 Tracé d'un électrocardiogramme qui débute avec trois cycles cardiaques normaux suivi d'un épisode de torsade de pointes (TdP).

1.1.2 Le syndrome du QT long acquis (ALQTS)

En plus d'être inné, le LQTS peut aussi être acquis (ALQTS) lorsque le fonctionnement du canal hERG est perturbé par des molécules cardiotoxiques. En effet, celui-ci est ciblé par des toxines, telles que ErgTx1 et BeKm-1 provenant du venin de scorpions *Centruroides noxius* et *Buthus eupeus*, respectivement¹⁵. Il peut également être perturbé, par effet secondaire, par des médicaments ayant des structures variées et appartenant à des classes pharmacologiques différentes (Tableau 1.1)^{1, 12, 15}. Étant donné qu'une quantité alarmante de composés ont la capacité d'inhiber le hERG, l'Organisation Mondiale de la Santé (OMS) maintient une base de données sur les médicaments bloquant le hERG causant des effets indésirables¹⁶. Lors de la conception de nouveaux médicaments, des tests *in vitro* sont à présent obligatoires afin de vérifier le potentiel de blocage du hERG¹⁷. C'est ainsi

qu'un grand nombre de médicaments d'ordonnance ont été retirés du marché et que plusieurs autres ne reçoivent pas l'approbation des agences de réglementation lors des phases cliniques⁷. Le rofécoxib, aussi connu sous son nom commercial *Vioxx*[®], en est un exemple célèbre. Ce médicament a été approuvé par l'agence américaine des produits alimentaires et médicamenteux (FDA, *Food and Drug administration*) en 1999 et retiré du marché en 2004 car une étude menée par la FDA concluait que le *Vioxx*[®] serait à l'origine de plusieurs milliers de décès aux États-Unis¹⁸.

Tableau 1.1 Structures et classes pharmacologiques de médicaments qui ont la capacité de causer une prolongation de l'intervalle QT ou des torsades de pointe sur l'électrocardiogramme.

Médicament	Structure	Classe pharmacologique
Bépridil		Antiarythmique
Cétirizine		Antihistaminique
Diphenhydramine		Antihistaminique
Prométhazine		Antihistaminique
Terfenadine (retiré du marché en 1998)		Antihistaminique
Fluvoxamine		Antidépresseur
Cisapride (retiré du marché en 2000)		Agent prokinétique
Rofécoxib (<i>Vioxx</i> [®]) (retiré du marché en 2004)		Anti-inflammatoire

En comparaison avec les autres canaux K_V , le hERG est particulièrement susceptible au blocage par les médicaments vu la taille supérieure de la cavité de son pore et de ses sites de liaison uniques. Plusieurs études ont démontré que la plupart des molécules hERG-actives interagissent avec le domaine du pore. Notamment, les résidus Tyr652 et Phe656 du segment S6 ainsi que la Thr623, la Ser624 et la Val625 de l'hélice du pore et du SF sont des sites ciblés par les molécules hERG-actives^{7, 9, 19-21}. Certaines études ont démontré par modélisation *in silico* que les chaînes latérales de ces acides aminés sont orientées vers la cavité centrale du pore où il est souvent indispensable d'avoir des résidus hydrophobes à certaines positions (652 et 656) pour accommoder des molécules de tailles et de structures différentes^{7, 9, 22, 23}. Par l'entremise d'attractions hydrophobes ou cation- π non spécifiques, ces interactions pourraient partiellement expliquer la diversité des molécules qui bloquent le canal hERG. En outre, la cavité du pore du hERG est plus large que les autres canaux K_V (12 Å)^{7, 9} ce qui mène à croire qu'il peut aussi accommoder une plus grande variété de molécules. D'ailleurs, certaines études démontrent que même des flavanoïdes alimentaires, tel que ceux provenant du thé vert et des agrumes, peuvent moduler l'activité du hERG en se liant à la Phe656 du domaine S6 et provoquer la prolongation de l'intervalle QT²⁴⁻²⁶.

1.1.3 La structure du hERG

Le hERG est composé de quatre sous-unités monomériques qui contiennent chacune six domaines transmembranaires (S1 à S6) (Fig. 1.5). Les quatre premières hélices (S1 à S4) constituent le domaine sensible au voltage (DSV) et sont liées au domaine du pore (hélices S5 à S6) via le segment intracellulaire S4-S5. Les sous-unités du hERG s'assemblent au niveau des domaines du pore pour former un tunnel qui coordonne la sortie des ions potassium ainsi qu'une « porte » qui contrôle l'ouverture et la fermeture du canal. Les hélices S5 et S6 du pore se rejoignent grâce au segment

extracellulaire qui comprend le segment S5P, l'hélice du pore (H_p) et le filtre de sélectivité (SF). Le segment S5P, qui rejoint le domaine transmembranaire S5 à l'hélice du pore, est particulièrement long (43 acides aminés) chez le hERG comparativement aux autres canaux K_v qui sont de 10 à 19 acides aminés (Fig. 1.6)^{27, 28}. Une étude RMN a été réalisée sur ce segment, dont j'ai participé mais qui ne sera pas présentée dans cette thèse (Annexe A). De plus, il comporte un SF ayant une séquence unique (SVGFG) au lieu du motif TVGYG étant hautement conservé parmi plusieurs canaux $K^{+21, 29}$. La structure du hERG n'a jamais été entièrement cristallisée, car l'expression et la purification du canal entier sont très ardues. Le domaine du pore du hERG contient plusieurs sites de modifications post-traductionnelles, tels que les sites de glycosylation sur Asn598 et Asn629, ainsi que la phosphorylation de la Tyr611^{30, 31}. Toutefois, Gong *et al.* ont démontré que la glycosylation n'était pas nécessaire pour exprimer des canaux hERG fonctionnels à la surface de la cellule³². La structure du hERG est alors principalement prédite par homologie de séquence avec des canaux K^+ similaires dont les structures ont été déterminées, tel que le domaine du pore des canaux potassiques bactériens KcsA en conformation fermée et celui du canal MthK en conformation ouverte³³⁻³⁶. Un modèle d'homologie construit à partir de la structure du canal MthK mais qui contient le domaine S6 et l'hélice du pore du hERG révèle l'alignement de deux rangées de quatre chaînes latérales dans la cavité du pore, dont celles des acides aminés Tyr652 et Phe656⁷.

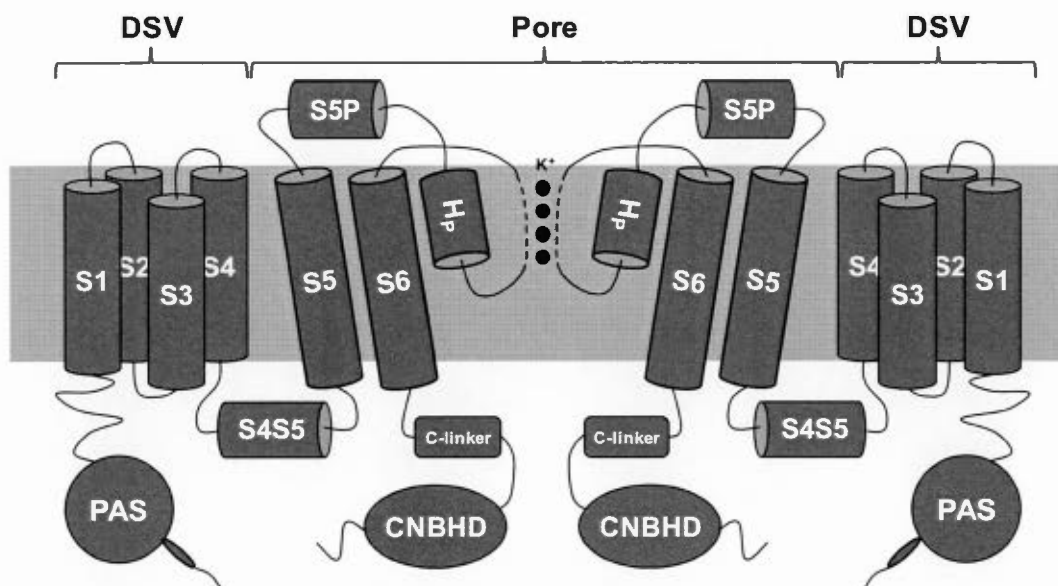


Figure 1.5 Schéma de la vue latérale de la topologie du canal hERG stabilisé dans une bicouche lipidique (rectangle gris pâle). Le domaine sensible au voltage (DSV) comporte les hélices transmembranaires S1 à S4, tandis que S5 à S6 constituent le domaine du pore. Le segment intracellulaire S4S5 relie ces deux domaines. Le filtre de sélectivité (SF) est représenté en pointillé et coordonne le passage des ions potassium (K^+). Les domaines intracellulaires N-terminal et C-terminal incluent le domaine PAS et CNBHD respectivement. Seuls deux des quatre sous-unités du canal sont représentées.

Le domaine N-terminal est la seule région du hERG dont la structure a été obtenue par cristallographie à rayons X³⁷⁻⁴⁰. Il contient le domaine PAS (Per. Arnt. Sim.) constituant cinq feuillets- β antiparallèles superposés d'une hélice 3_{10} et ayant deux hélices- α de chaque côté³⁷. Récemment, des études de résonance magnétique nucléaire (RMN) ont confirmé la structure cristallographique du domaine PAS et ont démontré que la queue N-terminale de ce domaine se structurait en hélice de 11 acides aminés³⁸⁻⁴⁰.

K _V 1.4	EADPTTH.....FQSIPD
K _V 2.1	EKDEDDTK.....FKSIPA
K _V 3.1	ERIGAQPN.....DPSASEHTHFKNIPI
K _V 4.3	EKGSSASK.....FTSIPA
K _V 11.1 (hERG)	IGNMEQPHMDSRIGWLHNLGDQIGKPYNSSGLGGPSIKDKYVT
	571 613

Figure 1.6 Alignement des séquences du segment S5P de plusieurs canaux K_V. Les numéros en bas de la figure représentent les positions dans la séquence du hERG⁴¹.

La structure du hERG se distingue à plusieurs niveaux si on la compare aux autres canaux K_V. Le domaine du pore comprend plusieurs acides aminés étant conservés chez les canaux K_V mais qui ne le sont pas chez le hERG. De ces résidus, certains sont proposés comme des sites ALQTS-actifs chez le hERG, tels que la Tyr652 et la Phe656, qui sont occupés par une Ile et une Val respectivement dans d'autres canaux^{7,9}. De plus, chez les autres canaux K_V, une proline est retrouvée à une ou aux deux positions adjacentes à la Phe656, ce qui a mené à suggérer que la présence de proline occasionnerait un coude au niveau du S6 réduisant l'espace à l'intérieur de la cavité du pore. Ceci aiderait à expliquer la raison pour laquelle la cavité interne du canal hERG est plus grande (12 Å)^{7,9}.

Le but de cette thèse est d'aider à avancer dans la compréhension de la structure et du fonctionnement du hERG à l'aide de la RMN. En biologie structurale, la RMN et la cristallographie à rayons X sont deux techniques complémentaires qui sont utilisées pour déterminer la structure de molécules, ou de complexes moléculaires, à l'échelle atomique. Chacune de ces techniques comporte ses avantages et inconvénients. La cristallographie étudie l'état cristallin d'une molécule, donc de manière périodique, où elle n'est pas limitée par la taille moléculaire. La cristallogenèse, n'étant pas évidente pour les macromolécules biologiques, constitue souvent l'étape limitante pour l'utilisation de la cristallographie, où elle se fait souvent par méthode d'essais-erreurs. La RMN est une technique non destructive qui permet d'étudier les protéines

en solution, donc à l'état naturellement dynamique et faisant jusqu'à environ une centaine de kilodaltons, tandis qu'à l'état solide, elle n'est pas limitée au poids moléculaire. La RMN a aussi l'avantage de permettre d'étudier les interactions entre molécules, comme celles d'une protéine et d'un ligand étant très utilisée en pharmacologie pour étudier les médicaments.

De manière générale, l'étude des protéines membranaires (PM) est complexe, car leur nature hydrophobe entraîne souvent des problèmes de solubilité dans un milieu aqueux⁴². Jusqu'à présent, seulement 3 % des structures protéiques de la *Protein Data Bank* (PDB) sont des PM, malgré le fait que les PM constituent 30 % des protéines exprimées chez l'humain. Parmi ces structures de PM, 5 % ont été déterminées par RMN⁴³⁻⁴⁵. Considérant que la plupart des PM ne peuvent être cristallisées ou étudiées par RMN des solutions vu leur taille et leur solubilité – c'est le cas du canal hERG dont la structure n'est toujours pas résolue – il est toutefois possible d'obtenir de l'information sur leur structure, leur orientation et leur localisation dans la membrane en étudiant des peptides dérivés de protéines dans des membranes modèles.

Étudier des peptides correspondant à différentes régions d'une PM s'avère une stratégie utile pour nous aider à résoudre sa structure entière. D'ailleurs, plusieurs études de RMN ont été faites sur des fragments peptidiques du hERG, dont l'hélice S5, le segment S5P, le H_P, le segment PS6, ainsi que le SF, afin de déterminer leur structure et fonction. Le premier segment transmembranaire du domaine du pore, le S5, se structure en hélice- α de 20 acides aminés d'après des expériences de RMN en solution du ¹H à deux dimensions, soit *total correlation spectroscopy* (TOCSY) et *nuclear overhauser enhancement spectroscopy* (NOESY)⁴⁶. Ces expériences sont décrites dans les sections 2.3.1 et 2.3.2 de cette thèse. Du côté C-terminal du S5, se trouve le segment S5P (Fig. 1.6) qui relie le S5 au H_P (Fig. 1.5). Le S5P se structure en hélice amphiphile dans le hERG et aurait le rôle de réguler l'inactivation^{27, 41, 47}. Le H_P se situe après le S5P et se structure en hélice- α ⁴⁶. Les structures des segments

S5P et H_P ont été déterminées avec des expériences de double quantum filtered correlated spectroscopy (DQF-COSY), TOCSY et NOESY⁴⁸⁻⁵⁰.

Le SF, constituant le motif d'acides aminés SVGFG dans le hERG, se trouve directement après le H_P et a le rôle de coordonner le passage des ions potassium vers l'extérieur de la cellule lorsque le canal est actif. Plusieurs études ayant obtenu des structures de canaux K_V par simulations de dynamique moléculaire et par cristallographie de rayons X, comme pour les canaux KcsA et KirBac1.1, démontrent que le SF doit être flexible pour adopter différentes conformations lors de l'activation et de la désactivation⁵¹⁻⁵⁶. Les oxygènes des carbonyls du squelette peptidique du SF orchestrent les mouvements des ions K⁺ déshydratés vers l'extérieur de la cellule. Par exemple, à l'état conducteur du canal KirBac1.1, ces oxygènes pointent vers le centre du pore, tandis qu'à l'état non conducteur, seuls ceux de la valine restent orientés vers le pore (Fig. 1.7)⁵⁴.

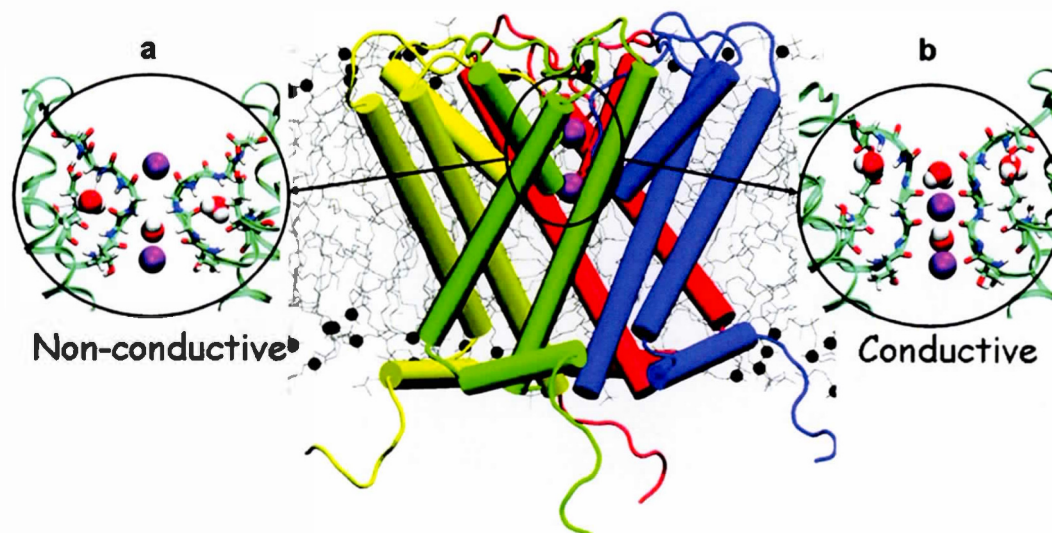


Figure 1.7 Simulation de dynamique moléculaire de la translocation d'ions K^+ (sphères mauves) et de molécules d'eau (sphères rouges et blanches) au travers la membrane par l'entremise du canal procaryote KirBac1.1. Les changements de structure du filtre de sélectivité (SF) sont associés aux différents états : non conducteur (a) et conducteur (b). Les hélices- α pour chaque monomère (colorés) sont entourées d'une bicouche de dioleoylphosphocholine (gris). L'image est reprise de Domene *et al.* avec permission⁵⁴.

Considérant son motif unique, sa prédisposition à être ciblé par des molécules hERG-actives et sa structure qui est toujours matière à débat, il est important de raffiner le modèle structural du SF du hERG en étudiant sa structure et ses interactions avec des médicaments cardiotoxiques ainsi qu'avec la membrane afin de mieux comprendre la fonction et le rôle du hERG dans le ALQTS. Dans cette thèse, l'étude de la structure et de la fonction d'un peptide qui correspond au SF et au fragment qui rejoint ce dernier au segment transmembranaire S6 est présentée au chapitre II²¹.

En plus de la boucle extracellulaire du domaine du pore, la boucle intracellulaire qui relie le DSV et le domaine du pore, la séquence Asp540 à Val549 qu'on appelle

S4S5, a aussi été étudiée par RMN afin de connaître sa structure. Cette boucle se trouve entre les domaines transmembranaires S4 et S5, et se structure sous forme d'hélice- α de 10 acides aminés⁵⁷. La structure cristalline du canal $K_v1.2$ ³³ ainsi que celle de la chimère $K_v1.2/2.1$ ⁵⁸ révèle que le segment *S4S5* se structure en hélice- α amphiphile parallèle à l'interface cytoplasmique de la membrane où un côté de l'hélice interagirait avec des lipides de la membrane et sera en proximité avec l'extrémité C-terminale du domaine transmembranaire *S6*^{34, 59}. Au chapitre III, le rôle important du segment *S4S5* est mis en évidence en identifiant deux résidus, Y542 et Y545, qui interagissent avec la membrane et certains domaines du hERG pour stabiliser la conformation ouverte du canal lors de la désactivation.

1.1.4 Mécanisme d'ouverture et de fermeture du hERG

Les mécanismes d'activation et de désactivation du canal hERG diffèrent des autres canaux K_v et ne sont toujours pas bien compris. Ils ne suivent pas nécessairement des processus réciproques, car ils impliquent plusieurs mouvements et sites d'interactions qui ne sont pas obligatoirement les mêmes en conformations ouverte et fermée⁶⁰. L'activation et la désactivation lentes du canal hERG pourraient être en partie dues aux mouvements lents du DSV, ou à une transmission lente des mouvements du DSV au domaine du pore^{61, 62}.

La dépolarisation de la membrane entraîne le mouvement du domaine S4 du côté cytosolique vers la surface cytoplasmique de la membrane au moyen des nombreux acides aminés chargés positivement qui sont sensibles au voltage⁶³⁻⁶⁵. Plusieurs auteurs pensent que le segment *S4S5* serait essentiel pour transmettre les changements conformationnels du DSV au domaine du pore puisque celui-ci les relie^{57, 59, 66-71}. Le *S4S5* est tiré par les déplacements du S4 et transmet ses mouvements à la porte d'activation pour mener à l'ouverture du canal (Fig. 1.8). La porte d'activation comporte les quatre régions C-terminales des domaines S6 (C-S6)

qui se croisent à l'interface cytoplasmique de la membrane^{36, 58}. Lors de l'activation, le S6 subirait des mouvements de rotation et de fléchissement où des interactions électrostatiques entre l'Asp540 du segment S4S5 et de l'Arg665 (C-S6) entreraient en jeu⁶⁷. Il y aurait aussi possiblement des interactions avec la Gly546 du S4S5 et le domaine cytoplasmique N-terminal pour maintenir l'ouverture du pore⁶⁹.

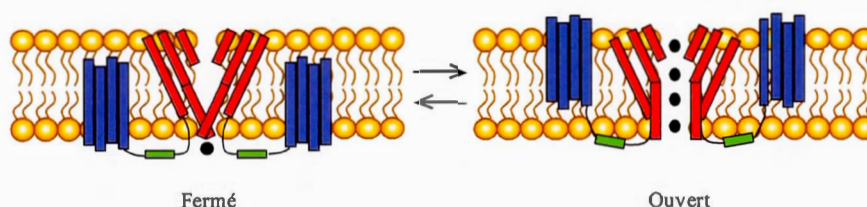


Figure 1.8 Mouvements des domaines du hERG suite à l'ouverture et la fermeture du canal. Le domaine sensible au voltage (DSV) est en bleu, le domaine du pore en rouge, le segment S4S5 en vert et les ions K^+ sont en noir.

Plusieurs groupes se penchent sur le rôle important du S4S5 lors de la déactivation^{57, 67, 70}. D'après les études électrophysiologiques sur une chimère du hERG, il est proposé que le S4S5 agirait comme levier en appliquant une force mécanique sur la porte d'activation tout en repositionnant l'Asp540 (S4S5) près de la Leu666 (C-S6) ce qui rétrécirait l'ouverture de la porte d'activation et la maintiendrait fermée^{33, 34, 59}.

Il est important d'étudier le rôle et la fonction du S4S5 afin de mieux comprendre le mécanisme d'ouverture et de fermeture particulier du hERG qui pourrait expliquer son rôle dans le LQTS. Dans cette thèse, une étude portant sur l'identification des résidus du segment S4S5 qui sont importants pour stabiliser la conformation ouverte du canal hERG sera présentée au chapitre III.

1.1.5 Environnement membranaire du hERG

La membrane plasmique des cardiomyocytes est aussi appelée le sarcolemme. Celle-ci agit comme barrière semi-perméable qui permet le passage d'ions afin de réguler la contraction et le relâchement des cellules musculaires du cœur. Le sarcolemme est composé de lipides, de protéines, et de glucides. Les lipides du sarcolemme sont majoritairement des phospholipides et du cholestérol (Tableau 1.2). Parmi les phospholipides, les plus abondants sont les phosphatidylcholines (PC) et les phosphatidyléthanolamines (PE) qui représentent 42 % et 30 % des phospholipides totaux, respectivement. La sphingomyéline (Sph) est un constituant lipidique retrouvé en grande majorité dans les membranes de cellules nerveuses où elle sert d'isolant, mais elle se retrouve aussi en faible quantité dans le sarcolemme à 11 %. Les lipides chargés, tels que la phosphatidylsérine (PS) et le phosphatidylinositol (PI) représentent environ 9 % des phospholipides totaux du sarcolemme⁷².

Tableau 1.2 Composition lipidique du sarcolemme des cardiomyocytes exprimé en pourcentage par rapport à la quantité totale de phospholipides. Les données sont recueillies de plusieurs études⁷³⁻⁷⁹ et la moyenne est présentée.

Lipides	Composition (%)	
	Moyenne	Écart type
PC	42	6
PE	30	4
PS et PI	9	3
Sph	11	5
Chol/PL (mol/mol)	0,5	0,1

PC: phosphatidylcholine, PE: phosphatidyléthanolamine, PS: phosphatidylsérine, PI: phosphatidylinositol, Sph: sphingomyéline, Chol: cholestérol, PL: phospholipides.

Les phospholipides sont composés de deux chaînes d'acides gras liées à un glycérol par deux de ses groupements hydroxyles. Le troisième groupement hydroxyle du glycérol est fixé à un phosphate qui est lié à un groupement polaire (Fig. 1.9). Dans les membranes biologiques, comme le sarcolemme, les phospholipides se structurent

sous forme de bicouches où les têtes polaires pointent vers l'extérieur et sont exposées au liquide interstitiel ou au cytoplasme, tandis que les chaînes acyles qui sont non polaires se trouvent au centre de la bicouche, dans le cœur hydrophobe (Fig. 1.9).

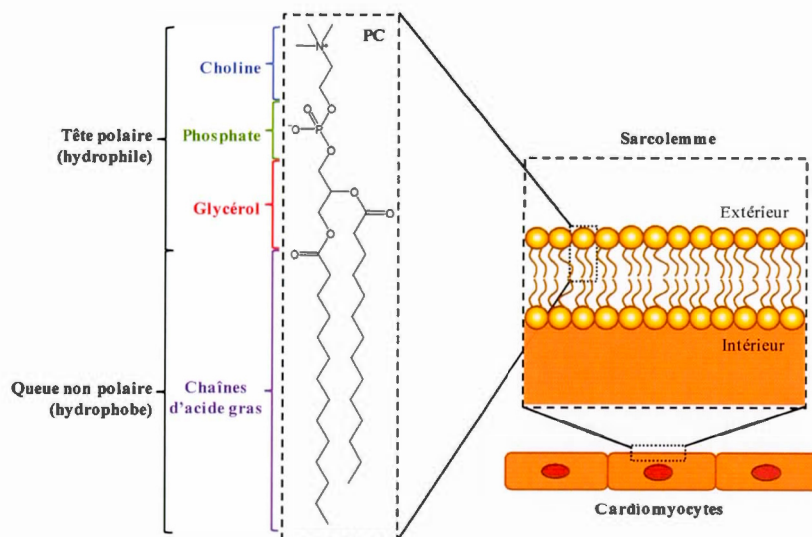


Figure 1.9 La membrane des cardiomyocytes, appelée sarcolemme, est majoritairement faite de phospholipides. PC : phosphatidylcholine.

1.2 Membranes modèles

La complexité de la membrane native est souvent problématique pour l'étude de protéines membranaires par des méthodes spectroscopiques. Les modèles lipidiques simplifiés ont une composition et une structure similaires aux biomembranes et permettent d'étudier la structure des protéines membranaires et leur interaction avec la membrane. Dans cette thèse, l'utilisation de membranes modèles a permis d'étudier le SF et le segment S4S5 du canal potassique hERG, qui seront discutés davantage dans les chapitres III et IV respectivement. Par la suite, nous avons développé un système membranaire modèle qui permettra d'étudier les protéines membranaires par

RMN, tout en simplifiant les étapes de purification des protéines (chapitre V). La théorie sur les méthodes RMN sera présentée au prochain chapitre (chapitre II).

1.2.1 Composition

Un modèle membranaire doit bien représenter la composition lipidique native des protéines membranaires afin de maintenir certaines propriétés physiques, telles que la morphologie, la courbure et l'épaisseur de la membrane. Il existe une grande diversité de lipides dans les cellules eucaryotes pour lesquels varient le groupement polaire et la longueur des chaînes acyles (14 à 24 carbones) qui peuvent contenir, ou non, des insaturations⁸⁰. Les têtes polaires des phospholipides déterminent la charge globale du lipide. Les lipides zwitterioniques comme la PC et la PE ont à la fois une charge négative et positive donc leur charge globale est neutre, tandis que celle des PI et PS est négative. Les membranes biologiques eucaryotes, incluant celle du sarcolemme, sont principalement composées de phospholipides, plus spécifiquement de PC (Tableau 1.2), alors celle-ci est souvent employée dans les membranes modèles.

1.2.2 Propriétés physiques et organisation des lipides

La manière dont les lipides s'organisent en solution dépend de la nature du lipide en question – ses chaînes acyles et sa tête polaire – ainsi que du solvant, du pH, de la force ionique et de la température⁸¹. Les lipides sont des molécules amphiphiles qui regroupent leurs domaines hydrophobes et exposent leurs domaines polaires au solvant aqueux. La forme d'un lipide au niveau moléculaire va déterminer s'il s'assemble en bicouche, en micelle ou en phase hexagonale (Fig. 1.10). La plupart des phospholipides ont une forme moléculaire cylindrique. Ils s'autoassemblent donc en bicouche, autrement dit deux monocouches antiparallèles superposées (Fig. 1.10B). Les détergents, les phospholipides n'ayant qu'une seule chaîne acyle,

ainsi que les phospholipides à chaînes courtes (huit carbones ou moins) ont une structure moléculaire de type conique. Ceux-ci forment des micelles, car leur tête polaire est plus grande que leur groupement hydrophobe (Fig. 1.10A). Les lipides ayant une forme géométrique de type cône inversé mènent à la formation de phases hexagonales (H_I), mais certains ont tendance à former des phases hexagonales inversées (H_{II}), telle que la PE (Fig. 1.10C). Les phases hexagonales sont retrouvées dans plusieurs processus biologiques tels que la fusion membranaire lors de l'endo- et l'exocytose, du recyclage membranaire et du trafic de protéines⁸².

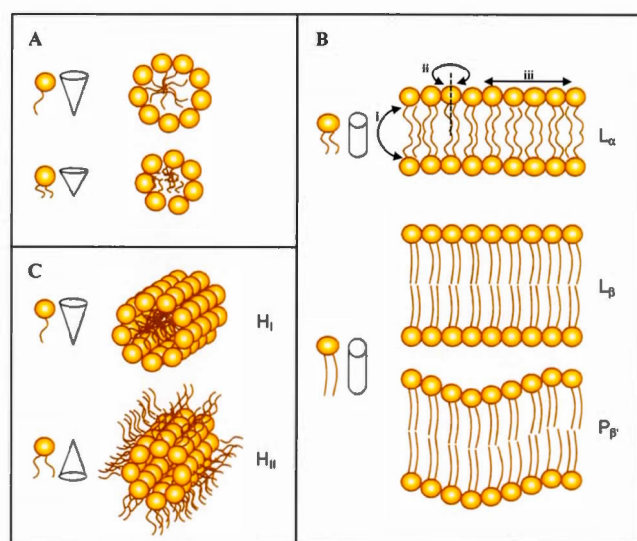


Figure 1.10 Formes moléculaires des lipides qui s'autoassemblent en solution sous forme de micelle (A), de bicouche (B) ou en phase hexagonale (C). Les lipides peuvent diffuser librement dans une bicouche en phase liquide cristalline (L_α) en effectuant des mouvements de *flip-flop* (i), de rotation (ii) et de diffusion latérale (iii). Les lipides peuvent aussi être en phase gel (L_β), où les chaînes sont ordonnées et rigides, ainsi qu'en phase gel ondulée (P_β). Certains lipides peuvent s'assembler en phase hexagonale (H_I) ou en phase hexagonale inversée (H_{II}).

À part la géométrie moléculaire, la concentration monomérique des surfactants est un facteur important à considérer, car celui-ci va influencer leur capacité à s'autoassembler. À des concentrations très faibles, les surfactants se trouvent sous forme de monomères. Plus la concentration du surfactant augmente, plus la quantité de monomère augmente jusqu'à un certain point de saturation, où l'augmentation de la concentration de monomère est quasi nulle. Cette concentration correspond à la concentration micellaire critique (CMC) – qui est propre à chaque surfactant (Tableau 1.3) – où les monomères s'auto-assemblent pour former des micelles. Certaines molécules amphiphiles peuvent aussi former des phases lamellaires, ce qui dépend majoritairement de leur forme moléculaire comme discuté ci-dessus.

Tableau 1.3 Concentration micellaire critique (CMC) de divers lipides et détergents communément employés pour les membranes modèles et pour la purification de protéines membranaires.

Surfactant	CMC (mM)	Références
DPPC	$4,6 \times 10^{-7}$	[1]
DMPC	6×10^{-6}	[1]
DHPC	15	[2]
Tween 80	12×10^{-3}	[3]
C ₁₂ E ₈	0,09	[3]
Triton X-100	0,2	[3]
CHAPS	8	[3]
Glycocholate de sodium	13	[3]

DPPC: dipalmitoyl-phosphatidylcholine (PC), DMPC: dimyristoyl-PC, DHPC: dihexanoyl-PC, Tween 80: monooléate sorbitane de polyoxyéthylène 80, C₁₂E₈: octaéthylèneglycol monododécyl éther, Triton X-100: éther de polyéthylèneglycol et d'octylphénol, CHAPS: 3-[diméthylammonio]-1-propanesulfonate [1] Avanti Polar Lipids, Inc. [2] Warschawski et al., 2011 [3] Luckey, 2008

La structure dynamique de la membrane biologique est cruciale pour permettre la diffusion de ses constituants, dont les PM, pouvant ainsi jouer un rôle important dans

plusieurs fonctions cellulaires. La composition de la membrane modèle va influencer sa fluidité. Le cholestérol, de la famille des stérols, occupe une proportion importante dans la membrane eucaryote (Tableau 1.2). Sa nature encombrante augmente le désordre des chaînes lipidiques compactes et stabilise celles étant mobiles ce qui augmente et diminue, respectivement, la fluidité de la membrane⁸³. De manière similaire, les PM sont aussi responsables des propriétés physiologiques de la membrane, étant donné qu'elles constituent environ la moitié du poids sec de celle-ci. La fluidité de la membrane est aussi influencée par la température du système. La bicouche peut adopter différentes phases lamellaires, par exemple la phase liquide cristalline (L_α), et la phase gel (L_β) (Fig. 1.10B). Lorsqu'en phase L_β , le domaine hydrophobe des lipides est beaucoup plus ordonné et rigide; les chaînes carbonées sont parallèles et occupent très peu d'espace latéral. Lorsque la température du système augmente au-delà de la température de transition (T_m), qui est propre à chaque lipide, la membrane transite en phase L_α où il y a présence de conformères gauches dans les chaînes acyles. L'énergie thermique transmise aux lipides fait en sorte que les chaînes acyles deviennent donc très mobiles pour permettre des mouvements de flexion ce qui engendre l'expansion latérale de la bicouche au détriment de son épaisseur qui, elle, diminue⁸⁴. De plus, la T_m d'un lipide augmente avec le nombre d'interactions lipidiques, alors plus les chaînes acyles sont longues, plus la T_m sera élevée (Tableau 1.4). À l'opposé, les insaturations des chaînes acyles diminuent les interactions entre les lipides donc font baisser la T_m . En plus des mouvements des chaînes acyles, les lipides eux-mêmes peuvent se déplacer librement dans la membrane soit par diffusion latérale (Fig. 1.10Biii), soit avec des mouvements plutôt rares de *flip-flop* (Fig. 1.10Bi), où les lipides sautent d'un feuillet à un autre, soit en tournant sur leur axe longitudinal pour effectuer des mouvements de rotation (Fig. 1.10Bii).

Tableau 1.4 Nomenclature des chaînes acyles de divers phosphatidylcholine (PC) saturés et insaturés ainsi que leur température de transition (T_m).

Lipides	Nomenclature	T_m (°C)
DLPC	C12:0	-2
DMPC	C14:0	24
DPPC	C16:0	41
DSPC	C18:0	55
POPC	C16:0-18:1 Δ 9-Cis	-2
DOPC	C18:1 Δ 9-Cis	-17

DLPC: dilauryl-phosphatidylcholine (PC), DMPC: dimyristoyl-PC, DPPC: dipalmitoyl-PC, DSPC: distearoyl-PC, POPC: palmitoyl-oleoyl-PC, DOPC: dioleoyl-PC.

Il existe une autre phase gel dite ondulée (P_β) qui n'apparaît pas dans les membranes biologiques, mais qui peut se trouver dans plusieurs modèles membranaires, notamment ceux faits de PC, de PG et de Sph⁸⁵⁻⁸⁷. La phase P_β (Fig. 1.10B) est formée dans des bicouches flexibles pour lesquelles le couplage entre les monocouches est faible, et ce, lorsque la température se trouve entre celle de la prétransition et de la T_m ^{88, 89}. Cette phase peut se manifester de deux manières, soit quand la bicouche est en phase L_α et que la température diminue jusqu'à la T_m , soit lorsque le système est chauffé jusqu'à la température de prétransition en partant d'une bicouche en phase L_β ⁸⁶.

1.2.3 Choix du modèle membranaire

Les protéines membranaires, dont le hERG, sont des molécules hydrophobes qui nécessitent des surfactants afin de pouvoir les manipuler en solution. Plusieurs modèles membranaires sont disponibles pour les étudier et donc celui-ci est choisi en fonction des besoins biologiques de la protéine et des besoins techniques pour l'expérience RMN à effectuer, tel que décrit dans un article de revue auquel j'ai participé mais qui ne sera pas présenté dans cette thèse (Annexe B)⁹⁰.

Les micelles sont utilisées pour extraire et solubiliser les PM, ainsi que pour effectuer des expériences de RMN en solution, car elles procurent une haute résolution spectrale. Quoiqu'elles peuvent être très utiles, leur morphologie ne ressemble pas du tout à celle d'une membrane biologique. Les micelles ont une courbure très élevée, ce qui expose les régions hydrophobes des lipides au solvant. Cette différence de morphologie peut empêcher le bon repliement des PM et nuire à leur structure et à leur fonction. Les détergents sont souvent utilisés pour extraire les PM de leur membrane native. Ils sont également utilisés pour solubiliser les PM. Enfin, ils sont utilisés pour réintroduire (reconstituer) les PM dans des membranes modèles biomimétiques. Ils sont donc à la fois très utiles et potentiellement nocifs, et il faut donc les éliminer de l'échantillon final, ou du moins de s'assurer qu'en faible quantité ils ne perturbent pas le repliement, la structure ou la fonction de la PM d'intérêt.

Les bicouches ont une épaisseur d'environ 4 nm en phase L_α et peuvent contribuer à maintenir l'activité des PM lorsqu'elles sont utilisées comme membranes modèles, tel que pour la kinase diacylglycérol (*DAGK*) qui a été reconstituée dans des bicelles de DMPC ou DPPC contenant le détergent CHAPSO, un analogue de sels biliaires⁹¹. Un modèle idéal doit adopter une morphologie similaire à l'environnement natif de la PM et ce, à des températures physiologiques. Les bicouches en solution se referment spontanément sur elles-mêmes pour former des vésicules sphériques. En RMN, plusieurs modèles peuvent être utilisés, tels que les vésicules unilamellaires de tailles petites, grandes et géantes (SUV, LUV, GUV), ainsi que les vésicules multilamellaires (MLV). Les SUV sont préparées par sonication et leur taille (20 à <100 nm), nettement inférieure à celle d'une cellule eucaryote – qui fait normalement de 10 à 100 μm ⁹² (Fig. 1.11). La petite taille des micelles leur impose une courbure importante, une épaisseur inférieure à celle d'une bicouche traditionnelle et une distribution asymétrique des feuilletts lipidiques interne et externe, ce qui rends les rends instables et qui exerce une pression sur les PM. Elles ne sont pas utilisées pour la détermination de structure des PM, car en RMN en solution leur taille reste trop

grande pour obtenir une résolution spectrale acceptable. De plus, elles ne sont pas stables, car la bicouche est mince et la densité des têtes polaires au niveau du feuillet lipidique externe est faible⁹³. Celles-ci sont plutôt utilisées pour étudier l'interaction de protéines solubles avec la membrane⁹⁴.

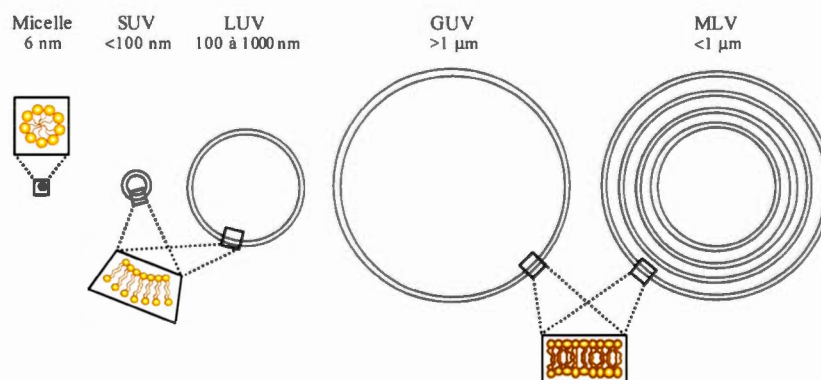


Figure 1.11 Schéma de divers modèles membranaires utilisés en RMN, telle que les micelles, les vésicules unilamellaires (SUV, LUV et GUV) et les vésicules multilamellaires (MLV). Les MLV, qui comportent plusieurs bicouches, ainsi que les GUV sont d'une taille supérieure et ont une morphologie membranaire locale qui ressemble à celle d'une biomembrane.

Les LUV sont préparées en filtrant une suspension lipidique par extrusion pour obtenir des objets ayant un diamètre entre 100 et 1000 nm (Fig. 1.11), tandis que les GUV, qui ont une taille supérieure à 1 µm, sont préparées en hydratant graduellement un film lipidique ou par électroformation^{92, 95}. La morphologie membranaire locale des GUV est plane et ressemble à celle d'une membrane biologique. Vue leur grande taille, ces modèles sont plutôt appropriés pour des expériences de RMN à l'état solide. Malgré tout, les GUV ne sont pas souvent employées comme modèles puisque la grande majorité de leur volume est occupé par le solvant plutôt que par la membrane, ce qui n'est pas très utile pour une technique si peu sensible comme la RMN.

Lorsque mis en solution, les lipides s'assemblent spontanément sous forme de vésicules multilamellaires (MLV) de différentes tailles de l'ordre de $1\text{ }\mu\text{m}$ de diamètre (Fig. 1.11)⁹². Cette organisation membranaire n'est pas retrouvée naturellement, mais la taille des agrégats ainsi que le degré de courbure des bicouches ressemble aux caractéristiques des biomembranes. De plus, les MLV sont avantageuses pour les études RMN, car leur concentration lipidique est très élevée.

Une bicouche planaire, où les régions hydrophobes sont exposées au solvant aqueux, n'est pas énergétiquement favorable, donc en général elle se referme sur elle même. Une autre option pour stabiliser sa région non polaire est d'ajouter des lipides à chaînes courtes (tels que la DHPC) sur les bords, créant ainsi des bicelles (Fig. 1.12)⁹⁶. Les surfactants non traditionnels peuvent également être employés, au lieu de lipides à chaînes courtes, pour préparer des bicelles, tel que les analogues de sels biliaires (CHAPSO, sodium glycocholate) et les détergents non ioniques, comme le Triton X-100, C_{12}E_8 et le Tween 80 (Tableau 1.4)⁹⁷⁻¹⁰⁰.

Au début des années 1990, les bicelles sont devenues très populaires vu leurs nombreux avantages⁹⁷. Leur composition et morphologie locales ressemblent beaucoup à celles des biomembranes. Les bicelles sont préparées en solubilisant le lipide et le détergent dans un milieu aqueux et en procédant à plusieurs cycles de congélation/décongélation/agitation jusqu'à ce que l'échantillon soit homogène. Elles sont très polyvalentes – le ratio molaire entre le lipide à chaîne longue et le lipide à chaîne court (ratio q) peut être modifié pour les employer en RMN des solutions, à q inférieur à 2,3 lorsqu'elles sont isotropes (Fig. 1.12A), et en RMN de l'état solide, où elles ont la particularité de s'orienter spontanément dans le champ magnétique supérieur à 1 Tesla et pour q supérieur à 2,3 (Fig. 1.12B et C)¹⁰¹. L'alignement est spontané de sorte que la normale (N) de la bicouche est perpendiculaire au champ magnétique et seulement lorsque le ratio molaire q est suffisamment élevé (supérieur à 2,3). Ceci est dû à la susceptibilité magnétique des phospholipides, qui sera abordée

plus en détail dans le chapitre I. De plus, c'est aussi un effet coopératif, alors si la concentration de lipides dans la bicouche n'est pas assez élevée, comme dans les bicelles isotropes, elles ne pourront pas s'aligner dans le champ magnétique.

Cette propriété est très intéressante, car elle permet entre autres d'étudier l'orientation des protéines (ou peptides) membranaires comme il sera détaillé au chapitre II¹⁰²⁻¹⁰⁴. Par exemple, le peptide antimicrobien alaméthicine a été étudié par RMN de l'état solide dans des bicelles de PC^{90, 104-107}. Les bicelles qui s'orientent dans le champ magnétique sont décrites dans la littérature comme étant soit des disques (Fig. 1.12A, B), soit des MLV perforées où les trous seraient stabilisés par des lipides à chaînes courtes (Fig. 1.12C). La topologie est équivalente dans les deux cas et par conséquent, il n'est pas possible de déterminer directement lequel des deux modèles est représenté en observant un seul spectre de RMN. Comme vu précédemment, la température va aussi affecter la morphologie des bicelles dans la mesure où la bicouche doit être en phase liquide cristalline ($L\alpha$), donc au-dessus de la T_m des lipides, pour qu'elles s'orientent spontanément dans le champ magnétique.

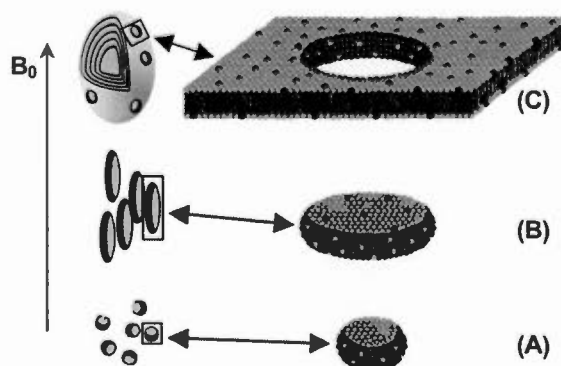


Figure 1.12 Schéma A) de bicelles isotropes et B) orientées dans le champ magnétique. C) Les MLV perforées peuvent également s'orienter dans le champ magnétique (B_0). La figure est adaptée de Triba *et al.* avec permission¹⁰⁴.

Toutefois, l'utilisation de bicelles est quelque peu restrictive¹⁰⁸ et peut limiter certaines applications. Par exemple, pour des applications de RMN de l'état solide, les bicelles de DMPC/DHPC s'orientent spontanément lorsque le champ magnétique est supérieur à 1 Tesla, et lorsque le ratio molaire est supérieur à 2.3 pour une concentration lipidique se situant entre 3 et 60 % (w/v) et à une température se situant entre 30 et 50 °C^{90, 96, 104, 109-112}. Il y a tout de même des progrès récents dans ce domaine, tels que l'optimisation de la gamme de température à laquelle certaines bicelles sont orientées¹¹³.

Il existe aussi d'autres structures qui s'orientent dans le champ magnétique, tel que les bicelles allongées (vermiculaire ou en forme de rubans)^{112, 114-116} et les liposomes déformés en ellipsoïdes aplatis ou allongés^{117, 118}. Même si elles n'ont pas la morphologie classique des bicelles, elles sont tout de même utiles pour les études RMN vu leur capacité de s'orienter dans le champ magnétique. Étant des vésicules, les liposomes ont une morphologie locale légèrement courbée qui mime davantage une biomembrane, relativement à la morphologie planaire des bicelles qui ont une forme discoïdale. De plus, ils présentent l'énorme avantage de posséder un intérieur et un extérieur, permettant d'éventuelles études de transport à travers la membrane, un élément important dans l'étude de PM telles que le hERG.

Comme vu précédemment, il existe de nombreux modèles membranaires et plusieurs approches pour les obtenir, chacun possédant des avantages et des inconvénients, et il est nécessaire de continuer de mettre au point de nouveaux systèmes et protocoles de reconstitution plus adaptés à certaines études. Dans le cadre de cette thèse, nous avons développé un nouveau système à base de lipides et de Tween 80, un détergent de faible CMC, ce qui évite la précipitation du complexe lipide-protéine, et nous avons étudié son potentiel dans le cadre d'études de PM par RMN. Ce système présente des avantages qui en font un choix prometteur pour des études structurales de PM.

1.3 Problématique et objectifs spécifiques

À ce jour, la structure intégrale du canal potassique hERG n'est toujours pas définie et son mécanisme d'ouverture et de fermeture particulier n'est toujours pas bien compris. Un des objectifs de cette thèse était donc de raffiner son modèle structural et dynamique afin de mieux comprendre son rôle dans le ALQTS. Plus particulièrement, étudier par RMN les segments intra- et extracellulaires du hERG, soit le SF et le S4S5. Plus précisément, au Chapitre II nous présentons la structure du SF sous faible et haute force ionique, ce qui reproduit les conditions physiologiques. Considérant la proximité de la boucle du pore à l'interface membranaire, nous avons aussi vérifié l'affinité du SF avec la membrane afin de clarifier son fonctionnement. Vu que plusieurs molécules LQTS-actives semblent cibler la région du pore, le rôle du SF dans le ALQTS a été étudié en vérifiant son interaction avec des médicaments cardiotoxiques.

De plus, notre objectif était de mieux comprendre les mécanismes d'ouverture et de fermeture particulier du hERG. Pour ce faire, nous avons identifié, au chapitre IV, les résidus du segment S4S5 qui sont responsables de la cinétique de désactivation particulièrement lente chez le hERG. Nous avons combiné des études de RMN et d'électrophysiologie. Chaque résidu du segment S4S5 du hERG a été muté à une alanine afin d'identifier la contribution individuelle de chaque résidu au phénotype de désactivation lente. Des études d'électrophysiologie ont permis de déterminer lesquels des mutants affectaient davantage les composantes du mécanisme d'ouverture et de fermeture, plus particulièrement la composante de désactivation. Ensuite, les mutations qui semblaient le plus perturber la cinétique de désactivation ont été sélectionnées pour les étudier sous forme de peptides qui correspondent à la séquence mutée du fragment S4S5. La proximité putative du segment S4S5 à la membrane cytosolique nous a ainsi incité à vérifier leur interaction avec la membrane par RMN.

Afin d'étudier les PM comme le hERG par RMN, elles doivent d'abord être extraites de leur environnement natif, solubilisées à l'aide de détergents et ensuite reconstituées dans des systèmes membranaires modèles qui pourront mimer la biomembrane. Avant la reconstitution, une étape d'élimination du détergent est souvent nécessaire, car la majorité des détergents ne peuvent offrir un environnement lipidique qui promeut le repliement correct et qui maintient la fonction des PM. Cette étape additionnelle est souvent longue et elle diminue le rendement protéique. Comme dernier objectif, nous voulons développer un système modèle membranaire pour des applications RMN. Au chapitre V, nous proposons un nouveau système membranaire modèle pour l'étude des PM par RMN qui utilise à la fois un détergent non ionique, le Tween 80, ainsi que des PC (DMPC ou DPPC). Nous démontrons que ces membranes modèles s'orientent dans le champ magnétique au-dessus de la T_m des PC et ce, sur une large gamme de ratios molaires (q). Le Tween 80 donne aux vésicules de PC des propriétés très élastiques de telle manière qu'elles se déforment dans le champ magnétique pour permettre une orientation spontanée. Les membranes modèles de PC/TW80 sont un bon outil pour déterminer l'orientation et la structure des PM en évitant l'étape de l'élimination du détergent.

CHAPITRE II

ÉLÉMENTS THÉORIQUES DE LA SPECTROSCOPIE DE RMN APPLIQUÉE AUX SYSTÈMES BIOLOGIQUES

2.1 Résonance magnétique nucléaire

La matière est faite d'atomes qui eux sont faits d'un noyau et d'électrons. Ces noyaux ont quatre propriétés physiques importantes : une masse, une charge électrique, un magnétisme et un spin¹¹⁹. La masse d'un atome provient majoritairement de la masse de son noyau. La charge électrique est très importante, car elle permet aux atomes de demeurer ensemble grâce aux forces électrostatiques entre les noyaux (chargés positivement) et les électrons (chargés négativement). Le magnétisme du noyau ressemble à celui d'un petit aimant qui interagit avec un champ magnétique. Celui-ci est si faible qu'il a très peu d'influence sur la structure atomique ou moléculaire. Le spin nucléaire est une propriété quantique plutôt abstraite. Le spin se comporte vaguement de la même manière que s'il tournait autour d'un axe, comme une petite planète¹²⁰.

Le spin d'un noyau peut interagir avec d'autres champs magnétiques provenant de son environnement, tels que des électrons environnants ou d'autres noyaux dans une même molécule. Il peut aussi interagir avec un champ magnétique externe (B_0) provenant d'un appareil. Le spin des noyaux permettent d'observer microscopiquement les structures internes et la dynamique des molécules par résonance magnétique nucléaire (RMN), et ce, de manière non destructive¹²⁰.

Seuls les noyaux ayant un numéro atomique (Z) ou un nombre de masse (A) impairs auront un nombre quantique de spin (I). Plusieurs isotopes de différents éléments peuvent avoir un nombre quantique de spin (Tableau 2.1).

Tableau 2.1 Propriétés d'isotopes nucléaires utiles en RMN des systèmes biologiques.

Isotope	Nombre quantique de spin (I)	Abondance naturelle (%)	Ratio gyromagnétique (γ : $10^7 \text{ rad} \cdot \text{T}^{-1} \cdot \text{s}^{-1}$)	Fréquence de Larmor à 14.1 T (MHz)
^1_1H	$\frac{1}{2}$	99,99	26,75	600
^2_1H	1	0,01	4,11	92
$^{13}_6\text{C}$	$\frac{1}{2}$	1,1	6,73	151
$^{14}_7\text{N}$	1	99,6	1,93	43
$^{15}_7\text{N}$	$\frac{1}{2}$	0,4	-2,71	61
$^{31}_{15}\text{P}$	$\frac{1}{2}$	100	10,84	243

Le spin d'un noyau peut être visualisé comme un vecteur, qu'on appelle le moment angulaire de spin (\vec{I}), pointant dans la direction de l'axe autour duquel il tourne (Fig. 2.1). Puisque les noyaux sont composés de particules chargées, ils ont aussi un magnétisme intrinsèque que l'on appelle le *moment magnétique nucléaire* ($\vec{\mu}$). Les moments angulaire et magnétique de spins sont étroitement liés. Leur proportionnalité est représentée par la constante nommée *ratio gyromagnétique* (γ) comme décrit dans l'équation suivante¹²¹

$$\vec{\mu} = \gamma \cdot \hbar \cdot \vec{I} \quad (2.1)$$

où $\hbar = h/2\pi$ et h est la constante de Planck. Le ratio gyromagnétique, qui est propre à chaque noyau, indique la force de la réponse d'un noyau dans un champ magnétique. Plus le γ est élevé, plus le noyau est sensible, et vice-versa (Tableau 2.1).

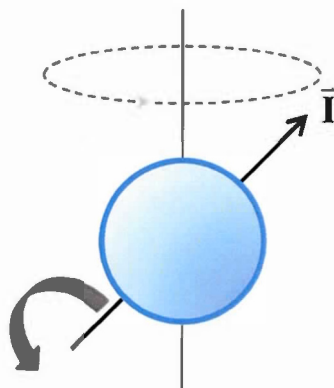


Figure 2.1 Spin d'un noyau ayant un moment angulaire de spin (\vec{I}) qui précesse autour d'un axe défini.

Le moment angulaire de spin (\vec{I}) n'est pas orienté de manière aléatoire; il a $2I + 1$ projections (états de spins) possibles auxquels sont associés des niveaux d'énergie. Pour un spin $1/2$, comme le ^1H ou le ^{31}P par exemple, il y a deux états de spins, soient $+1/2$ et $-1/2$. Sans champ magnétique externe, les $2I + 1$ projections ont la même énergie tandis qu'en présence de B_0 , il y a interaction entre ce dernier et le moment magnétique du noyau. Les états de spins n'ont donc plus la même énergie; c'est ce qu'on appelle l'*effet Zeeman* (Fig. 2.2). L'énergie de ces états est décrite comme suit :¹²¹

$$E = -\mu_z \cdot B_0 = -\gamma \cdot I_z \cdot B_0 \quad (2.2)$$

Elle dépend de la direction du moment angulaire de spin, du ratio gyromagnétique et de la force du B_0 . Alors, plus γ est élevé et plus B_0 est fort, plus l'énergie d'un niveau sera grande, et il y aura une plus grande séparation (ΔE) entre les niveaux d'énergie. Le signe « - » signifie que l'énergie est plus faible si $\vec{\mu}$ est dans la même direction que le B_0 ¹¹⁹. La population des états d'énergie de spins ($+1/2, -1/2$) est différente et suit la distribution de Boltzmann :

$$\frac{N_{\alpha}}{N_{\beta}} = e^{\Delta E/kT} \quad (2.3)$$

où N_{α} et N_{β} sont les nombres de population des états $+\frac{1}{2}$ et $-\frac{1}{2}$, respectivement, et k est la constante de Boltzmann ($1.3806 \times 10^{-23} \text{ J}\cdot\text{K}^{-1}$). La répartition des spins $+\frac{1}{2}$ et $-\frac{1}{2}$ est ce qui donne naissance à l'aimantation macroscopique, la source du signal RMN!

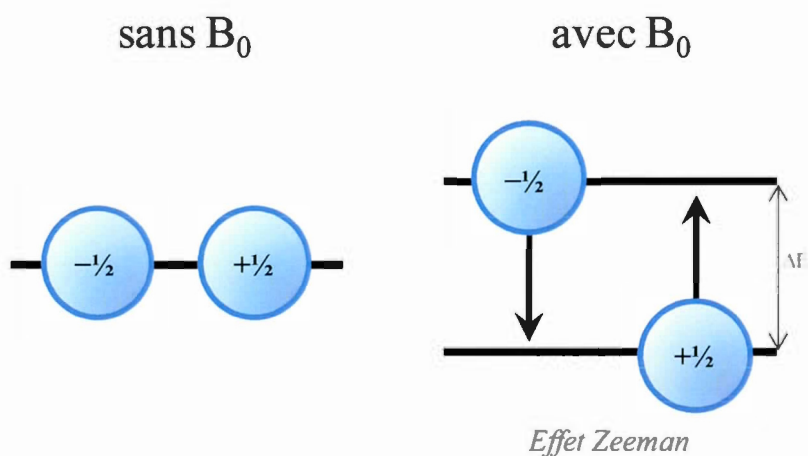


Figure 2.2 Niveaux d'énergie pour un spin $I = \frac{1}{2}$ avec et sans champ magnétique externe (B_0). En présence de B_0 , l'effet Zeeman lève la dégénérescence des niveaux d'énergie.

En présence de B_0 , le moment magnétique du spin d'un noyau adopte un mouvement en forme de cône avec un angle constant, qu'on appelle *précession* (Fig. 2.3). La fréquence de précession (fréquence de Larmor) d'un noyau dépend du γ et du B_0 , par conséquent, elle est propre à chaque noyau dans un champ magnétique donné (Tableau 2.1). Il est possible d'induire des transitions entre les états de spins (exciter) sélectivement à l'aide de radiation électromagnétique en appliquant une impulsion de radiofréquence ayant une énergie équivalente à celle de la transition (résonance). La

fréquence de résonance (ν) peut être calculée (en Hz) à l'aide de l'équation suivante¹²² :

$$\nu = \frac{\gamma \cdot B_0}{2\pi} \quad (2.4)$$

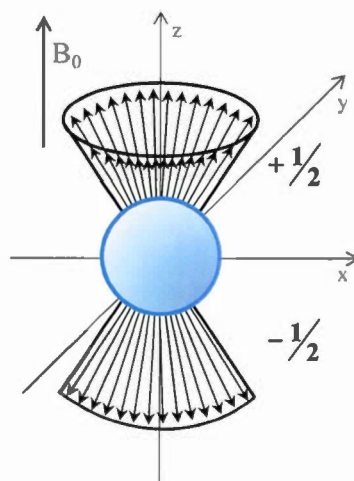


Figure 2.3 Mouvements de précession du spin d'un noyau ayant deux états de spin ($+1/2$ et $-1/2$) par rapport au champ magnétique B_0 défini selon l'axe y.

2.2 Inhomogénéités naturelles et couplages

Le champ magnétique perçu par le noyau (B_{effectif}) est légèrement inférieur à B_0 , car celui-ci est blindé par son environnement électronique local :

$$B_{\text{effectif}} = (B_0 - B') = B_0(1 - \sigma) \quad (2.4)$$

où σ est la constante de blindage. En présence du B_0 , le B_{effectif} d'un noyau n'est pas homogène, car l'environnement électronique local ainsi que les couplages donnent lieu aux inhomogénéités naturelles. Ces dernières peuvent être induites par les

électrons d'une liaison chimique (déplacement chimique, couplage scalaire), ou suite à des interactions dipolaires (couplage dipolaire), ce qui sera approfondi dans les sections qui suivent. Les inhomogénéités naturelles peuvent être exploitées afin d'obtenir de l'information structurale et spatiale^[21].

2.2.1 Déplacement chimique

Comme mentionné plus haut, la fréquence de résonance d'un noyau dépend principalement de son γ et du B_0 (Éq. 2.4). Toutefois, elle va aussi dépendre de sa position dans la molécule :

$$\nu = \frac{\gamma \cdot B_0(1-\sigma)}{2\pi} \quad (2.6)$$

La dépendance de l'environnement électronique sur la fréquence de résonance d'un noyau est ce que l'on appelle l'*effet du déplacement chimique*. Par exemple, A, un ^1H méthyl et B, un ^1H méthylène, alors le ^1H A sera plus blindé que B donc aura une fréquence, donc un déplacement chimique, plus faible. Le signal de RMN (déplacement chimique) est une source importante d'informations structurales, car il dépend des liens reliant les noyaux et de la structure des atomes voisins. Le déplacement chimique (δ) peut être calculé en partie par million (ppm) comme suit^[20, 121] :

$$\delta = 10^6(\nu - \nu_{ref})/\nu_{ref} \quad (2.7)$$

où ν_{ref} est la fréquence d'un composé de référence – comme les hydrogènes et carbones du tétraméthylsilane (TMS) pour la RMN du ^1H et du ^{13}C , respectivement.

2.2.2 Anisotropie du déplacement chimique (*chemical shift anisotropy*; CSA)

Dans une molécule, la densité électronique d'un noyau n'est pas uniforme dans toutes les directions – elle est anisotrope. Or, sa fréquence de résonance, donc son déplacement chimique, va dépendre de son orientation par rapport au B_0 . L'orientation est représentée par un tenseur (σ) qui est décrit par les trois axes principaux (σ_{xx} , σ_{yy} , σ_{zz}) (Fig. 2.4C). En RMN de l'état solide, c'est-à-dire les molécules qui ont des mouvements lents à l'échelle de la RMN, un échantillon qui n'est pas orienté va générer un spectre de poudre (Fig. 1.5A et B) consistant en une superposition de plusieurs pics fins à différentes fréquences de résonance correspondant à chaque orientation possible des noyaux dans l'échantillon. Le nombre de noyaux pour une orientation donnée déterminera l'intensité spectrale. Dans le cas des phospholipides dans une biocouche lipidique, les mouvements de rotation des molécules autour de l'axe de la normale de la bicouche produisent une symétrie axiale où σ_{xx} et σ_{yy} du tenseur CSA du ^{31}P sont moyennés (Fig. 1.5). Par conséquent, les fréquences des extrémités du spectre de ^{31}P permettent d'estimer le CSA ($\Delta\sigma$)¹²³ :

$$\Delta\sigma = \sigma_{//} - \sigma_{\perp} \quad (2.8)$$

où $\sigma_{//}$ et σ_{\perp} sont les déplacements chimiques pour les orientations parallèles (orientation à 0°) et perpendiculaires (orientation à 90°), respectivement. Le CSA est relié au spectre avec l'équation suivante¹²³ :

$$\Delta\nu(\theta) = \frac{2}{3} \Delta\sigma \frac{(3 \cos^2 \theta - 1)}{2} \quad (2.9)$$

où la fréquence (ν) est mesurée en Hz et elle dépend aussi de l'angle du noyau relativement au B_0 .

Pour un système biologique, le CSA peut nous informer sur la dynamique des lipides d'une membrane et de ses constituants. Par exemple, en RMN du phosphore (^{31}P) à

l'état solide (détailé dans la section 2.5.1), une augmentation des mouvements lipidiques va moyenner les orientations et réduire le CSA du spectre. De plus, l'orientation des protéines dans la membrane peut être déterminée par RMN puisque le CSA dépend de l'orientation des molécules (voir la section 2.5.3).

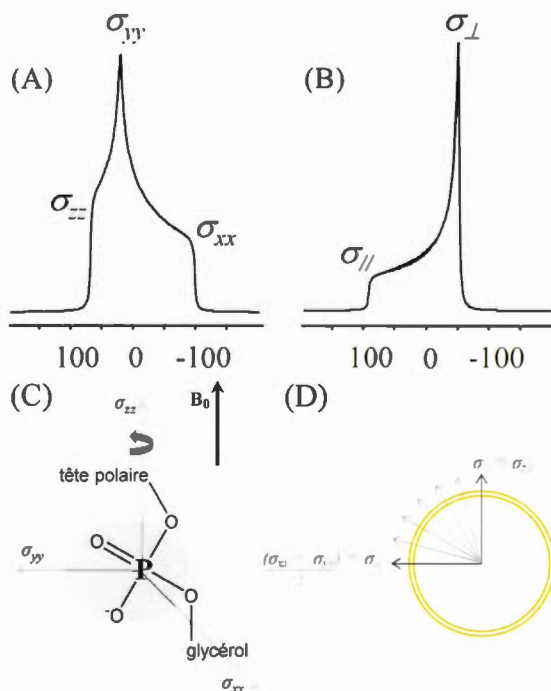


Figure 2.4 Spectres RMN du ^{31}P de phospholipides sans (A) et avec (B) mouvements de rotation axiale rapide selon l'axe z ; les images sont obtenues de Smith et Ekiel avec permission¹²⁴. C : Axes principaux du tenseur de CSA d'un phosphore lipidique qui tourne selon l'axe z . D : Orientations possibles des phospholipides d'un liposome non orienté.

2.2.3 Couplage scalaire (couplages J)

Le couplage scalaire est une interaction magnétique indirecte puisque les spins nucléaires sont couplés par l'entremise des électrons. Plus précisément, le noyau

magnétise légèrement les électrons environnants, ce qui génère un champ magnétique pouvant être ressenti par un noyau voisin dans une même liaison chimique. Ce phénomène est réciproque, de sorte que le noyau voisin va aussi magnétiser ses électrons pour générer un champ magnétique qui sera perçu par le premier noyau. Le couplage scalaire peut être homonucléaire (ex : ^1H - ^1H) ou hétéronucléaire (ex : ^1H - ^{13}C). Le couplage scalaire influence le spectre RMN de telle sorte que les signaux sont sous forme de multiplets. Le nombre de pics ($n+1$) dans un multiplet reflète le nombre de noyaux voisins équivalents (n). La fréquence qui sépare ces pics constitue la constante de couplage J ^{120, 121}. Malheureusement, ceci peut présenter des inconvénients : l'intensité sera distribuée sur tout les pics d'un multiplet donc la détection sera plus difficile, et pour les molécules plus complexes, les spectres sont encombrés ce qui complique leur interprétation. Il est possible d'employer le découplage pendant l'acquisition du signal, soit homo- ou hétéronucléaire, pour simplifier les spectres. Dans le cadre d'une expérience en RMN du ^{13}C par exemple, pour un couplage ^1H - ^{13}C , on applique un champ de radiofréquence à la fréquence Lamor du ^1H et on détecte à la fréquence du ^{13}C ¹²¹.

Le couplage des noyaux séparés par trois liaisons chimiques (3J) est très utile pour la détermination de la structure des peptides et des protéines. Le couplage $^3J_{\text{NH-H}\alpha}$ entre les protons (^1H) du groupement amide (N_H) et du carbone- α (H_α) aura une valeur caractéristique qui va dépendre de la structure secondaire du squelette peptidique, étant donné que les angles phi (ϕ) et psi (ψ) diffèrent (Fig. 2.5A)¹²⁵. Par exemple, une hélice- α à un angle ϕ de -60° tandis que celui d'un feuillet- β parallèle est -120° (Fig. 2.5B)¹²⁶.

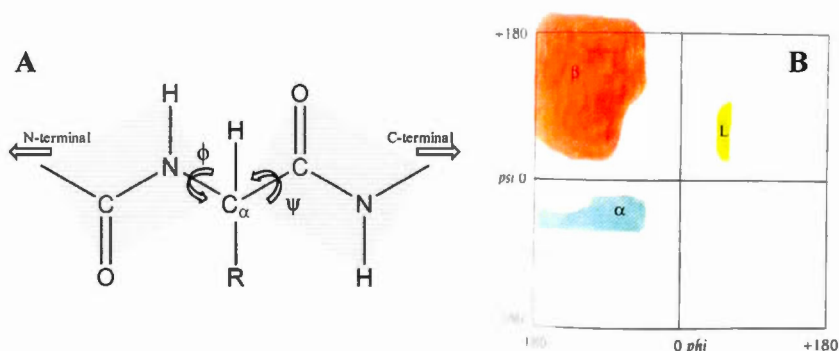


Figure 2.5 Structure secondaire des peptides et protéines. A) Les angles de torsion phi (ϕ) et psi (ψ) – rotation autour du carbone alpha (C_α) - d'un segment peptidique déterminant la structure secondaire. Les zones grises représentent les plans peptidiques rigides. B) Diagramme de Ramachandran qui montre les paires d'angles ϕ et ψ permises, incluant celles qui correspondent aux structures d'hélice- α avec un pas de rotation droit (bleu), de feuillet- β (rouge) et d'hélice- α avec un pas de rotation gauche (vert). L'image (B) est adaptée de Brändén et Tooze avec permission¹²⁶.

2.2.4 Couplage dipolaire

Un noyau ayant un spin non nul génère un champ magnétique avec lequel peut directement interagir un second noyau avoisinant. Cette interaction, dite dipolaire, ne nécessite pas de liaison chimique, car elle se fait à travers l'espace – elle peut donc être intra- ou intermoléculaire. Le couplage dipolaire (ω_D) est supérieure à celle du couplage scalaire et elle dépend surtout de la distance entre les noyaux (r) (Fig. 2.6), leur position relative (θ) par rapport à B_0 ainsi que du γ^{120} :

$$\omega_D^{\text{hétéro}} = \pm \frac{1}{2} \frac{\mu_0}{4\pi} \frac{\hbar \gamma_1 \gamma_2}{r_{12}^3} \left(\frac{3 \cos^2 \theta - 1}{2} \right) \quad (2.10)$$

dans le cas des couplages hétéronucléaires, et :

$$\omega_D^{homo} = \pm \frac{1}{2} \frac{3}{2} \frac{\mu_0}{4\pi} \frac{\hbar \gamma_1 \gamma_2}{r_{12}^3} \left(\frac{3 \cos^2 \theta - 1}{2} \right) \quad (2.11)$$

dans le cas des couplages homonucléaires. La dépendance angulaire du couplage dipolaire produit un dédoublement de pics sur le spectre RMN, et la distance entre les pics du doublet est appelée l'*éclatement dipolaire*. En solution, les mouvements rapides des molécules font que les angles des couplages dipolaires sont moyennés donc les éclatements ne peuvent être observés sur le spectre. Dans les systèmes anisotropes (RMN de l'état solide), les interactions dipolaires peuvent nous renseigner sur la structure et l'orientation des molécules, car chaque paire de noyaux couplés a une orientation différente par rapport au B_0 . Il existe toutefois des expériences RMN en solution (NOESY, ROESY) exploitant les interactions dipolaires, par l'intermédiaire de l'effet NOE (voir les sections 2.3.2 et 2.3.3), afin d'y extraire indirectement l'information sur le couplage dipolaire des noyaux pour déterminer la structure des molécules¹²¹.

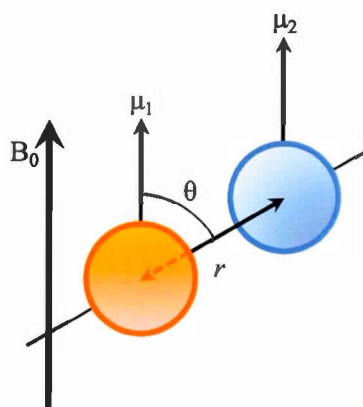


Figure 2.6 Couplage dipolaire entre deux noyaux. La force du couplage va dépendre de la distance (r) entre les deux noyaux (μ_1 , μ_2) et de leur orientation relative (θ) au champ magnétique externe (B_0).

2.2.5 Interaction quadripolaire

Les noyaux ont des charges qui sont distribuées de manière symétrique pour les noyaux de spin $\frac{1}{2}$. Pour le noyau de spin supérieur à $\frac{1}{2}$ (noyaux quadripolaires) les charges ne sont pas distribuées de manière symétrique mais plutôt avec deux dipôles. Le gradient de champ électrique (électrons) autour du noyau va donc interagir avec les noyaux quadripolaires¹²⁰. L'interaction quadripolaire modifie l'énergie des états de spins de sorte qu'il y a un dédoublement de pics sur le spectre, et ceux-ci sont espacés par un écart quadripolaire ($\Delta\nu_Q$) (Fig. 2.7). En RMN de l'état solide, cette interaction peut être exploitée comme dans le cas du deutérium (^2H) pour l'étude des membranes, tel que décrit dans les chapitres II à IV de cette thèse. La RMN du ^2H des systèmes membranaires est approfondie à la section 2.5.2.

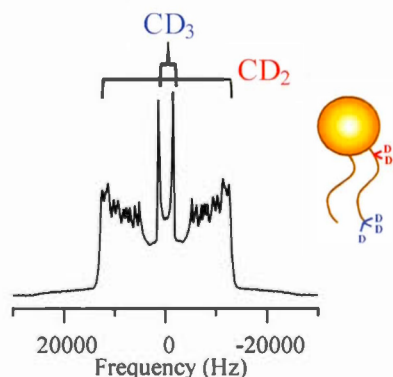


Figure 2.7 Spectre RMN du deutérium (^2H) d'un liposome. Les écarts quadripolaires des groupements CD_3 terminaux et des CD_2 près de la tête polaire des phospholipides ont été identifiés sur le spectre.

2.2.6 RMN en solution et RMN à l'état solide

La nature de l'échantillon va influencer l'expérience RMN à employer. Ce qui va surtout influencer le choix de la configuration du spectromètre RMN est le temps de corrélation (τ_c) des molécules que l'on veut étudier. Le τ_c est le temps que prend une molécule pour faire une rotation d'un radian (60°). Les molécules qui bougent rapidement – de l'ordre de la *ns* – dans un liquide ont un τ_c court, ce qui correspond à

la RMN en solution, tandis que la RMN de l'état solide convient aux molécules qui bougent lentement (τ_C long) dans un milieu solide ou visqueux, ou encore si elles sont de grande taille¹²⁰.

En RMN en solution, les fréquences de résonance des spins sont la conséquence des interactions avec le B_0 (effet Zeeman), avec d'autres spins (couplage scalaire) et avec le nuage électronique (déplacement chimique). Les autres interactions sont moyennées par le mouvement rapide des noyaux en solution présentant ainsi des pics fins sur le spectre. En RMN à l'état solide, la perte de mobilité des molécules fait en sorte que toutes les interactions ont un impact sur le spectre, incluant celles du couplage dipolaire et de l'effet quadripolaire que l'on ne voit pas en RMN en solution. Les pics sont ainsi larges à moins de faire tourner l'échantillon à l'angle magique (MAS; *magic angle spinning*), soit 54.7° l'angle auquel les contributions angulaires comme le couplage dipolaire (Éq. 2.10 et 2.11) et l'ADC (Éq. 2.9) deviennent nulles (Fig. 2.4).

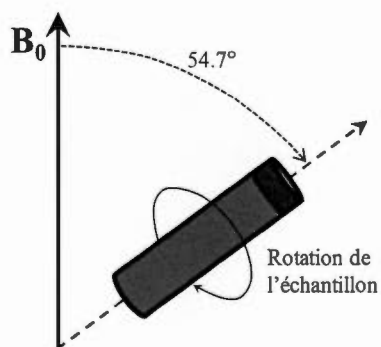


Figure 2.8 Schéma de la rotation à l'angle magique où l'axe de l'échantillon, se trouvant dans un rotor (cylindre gris), tourne à un angle de 54.7° par rapport au champ magnétique externe (B_0).

Dans cette thèse, la RMN en solution est employée pour étudier la structure des segments du hERG, leur interaction avec des médicaments ainsi qu'avec des systèmes modèles membranaires de petite taille (Chapitres III et IV). La RMN de l'état solide est utilisée pour étudier la perturbation de la membrane par les médicaments et les peptides du hERG (Chapitres III et IV), ainsi que pour

caractériser un nouveau modèle membranaire pour l'étude des peptides et PM (Chapitre V).

2.3 RMN bidimensionnelle du proton pour la détermination de la structure des peptides

La RMN bidimensionnelle (2D) rapporte de l'information sur les connectivités des noyaux à travers les liaisons (couplage scalaire), à travers l'espace (couplage dipolaire) ainsi que sur la dynamique moléculaire¹²⁷. Les expériences 2D ne sont qu'une série de spectres 1D ne se différenciant que par un certain délai dans la séquence afin de permettre aux noyaux d'évoluer en fonction de leur environnement et de leurs couplages. La RMN 2D a ses avantages : dans le cas d'attribution de pics, par exemple, on peut établir des corrélations entre les spins en identifiant, sur le spectre, les pics croisés dont les coordonnées correspondent aux déplacements chimiques des noyaux couplés (Fig. 2.9). Chaque noyau est forcément corrélé avec lui-même, ce qui est représenté par les pics sur la diagonale pour les couplages homonucléaires, ^1H - ^1H par exemple (Fig. 2.9). De plus, la RMN 2D offre une résolution spectrale supérieure à la RMN à une dimension (1D) étant donné que les pics du spectre 1D se chevauchent fréquemment. Les expériences 2D utilisées dans les chapitres III et IV de cette thèse, telles que la TOCSY, NOESY et ROESY, seront présentées dans les sections suivantes.

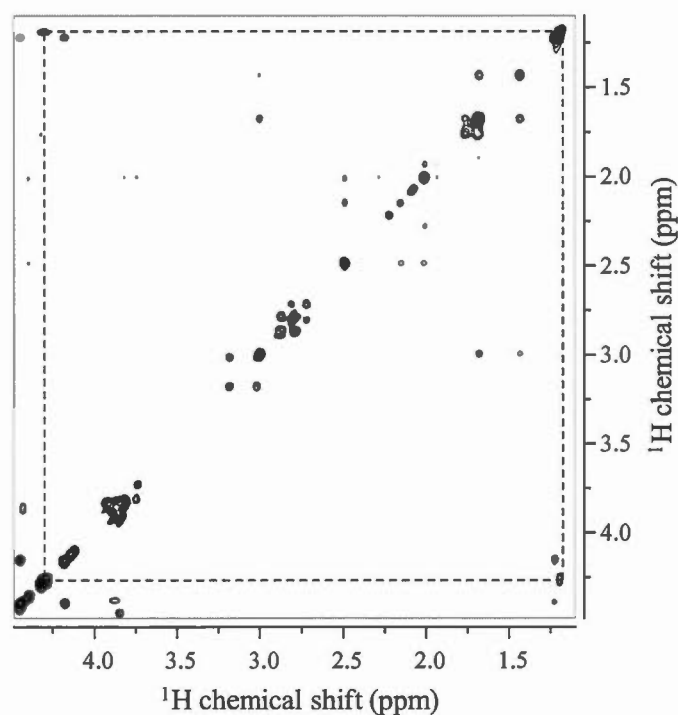


Figure 2.9 Spectre de RMN du ^1H de *Total Correlation Spectroscopy* (TOCSY). La ligne pointillée démontre la corrélation de deux pics sur la diagonale par l'entremise du pic croisé (coin gauche, en haut).

2.3.1 *Total Correlation Spectroscopy* (TOCSY)

Cette expérience permet de détecter toutes les corrélations homonucléaires (ex : ^1H - ^1H) entre les noyaux voisins qui sont couplés par l'intermédiaire d'une liaison chimique (scalaire) dans un même système de spins. La TOCSY⁴⁸ emploie un verrouillage de spins (*spinlock*) dans la séquence, qui consiste en une série d'impulsions pendant un temps de mélange (τ_m) (Fig. 2.10). La magnétisation ainsi verrouillée est transférée (transfert de polarisation), par l'entremise des noyaux qui sont directement couplés, à tous les noyaux, même à ceux qui ne sont pas directement

couplés. Si le τ_m est court, on détecte les couplages forts des noyaux avoisinants, tandis que si le τ_m est long, les noyaux éloignés, jusqu'à quatre liaisons chimiques, deviennent détectables sur le spectre de RMN.

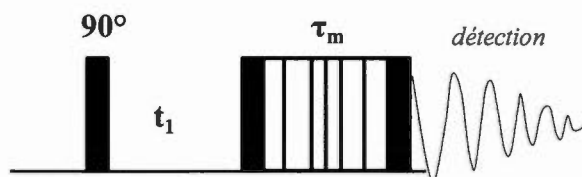


Figure 2.10 Séquence d'impulsions TOCSY. Impulsion de 90° suivie d'un délai (t_1) variable permettant l'évolution des spins avant le verrouillage ayant un temps de mélange (τ_m) précis. Le verrouillage consiste en une série d'impulsions de 90° et 180° ¹²⁸.

La TOCSY est utile pour étudier les protéines et les peptides, car chaque acide aminé représente un système de spins. On peut donc se servir de la TOCSY pour attribuer les ^1H d'une séquence d'acides aminés mais elle ne permet malheureusement pas de connaître sa structure primaire, car la présence de carbonyles sur le squelette protéique empêche le transfert d'aimantation. De plus, on peut suivre les changements de déplacements chimiques, comme pour l'exemple d'un peptide qui se lie à un ligand ou sice même peptide est exposé à un composé qui fait relaxer le signal rapidement, ce qui a été exploité avec le gadolinium (Gd^{3+}) au chapitre III de cette thèse.

2.3.2 Nuclear Overhauser Effect Spectroscopy (NOESY)

L'expérience NOESY⁴⁹ permet de voir les connectivités entre les noyaux qui sont proches dans l'espace ($< 5 \text{ \AA}$), ce qui inclut ceux qui sont couplés par des liaisons chimiques. Elle exploite le *Nuclear Overhauser Effect* (NOE) qui repose sur le couplage dipolaire entre deux noyaux. L'effet NOE se produit lorsque l'aimantation

d'un noyau est saturée en appliquant une faible impulsion à sa fréquence de résonance pendant un certain temps, ce qu'on appelle le découplage (Fig. 2.11). L'aimantation est transférée au noyau qui lui est couplé à travers l'espace, ce qui affecte l'intensité de son signal.

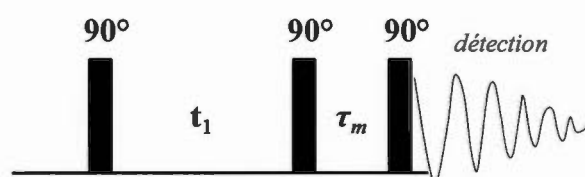


Figure 2.11 Séquence d'impulsions NOESY. Après la première impulsion de 90° , on laisse les spins évoluer pendant t_1 . La deuxième impulsion bascule l'aimantation des spins selon l'axe z afin que l'effet NOE se développe pendant τ_c . La dernière impulsion permet de procéder à la détection du signal¹²⁸.

En RMN en solution, les couplages dipolaires ne sont pas détectables, mais en exploitant la relaxation des spins, on peut obtenir de l'information structurale. La relaxation est définie par le retour à l'équilibre de l'aimantation des spins, en transférant son énergie à son environnement, après une impulsion de radiofréquence. Une expérience NOESY génère des signaux de corrélations (pics croisés) qui proviennent de la relaxation dipolaire. L'intensité des pics croisés dépend de la distance entre les deux noyaux :¹²⁹

$$NOE \propto \left\langle \frac{1}{r^6} \right\rangle f(\tau_c) \quad (2.12)$$

où r est la distance entre les deux noyaux couplés. L'intensité des pics est donc une information indispensable pour la détermination de structure des protéines et des peptides.

Le temps de corrélation (τ_c) est important pour les expériences NOESY, car il existe un τ_c , ou une fréquence, à laquelle le NOE ne peut s'établir pour un B_0 donné :

$$\omega_0 \tau_c \sim 1 \quad (2.13)$$

où ω_0 est la fréquence de Larmor en rad/s. Typiquement, les molécules ayant une masse molaire de 1 à 3 kDa sont désavantagées puisqu'elles ne montrent aucun pic croisé en NOESY, alors il faut soit avoir recours à l'expérience ROESY (ci-dessous), soit changer de spectromètre.

2.3.3 Rotating-frame Overhauser Effect Spectroscopy (ROESY)

Dans une expérience ROESY¹³⁰, le temps de mélange de la NOESY est remplacé par un verrouillage de spins comme dans la TOCSY (Fig. 2.12). Un verrouillage de spins plus faible est employé pour diminuer l'apparition des corrélations de la TOCSY. L'effet NOE d'une ROESY est toujours positif, jamais nul, peu importe le τ_c des molécules. Le verrouillage de spins génère un champ effectif (B_{effectif}) qui est perpendiculaire à B_0 et plus faible. La fréquence de transition des spins est donc aussi plus faible (voir Éq. 2.6) et la limite des mouvements moléculaires devient accessible sur une plus grande gamme de τ_c .

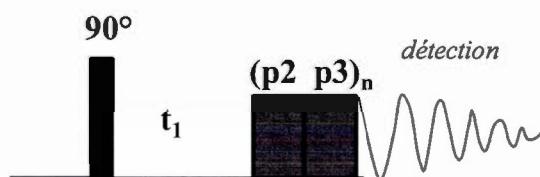


Figure 2.12 Séquence d'impulsion ROESY. Après la première impulsion de 90° , on laisse les spins évoluer pendant t_1 . Le temps de mélange de la NOESY est remplacé par un verrouillage de spins (p2, p3) plus faible que celui de la TOCSY¹²⁸.

2.4 Gradients de champs et saturation des résonances pour l'étude des interactions protéine-membrane

Étudier les interactions intermoléculaires, telles que protéine-membrane ou protéine-ligand, est indispensable pour mieux comprendre la fonction des protéines. Dans le chapitre II, les expériences de diffusion en RMN en solution *Pulsed Field Gradient Echo* (PGSE) et de *Saturation Transfer Difference* (STD) ont été employées pour analyser les interactions entre un peptide correspondant au SF du hERG, les médicaments cardiotoxiques impliqués dans le ALQTS et la membrane. Des expériences de STD ont aussi été employées au chapitre III pour distinguer les régions spécifiques de la membrane qui interagissent avec certains résidus du segment S4S5 du hERG.

2.4.1 *Pulsed Field Gradient Spin-Echo* (PGSE)

Il est possible de mesurer les mouvements aléatoires des molécules en solution en utilisant des expériences de diffusion. L'expérience de PGSE (Fig. 2.13A) sert à déterminer le coefficient de diffusion (D_s , en cm^2/s) des molécules en utilisant des gradients de champ pulsés (*Pulsed Field Gradient*, PFG)^{131, 132}. Normalement, la force du champ magnétique est homogène, mais en présence de gradients de champ – appliqués sous forme d'impulsion – elle varie de manière contrôlée selon la direction du gradient. L'effet du gradient sur les spins va dépendre de la force (G , en Gauss/cm) et de la durée (δ , en secondes) du gradient, ainsi que du ratio gyromagnétique (γ) et de la position du noyau dans l'échantillon (Fig. 2.13B).

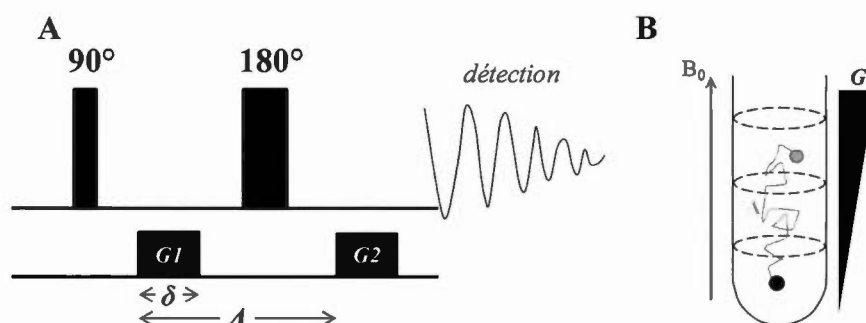


Figure 2.13 Expérience PGSE. A) Séquence d'impulsions qui consiste à appliquer une impulsion de 90° pour basculer les spins dans le plan xy . Le premier gradient ($G1$) sert à rendre B_0 temporairement inhomogène afin que la magnétisation soit différente d'un endroit à un autre dans l'échantillon. On applique ensuite une impulsion de 180° afin de rephaser l'aimantation des spins. Le second gradient ($G2$) permet de décoder les spins qui ont gardé en mémoire le champ qu'ils ont subi¹²⁸. B) Diffusion d'une molécule dans un tube RMN en présence de gradients de champ pulsés, où Δ est le temps de diffusion.

Le coefficient de diffusion est calculé d'après l'équation suivante :¹³²

$$S(G) = S(0) \exp[-(\gamma \delta G)^2 (\Delta - \delta/3) D_S] \quad (2.14)$$

où $S(G)$ est l'intensité du signal détecté après le gradient et Δ est le temps de diffusion (secondes), soit le délai entre les impulsions PFG. On peut déterminer le D_S à partir du graphique de $S(G)$ en fonction de la force du gradient (G), car les valeurs de γ , δ et Δ sont connues. Par la suite, on peut se servir des coefficients de diffusion pour estimer le pourcentage d'association des molécules afin de vérifier s'il y a interaction entre deux molécules. Cette application est détaillée au chapitre III à la section 3.4.3.1.

2.4.2 Saturation Transfer Difference (STD)

La détection des interactions spécifiques protéine-ligand par la technique STD^{85, 133} repose sur la diffusion d'un spin provenant d'une molécule ayant un poids élevé (>30 kDa)¹³⁴. Cette expérience nécessite un échange entre les formes liée et libre du ligand (Fig. 2.14). Les zones d'une molécule, irradiées par les impulsions, transfèrent leur aimantation aux régions du ligand participant à l'interaction. La diminution de l'intensité (I_{SAT}) des résonances du ligand est la conséquence du transfert de saturation (effet NOE) dû au couplage dipolaire avec la région de la molécule étant saturée. Une expérience de référence est aussi effectuée dans les mêmes conditions, sauf que l'on irradie loin de toutes les résonances d'intérêt (hors résonance) afin d'obtenir un spectre où l'intensité des pics n'est pas affectée par la saturation (I_0). À l'aide de l'équation suivante, on peut obtenir le spectre de différence (I_{STD}) :

$$I_{STD} = I_0 - I_{SAT} \quad (2.15)$$

On peut distinguer les régions des molécules qui interagissent, car seuls les signaux ayant reçu le transfert de saturation demeureront sur le spectre. Tout autre composé qui ne lie pas les régions irradiées ne recevra pas le transfert de saturation ($I_0 = I_{SAT}$).

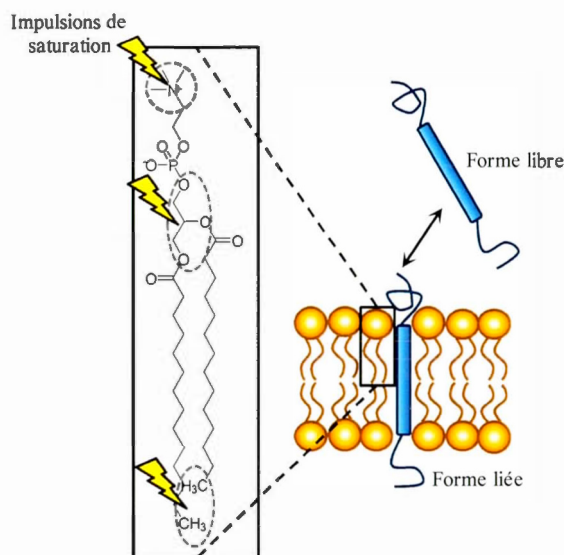


Figure 2.14 Expérience de STD pour localiser les peptides et les PM dans une membrane tel que réalisée au chapitre III. Les résonances des phospholipides sont saturées (éclairs) de manière spécifique : ^1H méthyles de la choline (tête polaire), ^1H du groupement glycérol (interface) et ^1H méthyles terminaux (cœur hydrophobe). La saturation est transférée aux ^1H peptidiques qui sont en contact avec la région irradiée.

Cette technique dépend de l'efficacité du transfert de saturation ainsi que du nombre de ligands dans la solution tel que discuter au chapitre III. Elle comporte toutefois des limites : si l'interaction entre les deux molécules est trop forte, l'aimantation transférée va diffuser vers d'autres noyaux réduisant les effets du STD sur le spectre de différence¹³⁵. Au contraire, si l'interaction est trop faible, tous les ligands seront à l'état libre, donc on n'observera pas l'effet du STD. La détection de signaux de STD faibles peut aussi être provoquée par une durée d'interaction qui est trop courte par rapport à la vitesse de relaxation de la magnétisation qui est transférée, et par un excès de ligands dans la solution, diluant ainsi la concentration de ligands saturés.

Des expériences de STD ont permis d'identifier, au chapitre III, les régions de la membrane, soit la surface (groupement choline), soit l'interface (groupement glycérol), soit le cœur hydrophobe (méthyle terminal) qui interagissent avec le segment SF du hERG (section 3.5.2) et avec des médicaments cardiotoxiques (section 3.5.4). Au chapitre IV, nous avons aussi vérifié avec des expériences STD les régions de la membrane qui interagissent avec le segment S4S5 du hERG (complément au chapitre IV).

2.5 RMN du phosphore-31 et du deutérium pour l'étude des systèmes membranaires

La RMN du ^{31}P et du ^2H ont été employés dans les chapitres III et IV pour déterminer le rôle de la membrane dans le ALQTS et pour le mécanisme d'ouverture et de fermeture du hERG respectivement, ainsi qu'au chapitre V pour caractériser les membranes modèles de PC-Tween 80 pour l'étude des PM par RMN.

2.5.1 RMN du phosphore-31

Le phosphore (^{31}P) est le noyau le plus fréquemment employé en RMN pour l'étude des systèmes lipidiques. En effet, les membranes ont une composition élevée en phospholipides (PL) et ceux-ci contiennent un groupement phosphate au niveau de leur tête polaire¹³⁶. En plus d'avoir un ratio gyromagnétique élevé, l'abondance naturelle du ^{31}P est de 100 %, ce qui élimine la nécessité de faire du marquage isotopique.

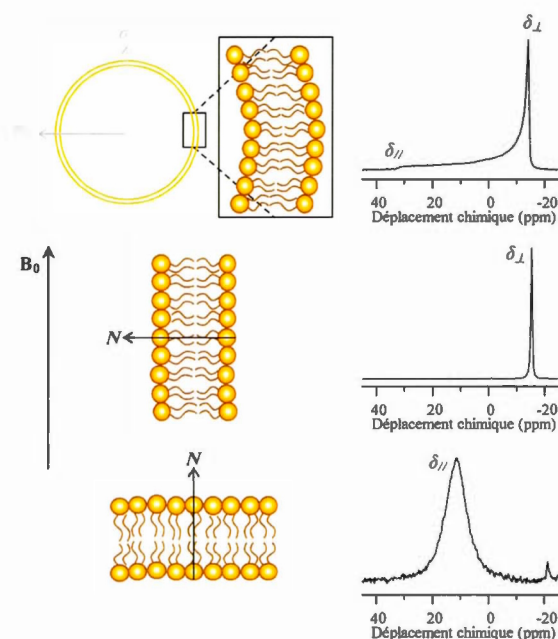


Figure 2.15 Comparaison des spectres RMN du ^{31}P de bicouches lipidiques non orientées et orientées. Les liposomes (sphériques) contiennent des lipides orientés à tous les angles par rapport à la direction du B_0 , ce qui est représenté par un spectre de poudre (haut). Les lipides qui sont alignés de manière perpendiculaire et parallèle sont représentés par les résonances δ_{\perp} et δ_{\parallel} , respectivement. Lorsque tous les lipides sont orientés à 90° par rapport à B_0 , on observe une seule résonance à δ_{\perp} (centre). De même, lorsque tous les lipides sont orientés à 0° , on observe une résonance à δ_{\parallel} (bas).

La RMN du ^{31}P ¹³⁷ est un outil pratique pour mesurer les changements de phases lamellaires des bicouches. La perturbation des lipides peut aussi être observée lorsqu'on étudie l'interaction de PM, de peptides et de petites molécules (par exemple, des médicaments) avec la membrane¹³⁶. De plus, la qualité d'orientation des PL par rapport au B_0 peut être déduite par la forme spectrale. Les PL d'une membrane en phase liquide cristalline subissent des mouvements rapides de rotation à symétrie axiale autour de l'axe de la normale (N) de la bicouche (Fig. 2.4B). Il y a donc des

fréquences distinctes pour les bicouches ayant leur normale parallèle et perpendiculaire au B_0 (Fig. 2.15). Par conséquent, le spectre de poudre du ^{31}P a une forme qui se distingue par un épaulement vers les hautes fréquences et un second vers les basses fréquences tel que vu à la section 2.2.2. L'écart entre ces épaulements représente le CSA^{100, 123, 138}. Les changements du CSA renseignent sur la dynamique des têtes polaires au niveau de la surface de la membrane.

2.5.2 RMN du deutérium (^2H)

L'utilisation de lipides deutérés (^2H) au niveau des chaînes acyles, commercialement disponibles, est aussi utile pour étudier la membrane. La deutération n'altère pas les propriétés de la membrane sauf pour sa température de transition (T_m) qui diminue de 3 à 5 °C¹³⁹.

Il est possible de vérifier l'ordre des chaînes lipidiques en mesurant l'écart quadripolaire ($\Delta\nu_Q$) des liens C-D sur le spectre RMN- ^2H (Fig. 2.7; Éq. 2.16)¹⁴⁰. Une augmentation des valeurs $\Delta\nu_Q$ est associée à l'augmentation de l'ordre des lipides, contrairement à une diminution qui est associée au désordre. L'ordre des chaînes deutérées nous renseigne donc sur la dynamique des lipides. Les lipides d'une bicouche en phase liquide cristalline sont continuellement en mouvement (Figure 1.10B). Les régions de la chaîne qui sont plus mobiles (méthyle terminal) auront un Δ_Q plus petit, tandis que les deutérons qui sont plus rigides (liens C-D près du groupement glycérol) auront une valeur Δ_Q plus élevée.

La valeur de $\Delta\nu_Q$ peut aussi nous renseigner sur l'orientation des membranes dans le champ magnétique. Les doublets du spectre ^2H ont une résolution accrue lorsque la bicouche est alignée par rapport au B_0 puisque les lipides adoptent une seule orientation et non une distribution de toutes les orientations possibles comme dans un système non orienté (Fig. 2.16, centre). De plus, si l'alignement de la normale de la

bicouche est parallèle au B_0 , les doublets ont un $\Delta\nu_Q$ deux fois plus élevé qu'un alignement perpendiculaire (Fig. 2.16, bas), car le celui-ci dépend de l'orientation relative au B_0 :

$$\Delta\nu_Q = \frac{3}{4} \frac{e^2 q Q}{h} (3 \cos^2 \theta - 1) S_{CD} \quad (2.16)$$

où $\frac{e^2 q Q}{h}$ est la constante de couplage quadripolaire d'un lien C-D aliphatique (~ 167 kHz), θ est l'angle entre la normale de la bicouche et le B_0 , et S_{CD} est le paramètre d'ordre des liens C-D^{141, 142}.

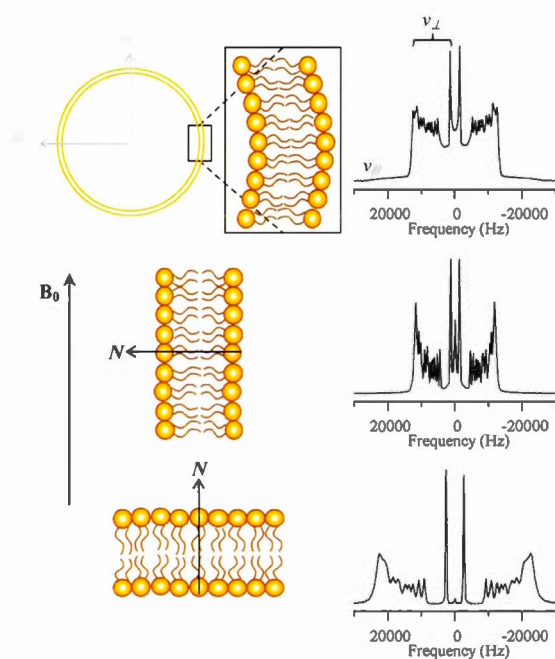


Figure 2.16 Comparaison des spectres de RMN du ^2H des chaînes acyles deutérées de bicouches lipidiques non orientées et orientées. Les liposomes (sphériques) contiennent des lipides orientés à tous les angles par rapport à B_0 , ce qui est représenté par un spectre de poudre (haut). Chaque doublet sur le spectre représente un lien C-D de la chaîne acyle. Les bicouches qui sont orientées de manière perpendiculaire et parallèle sont représentées par les résonances ν_{\perp} et ν_{\parallel} , respectivement.

Lorsque tous les lipides sont orientés à 90° par rapport à B_0 , les épaulements (ν_{\parallel}) disparaissent et les résonances ν_{\perp} ont une meilleure résolution (centre). Lorsque tous les lipides sont orientés à 0° , on perd également les résonances ν_{\parallel} et l'écart quadripolaire ($\Delta\nu_Q$) des résonances ν_{\perp} double (bas).

2.5.3 Susceptibilité magnétique

Certaines morphologies lipidiques des bicouches permettent aux membranes de s'aligner dans le champ magnétique. Ceci est dû à l'effet coopératif des lipides dont les chaînes acyles et les groupements esters possédant une susceptibilité magnétique anisotrope¹⁴³. Cette susceptibilité, normalement négative pour les PC, crée un moment magnétique macroscopique qui permet aux lipides de s'orienter avec l'axe longitudinale perpendiculaire au B_0 ¹³⁸. L'alignement permet de vaincre les mouvements browniens des lipides en solution et n'est donc possible que lorsqu'un nombre important de chaînes acyles sont ordonnées côte à côte et que le système lipidique est suffisamment mobile pour permettre l'orientation des membranes¹⁴⁴. Ceci dit, certains modèles de petite taille, tels que les bicelles isotropes, ne produisent pas un effet coopératif nécessaire à un alignement spontané.

Les membranes modèles orientées vont aussi aligner les PM et peptides qui y sont insérés afin d'exploiter les couplages dipolaires pour la détermination de structure des protéines¹⁰⁴. De plus, les membranes modèles orientées sont souvent utilisées pour vérifier l'orientation des protéines et peptides transmembranaires par rapport à la normale de la bicouche – une information qui est complémentaire aux informations structurales – tel que pour les domaines transmembranaires tOmpA et OmpX d'*Escherichia coli* ayant été incorporés dans des bicelles orientées^{102, 145}. Les protéines ou peptides sont marqués à l'azote-15 et le déplacement chimique ^{15}N diffère en fonction de leur alignement par rapport à B_0 . Par exemple, l'orientation et la structure de la protéine de l'enveloppe du bactériophage filamentueux *fd* ont été étudiées par RMN dans une bicouche lipidique avec des expériences 2D $^1\text{H}/^{15}\text{N}$ PISEMA¹⁰³.

L'orientation perpendiculaire relative au B_0 est limitée aux petites molécules (peptides, hormones, médicaments et phospholipides) qui subissent des mouvements axiaux symétriques et rapides. L'absence de ces mouvements, tel que pour les grosses

protéines, mène à des motifs de poudre sur le spectre de RMN plutôt que des pics fins¹⁴⁶. L'orientation perpendiculaire ($\beta_{nl} = 90^\circ$) est définie par un paramètre d'ordre S_{zz} :

$$S_{zz} \equiv \langle \frac{1}{2}(3 \cos^2 \beta_{nl} - 1) \rangle = -\frac{1}{2} \quad (2.17)$$

où β_{nl} représente l'angle moyen entre B_0 et la normale de la bicouche (N)¹⁴⁶. Par conséquent, l'écart entre les résonances du spectre de RMN diminue d'un facteur $\frac{1}{2}$.

L'orientation parallèle au B_0 est donc indispensable pour étudier les PM de grande taille¹⁴⁷. L'ajout d'ions paramagnétiques ayant une susceptibilité magnétique positive, tels que l'ytterbium (Yb^{3+}) et le gadolinium (Gd^{3+}), aux systèmes lipidiques alignés bascule leur orientation de manière à ce que $S_{zz} > 0$. Par conséquent, la résolution spectrale est améliorée, tel que vu précédemment avec la RMN du ^2H des bicouches orientées en ayant leur normale parallèle à B_0 (Fig. 2.16).

CHAPITRE III

AN NMR INVESTIGATION OF THE STRUCTURE, FUNCTION AND ROLE OF THE HERG CHANNEL SELECTIVITY FILTER IN THE LONG QT SYNDROME

Andrée E. Gravel, Alexandre A. Arnold, Érick J. Dufourc et Isabelle Marcotte

Biochimica et Biophysica Acta 1828 (2013) 1494–1502

Contribution des auteurs: IM a conçu, coordonné l'étude et participé à l'analyse des résultats. AEG, AAA, ÉJD et IM ont rédigé l'article. AEG a conçu, effectué et analysé les expériences de RMN. AAA et ÉJD ont assisté à la conception et l'acquisition des données RMN. Tous les auteurs ont approuvé la version finale du manuscrit.

3.1 Résumé

Les canaux potassiques dépendants du voltage *human ether-a-go-go-related gene* (hERG) qui se trouvent dans les membranes des cellules du cœur contiennent un filtre de sélectivité (SF) ayant une séquence unique (SVGFG), contrairement aux autres canaux potassiques (TVGYG). Le hERG entraîne le syndrome du QT long acquis (ALQTS) comme effet secondaire lorsqu'il est bloqué par des médicaments, ce qui mène à des arythmies ou à l'arrêt cardiaque. On croit que son domaine du pore, qui comprend le SF, est ciblé par les médicaments cardiotoxiques. Dans cette étude, nous examinons, avec des expériences de RMN en solution et à l'état solide, la structure et la fonction du segment L622-K638 du hERG qui contient le SF, ainsi que son rôle dans le ALQTS, en utilisant des médicaments ALQTS-actifs. Nous démontrons que le segment SF est non structuré en solution avec et sans ions K^+ , ce qui est cohérent avec la flexibilité requise pour que le canal change d'état de conductance ce qui a été

prédit par modélisation dans d'autres études. Nous démontrons aussi que le segment SF a le potentiel de perturber la membrane, mais que la présence d'ions K^+ annule cette interaction. Le motif du SF semble être une cible potentielle de la prométhazine pour le mécanisme du ALQTS, mais moins pour le bépridil, la cétirizine, la diphenhydramine et la fluvoxamine. L'affinité qu'a le SF pour la membrane est aussi influencée par la présence de médicaments, qui ont aussi tendance à perturber les modèles membranaires à base de DMPC. Ces résultats suggèrent que la membrane pourrait jouer un rôle dans le ALQTS en favorisant l'accès aux cibles transmembranaires ou intracellulaires du canal hERG, ou en perturbant la synergie lipide-protéine.

3.2 Abstract

The human ether-a-go-go-related gene (hERG) voltage-gated K^+ channels are located in heart cell membranes and hold a unique selectivity filter (SF) amino acid sequence (SVGFG) as compared to other K^+ channels (TVGYG). The hERG provokes the acquired long QT syndrome (ALQTS) when blocked, as a side effect of drugs, leading to arrhythmia or heart failure. Its pore domain - including the SF - is believed to be a cardiotoxic drug target. In this study combining solution and solid-state NMR experiments we examine the structure and function of hERG's L622-K638 segment which comprises the SF, as well as its role in the ALQTS using reported active drugs. We first show that the SF segment is unstructured in solution with and without K^+ ions in its surroundings, consistent with the expected flexibility required for the change between the different channel conductive states predicted by computational studies. We also show that the SF segment has the potential to perturb the membrane, but that the presence of K^+ ions cancels this interaction. The SF moiety appears to be a possible target for promethazine in the ALQTS mechanism, but not as much for bepridil, cetirizine, diphenhydramine and fluvoxamine. The membrane affinity of the

SF is also affected by the presence of drugs which also perturb model DMPC-based membranes. These results thus suggest that the membrane could play a role in the ALQTS by promoting the access to transmembrane or intracellular targets on the hERG channel, or perturbing the lipid-protein synergy.

3.3 Introduction

The human ether-à-go-go-related-gene (hERG) channels are voltage-gated potassium channels (K_v) located in the myocardium cell membranes and essential for heart function. The kinetics of the hERG functioning is atypical: it is characterized by slow activation and deactivation processes, and fast voltage-dependent inactivation⁹. Under membrane depolarization, the channel slowly proceeds from a closed to an open conformation to rapidly adopt an inactivated state that involves closing of the channel's outer mouth. During heart repolarization, the hERG reopens for a longer time before closing again. A resurgent I_{K_r} current is measured during this interval. If this K^+ current is disrupted by mutations or drugs, it prolongs the repolarization interval between Q and T waves on the electrocardiogram, thus provoking arrhythmia or heart failure⁹. The acquired form of this long QT syndrome (ALQTS) is the most common and occurs as a side effect of drugs when they generally block hERG channels. ALQTS is the first cause of delayed drug approval by the FDA and is frequently responsible for drug withdrawal from the market despite mandatory *in vitro* testing of all new drug entities for hERG-blocking potential^{148, 149}.

The hERG channel is composed of four monomeric subunits, each containing six transmembrane spanning helices (S1-S6). It has never been crystallized and its structure is predicted by homology studies with similar K^+ channels, such as the bacterial KcsA¹⁵⁰, the drosophila Shaker and the human Kv1.1²⁹, aided by electrophysiological, *in silico* and spectroscopic studies on hERG segments^{37, 47, 151-155}. The first four helices (S1-S4) compose the voltage sensor while S5 and S6

form the pore domain. S5 is connected to S6 by an extracellular loop more than twice the length of most K⁺ channels^{47, 156}, followed by the small pore helix and the K⁺-selective filter as illustrated in Fig. 3.1A. Interestingly, the selectivity filter (SF) of the hERG channel adopts a unique signature of Ser-Val-Gly-Phe-Gly as opposed to Thr-Val-Gly-Tyr-Gly for most potassium channels²⁹.

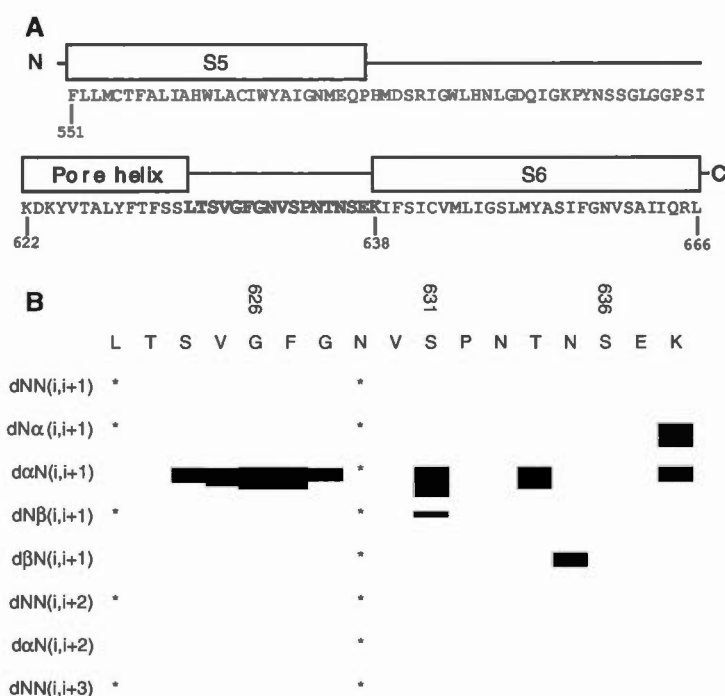


Figure 3.1 A) Amino acid sequence and predicted topology of the hERG channel pore domain (S5–S6)^{67, 155}. The bold text indicates the L622–K638 segment synthesized for NMR analysis. B) ¹H–¹H contacts for hERG L622–K638 in water obtained by ROESY with a 300 ms mixing time. Bar widths are proportional to cross peak intensities. Unassigned protons are marked with an asterisk.

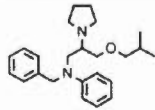
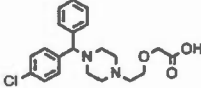
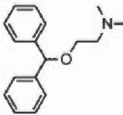
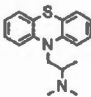
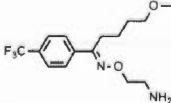
Considering the hERG channel's unique SF sequence, refining its structural model would be essential in order to gain a better understanding of its function. In K_v channels such as KcsA, the SF is thought to expose carbonyl oxygen atoms to the

extracellular solution to attract K^+ ions^{55, 157}. The filter would then adopt different conformations at high and low K^+ concentrations respectively corresponding to the conductive and non-conductive states^{55, 56}. Molecular dynamics (MD) studies and crystallographic X-ray structures support the SF's backbone flexibility at low K^+ concentrations as local structural changes in the TVGYG motif would be required to adopt the ion conduction conformation during ion movement⁵¹⁻⁵⁵. The conformational changes of the SF during the opening and closing of K^+ channel is still a matter of debate^{54, 158}. Therefore the first objective of this study was to verify conformation changes of the L622-K638 segment – which comprises the SF - with and without the presence of K^+ ions using standard two-dimensional (2D) solution nuclear magnetic resonance (NMR) experiments. According to sequence homology with other K^+ channels^{67, 155}, this segment corresponds to the linker connecting the pore helix to the S6 transmembrane helix (Fig. 3.1A). Considering the position of the SF of K^+ channels in cell membranes^{56, 157}, we have also studied the interaction of hERG's L622-K638 segment with model phospholipids membranes using solid-state NMR (SS-NMR) and saturation transfer difference (STD) experiments. Studying peptides from membrane proteins and channels using techniques such as circular dichroism (CD), molecular dynamics (MD) and NMR is a useful and commonly used strategy that provides invaluable structural information on proteins that are not easily overexpressed and purified such as the hERG mammalian channel. For example, its extracellular S5P (Annexe A) and intracellular S4-S5^{27, 38, 47, 154, 155, 159} linkers have been studied to gain a better insight into their structure and function, as well as the paddle domains of K_v channels such as K_v AP and HsapBK to cite a few¹⁶⁰. The L622-K638 moiety terminating a particularly long and flexible extracellular pore loop of the hERG is very well-suited for a segmental study⁴¹.

According to previous studies, some channel blockers would exert their activity by binding Thr623, Ser624 and Val625 located at the intracellular base of the SF^{19, 20}. Therefore another goal of this work was to investigate the role of the SF in the drug-

induced blockade of hERG leading to ALQTS. Five drugs with reported ALQTS activity were studied, each having different structures and belonging to various pharmacological classes as listed in Table 3.1. Bepridil is an antiarrhythmic drug with calcium antagonistic properties^{161, 162} while diphenhydramine, promethazine and cetirizine are antihistaminic H₁-receptor antagonists^{163, 164}. These four drugs have been suspected to block the hERG channel, most often by interacting with binding sites found in the hERG's pore cavity. However, fluvoxamine, a selective serotonin re-uptake inhibitor often prescribed to treat depression, does not appear to bind to this region. For some drugs, their large size alone would suggest their unlikeliness to fit in the pore cavity, such as the antibiotic erythromycin¹⁶⁵. The possibility of additional binding sites on the cytoplasmic or extracellular side of the hERG channel should thus be considered¹⁶⁵⁻¹⁶⁷. For that reason, we have studied the potential binding of LQTS-active drugs to the SF segment.

Table 3.1 Partition coefficients (log *P*), pharmacological classes and structures of studied LQTS-active drugs.

Drug	log <i>P</i>	Structure
Bepridil (antiarrhythmic)	5.2	
Cetirizine (antihistamine)	2.8	
Diphenhydramine (antihistamine)	3.3	
Promethazine (antihistamine)	4.4	
Fluvoxamine (antidepressant)	3.2	

Finally, we have investigated the role of the membrane in the ALQTS. Some drugs, such as promethazine, have a high affinity for membrane bilayers containing phosphatidylcholines (PCs) and can potentially disrupt the lipid-protein synergy^{167, 168}. This perturbation via non-specific hydrophobic and electrostatic interactions could indirectly block the hERG channel function. Using translational diffusion measurements, we have thus verified the affinity of the selected drugs for the model membranes. Additionally, the perturbation of polar head groups and acyl chains of model membranes was probed using ³¹P- and ²H-SS-NMR experiments, respectively. Coupled with STD experiments, this work provides an insight into the drugs' location with respect to the membrane and eventually on the membrane's role in the ALQTS.

3.4 Materials and Methods

3.4.1 Materials

The L622-K638 segment with sequence LTSVGFGNVSPNTNSEK comprising the hERG's SF was synthesized by GenScript Corporation (Piscataway, NJ, USA) with >95% purity. Protonated and deuterated dimyristoyl- and dihexanoylphosphatidylcholine (DMPC, DMPC-d₅₄, DHPC, DHPC-d₂₂) were purchased from Avanti Polar Lipids (Alabaster, AL, USA). Fluvoxamine maleate, promethazine hydrochloride and deuterium-depleted water were obtained from Sigma Aldrich (Oakville, ON, Canada), while deuterium oxide (D₂O) was purchased from CDN isotopes (Pointe-Claire, QC, Canada).

3.4.2 Sample preparation

Bicelles and multilamellar vesicles (MLVs) respectively used for solution- and solid-state NMR experiments were prepared by mixing freeze-dried DHPC and/or

DMPC in an aqueous solution at pH 4.5, then submitted to a series of freeze (liquid N₂)/thaw (50°C)/vortex cycles. The L622-K638 segment was mixed with the model membranes during their preparation and the peptide concentration was kept between 2 and 5 mM. The lipid concentration was maintained well above the critical micelle concentration (CMC). Solid-state NMR samples were prepared with deuterium-depleted water using a lipid/peptide (L/P) molar ratio of 100:1, a lipid/drug (L/D) molar ratio of 180:1 with a 80 % (w/v) hydration. A hydration percentage of 88% (w/v) was used for samples studied by solution NMR. ¹H diffusion NMR experiments were carried out in D₂O while all other high-resolution NMR experiments were performed using 10 % D₂O in water. Translational diffusion and saturation transfer difference (STD) measurements were carried out using DMPC/DHPC (q) molar ratios of 0.5 and 1, respectively. L/P molar ratios of 50:1 and 125:1 as well as a L/D molar ratio of 125:1 were employed.

3.4.3 Solution and solid-state NMR

All translational diffusion and STD experiments as well as TOCSY spectra and solid-state NMR experiments were recorded on a hybrid solution/solid-state Varian Inova Unity 600 (Agilent, Santa Clara, CA, USA) spectrometer operating at frequencies of 599.95 MHz for ¹H, 246.86 MHz for ³¹P and 92.125 MHz for ²H. A double-resonance 3-mm indirect z-gradient probe was used in the solution mode while a 4-mm broadband/¹H dual-frequency magic-angle-spinning probe head was employed for experiments on the solid state. The ¹H chemical shifts were internally referenced by adding 0.5 mM of 2,2-dimethyl-2-silapentane-5-sulfonic acid (DSS) set to 0.0 ppm. All ³¹P NMR spectra were externally referenced with respect to the signal of 85 % phosphoric acid set to 0 ppm.

ROESY spectra were recorded on a solution-state Bruker SB Advance DRX-400 (Bruker, Wissembourg, France) spectrometer operating at a 400.13 MHz for ¹H using a 5-mm probe. ¹H/¹³C heteronuclear single-quantum correlation (HSQC) spectra were

recorded at the Québec/Eastern Canada High Field NMR Facility on a Varian Inova 500 spectrometer operating at frequencies of 499.72 MHz for ^1H and 125.64 MHz for ^{13}C and equipped with a high-sensitivity 5-mm cold probe.

3.4.3.1 Translational diffusion experiments

^1H NMR self-diffusion measurements were carried out at 25 °C using the bipolar LED stimulated echo sequence¹³¹. A hard 90° pulse of 3.6 μs was used. The gradient pulse duration δ and diffusion time Δ were varied between 2-3 ms and 100-150 ms, respectively, to ensure that the echo intensities were attenuated by at least 80 %. 20k data points were obtained and typically 16 scans were acquired for each selected gradient strength with a recycle delay of 2 s. A complete attenuation curve was obtained by measuring 25 gradient strengths linearly incremented between 2.1 and 52.5 G/cm.

Translational diffusion coefficients (D_s) were calculated using the following equation:¹³²

$$S(G) = S(0)\exp[-(\gamma\delta G)^2(\Delta - \delta/3)D_s] \quad (3.1)$$

where $S(G)$ is the echo amplitude and γ is the ^1H gyromagnetic ratio. The gradient strength was calibrated using back calculation of the coil constant from the measurement of the diffusion constant of H_2O traces in D_2O using $D_s = 1.9 \times 10^{-5} \text{ cm}^2/\text{s}$ at 25 °C. The percentage of SF or drug bound to the bicelles was calculated using the following equation¹³³:

$$\% = \left[(D_{\text{obs}} - D_{\text{free}}^\phi) / (D_{\text{bound}} - D_{\text{free}}^\phi) \right] \times 100 \quad (3.2)$$

where D_{obs} is the diffusion coefficient of the bicelle-associated peptide or drug, D_{bound} is the diffusion coefficient of the bicelles in water, and D_{free}^ϕ is the corrected diffusion

coefficient of the peptide or drug in water where an obstruction factor (A) was introduced:

$$A = 1/(1 + 0.5\phi) \quad (3.3)$$

and

$$D_{free}^{\phi} = D_{free} \cdot A \quad (3.4)$$

where ϕ is the volume fraction of the obstructing particles, leading to an obstruction factor of 0.938 for spheroid objects, as detailed in previous work¹⁵⁴. In the case of drugs binding to SF, the obstruction factor was not necessary, and D_{obs} refers to SF-associated drug, D_{bound} to the diffusion coefficient of the SF and D_{free} to that of the drug in water. Diffusion coefficients were obtained by selecting 2 to 3 resonances on the spectra and experiments were repeated between 2 to 4 times.

2.4.3.2 Saturation transfer difference (STD)

The STD experiments consisted of a train of 50 ms Gaussian selective pulses separated by 0.1 ms delays and followed by a WET water suppression and detection⁸⁵. The saturation frequencies were alternated between the resonance to be saturated and -25 ppm. The resonances of the following DMPC groups have been saturated: $N(CH_3)_3$ (3.25 ppm), glycerol (4.03 ppm) and acyl chain terminal methyl (0.84 ppm). Gaussian pulses were applied with a radio-frequency field strength of 120 Hz and saturation times were varied between 250 ms and 5 s. The recycle delay was 4 s. Aromatic and amide protons were probed to avoid lipid resonance overlap. The resonances of protons giving the most intense STD curve were selected and all experiments done in duplicates.

2.4.3.3 High-resolution ^1H two-dimensional experiments

^1H total correlation spectroscopy (TOCSY) spectra were recorded on a 600 MHz Varian spectrometer using a 90° pulse of 5.5 ms, spin-lock times of 25, 100 and 250 ms with MLEV17 spin-lock fields of 15 kHz⁴⁸. A spectral width of 8 kHz was used in both dimensions with 1024 and 512 complex data points in the direct and indirect dimensions, respectively. 8 transients were accumulated with a repetition delay of 0.5 s. 2D rotating frame Overhauser spectroscopy (ROESY) spectra were recorded using a pulse length of 12 ms with mixing times of varying from 100 to 300 ms. A spectral width of 4.8 kHz was used in both dimensions with 2048 data points in F2 and 512 increments in F1. 16 scans were recorded with a repetition delay of 2 s. HSQC spectra were recorded using a ^1H 90° pulse ranging from 6.4 to 8.5 ms and a ^{13}C 90° pulse of 15.6 ms. A 8 kHz spectral width in F1 and F2 was used with 1024 data points in F2 and 200 increments in F1. 4 transients were accumulated with a repetition delay of 1.2 s.

2.4.3.4 Solid-state NMR (SS-NMR) experiments

^{31}P NMR spectra were recorded using a phase-cycled Hahn echo pulse sequence with gated broadband proton continuous wave decoupling at a field strength of 50 kHz¹³⁷. The interpulse delays were 33 μs and typically 1024 scans were acquired with a recycle delay of 5 s. The acquisition time was set at 10 ms with a 5 μs dwell time. ^2H NMR spectra were obtained using a solid echo pulse sequence¹⁴⁰ with interpulse delays of 20 μs and repetition delays of 0.5 s. This recycle delay was voluntarily set shorter than 5 times the longest relaxation time in a saturated fatty acyl chain (300 ms) to optimize the total acquisition sequence. This procedure does not affect the quadrupolar doublet positions that are extracted from the Pake patterns. At least 5000 data points were obtained and typically 5000 scans were recorded with an

acquisition time of 5 ms and 1 μ s dwell time. For all ^2H and ^{31}P NMR experiments, the 90° pulse length was varied between 2.8 and 3.4 μ s.

2.4.3.5 Data processing

Diffusion, STD and SS-NMR data were processed using matNMR¹⁶⁹. High-resolution 2D NMR spectra were processed using the NMRPipe package¹⁷⁰ and analyzed with the software NMRView for chemical shift assignment¹⁷¹.

3.5 Results

3.5.1 Structure of the SF segment in aqueous environment

To better understand the structure-function relationship of the hERG's SF, we have first investigated its structure in water by solution NMR with and without K^+ ions. So far, such studies of K^+ channel selectivity filters have targeted other K_V channels and were performed uniquely by molecular simulations^{22, 23, 29, 172}. We have used the synthetic segment L622-K638 comprising the SF as illustrated in Fig. 3.1A. About 95 % of the chemical shifts of this SF segment were assigned using TOCSY, ROESY and ^1H - ^{13}C HSQC experiments (Fig. 3.S1, Table 3.S1). As evidenced in Fig. 3.1B, no contacts indicative of a defined secondary structure were detected by 2D ROESY NMR experiments with mixing times up to 300 ms. Correspondingly no secondary structure was observed by CD measurements (data not shown).

The effect of K^+ ions on the SF's structure was then probed with 2D ^1H TOCSY experiments. This was done by analysing changes in chemical shifts of the L622-K638 segment at high and low K^+ concentrations selected to mimic the physiological intracellular (150 mM) and extracellular (10 mM) concentrations of myocardial cells. No variations in the proton resonances could be detected at both K^+ concentrations. Because ^{13}C nuclei are more sensitive to structural modifications,

^1H - ^{13}C HSQC correlation experiments were carried out and no changes in chemical shift could be seen (data not shown).

3.5.2 Interaction of the SF segment with the membrane

Considering that the extracellular loop to which the hERG's SF segment is connected is long and highly flexible, we have verified the possible interaction of the L622-K638 segment with the membrane. Since phosphatidylcholines (PCs) are the most abundant phospholipids in cardiomyocyte membranes, i.e. 34-52 % of total membrane phospholipids⁷², the model membranes employed for this study were prepared with PC. The 1D ^1H NMR spectra of the SF segment were recorded in water and in DMPC/DHPC bicelles, and comparison of these spectra in Fig. 3.2 reveal changes in the chemical shifts of the peptide's resonances. This suggests an interaction between this hERG segment and the model membranes.

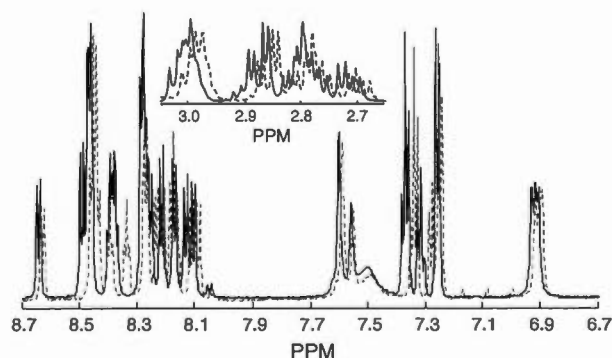


Figure 3.2 ^1H NMR spectra of the side chain region (top), amide and aromatic region (bottom) of SF (2 mM) in 10 % D_2O (black solid line), and with DMPC- d_{54} /DHPC ($q = 0.5$) bicelles (grey dashed line) at a lipid/peptide ratio of 50:1.

To further investigate this interaction, we have verified the affinity of the SF segment for the membrane environment using pulse field gradient (PFG) diffusion experiments. This technique allows measuring translational diffusion coefficients of

the L622-K638 hERG segment, drugs and PC bicelles in their free and bound states. If the SF segment interacts with the drugs and/or model membranes, the resulting diffusion coefficient will be averaged from the bound and free state (diffusion coefficients displayed in Table 3.S2). With these results, the percentage of SF segment bound to drugs and/or bicelles can then be estimated (Eq. 3.2). As shown in Table 3.2, 48 % of the SF segment binds to model membranes at a lipid/peptide molar ratio of 100:1. The addition of K^+ ions at low concentrations slightly decreases the SF segment's affinity for the membrane (46 %) while a high K^+ concentration lowers it by almost half (28 %).

Table 3.2 Calculated fraction of SF or drugs bound to the SF and to bicelles (with or without SF). Values are calculated according to Eq 3.2.

System	Fraction of bound SF or drug (%) ^a		
	SF	Bicelles	SF/Bicelles
SF	—	48	—
Bepidil	9	100	100 ^a (34) ^b
Cetirizine	14	100	100 ^a (49) ^b
Diphenhydramine	8	96	96 ^a (56) ^b
Fluvoxamine	3	100	100 ^a (50) ^b
Promethazine	37	100	100 ^a (66) ^b
SF/KCl (10 mM)	—	46	—
SF/KCl (150 mM)	—	28	—

^a Fraction of drug bound to Bicelles/SF samples.

^b Fraction of SF bound to Bicelles/drug samples.

The interaction of the SF segment with the model membranes was further investigated by SS-NMR at physiological temperature using MLVs made of DMPC with deuterated acyl chains. More specifically, the perturbation of the phospholipid polar headgroups can be revealed from the ^{31}P spectra since the chemical shift anisotropy (CSA) of this nucleus is sensitive to changes in orientation and

dynamics¹²³. The apolar region of the bilayer was probed by studying the quadrupolar splittings ($\Delta\nu_Q$) of the ^2H nuclei on the acyl chains as the quadrupolar interaction is highly responsive to motions^{141, 173}. The spectra presented in Fig. 3.3 without and with the SF segment are characteristic of phospholipids in a lamellar phase with axial symmetry^{123, 141}. Comparison of spectra in Fig. 3.3A shows a slight disruption of the model DMPC membranes when the SF segment is present. The phosphorus CSA decreases from 45.3 to 39.5 ppm with the SF segment while no changes in $\Delta\nu_Q$ are observed in the ^2H spectra. Consequently, the SF segment would mainly interact with the membrane surface. Both ^{31}P and ^2H SS-NMR spectra also display an isotropic peak in the presence of the SF segment, indicative of the coexistence of vesicles and rapidly-reorienting lipid structures, although the majority of the membrane would remain intact¹⁷⁴. Furthermore, when KCl is added at low (10 mM, Fig. 3.3B) and high (150 mM, Fig. 3.3C) concentrations to the SF/MLV samples, CSA and $\Delta\nu_Q$ values of ^{31}P and ^2H spectra, respectively, resemble those of a pure lipid system (DMPC MLV). Hence, the effect of the SF segment on model membranes seems to be cancelled when K^+ ions are present. ^{31}P and ^2H SS-NMR spectra of DMPC without and with KCl were recorded as controls and were superimposable (not shown) as expected for K^+ ions which have a weak effect on PC headgroups¹⁷⁵⁻¹⁷⁷.

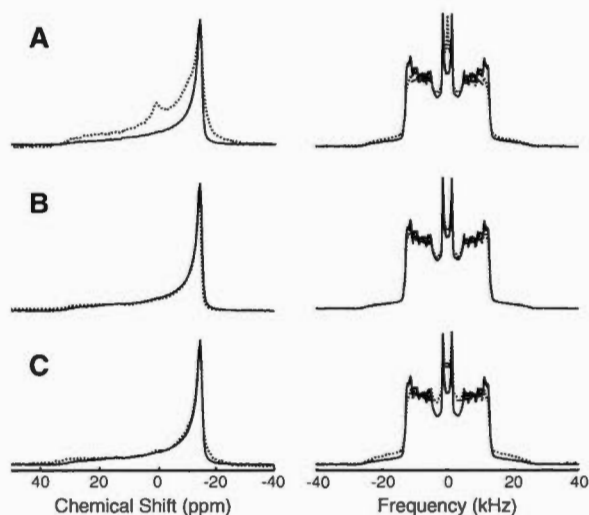


Figure 3.3 Effect of the SF on the ^{31}P (left) and ^2H (right) SS-NMR spectra of DMPC MLVs, with and without KCl, at 37 °C, with a lipid/SF molar ratio of 100:1. A) SF, B) SF with 10 mM KCl, C) SF with 150 mM KCl (dotted lines). The pure lipid spectra (solid line) are overlaid for comparison.

To better understand the interaction of the SF segment with the model membranes, STD experiments were conducted using DMPC/DHPC bicelles ($q=1$) by solution NMR. Mostly used to study the binding of ligands to protein, this technique can also help localizing a molecule in the membrane when interacting with the lipids⁸⁵. This is done by selectively saturating different lipid resonances, such as the choline group at the bilayer surface, the glycerol group at the polar/apolar interface, and the terminal methyl in the hydrophobic core. The effect of this saturation on the saturation transfer build-up of residues of the L622-K638 segment resonances can then help elucidating its position with respect to the membrane as was shown with amantadine¹³³, dynorphins¹⁷⁸ and the hERG's S5-P extracellular linker (Annexe A)¹⁵⁴. Bicelles were made of DHPC with deuterated lipid chains in order to probe the peptide penetration in the planar section of the bilayer and minimize contacts with high-curvature

regions. Variations in the saturation transfer build up were monitored for amide and aromatic protons of different residues along the peptide.

No transfers of saturation were observed on the protons of the SF segment (data not shown) at a L/P molar ratio of 50:1. The absence of STDs typically occurs if (1) all ligands are in the free state (not bound); (2) the binding is too strong; (3) the ligands are somewhere else in the membrane; (4) the dissociation of the ligands is slower than the relaxation rate of the magnetization that is transferred; or (5) if there is an excess of ligands obscuring the detection the ligands that are saturated as their concentration is too low in comparison to the free ligands⁸⁵. Because of the 48% association of the SF determined by translational measurements, points 1 and 2 can be ruled out. Point 3 is not likely as all regions of the phospholipids are probed, i.e. the $N(CH_3)_3$ of the choline group, the glycerol and terminal CH_3 group of DMPC acyl chains. Therefore in order to verify point 5, we have lowered the proportion of SF segment in the solution by increasing the L/P ratio to 125:1. As can be seen in Fig. 3.4, weak STDs could be detected with the choline headgroup exclusively for the aromatic ring protons of Phe627 located in the SVGFG motif. This result suggests that this residue is mainly responsible for the membrane interaction.

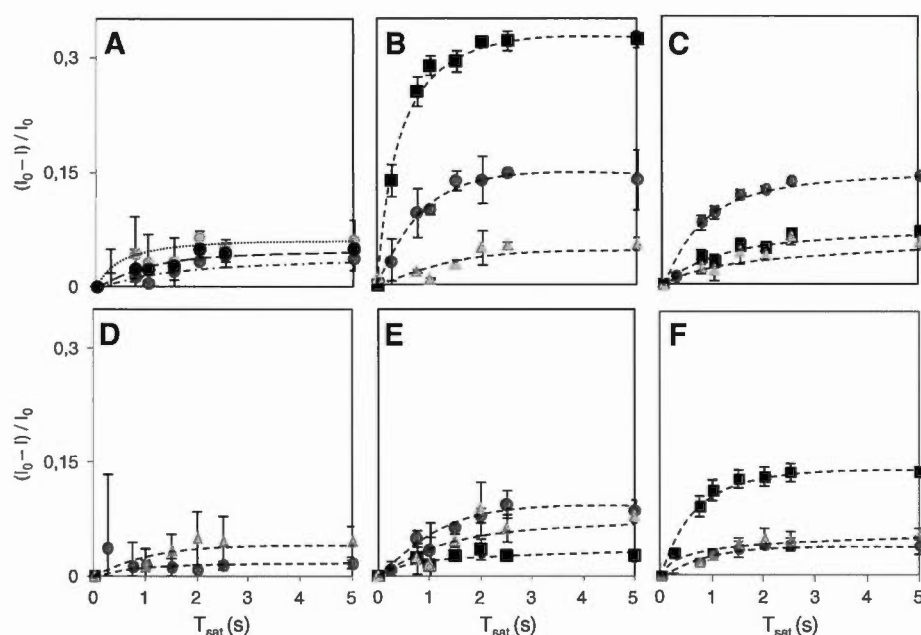


Figure 3.4 Observed saturation transfer difference curves for A) SF Phe627 ring protons $C^{(2,6)}H$ (dashed line), $C^{(3,5)}H$ (dash-dotted line) and $C^{(4)}H$ (dotted line), and aromatic protons for B) bepridil, C) cetirizine, D) diphenhydramine, E) fluvoxamine and F) promethazine in DMPC/DHPC- d_{22} bicelles when choline (\bullet), glycerol (\blacksquare) or terminal methyl (\blacktriangle) resonances of DMPC are saturated. Dashed and dotted lines are a guide to the eye.

3.5.3 Interaction of the SF segment with hERG-active drugs

Because the hERG's SF is a potential target for ALQTS-prone drugs, we have investigated the interaction of cardiotoxic drugs with this channel's segment. More specifically, bepridil, cetirizine, diphenhydramine, fluvoxamine and promethazine were selected. The association of the drugs to the peptide was determined by translational diffusion experiments. As shown in Table 3.2, out of all five drugs, promethazine has the highest affinity for the SF segment, 37 % of which is binding to it. Bepridil, cetirizine and diphenhydramine, on the other hand, demonstrate a weaker

affinity for the SF with 9, 14 and 8 % binding, respectively, whereas fluvoxamine only shows a 3 % association.

As a next step, we have verified the impact of the presence of drugs on the affinity of the SF segment for the membranes. The results are compiled in Table 3.2. The data demonstrate that the presence of some of the drugs promotes the peptide/membrane interaction by increasing SF segment binding affinity from 48 % to 56 % and 66 % with diphenhydramine and promethazine, respectively. Cetirizine and fluvoxamine have a negligible effect while bepridil decreases the SF segment association by 14 %.

3.5.4 Role of the membrane in the long QT syndrome

Since drugs responsible for ALQTS tend to have high logP values, the potential drug-membrane interaction was investigated. All the cardiotoxic drugs evaluated in this study have previously been reported to have an affinity for lipid membranes^{154, 179-181}. Hence, the possibility of an indirect blockage of the hERG channel through non-specific drug-membrane interactions cannot be ruled out. This hypothesis was first investigated using translational diffusion experiments, as previously described. Table 3.2 shows that all drugs have a high affinity for the membrane, their association ranging between 96 %-100 %. The values obtained for bepridil, cetirizine and diphenhydramine compare well with previously published data¹⁵⁴. We have also verified if the SF modifies the association of the drugs to the membranes, and Table 3.2 shows that their affinity is unchanged.

Considering the high affinity of the five cardiotoxic drugs for the PC bicelles, their interaction with model membranes was probed using SS-NMR experiments, as done with the SF. As shown in Fig. 3.5A, bepridil has no effect on the ³¹P SS-NMR spectrum of the DMPC membranes. The appearance of a small but measurable isotropic peak can be seen in the ³¹P and ²H SS-NMR spectra when cetirizine (5B),

diphenhydramine (5C) and promethazine (5E) are added to DMPC MLVs at a lipid/drug ratio of 180:1, indicating the formation of smaller vesicles. These drugs as well as fluvoxamine (5D) also have the effect of increasing the ^{31}P CSA, suggesting a reduced mobility of the phospholipid headgroups. Moreover, these spectra show a change in intensity between the 0° and 90° edges, with less lipids on the 90° edge which can be ascribed to a change in vesicle shape or transverse relaxation (T_2) effect caused by an increase in slow motions¹⁸². Analysis of the ^2H SS-NMR spectra shows that cetirizine has little effect on the phospholipid acyl chains, but a loss of resolution is seen for the quadrupolar splittings of the plateau positions (C2-C8, close to the glycerol backbone) with the other drugs, and more strikingly with diphenhydramine. Our results indicate that the LQTS-active drugs could either form smaller objects or change the lipid diffusion rate^{174, 183}.

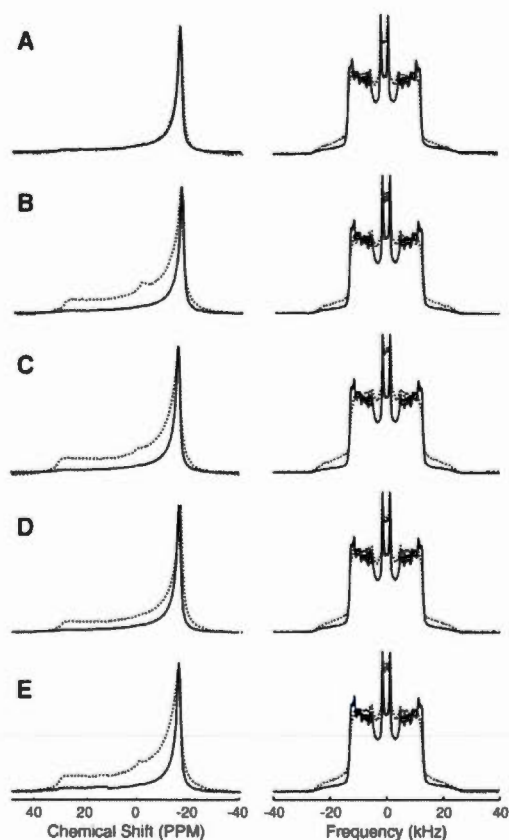


Figure 3.5 Effect of LQTS-active drugs on the ^{31}P (left) and ^2H (right) SS-NMR spectra of DMPC MLVs at 37°C with a lipid/drug molar ratio of 180:1. A) bepridil, B) cetirizine, C) diphenhydramine, D) fluvoxamine and E) promethazine (dotted lines). The pure lipid spectrum (solid line) is overlaid for comparison.

To localize the ALQTS-active drugs within the membrane while interacting with the bilayers, STD NMR experiments were carried out, as was done with the SF, in $q=1$ bicelles at a L/D molar ratio of 150:1. The effect of the saturation of the choline, glycerol and terminal methyl of the lipids on the aromatic protons of the hERG-active drugs is displayed in Fig. 3.4. Our data reveal that bepridil (4B) and promethazine (4F) aromatic groups are in proximity of the glycerol region of the membrane. Cetirizine (4C) and fluvoxamine (4E), on the other hand, show some interaction with the membrane surface, more specifically with the choline headgroups. The saturation transfers measured with diphenhydramine (4D) are remarkably low. Considering the 96% association of this drug to bicelles, its aromatic protons would thus be too tightly bound for an STD signal to be detected.

3.6 Discussion

Homology studies have offered insightful predictions of hERG's structure; however to better understand this channel's function and role in the ALQTS, we must first refine its structural model by experimental determination^{29, 150}. The use of peptides corresponding to specific regions of membrane proteins and channels, as opposed to full length proteins, is very helpful considering their difficult expression and purification. This is indeed particularly relevant for the notoriously long extracellular S5-S6 linker of the hERG channel for which peptides representing the S5-P portion were studied by CD and solution NMR (Annexe A)^{27, 47, 154, 155}. The TVGYG residues in the SF motif are highly conserved amongst K_V channels but the hERG channel has only retained valine and glycine residues in its SF, leading to an SVGFG sequence. Seemingly, the glycine residues are indispensable for the channel conformation where they offer the backbone flexibility needed when responding to the alternating outflow of K^+ ions and water molecules as shown with other K_V channels⁵⁶. Two steady states of the SF have actually been documented for KcsA, i.e., a conductive and a non-

conductive one respectively existing at high and low K^+ concentrations⁵⁴⁻⁵⁶. Although these conformations were seen on a millisecond timescale in computational studies of the KcsA channel and KirBac^{54, 184, 185}, they were not observed in our study for the hERG channel's SF segment on the NMR timescale, in the absence and presence of K^+ ions. If the transition rate between conformations is too fast, the resulting structure will be averaged. Thus, our 2D 1H NMR results suggest that hERG's SF is unstructured in water. This is in agreement with the flexibility expected for a segment that must be available for K^+ binding, H-bonding with water molecules, and which most likely spatially reorients during the channel functioning^{54, 184, 186}. According to MD studies on the KcsA^{55, 157}, the hydration shell of K^+ ions is partially removed in order to form electrostatic interactions with the carbonyl oxygen atoms of the SF's TVGYG backbone. This eventual ion binding to the carbonyls is likely not to perturb sufficiently the 1H and ^{13}C NMR signals, and we would thus be unable to detect any changes.

Our solution and SS-NMR experiments have shown that the hERG's SF segment has the potential to interact with the lipid membrane. This was first suggested by the change in the peptide's chemical shifts when added to isotropic bicelles (Fig. 3.2). The absence of peak broadening indicates, however, that the SF segment remains free to tumble in the bilayer and to diffuse laterally, as was observed by Wang *et al.* with amantadine¹³³. According to our diffusion experiments (Table 3.2), hERG's L622-K638 segment has a 48 % affinity for PC membranes. When "bound", this amphiphilic peptide would prefer the bilayer surface as only little effects are seen on the 2H SS-NMR spectrum using DMPC- d_{54} vesicles (Fig. 3.3). This is supported by a change in the headgroup dynamics suggested by the decrease in DMPC's CSA on the ^{31}P spectrum in Fig. 3.3 and by the STD experiments which could only detect saturation transfers between the $N(CH_3)_3$ of the choline headgroup and the aromatic protons of the L622-K638 peptide. The formation of fast-tumbling lipid assemblies could also be induced by the SF segment as revealed by the isotropic resonance on

the ^{31}P and ^2H spectra. Previous MD studies have shown interactions between the SF and the pore helix²⁹. The interaction between the SF segment and the membrane could potentially be of similar nature and enabled by the flexibility imparted by the particularly long linker between S5 and the pore helix (S5-P) which comprises 43 amino acid residues vs. 12-23 residues in most K^+ channels^{41, 47, 167}. As revealed by ^{31}P and ^2H SS-NMR, the addition of K^+ ions at both intra- (150 mM) and extracellular (10 mM) concentrations appear to cancel the SF segment's effect on the PC membranes. It is possible that K^+ ions compete with the amphiphilic L622-K638 hERG segment for an interaction with the phospholipid polar headgroups, most likely with the carbonyl groups where K^+ ions are known to bind¹⁷⁶. Altogether, our results suggest that the SF could interact with the membrane via its aromatic residue but that this interaction is most likely hindered by the local K^+ ions concentration.

Discovering new drug binding sites on hERG channels is fundamental when attempting to elucidate its role in the ALQTS. Our ^1H NMR translational diffusion measurements (Table 3.2) evaluated the potential binding of five LQTS-prone drugs to individual SF segments. The results show that promethazine has the highest affinity for the L622-K638 segment with an association close to 40 %. The SF segment could therefore be an additional binding site for this antihistamine drug which also binds Tyr652 and Phe656 on the S6 helix according to electrophysiological studies¹⁸¹. Previous published work has demonstrated that mutations to Thr623, Ser624 and Val625 on the SF as well as on Phe656 of the S6 reduced the channel block by bepridil²⁰. However, our translational diffusion experiments only reveal a low affinity (9 %) of this drug for the hERG's SF, suggesting that this channel's segment is not a primary target for bepridil. ^1H NMR translational diffusion experiments recently performed by our group had also showed a low affinity of this drug for the hERG's extracellular S5-P linker¹⁵⁴. We can hypothesize that bepridil needs the pore geometry to efficiently bind to sites in the

channel pore, or to more hydrophobic amino acid residues found on the transmembrane S6 helix.

Cetirizine, diphenhydramine and fluvoxamine also display a very weak binding affinity (14 % or below) for the L622-K638 hERG segment as shown in Table 3.2. ^1H NMR translational diffusion measurements reported 13 % and 9 % association of cetirizine and diphenhydramine, respectively, to the hERG's S5-P linker¹⁵⁴, yet the hERG blocking ability of cetirizine and its derivative diphenhydramine is still matter of debate¹⁸⁷⁻¹⁸⁹. As for fluvoxamine, it has been hypothesized that this antidepressant could bind to either the cytoplasmic or extracellular side of the channel and not to the pore cavity contrarily to most LQTS-active drugs^{166, 180}. Altogether, our results indicate that cetirizine, diphenhydramine and fluvoxamine are unlikely to bind the hERG's SF.

The hERG channel has a large pore cavity (12 Å) and, as described in the Introduction, has a particular kinetics^{9, 172}. It is in the open state for a longer time during the heart repolarization. According to computational studies, the SF would be flexible and change conformation during the functioning of K^+ -selective channels⁵⁴. Therefore we believe that the drugs' affinity for individual SF segments measured in this work gives a valuable insight on their potential to bind this segment in the actual hERG tetrameric organization. Combination of long-lasting open state and most likely mobile SF units certainly favors the access of drugs to sites in the pore domain and on the SF units. It should be noted that the L622-K638 hERG segment studied here comprises the SVGFG motif but also the amino acid residues connecting it to S6. It is thus also possible that drugs bind this short linker.

When probing the affinity of the five drugs for the model cardiomyocyte membranes, our ^1H NMR translational diffusion measurements revealed a 96 to 100 % association that is not affected by the presence of the peptide (Table 3.2). The STD measurements (Fig. 3.4) indicate that all hERG-active drugs tested prefer the polar

side of the bilayer. Bepridil and promethazine – which have the highest logP – seem to be located close to the glycerol region whereas cetirizine and fluvoxamine are nearer to the choline headgroups. Diphenhydramine – which shows the strongest effect on the ^{31}P and ^2H NMR spectra of the DMPC membranes – would be particularly close to the lipids considering the low STD values measured. In all cases, the phospholipid mobility would be reduced by the presence of the drugs with no perturbation of the hydrophobic core, as suggested by the ^{31}P and ^2H SS-NMR spectra (Fig. 3.5). The formation of smaller objects could also be induced by the drugs which, in some cases (cetirizine, diphenhydramine, and promethazine) could even disrupt the membrane and lead to the formation of smaller faster tumbling vesicles. Overall, our NMR study demonstrates that the tested drugs can interact with phospholipid membranes. This is in agreement with previous work reporting the interaction of promethazine with dipalmitoylPC (DPPC) membranes¹⁷⁹. Also, a study by van Balen *et al.*¹⁹⁰ proposed that the zwitterionic form of cetirizine – such as at the pH used in our study – interacts by weak electrostatic surface interactions with the polar headgroups of egg PC liposomes. Bepridil, cetirizine and diphenhydramine were also known to bind to DMPC/DHPC bicelles although they were found to slightly increase the phospholipid acyl chains ordering near the polar headgroup¹⁵⁴ as opposed to what is observed here with DMPC MLVs. The effect on bicelles was very small and could also have been ascribed to reduced bicelle wobbling.

The presence of cardiotoxic drugs in the membrane environment modifies the SF segment's association with the phospholipid bilayer, as evidenced in Table 3.2, and this would be correlated to the affinity of the SF segment for each individual drug. More specifically, promethazine has the highest (37 %) affinity for the SF segment, and its membrane association is increased by 18 % in the presence of this antihistamine. Correspondingly, no change in the membrane association of the SF segment is seen in the presence of fluvoxamine which has the lowest affinity (3 %) for this hERG moiety. As for intermediate cases such as diphenhydramine and

cetirizine which respectively have an 8 % and 14 % affinity for hERG's L622-K638 segment, their effect on its membrane association is either null (cetirizine) or within (8 % for diphenhydramine) the error limit of the method. This observation suggests that a fraction of the SF segment would interact directly with the lipid bilayer while another population would interact with membrane-bound drugs. This "attracting" effect of the drugs, however, appears to be not applicable to bepridil. Despite a 9 % affinity for the SF segment comparable to that of diphenhydramine, bepridil molecules bound to the bilayer reduce its membrane association by 14%. This effect could possibly be due to a competition for interaction sites in the lipid bilayer. Altogether, our results suggest that the association of hERG's L622-K638 segment with the membrane in the presence of drugs depends on factors such as the drug/segment, segment/membrane and drug/membrane affinity as well as the nature of the molecular interaction and the presence of K^+ ions. They also propose that modification of the membrane affinity of hERG moieties due to drug attraction or interference could affect the channel function – a mechanism that needs more investigation.

Besides channel obstruction, it is also possible that drug-membrane interactions can be indirectly involved in the ALQTS mechanism by facilitating the access of drugs to intracellular targets on the hERG channel, similarly to enkephalins that would need the membrane interaction prior to receptor binding¹⁹¹. As discussed in our previous study on hERG's S5-P linker¹⁵⁴, the interaction of drugs with the membrane could modify its local properties and perturb the channel functioning. The mechanical properties of biomembranes imparted by the nature of its lipid content are determinant for the structure and function of membrane proteins such as ion channels, as reviewed elsewhere. Perturbation of the membrane protein annular shell by drugs is suspected to play a role in the action mechanism of anesthetics and toxins¹⁹²⁻¹⁹⁴.

3.7 Conclusion

Our combined solution and SS-NMR study of the hERG's L622-K638 segment contributed to shed light on the SF structure and functioning as well as on its role in the ALQTS. We have shown that this SF segment is unstructured in an aqueous environment on the NMR timescale, with and without K^+ ions, in agreement with its expected flexibility required during the different channel conductive states. Moreover, the SF segment was shown to have a potential to interact with the phospholipid membrane surface – an interaction that would be hindered by the surrounding K^+ ions in its milieu. Our results indicate that the hERG's SF could be a binding site for promethazine and, thus, play a role in the ALQTS reported for this antihistamine. However, it would not be a primary target for bepridil, cetirizine, diphenhydramine and fluvoxamine. Finally, the high affinity of the cardiotoxic drugs for the lipid membrane as well as their effect on the membrane interaction of hERG's SF segment support the possibility of an indirect role of the membrane in the ALQTS.

3.8 Acknowledgements

A.G. wishes to thank the *Groupe de Recherche Axé sur la Structure des Protéines* (GRASP), the *Faculté des Sciences* of the *Université du Québec à Montréal* (UQAM), the *Centre Québécois sur les Matériaux Fonctionnels* (CQMF), the *Fonds de Recherche du Québec – Nature et Technologies* (FRQNT), the Canadian Institutes of Health Research (CIHR) Strategic Training Initiative in Chemical Biology and the Natural Sciences and Engineering Research Council (NSERC) of Canada for the award of scholarships. We would like to thank T. Sprules (Quebec/Eastern Canada NMR Center), A. Grélard and C. Courrèges (CBMN) for technical assistance and insightful discussions. This work was partly supported by the NSERC. I.M. is a member of the GRASP, CQMF, NanoQAM and Pharmaqam.

Table 3.S1 Proton chemical shifts of the hERG L622-K638 segment in water at 25 °C, pH 4.5.

Residue	NH	C α H	C β H	C γ H	Others
Leu ⁶²²	–	4.12	1.72, 1.76	1.67	C δ H 0.95
Thr ⁶²³	8.63	4.42	4.16	1.22	
Ser ⁶²⁴	8.47	4.48	3.82		
Val ⁶²⁵	8.20	4.13	2.07	0.91	
Gly ⁶²⁶	8.37	3.84			
Phe ⁶²⁷	8.15	4.62	3.18, 3.06		C ^(2,6) H 7.27 C ^(3,5) H 7.37 C ⁽⁴⁾ H 7.32
Gly ⁶²⁸	8.38	3.89			
Asn ⁶²⁹	–	–	–		–
Val ⁶³⁰	8.09	4.17	2.09	0.91	
Ser ⁶³¹	8.45	4.42	3.84		
Pro ⁶³²		4.45	2.27, 2.28	1.93, 2.00	C δ H 3.73, 3.81
Asn ⁶³³	8.27	4.35	2.72, 2.80		N δ H 6.91, 7.55
Thr ⁶³⁴	8.12	4.30	4.27	1.19	
Asn ⁶³⁵	8.45	–	2.78, 2.87		N δ H 6.92, 7.59
Ser ⁶³⁶	8.24	4.40	3.87		
Glu ⁶³⁷	8.27	4.39	2.01, 2.15	2.49	
Lys ⁶³⁸	8.24	4.31	1.77, 1.90	1.43	C δ H 1.68 C ϵ H 3.00 N ζ H 7.50

Table 3.S2 Translational diffusion coefficients of bicelles ($q=0.5$), SF and drugs used to calculate the fraction of bound peptide and drugs. $n = 2 - 4$.

System ^a	Component	Mean diffusion coefficient ($\times 10^{-10} \text{ m}^2 \cdot \text{s}^{-1}$)	$\sigma (\pm)$
SF	SF	1,82	0,12
SF/KCl10	SF	1,81	0,11
SF/KCl150	SF	1,72	0,05
BEP	BEP	3,93	0,12
CET	CET	3,78	0,12
DIP	DIP	4,82	0,14
FLU	FLU	4,21	0,10
PRO	PRO	4,74	0,19
Bic	Bic	0,55	0,02
SF/Bic	SF	1,15	0,01
	Bic	0,55	0,07
SF/KCl10/Bic	SF	1,21	0,06
	Bic	0,62	0,10
SF/KCl150/Bic	SF	1,30	0,29
	Bic	0,51	0,07
BEP/SF	BEP	3,75	0,16
	SF	1,73	0,01
CET/SF	CET	3,51	0,14
	SF	1,78	0,08
DIP/SF	DIP	4,59	0,12
	SF	1,85	0,17
FLU/SF	FLU	4,14	0,22
	SF	1,82	0,09
PRO/SF	PRO	3,69	0,19
	SF	1,88	0,17
BEP/Bic	BEP	0,47	0,03
	Bic	0,55	0,03
CET/Bic	CET	0,49	0,02
	Bic	0,56	0,01
DIP/Bic	DIP	0,70	0,02
	Bic	0,55	0,03
FLU/Bic	FLU	0,47	0,04
	Bic	0,56	0,01
PRO/Bic	PRO	0,47	0,09
	Bic	0,54	0,00
BEP/Bic/SF	BEP	0,45	0,02
	Bic	0,56	0,01
	SF	1,31	0,00
CET/Bic/SF	CET	0,48	0,03
	Bic	0,55	0,03
	SF	1,14	0,01
DIP/Bic/SF	DIP	0,69	0,01
	Bic	0,54	0,02
	SF	1,05	0,06
FLU/Bic/SF	FLU	0,44	0,01
	Bic	0,51	0,01
	SF	1,11	0,01
PRO/Bic/SF	PRO	0,45	0,00
	Bic	0,53	0,01
	SF	0,93	0,01

Example calculation – fraction of bound SF to the bicelles:

$$\begin{aligned}
 & [(D_{\text{obs}} - D_{\text{free}}) / (D_{\text{bound}} - D_{\text{free}})] \times 100 \\
 & [((1.15) - (1.82 \times 0.938)) / ((0.55) - (1.82 \times 0.938))] \times 100 \\
 & = 48 \%
 \end{aligned}$$

^a BEP (Bepiridil), CET (Cetirizine), DIP (Diphenhydramine), FLU (Fluvoxamine), PRO (Promethazine), KCl10 (10 mM KCl), KCl150 (150 mM KCl), Bic (Bicelles), SF (selectivity filter).

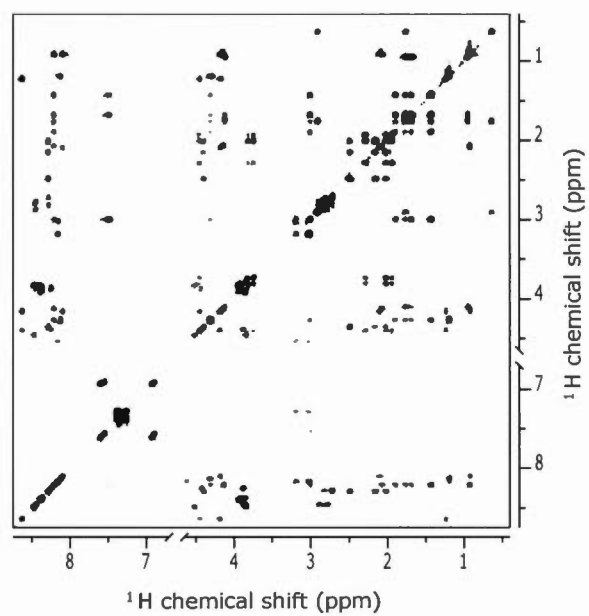


Figure 3.S1 ^1H TOCSY spectra of the hERG L622-K638 in 10 % D_2O at 20 °C.

CHAPITRE IIIV

TYROSINE RESIDUES FROM THE S4-S5 LINKER OF KV11.1 CHANNELS ARE CRITICAL FOR SLOW DEACTIVATION

Chai-Ann Ng¹, Andrée E Gravel¹, Matthew D Perry, Alexandre A Arnold, Isabelle
Marcotte et Jamie I Vandenberg

¹Ces auteurs ont contribué également à ce travail.

The Journal of Biological Chemistry, 291 (2016) 17293-17302

Contribution des auteurs: JIV a conçu et coordonné l'étude. CAN, AEG, IM et JIV ont rédigé l'article. CAN a conçu, effectué et analysé les expériences d'électrophysiologie. AEG a conçu, effectué et analysé les expériences de RMN. MDP et AAA ont assisté avec la conception et l'acquisition des données. Tous les auteurs ont contribué à la préparation des figures et ont approuvé la version finale du manuscrit.

4.1 Résumé

La désactivation lente des canaux Kv11.1 est critique pour leur fonction dans le cœur. Le segment S4-S5, qui lie le domaine sensible au voltage (DSV) à celui du pore, joue un rôle critique dans ce mécanisme de désactivation. Nous employons la spectroscopie RMN pour identifier la surface du segment S4S5 qui lie la membrane, ainsi que pour démontrer que deux résidus tyrosine étant hautement conservés dans la sous-famille de canaux KCNH sont associés à la membrane. La mutagenèse dirigée et les analyses électrophysiologiques démontrent que la Tyr542 interagit avec le domaine du pore ainsi qu'avec le DSV pour stabiliser la conformation active du canal, tandis que la Tyr545 contribue à la cinétique lente de désactivation, principalement en stabilisant l'état de transition entre les états actifs et fermés. Ainsi,

les deux résidus de tyrosine dans le segment S4S5 du Kv11.1 jouent un rôle critique, mais distinct, dans le phénotype de désactivation lente, qui est une particularité des canaux Kv11.1.

4.2 Abstract

Slow deactivation of Kv11.1 channels is critical for their function in the heart. The S4-S5 linker, which joins the voltage sensor and pore domains, plays a critical role in this slow deactivation gating. Here, we use NMR spectroscopy to identify the membrane bound surface of the S4S5 linker and show that two highly conserved tyrosine residues within the KCNH subfamily of channels are membrane associated. Site directed mutagenesis and electrophysiological analysis indicates that Tyr542 interacts with both pore domain and voltage sensor residues to stabilize activated conformations of the channel, whereas Tyr545 contributes to the slow kinetics of deactivation by primarily stabilizing the transition state between the activated and closed states. Thus the two tyrosine residues in the Kv11.1 S4S5 linker play critical but distinct roles in the slow deactivation phenotype, which is a hallmark of Kv11.1 channels.

4.3 Introduction

The rhythm of the heartbeat is primarily controlled by the co-ordinated activity of a range of voltage-gated ion channels^{195, 196}. Kv11.1, which is encoded by the human *ether-à-go-go*-related gene (hERG, official name: KCNH2)⁴, is responsible for the delayed rectifier current (I_{Kr}), which plays a critical role in cardiac repolarization^{5, 197}. Kv11.1 channels have unusual kinetics of gating, namely slow activation and deactivation but fast inactivation and recovery from inactivation¹⁹⁸. Consequently, these channels pass relatively little current during the plateau phase of the action

potential but deliver a large current during repolarization¹⁹⁹. The slow kinetics of deactivation during the early diastolic period also enables Kv11.1 channels to play a critical role in terminating ectopic beats that may otherwise lead to cardiac arrhythmias and sudden cardiac arrest^{198, 200}.

Kv11.1 channels have the typical topology of voltage-gated K⁺ channels, which includes cytoplasmic N-terminal and C-terminal domains, a voltage sensor domain (VSD) composed of the first four transmembrane segments (S1-S4) and a pore domain composed of the 5th and 6th transmembrane segments (S5, S6). Pore domains from each of the four subunits co-assemble to form the ion conduction pathway, as well as the gates that control activation and inactivation. The slow activation and deactivation kinetics of Kv11.1 channels are due in part to the slow movement of the VSD^{62, 201}. Motion of the VSD, in response to changes in the membrane electric field, facilitates opening and closing of the activation gate at the intracellular end of the pore domain by pulling on the S4S5 linker (residues 539-550), which connects the VSD to the activation gate at the cytoplasmic end of the pore⁵⁹. Numerous studies have emphasized the importance of the S4S5 linker for Kv11.1 gating^{57, 59, 66, 67, 69-71}. In addition to providing a direct link between the voltage sensor and pore domains, the S4S5 linker interacts with the cytoplasmic domains and is thought to mediate the influence of cytoplasmic domains on the kinetics of deactivation gating^{57, 70, 71}. Recently, Lörinczi *et al.* showed that when the S4S5 linker in Kv11.1 channels was disrupted (i.e., co-expressing a construct composed of residues 1-545 with another composed of residues 546-1159) the channels can still assemble and retain their slow activation kinetics, as well as rapid inactivation and recovery from inactivation kinetics, but they have much faster deactivation kinetics compared to full length wild-type (WT) channels²⁰². These data indicate that an intact S4S5 linker is not required for normal activation gating, but once the channels have opened an intact S4S5 linker is required to stabilize the activated state and thereby contributes to slow deactivation. Another important implication of this study is that activation and deactivation gating

are not simply reciprocal processes but rather the transition from the closed state to the open state likely follows a different pathway to the transition from the open state back to the closed state.

In the crystal structure of the Kv1.2/2.1 chimeric channel, which is thought to have captured the channel in the activated state⁵⁸, the S4S5 linker forms an α -helix that is located at the cytoplasmic membrane interface, with one surface interacting with the membrane and/or transmembrane regions of the channel when the activation gates are in the open conformation. In this study, we sought to identify key S4S5 linker residues that interact with the membrane and/or intramembrane protein domains to stabilize the open state of the channel. A combination of nuclear magnetic resonance (NMR) and electrophysiology experiments suggest that the two tyrosine sidechains (Tyr542 and Tyr545) point towards the membrane interior. Thermodynamic mutant cycle analysis experiments indicate that Tyr542 interacts with both pore domain and voltage sensor residues to stabilize the open state of the channel. Conversely, mutations to Tyr545 cause marked changes to the kinetics of deactivation but have much smaller effects on the voltage dependence of the distribution between open and closed states, which suggests that Tyr545 stabilizes an intermediate transition state in the pathway between the activated and closed states.

4.4 Experimental procedures

4.4.1 NMR spectroscopy

Materials—Peptide that contains the S4S5 linker (LVRVARKLDRYSEYGAVLF) was synthesized by GL Biochem Ltd. (Shanghai, China) with >98 % purity. Protonated and deuterated dimyristoylphosphatidylcholine (DMPC, DMPC-d₅₄) were purchased from Avanti Polar Lipids (Alabaster, AL, USA) while deuterated dodecylphosphocholine (DPC-d₃₈), deuterium-depleted water, and diethylenetriaminepentaacetic acid gadolinium (III) dihydrogen salt hydrate were

purchased from Sigma Aldrich (Oakville, ON, Canada). Deuterium oxide (D_2O) was obtained from CDN Isotopes (Pointe-Claire, QC, Canada). Phosphatidylcholines are abundantly found in biological membranes; consequently DMPC is frequently used in model membranes, while DPC has been previously used to determine the Kv11.1 S4S5 linker structure by NMR⁵⁷. DMPC/DPC bicelles are a more biologically relevant alternative, and have recently been introduced as a new membrane mimicking system for the NMR analysis of membrane proteins²⁰³.

NMR sample preparation—Bicelle and multilamellar vesicle (MLV) samples used for solution- and solid-state NMR respectively, were prepared by mixing freeze-dried DMPC and/or DPC in water. The mixture was submitted to a series of at least three freeze (liquid N_2) / thaw ($50\text{ }^{\circ}C$) / vortex shaking cycles. In all experiments, the peptide concentration was kept between 2 and 5 mM while the lipid concentration was maintained well above the critical micelle concentration (CMC) of the lipids. To ensure the stability of the model membranes, the hydration percentages were kept at 75 % for solid-state NMR and 90 % for high-resolution NMR using deuterium-depleted water and 10 % D_2O , respectively. Solution NMR experiments used lipid molar ratios ($q = \text{DMPC/DPC}$) of 0.25 and 1, as well as a lipid/peptide (L/P) molar ratio ranging from of 50:1 to 58:1. solid-state NMR samples were prepared at a L/P molar ratio of 100:1.

NMR experiments—All experiments except high-resolution solution experiments, were recorded on a hybrid solution/solid-state Varian Inova Unity 600 (Agilent Technologies, Mississauga, ON, Canada) spectrometer operating at frequencies of 599.95 MHz for 1H , 246.86 MHz for ^{31}P and 92.125 MHz for 2H . solid-state NMR experiments used a 4-mm broadband/ 1H dual-frequency magic-angle spinning (MAS) probehead. The 1H chemical shifts were internally referenced by adding 0.5 mM of 2,2-dimethyl-2-silapentane-5-sulfonic acid (DSS) set to 0.0 ppm while ^{31}P NMR spectra were externally referenced with respect to the signal of 85 % phosphoric acid

set to 0 ppm. All data was processed using MestReNova (Mestrelab Research, Santiago de Compostela, Spain).

^1H total correlation spectroscopy (TOCSY) spectra were recorded on a hybrid solution/solid-state Bruker Avance III-HD narrow bore spectrometer (Milton, ON, Canada) operating at a frequency of 599.95 MHz for ^1H with a broadband double resonance 5mm probe. A 90° pulse of 13 μs , and spin-lock time of 80 ms with MLEV17 spin-lock field of 10 kHz were employed⁴⁸. A spectral width of 6 kHz was used in both dimensions with 2048 and 256 complex data points in the direct and indirect dimensions, respectively. A total of 40 transients were accumulated with a repetition delay of 2 s.

^{31}P NMR spectra were recorded using a phase-cycled Hahn echo pulse sequence with gated broadband proton continuous wave decoupling at a field strength of 20 kHz¹³⁷. A 90° pulse length of 13 μs was used with interpulse delays of 33 μs . Typically 1024 scans were acquired with a recycle delay of 5 s. The acquisition time was set at 10 ms with a 5 μs dwell time. ^2H NMR spectra were obtained using a solid-echo pulse sequence¹⁴⁰ with a 90° pulse length of 2.8 μs , interpulse and repetition delays of 20 μs and 0.5 s, respectively. At least 5000 data points were obtained and typically 2048 scans were acquired with an acquisition time of 5 ms and 1 μs dwell time.

4.4.2 Electrophysiology Methods

We chose to use *Xenopus* oocytes for our electrophysiological recordings as this system enables high level expression of almost all channels including mutant channels that result in expression defects in mammalian systems²⁰⁴.

Molecular biology—The cDNA of Kv11.1 (a gift from Dr Gail Robertson, University of Wisconsin) was subcloned into a pBluescript vector, which contains the 5' untranslated region (UTR) and 3' UTR of the *Xenopus laevis* β -globin gene (a gift

from Dr Robert Vandenberg, University of Sydney). Site-directed mutagenesis of Kv11.1 cDNA was performed using the Quikchange method (Agilent Technologies, Mulgrave, VIC, Australia) and mutations confirmed by Sanger DNA sequencing. WT and mutant channel cDNAs were linearized with BamHI-HF (NEB, Ipswich, MA, USA) and cRNA was transcribed with T7 RNA polymerase using the mMessage mMachine kit (Ambion, Austin, TX, USA).

Oocyte preparation—Female *Xenopus laevis* frogs were purchased from Nasco (Fort Atkinson, WI, USA). The Garvan/St Vincent's Animal Ethics Committee granted approval (ID 14/30) for all animal experiments described in this study. Frogs were anaesthetized by immersion in 0.17 % w/v tricaine. One ovarian lobe was mobilized and ~5 mL removed. The follicular cell layer was digested by using 1 mg/ml Collagenase A (Roche, IN, USA) in Ca^{2+} -free ND96 solution containing (mM): NaCl 96, KCl 2, MgCl_2 1.0 and Hepes 5 (pH adjusted to 7.5 with 5 M NaOH) for ~2 hours. After rinsing with ND96 (as above, plus 1.8 mM CaCl_2) to remove the Collagenase A, stage V and VI oocytes were isolated and stored at 18 °C in ND96 supplemented with 2.5 mM pyruvic acid sodium salt, 0.5 mM theophylline and 50 $\mu\text{g}/\text{ml}$ gentamicin. *Xenopus laevis* oocytes were injected with cRNA and incubated at 18 °C for 24–48 h prior to electrophysiological recordings.

Electrophysiology—Two-electrode voltage-clamp experiments were performed at room temperature (~21 °C) using a Geneclamp 500B amplifier (Molecular Devices Corp, Sunnyvale, CA, USA). We used glass microelectrodes with tip resistances of 0.3–1.0 M Ω , when filled with 3 M KCl. Oocytes were perfused with ND96 solution (see above) during all experiments. A 50 ms +20 mV depolarization step from the holding potential of -90 mV was applied at the start of each sweep to enable off-line leak-current subtraction. We assumed that the current leakage was linear in the voltage range -150 to +40 mV. Data acquisition and analysis were performed using pCLAMP software (Version 10.2, Molecular Devices, Sunnyvale, CA, USA), Excel

software (Microsoft, Seattle, WA, USA) and Prism 6 (GraphPad Software Inc. La Jolla, CA, USA). All parameter values are reported as mean \pm standard error of the mean (SEM) for n experiments, where n denotes the number of different oocytes studied for each construct.

Data analysis— To measure the voltage dependence of activation, cells were depolarized from -70 to $+60$ mV for 3 s (exact voltage range depending on the mutant tested) followed by a step to -70 mV to measure tail current amplitude. Tail current amplitudes were normalized to the maximum tail current value and fitted with a Boltzmann function:

$$I/I_{\max} = \left[1 + e^{(V_{0.5}-V_t)/k} \right]^{-1} \quad (3.1)$$

where I/I_{\max} is the relative tail current amplitude, $V_{0.5}$ is the voltage at which 50 % of channels are deactivated, V_t is the test potential and k is the slope factor. To measure rates of activation, an envelope of tails protocol was used to obtain the rates of activation at $+20$ mV²⁰⁵. The peak tail current amplitudes recorded at -70 mV using different activation duration at $+20$ mV were fitted with a single exponential function to obtain a time constant for activation.

Rates of deactivation were measured from the hooked tail current traces recorded at voltages in the range -70 to -150 mV, following a 1 s depolarization step to $+40$ mV from a holding potential of -90 mV. The decaying phase of the current traces was fitted with a double exponential component to derive both components of channel deactivation. However, only the fast component, is reported in this study. To measure the voltage dependence of deactivation, cells were depolarized to $+40$ mV for 1 s, to ensure channels were fully activated, then stepped to voltages between $+60$ and -100 mV (exact voltage range depending on the mutant tested) for 3 s, followed by a step to -70 mV to measure tail current amplitude²⁰⁶⁻²⁰⁸. Tail current amplitudes were normalized to the maximum tail current value and fitted with a Boltzmann function

using equation 4.1. In experiments in which the free energies associated with voltage-dependent deactivation were examined, the same datasets were fitted with the thermodynamic form of the Boltzmann equation:

$$I/I_{max} = \left[1 + e^{(\Delta G^0 - z_g EF)/RT} \right]^{-1} \quad (4.2)$$

where ΔG^0 is the work done at 0 mV, z_g is the effective number of gating charges moving across the membrane electric field (E), F is the Faraday constant, R is the universal gas constant, and T is the absolute temperature. From equation 4.2, we can also calculate the effect of a mutation on ΔG^0 as follows:

$$\Delta\Delta G_{mt}^0 = \Delta G_{mut}^0 - \Delta G_{WT}^0 \quad (4.3)$$

Double mutant cycle analysis — To investigate whether two residues interact to stabilize the open and/or closed states we used thermodynamic mutant cycle analysis. The interaction energy, $\Delta\Delta G_{int}^0$, between two mutants was calculated as the difference in free energy of the double mutant compared to the sum of the free energy differences of the individual mutants:

$$\Delta\Delta G_{int}^0 = \Delta\Delta G_{mut1+mut2}^0 - (\Delta\Delta G_{mut1}^0 + \Delta\Delta G_{mut2}^0) \quad (3.4)$$

Absolute $\Delta\Delta G_{int}^0$ values of greater than 4.2 kJ mol⁻¹ (i.e. 1 kcal mol⁻¹) were considered significant²⁰⁹⁻²¹⁴.

Statistical analysis — We used one-way ANOVA with Bonferroni post-test analysis to compare rates of deactivation and $V_{0.5}$ of deactivation, or an unpaired t -test when comparing the $\Delta\Delta G^0$ values of double mutants ($\Delta\Delta G_{mut1+mut2}^0$) compared to the sum of $\Delta\Delta G^0$ values of individual mutants ($\Delta\Delta G_{mut1}^0 + \Delta\Delta G_{mut2}^0$) in double mutant cycle analysis experiments. p -values <0.05 were considered significant.

Homology modelling — The crystal structure of a Kv1.2/2.1 channel chimera⁵⁸ was used to generate the homology model of Kv11.1 using Swiss PdbViewer²¹⁵ and the final structure was optimized by using SWISS-MODEL Workspace^{216, 217}.

4.5 Results

An alignment of the S4S5 linkers of different voltage-gated potassium channels is shown in Figure 4.1. The most highly conserved residues are the charged arginine residues from the distal S4, and a glycine residue in the middle of the S4S5 linker. There are also two leucine residues in the S4S5 linker that are highly conserved in the Kv1-Kv9 channels but are replaced by tyrosines in Kv10-12 channels. In the crystal structure of Kv1.2/2.1 chimera, the leucine residues in the S4S5 linker are orientated towards the lipid membrane. It has been shown previously that the S4S5 linker is critical for channel activation and deactivation in Kv11.1^{57, 66, 67, 69} and that many of the S4S5 residues contribute to the slow gating kinetics. Previous studies, however, have largely focused on how the S4S5 linker interacts with cytoplasmic domains. For example: Asp540 interacts with the bottom of the S6 transmembrane domain to stabilize the closed state of Kv11.1 channel⁶⁷ and cysteine scanning studies have suggested that the S4S5 domain interacts with the N-terminal tail⁷¹. The tyrosine residues, however, have not been extensively studied. Our sequence homology analysis, coupled to the location of the S4S5 linker in crystal structures of the activated state, suggest that the two tyrosine residues are likely to contribute to interactions with the membrane and/or intra-membrane domains of the channel.

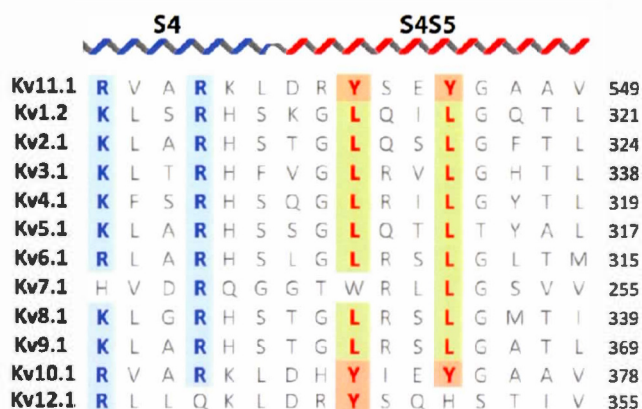


Figure 4.1 Tyrosine residues are conserved among the KCNH family. Sequence alignment of Kv channels for S4 and S4S5 linker regions. Arginine residues in S4 are highlighted in blue and tyrosine residues, conserved

within the KCNH family (Kv10-12), are highlighted in orange. In place of tyrosine, almost all other Kv channels have a leucine at the equivalent sites (green boxes). The topology above the alignment is based on the crystal structure of Kv2.1/1.2 chimeras (2R9R).

To determine if the equivalent residues in Kv11.1 (Tyr542 and Tyr545) are likely to be oriented towards the lipid membrane, we studied the interaction of a peptide (Leu532–Phe551) that contains the S4S5 linker of Kv11.1 channel with dimyristoylphosphatidylcholine (DMPC) or DMPC/dodecylphosphocholine (DPC) model membranes (Figure 4.2). First, solution NMR was used to gain insight into whether the S4S5 linker interacts with the lipid membrane. We recorded 1D ^1H -NMR spectra of the S4S5 peptides in water (Figure 4.2Ai) and in the presence of DMPC/DPC bicelles (Figure 4.2Aii). Comparison of the spectra shows changes in the chemical shifts and significant broadening of the peptides' resonances, consistent with an interaction between the peptide and the model membranes²¹. Phosphorus (^{31}P) and deuterium (^2H) solid-state NMR experiments were then employed to further investigate the interaction of the S4S5 peptide with the membrane using DMPC multilamellar vesicles (MLVs). Since phospholipids harbour a phosphate in their polar headgroup, ^{31}P NMR spectra were acquired to monitor change at the membrane surface. Broad power spectra are characteristic of non-oriented MLVs and represent

the superposition of all chemical shifts from the distribution of orientations in the magnetic field (Figure 4.2*B**i*), with the 90° edge on the right and 0° on the left.

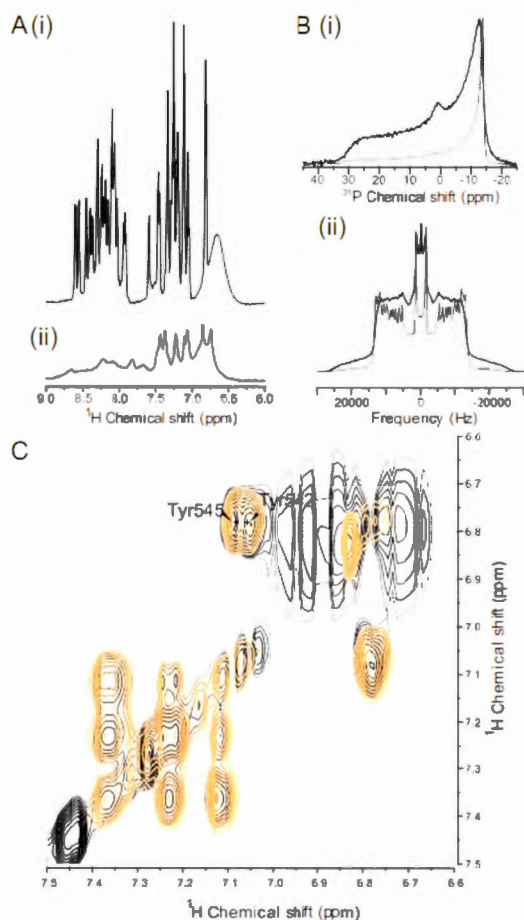


Figure 4.2 Tyrosine residues within the S4S5 linker of Kv11.1 are orientated towards the lipid membrane. *A*, S4S5 peptide (Leu532–Phe551) interacts with the lipid membrane as the amide and aromatic resonances of the ¹H NMR spectra of the WT peptide in DMPC/DPC-d₃₈ are very broad (*panel ii*) compared to S4S5 peptide in 10 % D₂O (*panel i*). *B*, Pure ³¹P (*panel i*) and ²H (*panel ii*) solid-state NMR spectra of DMPC-d₅₄ MLV model membranes (grey) and with S4S5 peptide (black) showing the S4S5 peptide interacts with the lipid membrane. *C*, ¹H TOCSY spectra of the S4S5 peptide solubilized with DMPC-d₅₄/DPC-d₃₈ in 10 % D₂O (black) and with 0.5 mM Gd³⁺

(orange) showing the tyrosine residues (Tyr542 and Tyr545) are protected from soluble paramagnetics by the lipids as the aromatic signals for the Tyr542 and Tyr545 remain.

To probe the bilayer's hydrophobic core, phospholipids with perdeuterated acyl chains (DMPC-d₅₄) were used. The spacing between each doublet on the ²H NMR spectrum is known as the quadrupolar splitting ($\Delta\nu_Q$) and gives insight on the degree

of organisation of the acyl chains (Figure 4.2bii). The largest splitting corresponds to the CD₂ bonds closer to the headgroup, while the smaller splitting corresponds to the most mobile CD₃ group at the end of the lipid chain. Pure lipids ³¹P (Figure 4.2Bi, grey) and ²H (Figure 4.2Bii, grey) spectra were recorded as a reference. The peptide disrupts model DMPC membranes suggesting the formation of fast-tumbling lipid assemblies, as revealed by the isotropic resonance on the ³¹P and ²H spectra (Figure 4.2B, black). Moreover, the ³¹P spectra for the peptide (Figure 4.2Bi, black) shows a change in intensity between the 0° and 90° edges of model membranes (Figure 4.2Bi, grey), with less lipids on the 90° edge which can be ascribed to a change in vesicle shape or transverse relaxation (T₂) effect caused by an increase in slow motions. The peptide mainly interacts with the surface of the membrane since no changes in Δν_Q of ²H spectra are observed, indicative of no deep insertion in the hydrophobic core of the membrane¹⁴². Whilst these data suggest that the S4S5 linker is directly involved in membrane interaction, the orientation of the tyrosine residues was further probed by adding soluble paramagnetic gadolinium lanthanide ions (Gd³⁺) to the samples. The Gd³⁺ ions attenuate the proton signals of the peptide residues that are solvent-exposed⁴⁶. In agreement with solid-state NMR, the TOCSY spectrum of the linker (Figure 4.2C) shows that the tyrosine ring protons are protected from the effect of Gd³⁺. This suggests that Tyr542 and Tyr545 are located facing the membrane.

We first performed alanine-scanning mutagenesis on the S4S5 residues (Asp540-Val549) to investigate how individual residues in the S4S5 linker contribute to the voltage dependence of the distribution between closed and open states (activation) as well as the rate of activation of Kv11.1 channels. Figure 4.3Ai shows the 3 s activation protocol and exemplar traces for WT Kv11.1 channels. The V_{0.5} of activation for WT (-23.9 ± 1.3 mV, n=5). Most of the mutants altered the V_{0.5} of activation when compared to WT with the largest shifts seen for S543A, G546A and A548V (Figure 4.3Aii). The changes observed for Y542A (-7.2 ± 1.5 mV, n=4) and

Y545A (-36.0 ± 1.2 mV, $n=5$) were more modest. Figure 4.3Bi shows the protocol, and typical family of current traces, used to measure the rate of activation at +20 mV (see methods for more details). The time constant for WT (102.5 ± 6.1 ms, $n=8$) and mutants are summarized in Figure 4.3Bii as well as in Table 4.1. Notably, both Y542A and Y545A did not significantly perturb the rate of activation at +20 mV compared to WT.

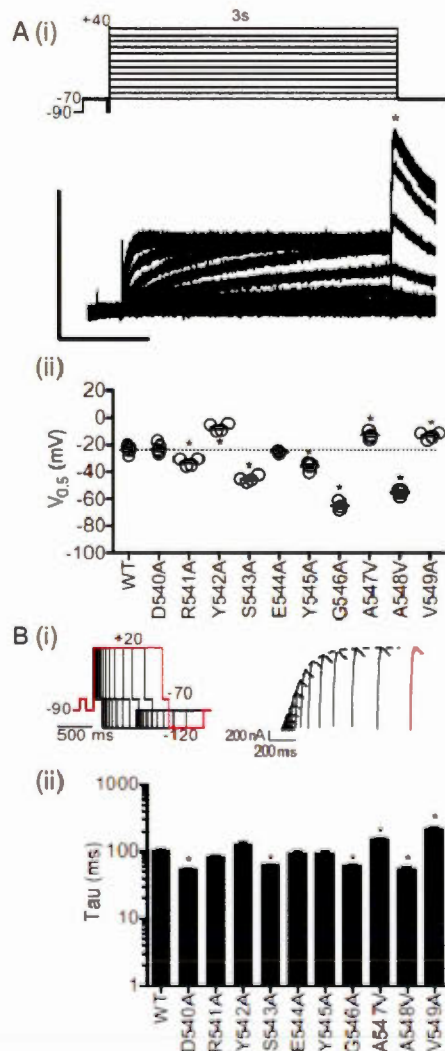
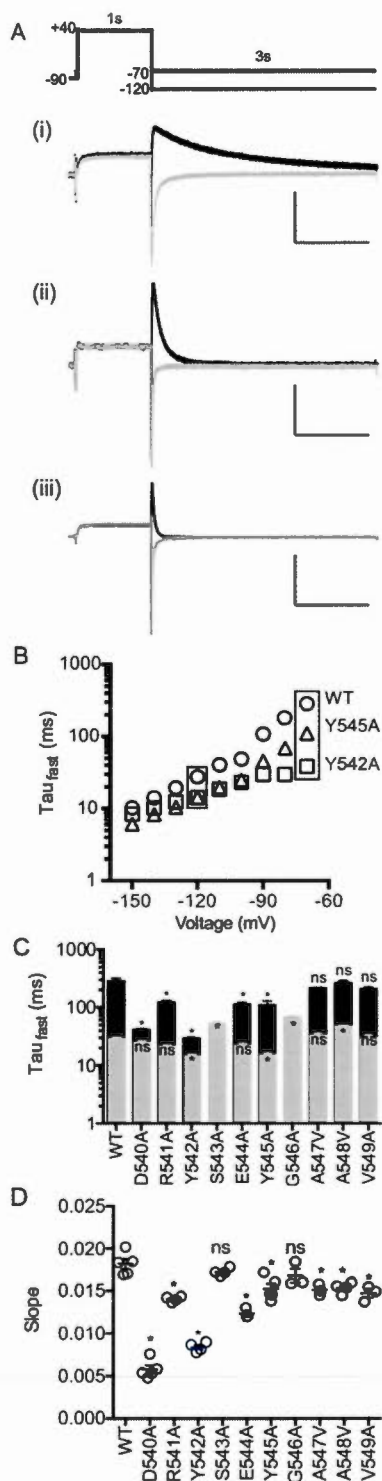


Figure 4.3 Activation properties for S4S5 mutants. *A*, 3 s isochronal activation protocol and example traces of WT. X- and Y-axis are 1 s and 0.25 uA, respectively (*panel i*). The peak tail currents (*) derived from 3 s isochronal activation were fitted with a Boltzmann equation to derive $V_{0.5}$ of activation (*panel ii*). The values for all mutants are summarized in Table 4.1. *B*, Envelope of tail protocol to elicit the tail current at -70 mV after activation at +20 mV. One of the traces and its respective protocol are highlighted (*panel i*). The time constants of activation at +20 mV for WT and S4S5 mutants are summarized in *panel ii*. All summary data are presented as mean \pm S.E.M and statistical comparisons made using one-way ANOVA with Bonferroni post-test. Significant differences ($p < 0.05$) are highlighted with asterisks. The values for all mutants are summarized in Table 4.1.

Mutant	Activation $V_{0.5}$ (mV) (<i>n</i>)	Time constant of activation at +20mV(ms) (<i>n</i>)
WT	-23.9±1.3 (5)	102.5±6.1 (8)
D540A	-23.1±1.7 (5)	55.2±2.2 * (5)
R541A	-33.2±1.3 * (4)	87.0±3.6 (5)
Y542A	-7.2±1.5 * (4)	128.0±11.0 (6)
S543A	-45.5±1.2 * (4)	64.2±1.6 * (7)
E544A	-25.7±0.7 (3)	97.8±2.6 (6)
Y545A	-36.0±1.2 * (5)	97.3±4.5 (7)
G546A	-65.2±2.2 * (3)	63.0±2.8 * (5)
A547V	-13.0±1.8 * (3)	157.2±6.0 * (6)
A548V	-55.3±0.8 * (5)	55.0±5.1 * (7)
V549A	13.3±1.1 * (4)	225.8±15.0 * (7)

Table 4.1 Summary of the values for the 3 s isochronal deactivation $V_{0.5}$, rates of deactivation at -70 mV and -120 mV for S4S5 alanine mutants. Data is presented as mean ± S.E.M (*n*) where *n* denotes number of individual recordings. Only $p < 0.05$ versus WT are reported as significant using one-way ANOVA with Bonferroni post-test.

Previous studies have suggested that activation and deactivation are not simply reciprocal processes but rather occur via different pathways^{202, 208}. We therefore investigated whether any of the S4S5 mutants preferentially altered the deactivation phenotype. Figure 4.4A shows typical examples of 3 s tail current traces recorded at -70 mV (black) and -120 mV (grey) for WT (*i*), Y545A (*ii*) and Y542A (*iii*) following a 1 s step to +40 mV to fully activate the channels. The time constants for the fast component of deactivation in the voltage range from -70 to -150 mV for these three channels are shown in Figure 4.4B. The rates of deactivation of Y545A (triangle) are 2-3 times faster than WT (circle) at all voltages measured. For Y542A (square) the rate of deactivation is more than 10 times faster than WT at -70 mV but at -150 mV there is almost no difference in the rates of deactivation for WT and Y542A channels. A summary of the time constant for the fast component of deactivation at -70 mV (black) and -120 mV (grey) for all S4S5 alanine mutants is shown in Figure 4.4C and in Table 4.2. Figure 4.4D shows a plot of the voltage dependence of the rates of deactivation for all the S4S5 alanine mutants. Mutation to the three charged residues (D540A, R541A and E544A) all reduced the voltage dependence of the rates of deactivation. Conversely, mutations to the uncharged



residues caused only modest changes to the voltage dependence of the rates of deactivation, with the notable exception of Y542A.

Figure 4.4 Kinetics of deactivation for S4S5 alanine mutants. *A*, Cells were depolarized to +40 mV for 1 s and followed by repolarization to -70 and -120 mV for 3 s. Example deactivation current traces acquired at -70 (black) and -120 mV (grey) for WT (*panel i*), Y545A (*panel ii*) and Y542A (*panel iii*). X- and Y- axes are 1 s and 0.25 uA, respectively. *B*, Comparison of time constants of deactivation for WT (circle), Y545A (triangle) and Y542A (square) corresponding to the test voltage range of -150 to -70 mV. *C*, Time constants for the fast component of deactivation at -70 mV (black) and -120 mV (grey) for S4S5 alanine mutants (mean \pm S.E.M). *D*, Summary of the voltage-dependence of the rates of deactivation (mean \pm S.E.) for WT and S4S5 mutants. All summary data are presented as mean \pm S.E.M and statistical comparisons made using one-way ANOVA with Bonferroni post-test. Significant differences ($p < 0.05$) are highlighted with asterisks. The values for all mutants are summarized in Table 4.2.

Table 4.2 Summary of the values for the 3 s isochronal deactivation $V_{0.5}$, rates of deactivation at -70 mV and -120 mV for S4S5 alanine mutants. Data is presented as mean \pm S.E.M and n denotes number of individual recordings. Only $p < 0.05$ versus WT are reported as significant using one-way ANOVA with Bonferroni post-test.

Mutant (n)	Deactivation $V_{0.5}$ (mV)	Time constant of deactivation at -120 mV (ms)	Time constant of deactivation at -70 mV (ms)
WT (5)	-61.3 ± 0.5	27.8 ± 1.3	286.2 ± 32.4
D540A (5)	-25.6 ± 2.0 *	23.8 ± 1.4	41.7 ± 1.4 *
R541A (4)	-46.3 ± 0.8 *	20.4 ± 0.9	124.9 ± 7.5 *
Y542A (5)	-1.6 ± 1.1 *	14.3 ± 0.5 *	29.7 ± 0.7 *
S543A (4)	-78.6 ± 0.6 *	49.3 ± 3.6 *	N/A
E544A (3)	-40.3 ± 1.4 *	21.1 ± 1.8	113.7 ± 9.0 *
Y545A (5)	-46.4 ± 1.1 *	14.4 ± 1.1 *	110.4 ± 18.6 *
G546A (4)	-82.0 ± 0.2 *	64.7 ± 2.2 *	N/A
A547V (3)	-56.5 ± 1.1	31.2 ± 2.8	217.3 ± 3.4
A548V (5)	-64.8 ± 0.6	45.1 ± 1.7 *	268 ± 21.8
V549A (4)	-53.3 ± 1.1 *	28.4 ± 3.1	208.7 ± 15.9

We next investigated how S4S5 mutants affected the voltage dependence of the distribution between open and closed states when starting from the open state, i.e. we measured 3 s isochronal deactivation curves to derive the $V_{0.5}$ of steady-state deactivation²⁰⁷. Figure 4.5A shows WT Kv11.1 channels recorded from a 3 s isochronal deactivation protocol. The midpoint of the voltage dependence of deactivation $V_{0.5}$ derived by fitting the normalized amplitude of the -70 mV tail currents for WT (circle), Y542A (square) and Y545A (triangle) using Boltzmann function (Equation 4.1) were -61.3 ± 0.5 mV ($n=5$), -1.6 ± 1.1 mV ($n=5$) and -46.4 ± 1.1 mV ($n=5$) respectively (Figure 4.5B). Y542A caused the largest depolarizing shift in the $V_{0.5}$ of deactivation of all the S4S5 alanine mutants whereas Y545A caused a more modest but still statistically significant depolarizing shift in the $V_{0.5}$ of deactivation (Figure 4.5C).

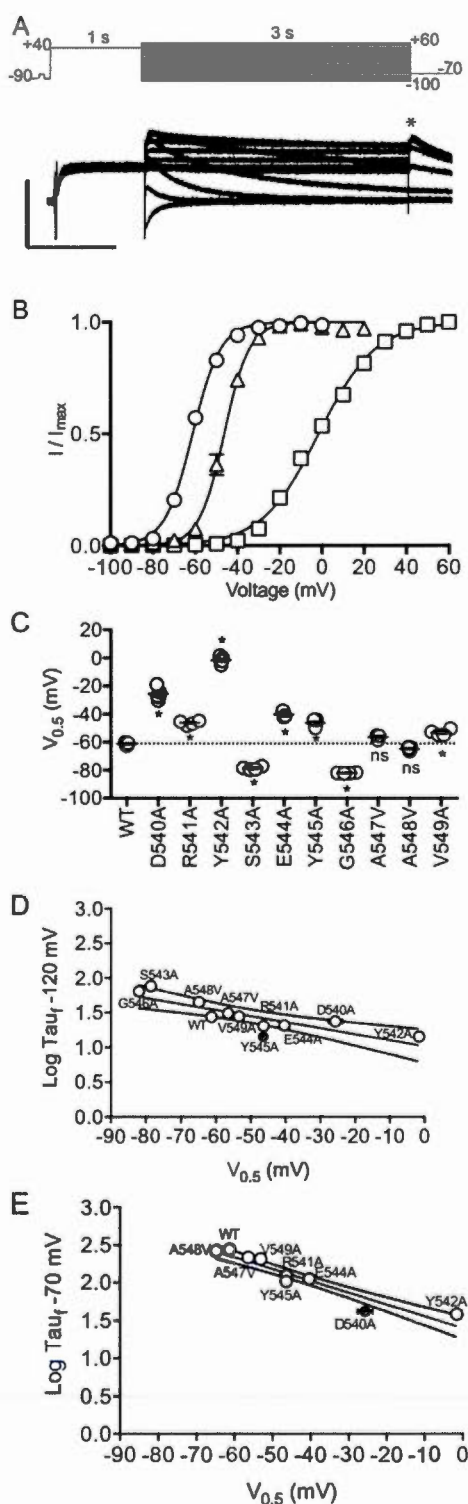


Figure 4.5 Voltage dependence of the distribution between open and closed states for S4S5 mutants. *A*, 3 s isochronal deactivation protocol and example traces for WT. X- and Y-axes are 1 s and 0.25 uA, respectively. *B*, The peak tail currents (*) derived from 3 s isochronal deactivation were fitted with Boltzmann equation to derive $V_{0.5}$ values. The $V_{0.5}$ values are WT: -61.3 ± 0.5 mV (mean \pm S.E.M, $n=5$; circle), Y545A: -46.4 ± 1.1 mV (mean \pm S.E.M, $n=5$; triangle) and Y542A: -1.6 ± 1.1 mV (mean \pm S.E.M, $n=5$; square). *C*, Summary of the deactivation $V_{0.5}$ of all S4S5 alanine mutants. Only $p < 0.05$ versus WT are reported as significance using one-way ANOVA. The 3 s isochronal deactivation $V_{0.5}$ values for all mutants are summarized in Table 4.2. *D* and *E*, Relationship between time constants of deactivation for S4S5 alanine mutants at -120 mV and -70 mV, respectively, and their corresponding deactivation $V_{0.5}$. Linear regression was applied (straight line) with 95 % confidence interval (CI) of the fit. Residues outside the 95 % CI are highlighted as filled circles.

Perturbations to the rates of deactivation in the S4S5 alanine mutants could be caused by either a change in the electrochemical driving force for deactivation and/or due to a change in the transition state energy barrier separating the open and closed states, i.e., there can be thermodynamic and/or kinetic components. To explore these two components, we have plotted the time constants for the fast component of deactivation at -120 and -70 mV versus the $V_{0.5}$ for 3 s isochronal deactivation for all S4S5 alanine mutants (Figure 4.5D-E). When kinetics were measured at -120 mV, most of the alanine mutants, with the notable exception of Y545A, reside within the 95 % confidence interval obtained from a regression line fitted to the rate of deactivation *versus* isochronal deactivation $V_{0.5}$ data. This suggests that much of the change in the rates of deactivation at -120 mV for these S4S5 alanine mutants can be explained by changes in the thermodynamics of deactivation gating. Conversely, for Y545A, the rate of deactivation is much faster than would have expected from the simple change in the $V_{0.5}$ of deactivation. Consistent with this data at -120 mV, the change in the rates of deactivation at -70 mV for the S4S5 alanine mutants can also be explained by changes in the thermodynamics of deactivation gating, except for D540A and Y545A, whose mean values lie outside of the 5-95 % confidence intervals. Note that S543A and G546A were excluded from analysis as these mutant channels did not deactivate at -70 mV. Our data show that whereas Y542A clearly affected the thermodynamics of deactivation gating, Y545A appeared to have a significant kinetic component on top of the alteration to the thermodynamics of deactivation gating.

As alanine mutagenesis of the two tyrosine residues appear to have quite distinct phenotypes in terms of effects on activation/deactivation, but both resulted in accelerated rates of deactivation with minimal perturbation on the rate of activation. We thus focus our investigation on the deactivation phenotypes of Tyr545 and Tyr542. Each tyrosine residue was mutated to Ala, Leu, Ile, Phe or Trp. All of the Tyr542 and Tyr545 mutants resulted in accelerated rates of deactivation, with the

exception of Y545F (Figure 4.6A). Mutations at Tyr542 tended to cause greater perturbations to the $V_{0.5}$ of deactivation than mutations at Tyr545 (Figure 4.6B). A plot of the perturbation to the rate of deactivation (measured at -70 mV) versus the change in $V_{0.5}$ of deactivation, for the groups of mutants at Tyr542 and Tyr545, highlights that mutations to Tyr542 predominantly affect the thermodynamics of channel deactivation, whereas mutations to Tyr545 cause relatively more perturbation to the kinetics of deactivation gating (Figure 4.6C).

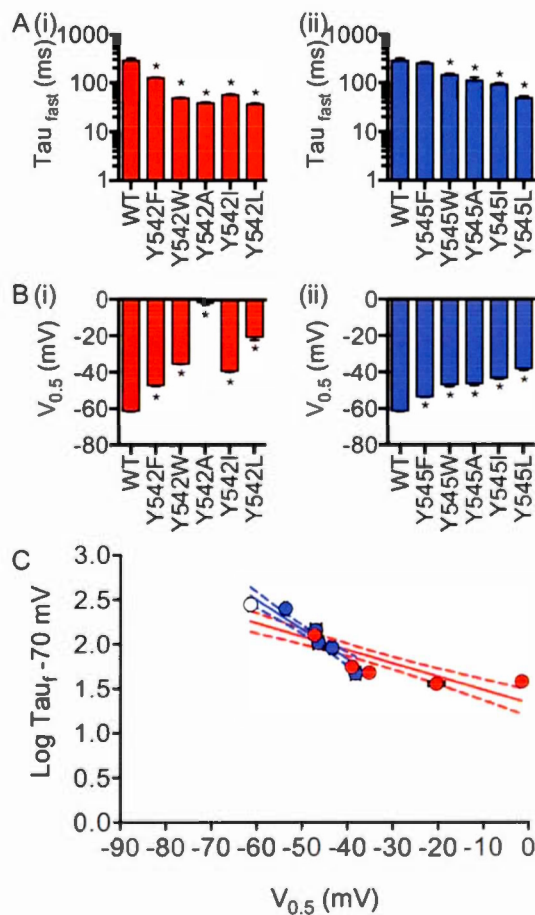


Figure 4.6 Tyr545 (blue) is functionally different to Tyr542 (red). *A*, Time constants of deactivation at -70 mV for different Tyr542 (*panel i*) and Tyr545 (*panel ii*) side-chain residues. *B*, 3 s isochronal deactivation $V_{0.5}$ for Tyr542 (*panel i*) and Tyr545 (*panel ii*) side-chain residues. Data is presented as mean \pm S.E.M. Only $p < 0.05$ versus WT are reported as significant using one-way ANOVA with Bonferroni post-test. *C*, Relationship between rates of deactivation for different WT (white), Tyr542 (red) and Tyr545 (blue) side-chain residues at -70 mV and their corresponding deactivation $V_{0.5}$. Linear regression with 95 % confidence interval was fitted to each dataset.

As mutations to Tyr542 significantly perturbed the voltage dependence of the equilibrium distribution of the open and closed states, we probed for residues that might interact with Tyr542 in the open or closed state by using double mutant cycle analysis. Based on our homology model (Figure 4.7A), Tyr542 lies in close proximity to Val535 and Arg537 in S4 and Ile560 in S5. Figure 4.7Bi shows the 3 s isochronal deactivation curves for WT (black circle), I560A (black square), Y542A (white circle) and I560A+Y542A (grey circle). I560A is WT-like whereas Y542A has a large depolarizing shift. The double mutant I560A+Y542A has an intermediate phenotype between I560A and Y542A. The method for calculating interaction energies and a plot of the $\Delta\Delta G^0$ values for I560A, Y542A and I560A+Y542A are shown in Figure 4.6Bii. The $\Delta\Delta G^0$ value for I560A+Y542A (grey bar) is less than the sum of the $\Delta\Delta G^0$ values for the two individual mutants, indicative of an energetic interaction between these two residues. In addition to Ile560, the double mutant cycle analysis indicates that Tyr542 is energetically coupled to Val535 and Arg537 (Figure 4.7C). In contrast, double mutant cycle analysis of Y545A with three residues (Ile560, Ser654 and Asn658) did not reveal any significant energetic interactions (Figure 4.7C). A summary of the experimental $\Delta\Delta G^0$ values for all single and double mutants and their interaction energies are shown in Table 4.3.

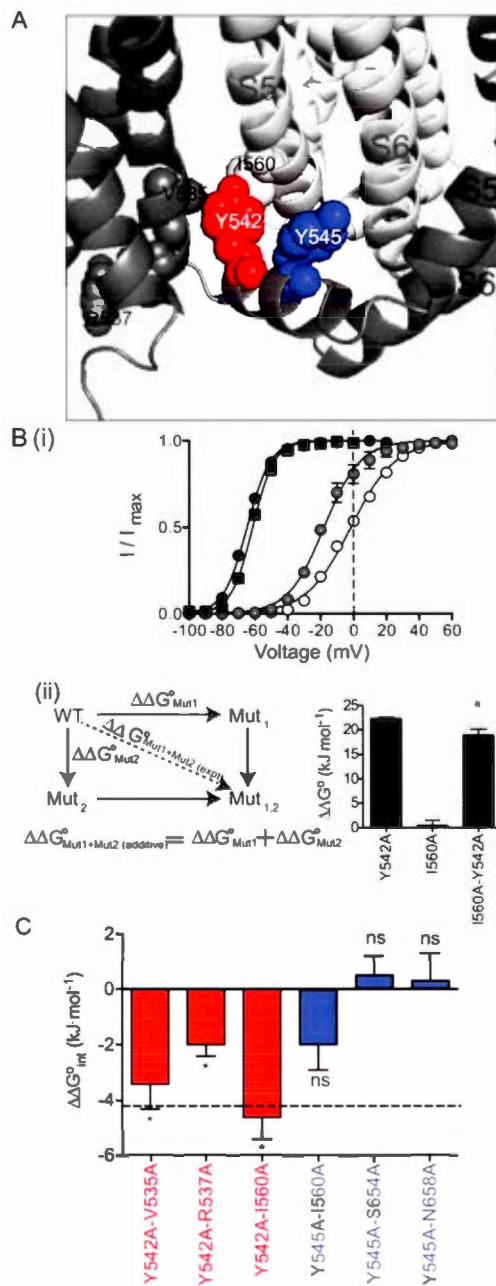


Figure 4.7 Double mutant cycle analysis of Tyr542 and Tyr545. *A*, Orientation of Tyr542 (red) and Tyr545 (blue) within the S4S5 linker and the residues that were energetically coupled. *B*, 3 s isochronal deactivation curves for WT (black circle), I560A (black square), Y542A (white circle) and I560A+Y542A (grey circle). 0 mV was indicated by dotted lines to show the differences between the individual and double mutations (*panel i*). The additivity effect $\Delta\Delta G^0_{\text{Mut1+Mut2 (additive)}}$ is the summation of $\Delta\Delta G^0$ from the individual mutation (*panel ii*). Comparison between the $\Delta\Delta G^0$ obtained from experiment (black) and additivity effect (grey) for double mutant I560A and Y542A are shown on the right of *panel ii*. *C*, Summary of the double mutant cycle analysis displayed as the $\Delta\Delta G^0_{\text{Mut1+Mut2 (int)}}$ for the Tyr542 double mutants (red) and Tyr545 double mutants (blue). * indicates statistical differences,

$p < 0.05$ using an unpaired t -test when comparing the experimentally derived $\Delta\Delta G^0$ for the double mutant with the sum of the $\Delta\Delta G^0$ values for the two individual mutants. Only the double mutant I560A-Y542A has an interaction energy greater than 4.2 kJ mol^{-1} , indicated by the dotted line. Data is presented as mean \pm S.E.M.

4.6 Discussion

Kv11.1 channels have unusual kinetics, which include rapid recovery from inactivation and slow deactivation. In the heart, the slow deactivation kinetics play a particularly important role in the suppression of propagation of ectopic beats that occur during the early diastolic interval¹⁹⁸. The S4S5 linker clearly plays a critical role in deactivation gating of voltage-gated K⁺ channels, including Kv11.1 channels^{57, 67, 70}. Here, we have shown that two tyrosine residues in the S4S5 linker, Tyr542 and Tyr545, play important, but distinct, roles in stabilizing the open state of the Kv11.1 channel and thus in mediating the slow deactivation gating of Kv11.1 channels.

Tableau 4.3 Summary of the values for the $\Delta\Delta G^0$ (mean \pm S.E.M) and n denotes number of individual recordings.

Mutant (n)	$\Delta G^0_{(expt)}$ (kJ·mol ⁻¹)	$\Delta\Delta G^0_{(Mut-WT)}$ (kJ·mol ⁻¹)	$\Delta\Delta G^0_{(Mut1+Mut2)}$ ($\Delta\Delta G^0_{(Mut1)} + \Delta\Delta G^0_{(Mut2)}$) (kJ·mol ⁻¹)
WT(5)	-22.7 \pm 0.6	-	
Y542A(5)	-0.3 \pm 0.2	22.3 \pm 0.2	
V535A(3)	-20.8 \pm 1.8	1.8 \pm 1.8	
R537A(4)	20.1 \pm 0.6	2.6 \pm 0.6	
I560A(3)	-22.1 \pm 1.0	0.5 \pm 1.0	
Y542A-V535A(5)	-1.8 \pm 0.1	20.8 \pm 0.1	-3.4 \pm 0.9*
Y542A-R537A(3)	0.3 \pm 0.1	22.9 \pm 0.1	-2.0 \pm 0.4*
Y542A-I560A(4)	-4.4 \pm 1.1	18.2 \pm 1.1	-4.6 \pm 0.8*
Y545A(5)	-19.5 \pm 0.6	3.2 \pm 0.6	
I560A(3)	-22.1 \pm 1.0	0.5 \pm 1.0	
S654A(4)	-23.7 \pm 1.0	-1.1 \pm 1.0	
N658A(4)	-17.2 \pm 1.1	5.5 \pm 1.1	
Y545A-I560A(4)	-21.0 \pm 1.2	1.7 \pm 1.2	-2.0 \pm 0.9
Y545A-S654A(3)	-20.1 \pm 0.4	2.6 \pm 0.4	0.5 \pm 0.7
Y545A-N658A(4)	-13.7 \pm 1.2	8.9 \pm 1.2	0.3 \pm 1.0

* means statistically different from their corresponding additive effect

In this study, mutations to Tyr542 resulted in large shifts in the voltage dependence of the equilibrium distribution between the open and closed states, with all mutants shifting the equilibrium in favour of the closed state (Figure 4.6Bi). All Tyr542 mutants also resulted in an acceleration of the rates of deactivation (Figure 4.6Ai). These results are consistent with a role for Tyr542 in stabilizing the open state of the channel (Figure 4.6Di). Mutating Tyr542 to alanine caused a marked acceleration of the rates of deactivation with a shallow slope (Figure 4.4D). The fact that the slope of the voltage dependence of rates of deactivation for Y542A is much shallower than that of WT or Y545A suggests that the native Tyr542 interacts with, and so influences, the motion of the VSD during deactivation. This conclusion is consistent with our mutant cycle analysis experiments indicating an energetic interaction between Tyr542 and Arg537, as well as with Val535 and Ile560 (Figure 4.7), although only the interaction with Ile560 exceeds the 1 kcal mol^{-1} threshold that is often used to indicate biologically relevant interactions²⁰⁹⁻²¹⁴.

In contrast to Tyr542, mutations to Tyr545 caused less perturbation to the voltage dependence of the equilibrium distribution between the open and closed states (Figure 4.6Bii) but still caused a marked acceleration of the rates of deactivation (Figure 4.6Bi). This suggests that Tyr545 might form important interactions that stabilize the transition state complex; however these interactions are destabilized by mutations, i.e. lower the energy barrier for channel deactivation. This suggestion is also consistent with the thermodynamic mutant cycle analysis experiments, which showed that there were no significant energetic interactions involving Tyr545 and other residues in the stable end states. However, at this stage we cannot determine the nature of such interactions. They could be with transmembrane domain residues and/or with the membrane lipids. Given that the NMR experiments suggest that the peptide mainly interact with the surface of the membrane (since there were no changes in Δv_Q of ^2H spectra), if there are any specific interactions between Tyr545

and the membrane these would most likely involve interactions with the lipid headgroups.

The S4S5 linker is thought to be essential to transmit conformational changes of the voltage sensor to the pore domain, as evidenced by its proximity to the S6 helix in the crystal structure of the Kv1.2 channel, as well as its direct interaction with the S6 domain⁶⁷. Previous studies of the S4S5 linker in Kv11.1 channels have focused on its role in linking the voltage sensor domain to the activation gate at the intracellular end of the pore domain^{59, 67}, as well as its role in mediating interactions with cytoplasmic domains that can also modulate deactivation gating⁷¹. Our NMR studies of a peptide that contains the Kv11.1 S4S5 linker in a model membrane indicate that both Tyr542 and Tyr545 are likely to point towards the membrane, which is consistent with the homology model based on the structure of the activated Kv1.2/2.1 channel (see Fig. 4.7A). This suggests that the S4S5 linker could also have important interactions with the membrane directly and/or with residues in the transmembrane domains of the channel. We have clear evidence that Tyr542 interacts with other transmembrane domain residues. However, the relatively small magnitude of this interaction (e.g. -4.6 kJ mol^{-1} for Y542A-I560A) suggests that other factors might be involved, which could include interactions between Tyr542 and the membrane. Tyr545 interactions with the membrane contributing to the stabilization of the transition state in the pathway connecting the activated state with the closed states are also plausible but we do not yet have definitive proof of such interactions.

Recently, Lörinczi *et al.*²⁰² showed that cutting the S4S5 linker of Kv11.1 channels in half could still produce functional channels with normal activation but accelerated deactivation. This indicates that the major role of S4S5 linker is to stabilize the open state and it is conceivable that the split S4S5 linker in the Kv11.1 prevents the interaction promoted by the S4S5 linker with other parts of the channel in the activated state. It is also possible that the split S4S5 may disrupt its interaction with

the lipid membrane. It is unlikely that a split S4S5 linker would maintain a continuous helix that lies parallel to the membrane in the activated state of the channel^{33, 218-222}. Our functional studies provide complementary information that is consistent with recent findings²⁰² by showing that the two conserved tyrosine residues play important but distinct roles in stabilizing the open state of Kv11.1 channels.

4.7 Complément au chapitre: *Saturation transfer difference* (STD) par RMN en solution

Nous avons effectué des expériences de STD par RMN en solution afin d'identifier les régions spécifiques de la membrane interagissant avec le segment S4S5⁸⁵. Malheureusement les résultats n'ont pas été retenus dans la révision publiée de l'article. Tel que décrit au chapitre I (section 1.4.2), l'expérience STD consiste à irradier différentes résonances lipidiques, telles que les groupements choline se trouvant à la surface de la membrane, les groupements glycérols qui sont à l'interface polaire/apolaire, ainsi que les méthyles terminaux des chaînes acyles qui sont au centre du cœur hydrophobe de la membrane. La saturation des lipides est transmise aux résidus du segment S4S5 qui sont à proximité aidant ainsi à identifier leur position dans la membrane.

Afin de différencier les résidus tyrosines (Y542 et Y545) du segment du hERG, nous avons fait les mesures de STD avec deux peptides mutants : Y542W et Y545W – i.e. que la tyrosine a été remplacée par une tryptophane. Ceci nous a permis d'identifier l'effet des tyrosines sur l'interaction avec la membrane.

4.7.1 Matériel et méthode

Les peptides S4S5 (LVRVARKLDRYSEYGAVLF), Y542W (LVRVARKLDRWSEYGAVLF) et Y545W (LVRVARKLDRYSEWGAVLF) ont

été synthétisés à >98 % de pureté par *GL Biochem Ltd.* (Shanghai, China). Les lipides dimyristoyl-PC protonés (DMPC) ont été achetés de *Avanti Polar Lipids* (Alabaster, AL, USA) tandis que le dodécyl-PC deutéré (DPC-d₃₈) provient de Sigma Aldrich (Oakville, ON, Canada). L'oxyde de deutérium (D₂O) a été obtenu de *CDN Isotopes* (Pointe-Claire, QC, Canada).

Les mesures de STD ont été effectuées avec des bicelles de DMPC/DPC-d₃₈ ayant un ratio molaire $q = 1$, ainsi qu'un ratio lipide/peptide de 50:1. La DPC deutérée a été employée afin d'alléger les spectres ¹H, ainsi que pour identifier les interactions du peptide dans la région plane de la membrane, minimisant ainsi la détection des contacts peptidiques avec la région courbée des bicelles où la DPC prédomine. Les échantillons de bicelles, contenant 2 mM de peptide, ont été préparés en mélangeant les lipides et le peptide lyophilisés dans une solution de 10 % D₂O et en effectuant des cycles de congélation (N₂ liquide), décongélation (50°C) et de vortex un minimum de trois fois. La concentration lipidique a été maintenue largement au-dessus de la concentration micellaire critique (CMC). Le pourcentage d'hydratation des échantillons a été maintenu à 88 % masse/volume (w/v).

4.7.2 Expériences de STD

Les expériences de STD ont été enregistrées sur un spectromètre *Varian Inova Unity 600* hybride (solution/état solide) (Agilent, Santa Clara, CA, USA) opérant à une fréquence de 599.95 MHz pour le ¹H. Une sonde 3 mm double résonance de gradient-z indirecte a été employée en RMN des solutions. Les déplacements chimiques du ¹H ont été référencés de manière interne en ajoutant 0.5 mM d'acide 2,2-diméthyl-2-silapentane-5-sulfonique (DSS) qui a été réglé à 0.0 ppm.

Les expériences de STD consistent en une série d'impulsions gaussiennes sélectives de 50 ms séparées de délais de 0.1 ms et suivies d'une suppression d'eau *WET*^{85, 133}.

Les fréquences de saturation ont été alternées entre la résonance qui devait être saturée (*on-resonance*) et -25 ppm (*off-resonance*). Les résonances des groupements de la DMPC qui ont été saturées sont les suivantes : la choline ($\text{N}(\text{CH}_3)_3$) à 3.25 ppm, le glycérol à 4.03 ppm, et les méthyles terminaux des chaînes acyles à 0.84 ppm. Les impulsions gaussiennes ont été appliquées à un champ de radio-fréquence ayant une puissance de 120 Hz et les temps de saturation variaient de 250 ms à 5 s. Le délai de recyclage était de 4 s avec 32 scans.

Les variations causées par le transfert de saturation sur les pics des protons (^1H) des groupements amides et aromatiques ont été examinés afin d'éviter le chevauchement avec les résonances lipidiques. Toutes les expériences ont été dupliquées.

4.7.3 Résultats et discussion

Les effets de la saturation des groupements choline, glycérol et méthyles terminaux de la DMPC ont été observés sur les protons (^1H) aromatiques C(2,6)H et C(3,5)H de la Tyr542 et de la Tyr545 des segments S4S5, Y542W et Y545W du hERG (Fig. 4.8). Nos résultats démontrent des grandes barres d'erreurs, puisque l'intensité des pics n'était pas facilement mesurable sur les spectres avec saturation (*on resonance*). Tel qu'expliqué à la section 1.4.2 du chapitre I, si l'interaction entre le peptide et la membrane est trop forte, tel que semble être le cas pour le segment S4S5 (Fig. 4.2), ceci peut entraîner des mauvais résultats en STD. Idéalement, les mesures STD sont optimales lorsque les peptides peuvent échanger librement entre l'état lié et libre¹³⁵. Le segment S4S5 semble avoir une forte affinité pour la membrane. La concentration du peptide en solution (état libre) étant trop faible, les effets de la saturation ne peuvent être détectés de manière reproductible. Ces résultats appuient les conclusions de la publication, à savoir que les Tyr542 et 545 interagissent avec la membrane.

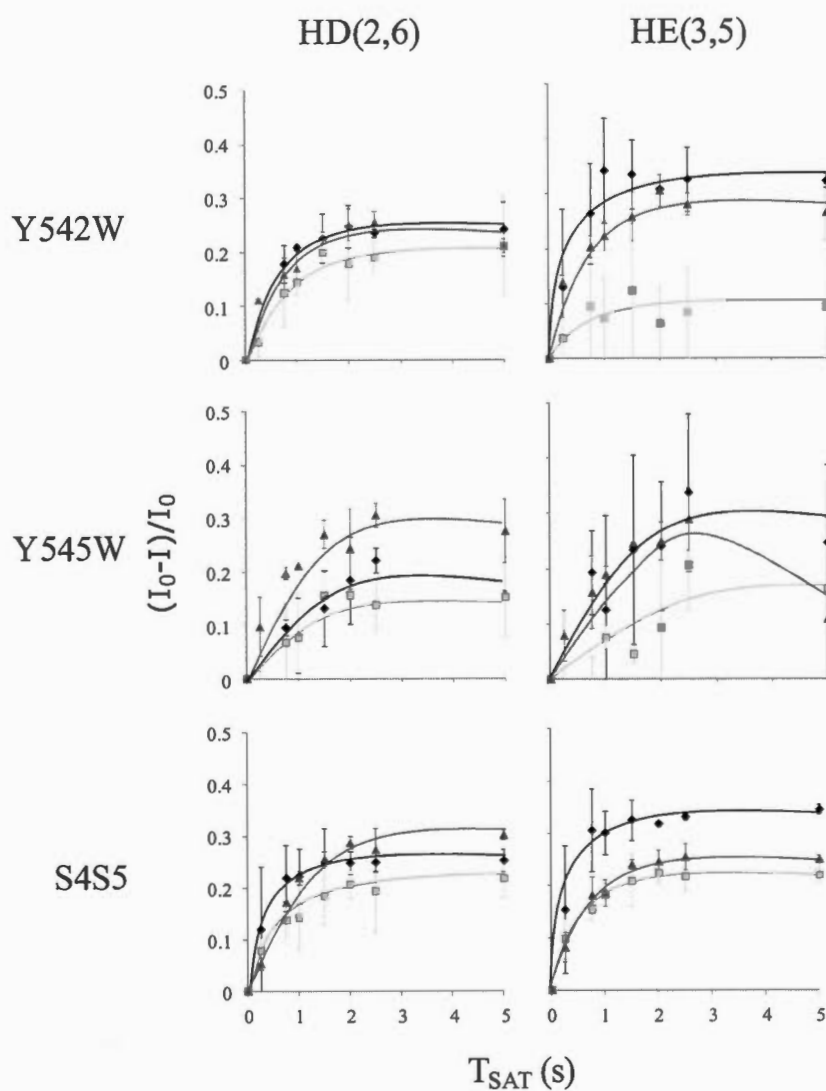


Figure 4.S1 Courbes STD des protons aromatiques ($C^{(2,6)}H$ and $C^{(3,5)}H$) des Tyr542 and Tyr545 des peptides S4-S5 du hERG (Y542W, Y545W, S4S5) solubilisés dans des bicelles de DMPC/DPC- d_{38} $q=1$ à 25 °C lorsque les groupements choline (◆), glycérol (■), and méthyl terminaux (▲) de la DMPC sont saturés.

CHAPITRE V

CHARACTERIZATION OF MAGNETICALLY-ORIENTABLE TWEEN-BASED MODEL MEMBRANES FOR NMR APPLICATIONS

Andrée E. Gravel, Alexandre A. Arnold, Matthieu Fillion, Michèle Auger et Isabelle
Marcotte

Article en soumission à Langmuir.

Contribution des auteurs : IM a conçu, coordonné l'étude et participé à l'analyse des résultats. AEG, AAA, MF, MA et IM ont rédigé l'article. AEG a conçu, effectué et analysé les expériences de RMN. MF a conçu, effectué et analysé les expériences d'infrarouge. AAA a assisté avec la conception et l'acquisition des données RMN.

5.1 Résumé

Dans cette étude, nous proposons un nouveau système mimétique membranaire qui contient un détergent qui élastifie la membrane, plus communément connu sous le nom de *Tween 80* (TW80) et formant des systèmes orientés visant des applications de RMN à l'état solide. Le TW80 est un esther d'acide gras (oléate) de sorbitane polyoxyéthylène reconnu pour être un surfactant non ionique doux. Les systèmes de membranes modèles phosphatidylcholine (PC)/TW80 ont été caractérisés par RMN du ^{31}P et ^2H ainsi que par spectroscopie infrarouge. Les bicouches étant composées de dimyristoylPC (14:0) ou de dipalmitoylPC (16:0) s'auto-assemblent avec le TW80 pour former des structures allongées s'orientant et maintenant leur alignement sur une gamme étendue de ratios molaires et de températures. Le détergent TW80 pourrait être exploité afin d'extraire de manière efficace des protéines membranaires et d'améliorer l'orientation des membranes en évitant l'élimination du détergent.

5.2 Abstract

In this study, we provide a new membrane mimetic system made of a membrane softening detergent commonly known as Tween 80 (TW80), to form oriented systems for solid-state NMR applications. TW80 is a fatty acid ester (oleate) of sorbitan polyethoxylate known to be a mild non-ionic surfactant. Phosphatidylcholine (PC)/TW80 model membrane systems were characterized by ^{31}P and ^2H solid-state NMR as well as infrared spectroscopy. Bilayers made of dimyristoylPC (14:0) or dipalmitoylPC (16:0) were shown to self-assemble with TW80 to form elongated oriented structures which maintain alignment over a wide range of molar ratios and temperatures. TW80 detergent could be exploited to allow for efficient membrane protein extraction and enhanced membrane orientation by avoiding detergent removal.

5.3 Introduction

The plasma membrane acts as a semi-permeable barrier which separates and compartmentalizes the cell. It also plays an important role in many biological processes such as protein scaffolding and cell signaling. It is thus essential to investigate the organization and any perturbations of this important biological lipid bilayer at a molecular level. The complexity of a native biological membrane can be problematic for some spectroscopic methods, such as nuclear magnetic resonance (NMR), thus membrane mimetic systems are useful tools to better understand the membrane structure and interactions.

A variety of model membranes exist, such as micelles, liposomes, or bicelles, depending on biological and experimental requirements. As summarized by Warschawski *et al.*, several criteria should be considered when choosing a membrane mimetic system. First, the lipids must mimic as closely as possible the native environment in order to maintain innate structures and functions. Also, the model

must allow the acquisition of high quality spectra. Some physical parameters are best to be taken into consideration, such as the temperature range stability, which should cover that of the experiment to be performed and should preserve the sample life in time. Furthermore, morphology, size, and composition of model membranes will dictate the NMR experiment to be used.

Bicelles, or bilayered micelles, are useful tools for studying membrane proteins (MPs) by NMR since their composition and local morphology resemble those of biomembranes⁹⁰. Commonly comprised of dimyristoylphosphatidylcholine (DMPC) and dihexanoylPC (DHPC) as the long- and short-chain lipids, respectively, DMPC can be substituted by a variety of saturated and unsaturated lipids with zwitterionic or charged headgroups. Bicelles can also be prepared by mixing a lipid with a non-lipid surfactant such as Triton X-100⁹⁹ and CHAPSO⁹⁷. Often found as disks, bicelles can also form vesicles or perforated vesicles depending on the long-to-short-chain lipid molar ratio (q) and temperature¹⁰⁴. Bicelles are known to spontaneously align in the magnetic field where the bilayer normal is perpendicular to the magnetic field direction. This is due to the magnetic susceptibility anisotropy of the phospholipids¹⁰¹. The perpendicular alignment is achieved when the temperature is above the lipids' gel-to-fluid phase transition temperature (T_m), and when the q ratio and total lipid concentration are high enough⁹⁰. Oriented bicelles are of great interest for solid-state NMR applications since, notably, they allow determining of the orientation of transmembrane peptides and proteins^{102, 103, 145}. The positioning of MPs with respect to the membrane is of great importance since it will give insight on the protein function and interaction mechanism. It is also possible to achieve a parallel alignment of bicelles with respect to the external magnetic field by adding small amounts of paramagnetic lanthanide ions¹⁴⁶. This strategy improves spectral resolution since, for example, it doubles the ¹⁵N and ²H NMR frequency ranges, thus the protein orientation relative to the surrounding membrane, becomes independent of its azimuthal orientation and axial diffusion rate²²³.

Detergents, such as n-dodecyl-PC (DPC) and n-dodecyl- β -D-maltoside (DDM) are commonly used in protein purification. In an aqueous environment, these surfactants spontaneously form micelles which are frequently used for structural studies of MPs by solution NMR because of their fast tumbling which averages out orientation-dependent interactions, thus increasing spectral resolution²²⁴⁻²²⁶. However, the micelles' morphology is different to that of biomembranes; therefore detergents are often removed before membrane reconstitution. Detergent removal can be tedious and time consuming and can significantly lower the MP yield. A more suitable alternative to using detergent-only models for NMR studies of MPs would be opting for a combination of lipids and detergents. Such model more closely resembles the natural lipid bilayers while maintaining spectral resolution. We propose a new membrane model made of phospholipids and a commonly used detergent, Tween 80.

Polysorbate 80, also commercially known as Tween 80[®], is a fatty acid ester (oleate) of sorbitan polyethoxylate with a multi-headed structure of four hydrophilic moieties, one of which is extended by an alkyl chain (Fig. 5.1A). This mild non-ionic surfactant is known for its uses as an excipient in the pharmacology industry and as an emulsifier in the food industry, but also for extracting soluble and membrane-bound proteins²²⁷⁻²³⁰. Tween 80 (TW80) has been known for increasing protein extraction yields while maintaining the enzymatic functions of proteins like *Aspergillus niger*'s lipase²³¹ and a putative hemolysin extracted from *Pasteurella multocida*²³². A lesser known use for TW80 is as a bilayer softening component to generate transferosomes. These elastic liposomes are utilized as transdermal delivery systems to enhance drug permeation in a tissue of interest, such as the skin^{233, 234}.

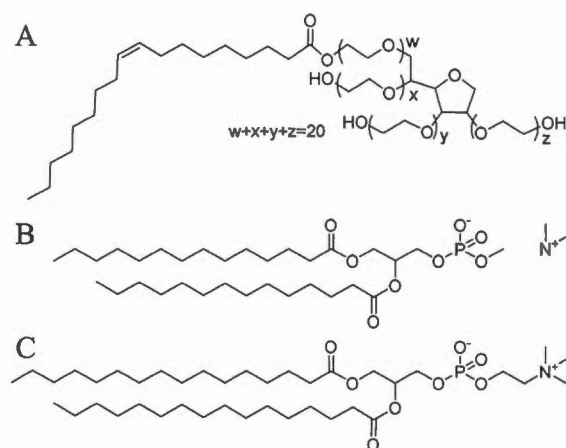


Figure 5.1 Molecular structures of Tween 80 (A), dimyristoyl-PC (B) and dipalmitoyl-PC (C).

In this work, we examined the possibility of combining the membrane softening ability of Tween 80 with the phospholipids' propensity to align in a magnetic field to form oriented model membranes for solid-state NMR applications. The same surfactant would thus be exploited not only to extract membrane proteins but also to enhance the membrane orientation, thus preventing the detergent removal step. Phosphatidylcholines – abundantly found in biological membranes and also known for maintaining the activity of MPs⁹¹ – were used. More specifically, we have chosen DMPC frequently used in model membranes for NMR studies, as well as dipalmitoyl-PC (DPPC) which acyl chain length more closely resembles that of eukaryote biomembranes (Fig. 5.1B and C). We established the adequate surfactant-lipid (q) molar ratios for membrane orientation and measured the quality of this orientation. Because the softening ability of surfactants is a well-known property, we anticipate that our proposed approach could be generalized to other surfactants²³⁵. In addition, the formation of soft and magnetically-orientable bilayers is less restrictive than the requirements for adopting a bicelle morphology. The first report of magnetically-induced bilayer orientation was of *Escherichia coli* phospholipid extracts²³⁶. This has also been observed with other studies which required lipid mixtures to achieve liposome orientation²³⁷, such as DMPC or DPPC liposomes containing detergents^{97, 238}.

5.4 Materials and Methods

5.4.1 Materials

Protonated and deuterated dimyristoyl- and dipalmitoylphosphatidylcholine (DMPC, DMPC-d₅₄, DPPC, DPPC-d₆₂) were purchased from Avanti Polar Lipids (Alabaster, AL, USA) while OmniPur polyoxyethylene (20) monooleate (TW80) was obtained from EMD Millipore (Billerica, MA, USA), and cholesterol was purchased from MP Biomedicals (Solon, OH, USA). Deuterium-depleted water and ytterbium (III) nitrate pentahydrate (99.9 % purity) were obtained from Sigma Aldrich (Oakville, ON, Canada) and deuterium oxide (D₂O) from CDN Isotopes (Pointe-Claire, QC, Canada).

5.4.2 Sample preparation

PC/TW80 model membranes were prepared by mixing freeze-dried DMPC or DPPC with a viscous TW80 solution, and then submitted to a series of freeze (liquid N₂) / thaw (50°C) / vortex shaking cycles. Cholesterol was mixed with the phospholipid powders when sterol-containing membranes were prepared. The lipid concentration was maintained well above the critical micelle concentration (CMC) of TW80 (12 nM). Solid-state (SS-) NMR samples were prepared with ²H-depleted water at 80% (w/v) hydration. Samples of lanthanide-doped membranes were prepared at minimal ytterbium (Yb³⁺) concentration necessary for parallel alignment, therefore molar ratios (PC/Yb³⁺) were of 105 for DMPC¹⁴⁷ and 88 for DPPC. All samples were at least duplicated.

5.4.3 NMR experiments

Most SS-NMR experiments (³¹P and ²H for DMPC/TW80 and DPPC/TW80 at all tested q ratios with and without lanthanides including duplicates) were recorded on a

hybrid solution/solid-state Varian Inova Unity 600 (Agilent, Santa Clara, CA, USA) spectrometer operating at frequencies of 599.95 MHz for ^1H , 246.86 MHz for ^{31}P and 92.13 MHz for ^2H . A double-resonance 5-mm probe was used in the solution mode while a 4-mm broadband/ ^1H dual-frequency magic-angle-spinning (MAS) probe head was employed for solid-state experiments. The remaining SS-NMR experiments (DMPC/TW80 and DPPC/TW80 orientation times, T_m measurements as well as additional duplicates previously done on the 600 MHz spectrometer) were recorded on a Bruker 400 Avance III HD (Milton, ON, Canada) spectrometer operating at frequencies of 161.94 MHz for ^{31}P and 61.41 MHz for ^2H using a double resonance 4 mm MAS probe or a triple resonance 1.9 mm MAS probe operating in dual-resonance mode.

^{31}P SS-NMR spectra were externally referenced with respect to 85 % phosphoric acid set to 0 ppm while ^{31}P solution NMR spectra were referenced at 3.38 ppm with a sealed internal capillary containing phosphate ions at pH 11 which was previously referenced with 85 % H_3PO_4 . SS-NMR data were processed using MestReNova software (Mestrelab Research, Santiago de Compostela, Spain). For experiments with the Varian 600 spectrometer, ^{31}P SS-NMR spectra were recorded using a phase-cycled Hahn echo pulse sequence¹³⁷ with gated broadband proton continuous wave decoupling at a field strength of 50 kHz. The interpulse delays were 33 μs and typically 1024 scans were acquired with a recycle delay of 5 s. The acquisition time was set at 20 ms with a 1 μs dwell time. ^2H SS-NMR spectra were obtained using a solid echo pulse sequence¹⁴⁰ with interpulse delays of 12 μs and repetition delays of 0.5 s. This recycle delay was voluntarily set shorter than 5 times the longest relaxation time in a saturated fatty acyl chain (300 ms) to optimize the total acquisition sequence. This procedure does not affect the quadrupolar doublet positions that are extracted from the Pake patterns. At least 5000 data points were obtained and typically 2048 scans were recorded with an acquisition time of 5 to

20 ms and 1 μ s dwell time. For all ^2H and ^{31}P SS-NMR experiments, the 90° pulse length varied between 2.8 and 4 μ s.

For experiments acquired with a Bruker 400 spectrometer and 4-mm probe, ^{31}P SS-NMR spectra were recorded as described above. However, the interpulse delays were 34 μ s and the acquisition time was set at 100 ms with a 5 μ s dwell time. ^2H NMR spectra were obtained also as above with interpulse delays of 60 μ s and repetition delays of 1 s and an acquisition time of 30 ms and 0.5 μ s dwell time. The 90° pulse length was 3 μ s for all ^2H and ^{31}P SS-NMR experiments.

For experiments acquired on Bruker 400 spectrometer with the 1.9-mm probe, ^{31}P SS-NMR spectra were recorded as described above with interpulse delays of 34 μ s. The acquisition time was set at 20 ms with a 5 μ s dwell time. ^2H NMR spectra were obtained as described above with interpulse delays of 60 μ s, repetition delays of 0.5 s, and an acquisition time of 30 ms and 0.5 μ s dwell time. For all ^2H and ^{31}P NMR experiments, the 90° pulse length was 2.5 μ s.

5.4.4 ^{31}P spectra fitting

We wrote a MATLAB program to determine the deformation of the PC/TW80 model membranes from the ^{31}P spectra lineshape. The extent of vesicle deformation is described with a c/a ratio, where c and a are the major and minor axes for the ellipsoid, respectively (Fig. 5.4). The c/a value depends on curvature-elastic properties of the membrane as described by Dubbinyi *et al.*:

$$c - a = r_0^3 \frac{H^2 \Delta \chi}{12K} \quad (3.1)$$

where r_0 is the radius of non-deformed liposome in cm, $\Delta\chi$ is the magnetic susceptibility of phospholipid molecules, K is the curvature-elastic modulus in dynes and H is the intensity of the magnetic field in gauss^{138, 239}.

To simulate ^{31}P spectra for fitting with experimental ^{31}P spectra, Δ (CSA), ν_P (chemical shift of 90° orientation) and β (resonance width) were obtained from simulated spectra fitted to experimental spectra of pure PC vesicles (DMPC or DPPC MLV). The ellipsoid ratio (r), which is the ratio of the major (c) and minor (a) axes of an ellipsoid (Fig. 5.4), was then adjusted to obtain the best-fit spectrum.

5.4.5 Fourier transform infrared spectroscopy

Samples were prepared by weighting the desirable quantity of perdeuterated DMPC or DPPC and TW80. The total mass of phospholipids and detergent was 4 mg and the phospholipids (DMPC or DPPC) : Tween 80 molar ratio (q) was 3 or 4 for DMPC, and 3 or 9 for DPPC. Hydration of sample was done with 11.2 μL of D_2O , giving a total proportion of 20 % (w/w) lipids in buffer. The formation of vesicles was ensured by performing 5 cycles of vigorous vortexing, freezing (liquid N_2), and thawing (50°C). The sample was then deposited between two windows of CaF_2 . All samples were duplicated.

Experiments were performed using a Magna 560 FTIR spectrometer from Nicolet (Thermo Scientific, Madison, WI) equipped with a nitrogen-cooled MCT (HgCdTe) A detector. The temperature was adjusted using a home-build temperature controller ($\pm 1^\circ\text{C}$) and the stabilization time for each temperature was 3 minutes. Samples were deposited between two CaF_2 windows (Spectral Systems, Hopewell Junction, NY) and a Mylar film spacer of 13 μm (Goodfellow Cambridge Ltd., Huntingdon, U.K.). Spectra were recorded via the acquisition of 128 interferograms at a resolution of 4 cm^{-1} using a Happ-Genzel apodization. Grams/7 AI (Galactic Industries Corp.,

Salem, NH). The D₂O spectrum was subtracted from each series of spectra. Then, the 3100-2700 cm⁻¹ region was baseline-corrected with a cubic function.

5.5 Results

5.5.1 NMR characterization of PC/TW80 model membranes

Phospholipids harbour a phosphate in their polar headgroup which allows observing by ³¹P SS-NMR changes in the morphology and orientation of model membranes. The ³¹P chemical shift depends on the orientation of the phospholipids with respect to the external magnetic field (B_0). The chemical shift anisotropy (CSA, $\Delta\sigma$) thus represents the superposition of all chemical shifts for the distribution of orientations of the phospholipids in non-oriented samples. The CSA is also indicative of the dynamic properties of the phospholipids as increased lipid motions will result in spectral averaging. For phospholipids with axial symmetry, the CSA can be written as follows:

$$\Delta\sigma = \sigma_{\parallel} - \sigma_{\perp} \quad (3.2)$$

where σ_{\parallel} and σ_{\perp} are the parallel and perpendicular components of the CSA tensor which can be measured from the 0° (left edge) and 90° (right edge) frequencies of the powder spectrum of non-oriented static samples¹²³. For oriented samples, only a single well-resolved ³¹P resonance remains at the right edge.

Lipids with deuterated acyl chains (DMPC-d₅₄ and DPPC-d₆₂) we used to probe the hydrophobic core of the membrane by ²H SS-NMR. The doublet spacing of individual CD₂ bond resonances, also call the quadrupolar splitting ($\Delta\nu_Q$), gives insight on the degree of organization of the acyl chains. The $\Delta\nu_Q$ is defined as follows:

$$\Delta\nu_Q = \frac{3}{4} \frac{e^2 q Q}{h} (3 \cos^2 \theta - 1) S_{CD} \quad (3.3)$$

where $\frac{e^2 q Q}{h}$ is the static quadrupolar coupling constant (~ 167 kHz), θ is the angle between the bilayer normal and the external magnetic field, and S_{CD} is the order parameter of ^2H in C- ^2H bonds^{141, 173}. An increase (decrease) in $\Delta\nu_Q$ is characteristic of an increase (decrease) in lipid order^{142, 173}.

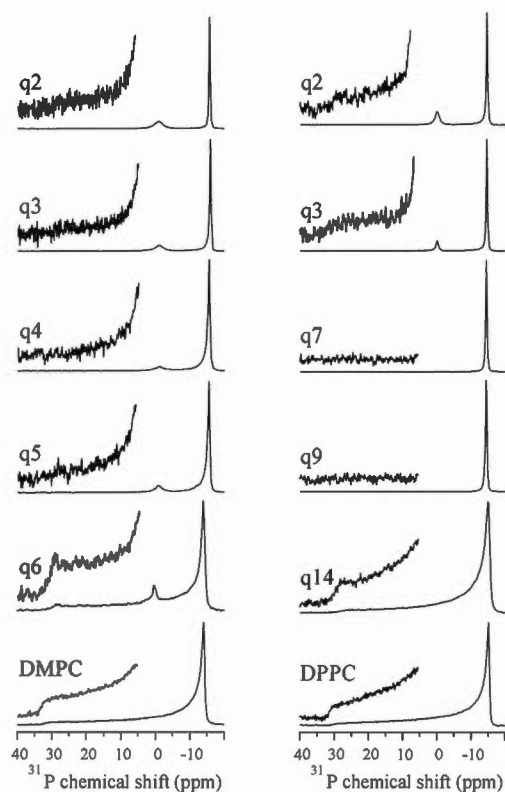


Figure 5.2 ^{31}P NMR spectra of DMPC/TW80 (left) and DPPC/TW80 (right) at 37°C and 57°C , respectively, for different molar ratios (q). Pure phospholipid spectra (bottom) are shown for comparison. The magnifying factor of pure lipid and non-oriented insets (DMPC/TW80 q_6 and DPPC/TW80 q_{14}) is 10X. All other insets for oriented molar ratio are magnified 100X.

Model membranes were prepared using phospholipids with 14 and 16 carbon acyl chains (DMPC and DPPC, respectively). We first established the phospholipid:TW80 molar ratios and temperature range at which the bilayer is oriented by ^{31}P and ^2H SS-NMR, as summarized in Table 5.S1, and presented in Fig. 5.2 and 5.3. Fig. 5.2 shows the orientation as a function of q for both PC/TW80 systems at $\sim 15^\circ\text{C}$ above the lipids' T_m . DMPC/TW80 aggregates spontaneously align at molar ratios ranging from $q2$ to $q5$, while DPPC/TW80 systems have a broader alignment range of $q2$ to $q13$. The ^{31}P SS-NMR spectra show that a sharp signal appears at -15 ppm which corresponds to the 90° edge of pure PC powder spectra (Fig. 5.2), indicating the perpendicular orientation of the membrane normal (N) with respect to B_0 (Fig. 5.4). A small peak at 0 ppm emerges on the ^{31}P SS-NMR spectra primarily at low q ratios, likely due to the presence of rapidly reorienting PC-TW80 mixed micelles. A small residual powder pattern appears at high q ratios. In most cases it remains absent, or below detection, but its presence, even when aggregates are aligned, suggests that PC/TW80 vesicles adopt a prolate-type morphology (Fig. 5.4) as opposed to a bilayered disk shape, like bicelles.

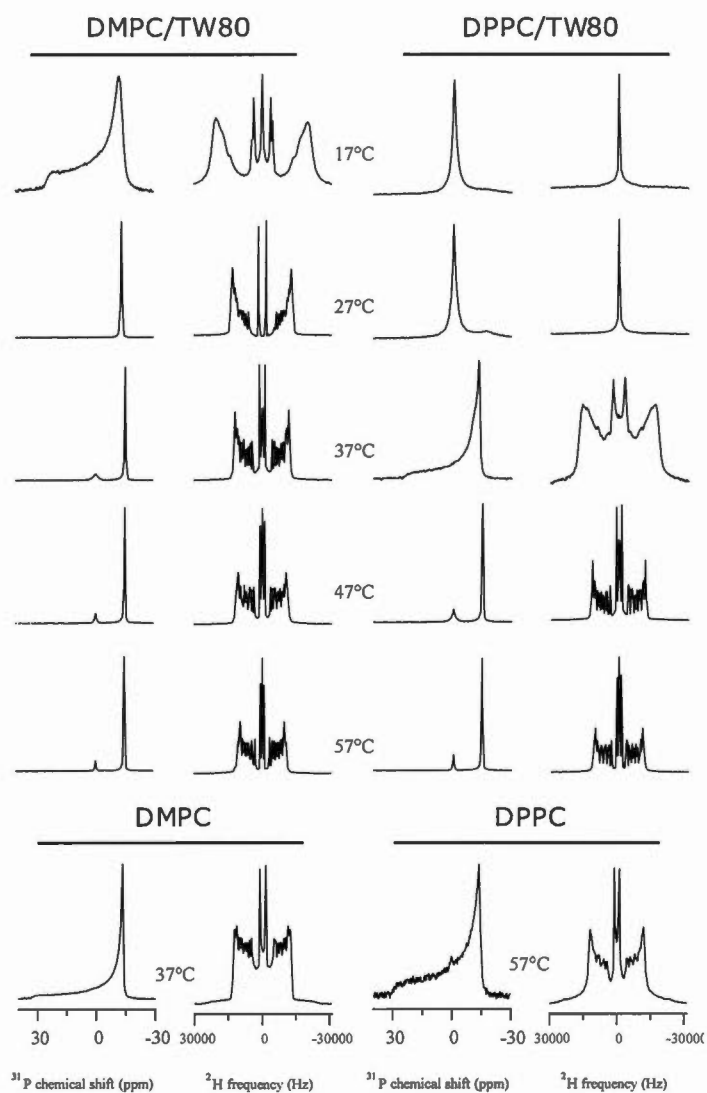


Figure 5.3 ^{31}P (first and third columns) and ^2H (second and last columns) NMR spectra of DMPC/TW80 (left) and DPPC/TW80 (right) with q_3 at different temperatures. Pure lipid spectra of DMPC (bottom, left) and DPPC (bottom, right) are displayed for comparison.

Table 5.S1 as well as Fig. 5.3 show that the temperature is not a limiting factor for membrane orientation, as long as the experiments are carried out above the

phospholipids' T_m which is 23 °C for DMPC and 42 °C for DPPC²⁴⁰. Similarly to ^{31}P SS-NMR, ^2H spectra of PC/TW80 membranes above the T_m are characteristic of bilayer alignment where the individual ^2H signals are well resolved and the shoulders representing the 0° orientation are completely absent (Fig. 5.3). The $\Delta\nu_Q$ of ^2H spectra for PC/TW80 bilayers do not change with increasing TW80 content (data not shown). Furthermore, the oriented systems remain aligned well above the phospholipids' T_m (Table 5.S1). Just below the PC transition temperature, at 17 °C and 37 °C for DMPC/TW80 and DPPC/TW80 respectively, both ^{31}P and ^2H powder spectra were poorly resolved (Fig. 5.3). At these temperatures, significantly broader ^2H $\Delta\nu_Q$ and ^{31}P CSA imply the formation of large size aggregates with reduced elasticity. At even lower temperatures a single isotropic peak is obtained (Fig. 5.3). This isotropic chemical shift near -0.8 ppm most likely corresponds to a small population of aggregates that are undergoing rapid motions, seemingly organised as mixed micelles¹⁰⁴.

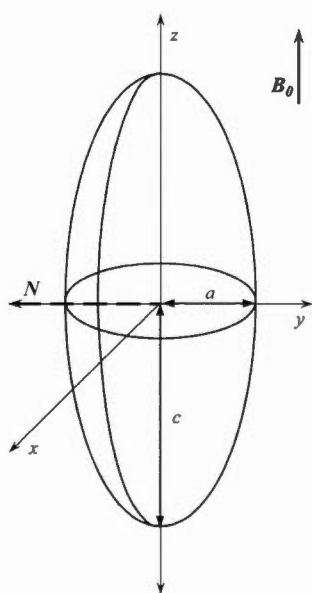


Figure 5.4 Geometric model of an ellipsoid in a xyz plane where c and a are the major and minor axis, respectively, B_0 is the external magnetic field, and N the membrane normal.

We further investigated the conditions favoring the assembly of PC and TW80 as mixed micelles and as oriented aggregates. Influencing these two morphologies are

the surfactant molar ratio (q) and the temperature. Our results show that in most conditions there is a coexistence of both morphologies with some exceptions, as with DPPC/TW80 at $q = 7$ (Fig. 5.2), for example. With both DMPC/TW80 and DPPC/TW80 systems, the intensity of the isotropic peak decreases when the q ratio increases (Fig. 5.S1). This indicates that the vesicle morphology is favored when the PC content is high. Furthermore, an increase in temperature leads to a smaller fraction of mixed micelles for DPPC/TW80 (Fig. 5.S1B). The influence of the temperature is not as trivial for DMPC/TW80 (Fig. 5.S1A). In order to limit the aggregates to a single morphology which can be oriented in the magnetic field, we thus recommend using higher molar ratios, *i.e.*, $q7$ to $q9$ for DPPC/TW80 and $q3$ to $q5$ for DMPC/TW80, with temperatures at least 15°C above the PC's T_m . This also prompted us to focus especially on molar ratios of $q3$ for DMPC/TW80 and $q9$ for DPPC/TW80 for further characterisations.

It is often desirable to use systems whose membrane normal is parallel to B_0 since the axial movements of transmembrane peptides are negligible, as opposed to introducing powder motifs on the spectra when perpendicular to B_0 ¹⁴⁶. Parallel alignment can be achieved by altering the magnetic susceptibility anisotropy of the membrane by adding small amounts of trivalent lanthanide ions¹⁴⁶. The alignment of PC/TW80 systems with their membrane normal parallel to the magnetic field is shown by ³¹P and ²H SS-NMR in Fig. 5.5. Indeed, the addition of Yb³⁺ to DMPC/TW80 aggregates at a PC/Yb³⁺ molar ratio of 105 “flipped” the bilayer normal from perpendicular ($\theta = 90^\circ$) to parallel ($\theta = 0^\circ$) to B_0 . The spectral signature of a parallel alignment is characterized by a resonance shift to low fields (20 ppm) for ³¹P spectra, and a doubling of the quadrupolar splitting (26 to 52 kHz) for ²H spectra (Fig. 5.5, right). Also, paramagnetic ions tend to broaden resonances¹⁴⁶, as observed on the ³¹P spectrum (Fig. 5.5, bottom left).

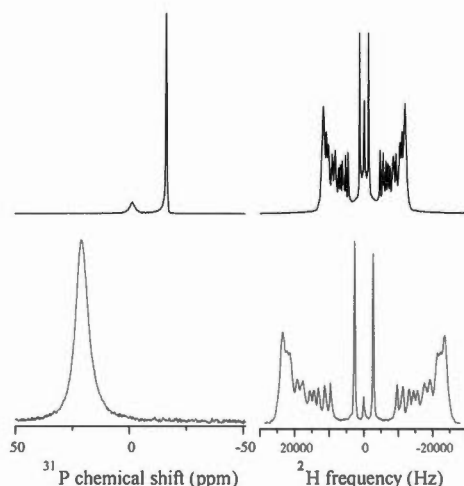


Figure 5.5 ^{31}P (left) and ^2H (right) NMR spectra of DMPC/TW80 q_3 at 37 °C without (top) and with (bottom) lanthanide ions using a DMPC/ Yb^{3+} molar ratio of 105:1.

The magnetic susceptibility of the phospholipids induces a perpendicular alignment of PC/TW80 systems in the magnetic field. This can result in vesicle deformation to a prolate shaped ellipsoid. The extent of deformation depends on curvature-elastic properties of the membrane (Eq. 5.1). We fitted the ^{31}P SS-NMR spectra to determine the degree of vesicle deformation of our systems at different molar ratios of PC and TW80 (Fig. 5.6)¹³⁸. All PC/TW80 spectra fitting of lower q ratios suggest highly elongated systems (Fig. 5.6, bottom). With increasing molar ratios, the extent of deformation (c/a) decreases and ultimately plateaus at 16 for DMPC/TW80 and at 25 for DPPC/TW80. The aggregates' morphology transitions to spherical when DMPC/TW80 reaches a molar ratio of 6, and 14 for DPPC/TW80. In these conditions, the aggregates are no longer aligned in the magnetic field.

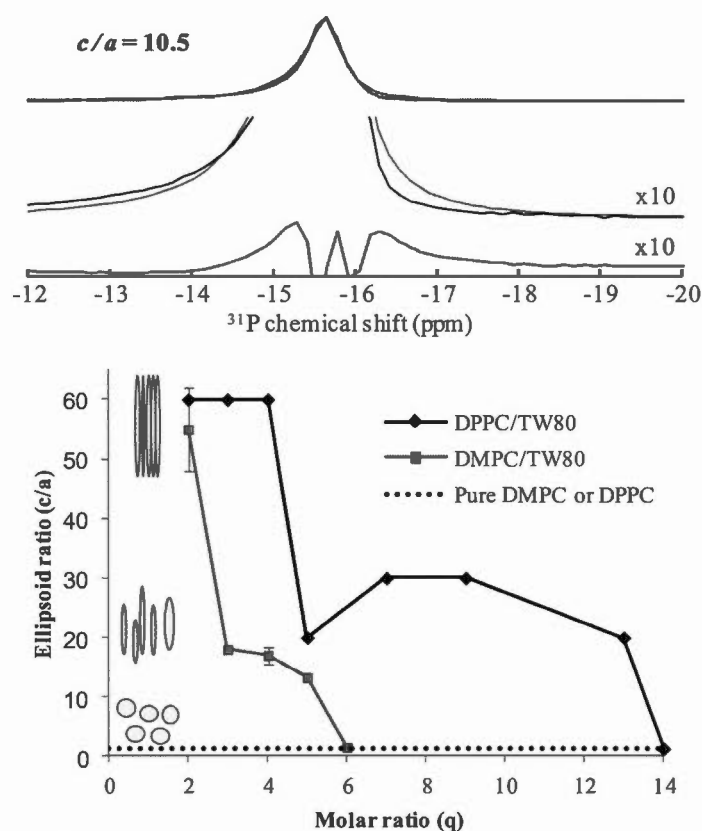


Figure 5.6 ^{31}P SS-NMR spectra fitting using Eq. (5.1). Top: DMPC/TW80 $q = 3$ at 37°C spectrum (black) overlaid with best-fit spectrum (grey) which corresponds to best-fit ellipsoid ratio (c/a) (top panel). Baseline zoom (10X) of spectra fitting (middle panel) and 10X zoom of fit residuals (lower panel). Bottom: Best-fit ellipsoid ratios of DMPC/TW80 systems (grey) and DPPC/TW80 (black) plotted against the surfactant molar ratio. PC/TW spectra used for ^{31}P fitting were recorded at 37°C and 57°C for samples containing DMPC and DPPC respectively. Experimental ellipsoid ratio of pure PC (dotted line) was added for comparison.

When lipid systems are orientated, their bilayer normal is either parallel (with lanthanides) or perpendicular relative to the direction of the magnetic field. Oriented vesicles deform to oblate (σ_{\parallel}) or prolate (σ_{\perp}) ellipsoids, where the extent of the

deformation is described by the ellipsoid ratio (r) which depends on the curvature-elastic properties of the membrane (Eq. 5.1)¹³⁸. The ellipsoid ratio (c/a) is proportional to the magnetic field intensity (H); therefore vesicles should have a higher r value at higher magnetic fields. This was verified by recording PC/TW80 ^{31}P and ^2H SS-NMR spectra at 9.4 and 14.1 T (400 and 600 MHz) (Fig. 5.7A). ^{31}P SS-NMR spectra were fitted to determine the extent of deformation. As expected for oriented liposomes, the ellipsoid ratios were higher ($r = 15$) at 600 MHz than at 400 MHz ($r = 5$). The orientation improvement is also revealed by the ^2H NMR spectra which show an improved resolution of the quadrupolar splittings along the lipid acyl chains at higher field. Cholesterol (20 mol%) was added to the PC/TW80 systems in an attempt to alter the bilayers' fluidity (Fig. 5.7B). The rigidifying effect of cholesterol is revealed by the increase in the quadrupolar splittings on the ^2H NMR spectrum. As shown by Vist and Davis with DPPC, the C-C bonds in the acyl chain are mostly in a more ordered all-trans conformation in the presence of 20 mol% cholesterol, as opposed to the disorder induced by the rapid gauche-trans isomerization in pure phospholipids in the fluid phase⁸³. However its presence did not affect the lipid headgroup mobility but did improve the bilayer orientation, as shown on the ^{31}P NMR spectrum which is similar to the PC/TW80 membranes.

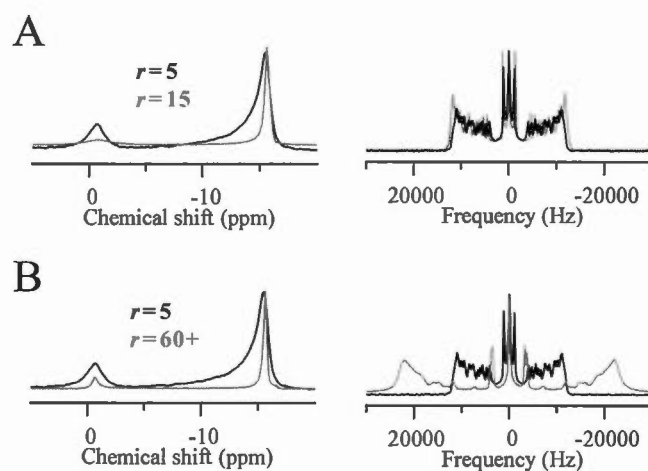


Figure 5.7 Quality of orientation as a function of the magnetic field strength (A) and of the vesicle elasticity (B). ^{31}P (left) and ^2H (right) SS-NMR spectra of DMPC/TW80 $q3$ model membranes at 37 °C. ^{31}P spectra were fitted using Eq. (5.1). Best-fit ellipsoid ratios (r) are given above ^{31}P spectra. (A) Spectra were recorded on 400 (black) and 600 MHz (grey) spectrometers. (B) Spectra of lipid mixture with (grey) and without (black) 20 mol% cholesterol.

5.5.2 Properties of phospholipids and TW80

We studied the thermotropism of PC lipids in the presence of TW80 by FTIR spectroscopy²⁴¹ to better understand the partitioning of these two surfactants. Spectra of various mixtures of DMPC/TW80 ($q3$, $q4$) and DPPC/TW80 ($q3$, $q9$) were acquired along with pure lipid spectra for comparison. The wavenumbers for the CD_2 symmetric stretching vibration ($\nu_s\text{CD}_2$) were plotted as a function of temperature in order to obtain thermotropic curves (Fig. 5.8A, B).

As expected, the higher the PC content, compared to TW80, the more the thermotropic curves resembles that of pure PC (Fig. 5.8A, B). Additionally, TW80

slightly disrupts the cooperative nature of the lipids since a larger temperature span is needed to transition from a gel to liquid-crystalline state (Fig. 5.8A, B). The decrease in lipid cooperativity also suggests that the PC and TW80 molecules are not segregated. This is further confirmed by the phase transition temperature of the lipids as determined from the FTIR thermotropism curve (Table 5.S2). Indeed, the presence of TW80 does not significantly affect the PC's T_m . However, the transition between phases for DMPC/TW80 requires a larger range of temperatures to reach the final liquid-crystalline phase (Fig. 5.S2). This is somewhat expected since the lipid mixture has a larger difference in acyl chain length (14:0 for DMPC and 18:1 for TW80) and this often results in lower miscibility characteristics where it is not uncommon to see a broadening of the phase transition²⁴⁰. Moreover, for DMPC/TW80, the wavenumbers before and after the transition phase are at slightly higher values ($\sim 0.5\text{ cm}^{-1}$) than with pure DMPC (Fig. 5.8A) indicating a higher conformational disorder of the acyl chains.

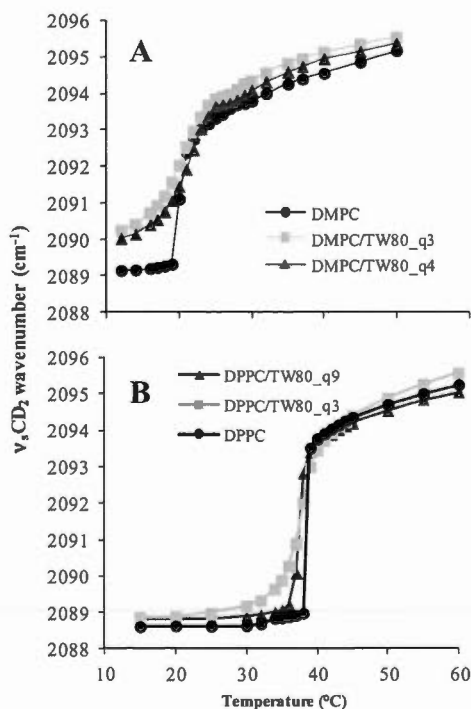


Figure 5.8 Temperature dependence of CD_2 symmetric stretching vibration ($\nu_s\text{CD}_2$) for PC/TW80 samples by FTIR spectroscopy. Thermotropic curves for DMPC (A), and DPPC (B) with and without TW80 at different molar ratios. All samples were duplicated and since the replicas reproduced very well (data not shown), the average of the $\nu_s\text{CD}_2$ values was used to plot the curves.

5.6 Discussion

In this work, we have characterized PC/TW80 model membranes – a system that orients in the magnetic field and uses a gentle non-ionic detergent employed for protein purification. Instead of the classical bicelle morphology where the detergent and lipids are mostly segregated, these bilayers showed to adopt a prolate shape (Fig. 5.4) in which PC and TW80 molecules are not segregated, as revealed by FTIR analysis. TW80 is indeed regularly used for the conception of transferosomes in which it acts as a bilayer softening component. TW80 thus increases the elasticity of PC bilayers, allowing them to easily deform and achieve orientation in the magnetic field. Similar effects of peptides such as met-enkephalin and melittin have been reported in the past on phospholipid membranes^{242, 243}. TW80 seems to have a much greater fluidizing effect on DPPC bilayers since a smaller proportion of the detergent was needed to maintain bilayer orientation.

The reversible transition from liposomes to mixed micelles which is caused by the partitioning of the detergent in a lipid bilayer is a well-documented process²⁴⁴. As the detergent content increases, detergent molecules partition into the membrane until reaching a saturation point. Further detergent addition leads to the disintegration of the membrane where detergent-saturated bilayers and lipid-detergent mixed micelles coexist. This phenomenon was observed in our study with PC/TW80 by ³¹P and ²H SS-NMR where an isotropic peak was present at low q ratios. Also, the perturbation of the lipids' cooperativity induced by TW80 was revealed by FTIR as a larger temperature span was needed to transition from a gel to liquid-crystalline state (Fig. 5.8). These results thus indicate that the closer the length of the PC acyl chain to that of TW80 (18 carbons with one unsaturation), the more stable the system. This is consistent with the NMR data (Fig. 5.2) where DPPC/TW80 systems (16 carbons) can orient over a wider span of q as compared to DMPC/TW80 systems (14 carbons). Most likely, the higher the difference in acyl chain length between PC and TW80

would reduce the compaction of the hydrophobic domain since they would take up more volume, resulting in conformational disorder.

Likewise, a mixture of a non-ionic detergent, Triton X-100 (TX-100), with PC has also been studied by several spectroscopic techniques^{99, 245}. Park *et al.* have more recently reported the orienting properties and practicality for membrane protein applications of PC/TX-100 aggregates by SS-NMR when used at a molar ratio of $q5^{99}$. Goni *et al.* have characterized the interaction of TX-100 with PC liposomes using differential scanning calorimetry (DSC), FTIR and NMR²⁴⁵. Similarly to TW80, TX-100 produces an isotropic peak on ^2H SS-NMR spectra, representative of fast-tumbling objects. As the detergent proportion increases (from $q10$ to $q3$) the $\Delta\nu_Q$ of the ^2H spectra decrease, caused by the partitioning of detergent molecules in the bilayer, thus disrupting the ordering of the lipid acyl chains. At $q3$ no $\Delta\nu_Q$ changes are observed until $q1.22$ when $\Delta\nu_Q$ collapsed. An isotropic peak also appears on ^{31}P spectra of PC/TX-100 liposomes when the molar ratio is below $q3$, and when $q < 1.22$ only isotropic components are present. Correspondingly, no changes in $\Delta\nu_Q$ were observed in our study as the TW80 concentration increased, indicating that the lipid chain order was maintained regardless of the TW80 content. FTIR experiments were also conducted to study the gel-to-liquid crystalline phase transition of PC/TX-100 systems. Contrary to TW80, TX-100 lowers the T_m of DPPC and DMPC by $\sim 10^\circ\text{C}$ which is attributed to a decrease in energy of the hydrophobic bonds between the PC acyl chains where their interaction would be perturbed.

The use of mild detergents used in MP purification to enable the magnetic orientation of lipid bilayers, such as TW80, paves the way to explore a variety of new membrane systems for the study of MPs and peptides. The formation of “elastosomes” is a promising alternative to bicelles which orientation and morphology can be perturbed by the insertion of a peptide or protein¹⁵⁴. The formation of long ellipsoids is most likely to reduce the orientation mosaicity of the

bilayers, as compared to bicelles. Moreover, PC/TW80 membranes orient over a wide range of temperature and q ratios, and thus have a less restrictive phase diagram as compared to bicelles, which can limit certain applications¹⁰⁸.

5.7 Conclusion

TW80-based model membranes made of DMPC or DPPC were shown to be a close mimic of biomembranes since a very low concentration of detergent is needed to achieve bilayer orientation in the magnetic field. They also offer a wide range of molar ratios and temperatures to perform SS-NMR experiments, especially with DPPC. The same detergent can be used to extract membrane proteins and enhance membrane orientation while avoiding detergent removal. PC/TW80 model membranes are a great example on how to exploit a membrane softening detergent for the study of MPs. In the future, the activity of proteins in PC/TW80 elastosomes should be evaluated.

5.8 Acknowledgements

The authors would like to thank F. Paquet-Mercier for his technical assistance with the infrared spectroscopy experiments, and D.E. Warschawski for stimulating discussions. A.G. wishes to thank the Natural Sciences and Engineering Research Council (NSERC) of Canada for the award of scholarships. M.F. would like to acknowledge graduate scholarship from the *Fonds de recherche du Québec Nature et Technologies* (FRQNT). This work was supported by an NSERC discovery grant, the Canadian Foundation for Innovation (CFI), the FRQNT, the *Regroupement québécois de recherche sur la structure, la fonction et l'ingénierie des protéines* (PROTEO), the *Centre de recherche sur les matériaux avancés* (CERMA) and the *Centre québécois sur les matériaux fonctionnels* (CQMF).

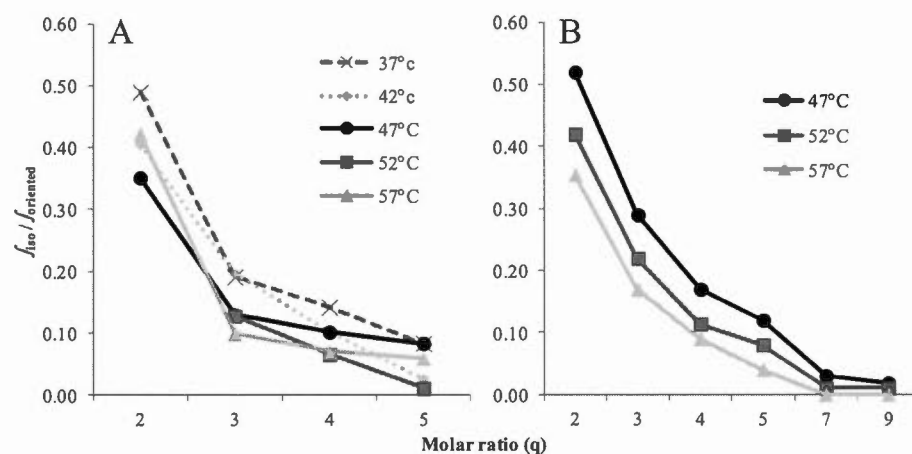


Figure 5.S1 Molar ratio (q) and temperature influence the morphology of PC/TW80 aggregates. The isotropic and oriented resonances from DMPC/TW80 and DPPC/TW80 ^{31}P spectra were integrated and the resulting ratios for the integration values ($J_{\text{iso}}/J_{\text{oriented}}$) were plotted as a function of the molar ratio. This was done for several temperatures above the T_m . Error bars included for DMPC/TW80 (37, 47 and 57 °C) and well as for DPPC/TW80 (47 and 57 °C, $q_{2,3}$ and 9).

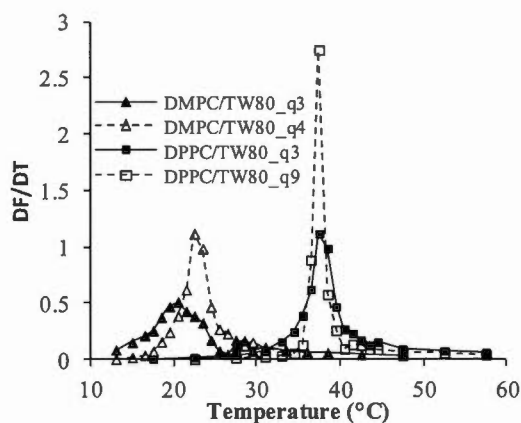


Figure 5.S2 First derivative of the thermotropic curves for DMPC/TW80 and DPPC/TW80 at different molar ratios is plotted as a function of temperature to determine the temperature of phase transition (T_m).

Table 5.S1 Summary of all ^{31}P NMR experiments of PC/TW80 model membranes at different molar ratios and temperatures (A). NMR experiments for PC/TW80 samples doped with Ytterbium (Yb^{3+}) for $q = 3$ at different temperatures (B).

A	DMPC/TW80																	DPPC/TW80									
	Temperature (°C)																										
	Molar ratio (q)	17	22	25	27	32	37	42	47	52	57	62	67	72	77	87	92										
Solution NMR	0.25	-	-	I	-	-	I	-	-	-	I	-	-	-	-	-	-	-	-	-	-	-	-	-	-	-	-
	0.5	-	-	I	-	-	I	-	-	-	I	-	-	-	-	-	-	-	-	-	-	-	-	-	-	-	-
	0.75	-	-	I	-	-	I	-	-	-	I	-	-	-	-	-	-	-	-	-	-	-	-	-	-	-	-
	1	-	-	I	-	-	I	-	-	-	I	-	-	-	-	-	-	-	-	-	-	-	-	-	-	-	-
	1.5	-	-	I	-	-	I	-	-	-	I	-	-	-	-	-	-	-	-	-	-	-	-	-	-	-	-
	0.5	N*	N*	N*	N*	N*	N*	N*	N*	N*	N*	N*	N*	N*	N*	N*	N*	-	-	-	-	-	-	-	-	-	-
	0.75	N*	N*	N*	N*	N*	N*	N*	N*	N*	N*	N*	N*	N*	N*	N*	N*	-	-	-	-	-	-	-	-	-	-
	1	N*	N*	N*	N*	N*	N*	N*	N*	N*	N*	N*	N*	N*	N*	N*	N*	-	-	-	-	-	-	-	-	-	-
	2	N*	-	A*	-	A*	-	A*	-	A*	-	A*	-	A*	-	A*	-	-	-	-	-	-	-	-	-	-	-
	3	N*	-	A*	-	A*	-	A*	-	A*	-	A*	-	A*	-	A*	-	-	-	-	-	-	-	-	-	-	-
	4	N*	-	A*	-	A*	-	A*	-	A*	-	A*	-	A*	-	A*	-	-	-	-	-	-	-	-	-	-	-
	5	N*	-	A*	-	A*	-	A*	-	A*	-	A*	-	A*	-	A*	-	-	-	-	-	-	-	-	-	-	-
	6	N	-	N	-	N	-	N	-	N	-	N	-	N	-	N	-	-	-	-	-	-	-	-	-	-	-
SS-NMR	7	-	-	-	-	-	-	-	-	-	-	-	-	-	-	-	-	-	-	-	-	-	-	-	-	-	-
	9	-	-	-	-	-	-	-	-	-	-	-	-	-	-	-	-	-	-	-	-	-	-	-	-	-	-
	13	-	-	-	-	-	-	-	-	-	-	-	-	-	-	-	-	-	-	-	-	-	-	-	-	-	-
	14	-	-	-	-	-	-	-	-	-	-	-	-	-	-	-	-	-	-	-	-	-	-	-	-	-	-
		-	-	-	-	-	-	-	-	-	-	-	-	-	-	-	-	-	-	-	-	-	-	-	-	-	-
		-	-	-	-	-	-	-	-	-	-	-	-	-	-	-	-	-	-	-	-	-	-	-	-	-	-
		-	-	-	-	-	-	-	-	-	-	-	-	-	-	-	-	-	-	-	-	-	-	-	-	-	-
		-	-	-	-	-	-	-	-	-	-	-	-	-	-	-	-	-	-	-	-	-	-	-	-	-	-
		-	-	-	-	-	-	-	-	-	-	-	-	-	-	-	-	-	-	-	-	-	-	-	-	-	-
		-	-	-	-	-	-	-	-	-	-	-	-	-	-	-	-	-	-	-	-	-	-	-	-	-	-
		-	-	-	-	-	-	-	-	-	-	-	-	-	-	-	-	-	-	-	-	-	-	-	-	-	-
		-	-	-	-	-	-	-	-	-	-	-	-	-	-	-	-	-	-	-	-	-	-	-	-	-	-

A: Aligned
N: Not aligned
I: Isotropic
*: experiments also done by ^1H NMR

B

DMPC/TW80/Yb3+ q3								DPPC/TW80/Yb3+ q3									
Temperature (°C)																	
17	27	37	47	57	67	77	17	22	27	32	37	42	47	52	57	67	77
N*	A*	A*	A*	A*	A*	A*	N*	N*	N*	N*	N*	N*	N*	A*	A*	A*	A*

Table 5.S2 Phase transition temperatures (T_m) for DMPC and DPPC without and with TW80 at various molar ratios obtained by FTIR. T_m was obtained by applying a first derivative on the IR thermotropic curve and plotting it as a function of temperature (Fig. 5.S2). The resulting maximum, which represents the inflexion point of the thermotropic curve, is the T_m . Also noteworthy, the acyl chains of the PC lipids used in our IR experiments are deuterated (DMPC- d_{54} and DPPC- d_{62}). Deuteration is known to decrease the T_m by 3 to 5 degrees compared to the protonated dispersions^{246, 247}.

Sample	T_m (°C)
DMPC	19.5
DMPC/TW80 q3	20.5
DMPC/TW80 q4	22.5
DPPC	38.5
DPPC/TW80 q3	37.5
DPPC/TW80 q9	37.5

CHAPITRE VI

CONCLUSIONS ET PERSPECTIVES

Les résultats de cette thèse peuvent être subdivisés en deux parties : l'étude du rôle et du fonctionnement du hERG et le développement de membranes modèles. Dans la première section, on a étudié la structure, la fonction et le rôle du filtre de sélectivité du hERG qui serait impliqué dans le syndrome du QT long (chapitre III) ainsi que le rôle du segment S4S5 dans le mécanisme d'ouverture et de fermeture du canal hERG (chapitre IV). Par ailleurs, nous avons développé un nouveau modèle membranaire pour des applications structurales en RMN (chapitre V). Les conclusions de ces études sont présentées ainsi que les perspectives futures.

6.1 Résumé et conclusions du rôle et de la fonction du hERG

6.1.1 Étude de la structure, de la fonction et du rôle du filtre de sélectivité du hERG

Le hERG reçoit énormément d'attention depuis sa découverte en 1994 puisque celui-ci est ciblé par une large gamme de médicaments cardiaques et non cardiaques qui peuvent engendrer des arythmies potentiellement fatales, un effet secondaire entièrement non désiré⁴. Étant donné les nombreuses différences par rapport aux autres canaux potassiques qui dépendent du voltage, il est primordial d'étudier la structure du hERG, car celle principalement prédite par homologie de séquences n'est pas suffisante pour bien comprendre sa fonction et son rôle dans le ALQTS. L'utilisation de peptides correspondants aux régions spécifiques du hERG s'avère être une stratégie très utile, tel que démontré au chapitre III, où l'on décrit l'étude d'un peptide de 17 acides aminés qui comporte le filtre de sélectivité du hERG. Cette

étude est importante, car la région du hERG est ciblée par les médicaments cardiotoxiques, dont les acides aminés Thr623, Ser624 et Val625 du SF^{19, 20}. Notre étude démontre que le SF est non structuré, avec et sans potassium. Ceci est en accord avec la flexibilité requise pour qu'il puisse s'adapter aux changements de conformations nécessaires pour coordonner le passage des ions K^+ (Fig. 1.7)^{54, 184, 186}. On démontre aussi qu'il aurait la possibilité d'interagir avec la membrane, vu sa proximité et son affinité pour la surface de la membrane, et que cette interaction diminue en présence d'ions K^+ . Certaines études démontrent l'importance des interactions lipide-protéine pour stabiliser les changements de conformation des canaux K_V ²⁴⁸⁻²⁵⁰. De plus, nous avons étudié l'interaction du SF avec des médicaments cardiotoxiques, dont le bépripil, la cétirizine, la diphenhydramine, la prométhazine et la fluvoxamine, provenant de différentes classes pharmacologiques, ayant des structures variées et étant reconnus pour leurs risques à prolonger l'intervalle QT et à induire des torsades de pointes. La prométhazine aurait le potentiel de cibler le SF pour induire le ALQTS. Nos résultats appuient la possibilité du rôle *indirect* de la membrane dans le ALQTS, car les médicaments cardiotoxiques ont une haute affinité pour celle-ci, et leur présence affecte l'affinité qu'a le SF pour la membrane. Il y a déjà 20 ans, Sargent et Schwyzer ont décrit le rôle catalyseur de la membrane pour les interactions ligand-récepteur²⁵¹. Pour mieux comprendre le mécanisme du ALQTS, il est important d'étudier le rôle potentiel de la membrane via ses interactions avec les molécules hERG-actives. Certaines études démontrent que les molécules amphiphiles, telles que le médicament thiopental de sodium et la toxine SGTx1, peuvent modifier les propriétés mécaniques de la membrane et accéder à certains sites de liaison du DSV de canaux K_V en se partitionnant dans la membrane^{252, 253}. Les connaissances sur le rôle de la membrane ont été avancées par Chartrand *et al.* dans un article auquel j'ai contribué (Annexe A). Notre étude apporte donc des nouvelles connaissances au niveau de la structure et du fonctionnement du SF ainsi que du mécanisme cardiotoxique des médicaments.

6.1.2 Rôle du segment S4S5 dans le mécanisme d'ouverture et de fermeture du hERG

Le mécanisme d'ouverture et de fermeture du hERG est unique, mais primordial pour la régulation normale des battements cardiaques chez l'humain. Au cours des dernières années, plusieurs études ont confirmé l'importance du rôle du segment intracellulaire S4S5 pour l'activation et la désactivation du canal hERG^{59, 66, 67, 69, 71, 155}.

La séquence du S4S5 des canaux K_v1 à K_v9 contient deux résidus leucine qui sont hautement conservés, mais remplacés par des tyrosines dans les canaux K_v10 à K_v12²⁵⁴. La structure du canal K_v1.2 ayant été cristallisée démontre que ces leucines se retrouvent du côté du segment S4S5 qui fait face à la membrane⁵⁸. De plus, la structure par RMN d'un peptide de 20 acides aminés correspondant au segment S4S5 du hERG a été déterminée et démontre une hélice amphipathique où son côté hydrophobe contient les tyrosines Y542 et Y545⁵⁷. Au chapitre IV, on a confirmé que les résidus Y542 et Y545 du segment S4S5 interagissent avec la membrane et/ou avec des domaines protéiques du hERG pour stabiliser la conformation ouverte de ce canal lors de la désactivation. La structure cristalline du chimère K_v1.2/2.1 révèle que les deux tyrosines du segment S4S5 pointent vers la membrane et sont entourées d'une concentration importante de lipides⁵⁸. Notre étude affirme que le segment S4S5 interagit avec plusieurs cibles (domaines du hERG et la membrane) afin de transmettre les mouvements du DSV au domaine du pore pour permettre son ouverture/fermeture. Certaines études ont constaté l'interaction du S4S5 avec la région intracellulaire du pore ainsi qu'avec les domaines cytoplasmiques^{59, 67, 71}. Par électrophysiologique, nous avons démontré que la Y542 du segment S4S5 du hERG interagit avec le DSV pendant la désactivation pour stabiliser la conformation ouverte. De plus, nous démontrons que la Y542 interagissait avec des résidus des domaines transmembranaires, mais les interactions faibles indiquent qu'il y aurait d'autres facteurs à considérer, dont l'interaction avec la membrane. D'autre part, la

Y545 semblerait plutôt stabiliser un état intermédiaire entre la conformation ouverte et fermée. La nature de ces interactions ne peut être déterminée pour l'instant, mais il se pourrait que ce soit avec la membrane. Les tyrosines Y542 et Y545 stabilisent la conformation ouverte des canaux Kv11.1 où ils joueraient des rôles distincts, mais importants pour conférer au hERG sa désactivation particulièrement lente. Notre étude clarifie donc le fonctionnement particulier du canal potassique hERG via l'étude RMN et d'électrophysiologie du segment S4S5 important pour la santé humaine.

6.2 Vers de nouvelles membranes modèles pour les études de RMN – Résumé et conclusions

Dans un contexte d'études structurales de protéine membranaires par RMN, il est inévitable de s'intéresser aux membranes modèles dans lesquelles ces protéines pourraient être réinsérées. Dans le cadre de cette thèse, nous avons voulu développer un nouveau système membranaire modèle, composé de lipides et de Tween 80, un détergent « doux », et d'en étudier les propriétés.

Une variété de modèles membranaires existent déjà, tels que résumés dans l'introduction et dans l'article de revue (Annexe B) auquel j'ai participé⁹⁰. Alors que les détergents sont souvent employés pour la détermination de structure des PM par RMN, leur morphologie ne ressemble pas du tout à l'environnement natif des PM. Il est souvent souhaité de les éliminer lors que la purification des PM – une étape fastidieuse et longue diminuant souvent le rendement final en protéines réinsérées dans les membranes.

Nous avons donc développé un nouveau modèle membranaire composé d'un mélange de détergents et de lipides pour des applications en RMN à l'état solide qui évite l'étape de l'élimination du détergent. Ce système, composé de TW80 et de DMPC ou de DPPC, a été caractérisé par RMN de l'état solide et par infrarouge. Nous

démontrons la grande utilité du système PC/TW80 pour des applications RMN puisqu'il s'oriente dans le champ magnétique sur une large gamme de températures et de ratios molaires. À la différence des bicelles, cependant, le système PC/TW80 est formé de liposomes et non pas de disques, ce qui en fait un modèle plus proche dans sa morphologie de la cellule biologique. Il est possible de faire basculer l'orientation des systèmes PC/TW80 avec l'utilisation d'une faible quantité d'agents paramagnétiques de sorte que la normale de la bicouche soit parallèle (au lieu de perpendiculaire) au champ magnétique. Nos résultats de FTIR confirment que nos systèmes adoptent une morphologie ellipsoïdale, car les molécules PC et de TW80 ne sont pas ségréguées comme pour les bicelles. Les bicelles ont la caractéristique d'effectuer un mouvement dynamique que l'on appelle le *wobbling*, qui peut aussi être induit ou amplifié par l'interaction avec les protéines et les peptides membranaires. Ce mouvement dynamique va moyenner la distribution des orientations lipidiques, décrivant en partie le paramètre d'ordre S_{CD} (Éq. 2.16), et donc, réduire l'écart quadripolaire ($\Delta\nu_Q$). Il est facile d'imaginer que les élastosomes de PC/TW80 – liposomes hautement déformés dans le champ magnétique – subiront potentiellement moins cet effet de *wobbling* vu leur longue taille, surtout à des ratios molaires (q) faibles (Fig. 5.6). L'effet des protéines sur les systèmes PC/TW80 reste à être évalué. La taille et la morphologie de membranes modèles, en général, peuvent changer lorsque l'on ajoute les protéines (ou peptides), tel qu'observé avec le peptide transmembranaire KALP21 dans des petites bicelles²⁵⁵. De plus, l'effet d'ajouter une protéine ne sera pas nécessairement le même pour une autre, tout comme un peptide transmembranaire n'affectera pas la bicouche de la même manière qu'un peptide qui se lie à la surface²⁵⁶. Le choix du modèle, plus précisément sa taille, va aussi influencer certains paramètres, tel que le degré de solvation des têtes polaires lipidiques et donc celle de la protéine (ou du peptide). Les systèmes lipidiques de grande taille ont tendance à être des meilleurs mimétiques pour cette raison, car ils incorporent mieux les protéines et les peptides. Toutefois, ils sont limités à des techniques qui accommodent leur grande taille, telles que la RMN de l'état solide.

Le TW80 est utilisé régulièrement pour la conception de transférosomes, des systèmes vésiculaires permettant la livraison transdermique où il agit comme agent qui ramollit les bicouches^{233, 234}. Il pourrait donc être utilisé pour transférer d'autres molécules membranaires, telles que les PM. Dans notre étude, le TW80 augmente l'élasticité des bicouches de PC afin qu'elles puissent se déformer et s'orienter dans le champ magnétique. Ce système mime bien la biomembrane, en fait de composition et de morphologie, en plus d'être très intéressant pour les applications RMN. L'utilisation de TW80 pour purifier les PM, les réintroduire dans une membrane modèle et pour orienter les bicouches dans le champ magnétique ouvre la possibilité d'explorer une nouvelle variété de systèmes membranaires pour l'étude de peptides et de PM par RMN. Parmi ces PM, l'étude structurale du hERG bénéficiera du développement de nouveaux systèmes membranaires parallèlement au développement de nouvelles techniques biologiques pour produire le hERG de façon abondante et permettre de l'extraire de sa membrane native, de le purifier et de le reconstituer dans une membrane lipidique.

6.3 Perspectives pour l'étude du canal hERG et de la membrane par RMN

Dans cette thèse, nous avons raffiné le modèle structural du hERG en déterminant la structure de son SF, dans des conditions mimant les concentrations intra- et extracellulaires de potassium, et en étudiant son interaction avec la membrane et des médicaments cardiotoxiques afin de mieux comprendre son rôle dans le ALQTS (chapitre III). De plus, nous avons contribué à améliorer les connaissances sur le mécanisme d'ouverture et de fermeture particulier du hERG en étudiant le rôle du segment S4S5 et de la membrane dans la désactivation lente (chapitre IV).

Le hERG a longtemps été considéré comme une mauvaise cible, car son blocage occasionne des effets secondaires non désirés et potentiellement fatals²⁵⁷. Les analyses de dépistage du blocage du hERG et de la prolongation de l'intervalle QT

sur l'électrocardiogramme ne sont pas infaillibles. Par conséquent, l'inhibition du hERG, de même que pour la prolongation de l'intervalle QT, ne restent que des marqueurs de risque pour l'arythmogénèse²⁵⁸. De ce fait, il est estimé que près de 60 % des nouveaux médicaments thérapeutiques étant considérés hERG-actifs sont abandonnés au stade précoce du processus de développement de médicaments même si leur potentiel d'induire les torsades de pointe (TdP) n'est pas connu²⁵⁸. Il est alors essentiel de raffiner le modèle structural du hERG afin de mieux comprendre son fonctionnement et son rôle dans le ALQTS.

6.3.1 Raffiner le modèle structural et mieux comprendre la fonction du hERG

Pour mieux comprendre la fonction des protéines membranaires en général, et du hERG en particulier, on doit étudier sa structure. Pour ce faire, on peut adopter plusieurs stratégies. Idéalement, le hERG serait étudié *in vivo*, c'est-à-dire dans un organisme vivant. Cette stratégie est très difficile à réaliser en raison de la diversité moléculaire de l'échantillon compliquant l'analyse spectroscopique. Par contre, ce domaine d'étude commence progressivement à être exploré en RMN en solution et à l'état solide^{259, 260}. Par exemple, le groupe Marcotte développe des outils pour étudier les cellules intactes, donc *in vivo*, par RMN de l'état solide²⁶¹. On peut donc envisager, possiblement dans un avenir proche, pouvoir surexprimer des protéines marquées dans des cellules pour ensuite les étudier dans leur environnement natif. Par exemple, la surexpression du hERG pourrait être effectuée dans des œufs de *Xenopus laevis* étant donné que sa surexpression a déjà été réalisée. On peut aussi étudier le hERG *in cell*, autrement dit comme *in vivo* sauf que les cellules ne sont pas vivantes pendant l'analyse de RMN. Les cellules étant mortes, il y a moyen de vérifier que l'environnement natif n'est pas perturbé tel que démontré par le groupe de Baldus qui a surexprimé la PM PagL de *Pseudomonas aeruginosa* dans une souche mutante d'*Escherichia coli* (*E. coli*)²⁶².

Comme troisième stratégie, on peut exprimer le hERG en entier, le purifier et le reconstituer dans une membrane artificielle. Le choix du système d'expression est important ce qui est surtout vrai pour les protéines membranaires d'origine humaine. Par exemple, on peut employer un système d'expression bactérien, tel qu'*E. coli* qui est de loin l'organisme le plus utilisé pour la surexpression des protéines comme le témoigne la structure tridimensionnelle de la rhodopsine sensorielle de la cyanobactérie *Anabaena*, un homodimère de 81 kDa, qui a été obtenu par RMN de l'état solide^{263, 264}. En principe, les bactéries permettent d'obtenir un rendement protéique supérieur aux organismes eucaryotes, tels que les levures, mais ce n'est souvent pas le cas pour les protéines membranaires humaines, comme le hERG. Étant donné la taille de certaines PM, celle du monomère hERG étant de 127 kDa, leur surexpression dans un système bactérien est souvent toxique pour les bactéries, ou mène à la formation de corps d'inclusion. Cette stratégie présente plusieurs défis mais il y a beaucoup de progrès dans ce domaine pour les PM²⁶⁵.

On peut aussi choisir d'étudier les segments de la protéine plutôt que la protéine entière, tel que décrit aux chapitres III et IV. Cette stratégie est utile pour aider à résoudre sa structure entière. De plus, il est possible d'étudier les interactions entre le hERG (ou ses segments) et ses partenaires, tels que les médicaments cardiotoxiques (chapitre II) ou d'autres protéines (ou domaines protéiques du hERG), afin de nous renseigner davantage sur son fonctionnement et son implication dans le ALQTS. De même, on pourrait confirmer certaines interactions en substituant les résidus que l'on soupçonne être importants pour les interactions hERG-partenaire et les remplacer par des acides aminés de nature semblable. L'interaction avec le partenaire serait vérifiée par RMN, mais cette fois-ci avec les protéines (ou peptides) mutants. Il serait aussi intéressant de vérifier par RMN si la structure du hERG (ou de ses segments) change en présence des médicaments hERG-actifs, ou autres domaines du hERG dans le cas des segments.

Si l'on choisit de purifier le hERG en entier, il doit être reconstitué dans un environnement qui ressemble à son environnement natif afin de conserver sa structure et fonction naturelles. Vu sa taille énorme (plus de 500 kDa pour sa forme tétramérique), cela représente un défi colossal. En RMN en solution, on peut utiliser des solvants organiques, mais ils maintiennent rarement la structure native des PM, ou des micelles de détergents, qui imposent un haut degré de courbure aux PM. En plus de former de gros complexes avec des détergents, les protéines membranaires de grande taille, incluant le hERG, ne sont pas appropriées pour la RMN en solution, telles que décrit au chapitre III, car elle est limitée à des tailles de 100 kDa. Pour étudier la structure du hERG en RMN en solution, il serait envisageable d'étudier plutôt de longs peptides, tels que des domaines transmembranaires intégrés dans des membranes par exemple, car la région transmembranaire de ce canal (S1 à S6) ne représente que 22 % des résidus totaux. Pour des raisons de confidentialité, mes contributions dans un autre projet, concernant l'expression et la purification du domaine du pore du hERG (S5 à S6), ne seront pas présentées dans cette thèse.

En RMN de l'état solide, on peut utiliser des membranes modèles, mais pour obtenir une résolution spectrale semblable aux molécules qui se réorientent rapidement en solution, on peut employer deux stratégies : les membranes orientées ou la rotation à l'angle magique. La rotation à l'angle magique utilise des membranes modèles non orientées et consiste à faire tourner l'échantillon à haute vitesse à un angle de 54.7° par rapport au champ magnétique externe pour moyenner les interactions qui dépendent de l'orientation des noyaux afin d'obtenir des pics fins⁹⁰. Le hERG en entier pourrait difficilement être reconstitué dans des membranes modèles orientées, vu sa taille et sa complexité (tétramère). Par contre, l'étude des longs segments transmembranaires du hERG pourrait profiter de ce modèle, tel que celui que nous avons développé avec le Tween 80, où l'environnement lipidique se rapproche de celui de la biomembrane tout en permettant d'étudier sa structure et son orientation, ce qui est décrit plus en détail aux chapitres II et V.

Plusieurs études mettent beaucoup d'emphasis sur le rôle du segment S4S5 pour transmettre les mouvements du domaine sensible au voltage (DSV) à la porte d'activation (région intracellulaire du pore)^{59, 67}. La proximité du segment S4S5 avec l'hélice S6 du hERG en conformation fermée a été démontrée ainsi que sa proximité avec la région distale du domaine intracellulaire N-terminal en conformation ouverte (domaine PAS)^{67, 71}. Le groupe de Kong a étudié l'interaction du segment S4S5 avec le domaine N-terminal par titrage par RMN en solution³⁸. Ils ont aussi démontré que le segment S4S5 (nonapeptide) se structurait en hélice- α ¹⁵⁹. De même, le groupe de Vandenberg a obtenu la structure d'un peptide S4S5 de 20 acides aminés s'organisant en une hélice- α plus longue que celle qui a été signalée par Gayen *et al.*⁵⁷ La longueur du nonapeptide peut faire questionner la validité de la structure, surtout que Gayen *et al.* considèrent qu'un seul tour d'hélice est suffisant pour satisfaire aux critères structuraux d'une hélice- α . Il serait donc intéressant de vérifier les interactions du segment S4S5 plus long (chapitre IV) avec le domaine N-terminal du hERG par RMN en solution. En utilisant un protocole déjà établi par le groupe de MacKinnon³⁷, le domaine N-terminal peut-être facilement exprimé avec ou sans marquage isotopique. La RMN en solution peut ensuite servir pour attribuer les résonances des peptides S4S5 et N-terminal afin d'y déterminer les sites de liaison sur le domaine N-terminal en présence du segment S4S5, et vice versa. Similairement, le groupe de Barros a fait une étude électrophysiologique pour vérifier la proximité de régions spécifiques du S4S5 avec ceux du domaine N-terminal du hERG dans des oocytes de *Xenopus laevis*⁷¹. Ils ont introduit des résidus cystéine par mutagenèse dirigée aux résidus du N-terminal et du S4S5 qu'ils soupçonnaient interagir ensemble. Par la suite, ils ont vérifié la présence de liaisons disulfures qui leur a confirmé leur proximité.

6.3.2 Développement de nouvelles membranes modèles avec d'autres détergents

On a longtemps pensé que les lipides n'étaient que des molécules amphiphiles servant de support, et que seules les protéines effectuaient les tâches physiologiques. En fait, les cellules contrôlent avec précision leur composition membranaire afin de moduler la distribution et l'activité des protéines qui la compose²⁶⁶. Différentes espèces lipidiques (cholestérol, lipides saturés/insaturés, chargés/neutres) peuvent accomplir diverses fonctions, telles que la formation de radeaux lipidiques, leur implication dans la signalisation cellulaire et même la régulation de canaux ioniques²⁶⁷. Entre autres, le mésappariement hydrophobe entre les PM et la bicouche est un mécanisme de contrôle servant à trier les protéines de l'appareil de Golgi, du réticulum endoplasmique et de la membrane plasmique^{268, 269}. Par exemple, les cellules font varier leur composition en cholestérol – qui a tendance à épaissir la bicouche lipidique. L'on retrouve une quantité plus importante de cholestérol dans la membrane plasmique, moins dans l'appareil de Golgi et encore moins dans le RE, ce qui est proportionnel à leurs épaisseurs respectives²⁷⁰.

L'importance de la membrane a aussi été mise en évidence dans les chapitres III et IV où elle aurait un rôle indirect dans ALQTS et dans le mécanisme d'ouverture et de fermeture du hERG. De ces faits, il est indispensable de développer de nouveaux systèmes membranaires qui peuvent à la fois mimer adéquatement l'environnement natif des protéines d'intérêt, ainsi qu'améliorer les analyses biophysiques.

Par RMN, certains types d'études des PM, telles que *polarization inversion spin exchange at the magic angle* (PISEMA) et la RMN de l'azote-15, est facilitée lorsque le système protéine-membrane est aligné dans le champ magnétique^{271, 272}, tel que discuté aux chapitres I et IV. Certains détergents, tels que le Tween 80, peuvent agir comme ramollissant de membranes. C'est en conférant une morphologie plus élastique à la membrane qu'elle se déforme à haut champ magnétique dû à l'anisotropie de susceptibilité magnétique des phospholipides qui la constituent.

Idéalement, ce même surfactant peut aussi servir d'agent solubilisant lors de l'extraction des PM et comme intermédiaire de reconstitution. En principe, cette stratégie pourrait être utilisée pour des mélanges de PC et d'autres détergents communément utilisés avec les PM. Choisir un détergent pour l'étude de protéines membranaires n'est pas toujours facile, car il n'existe aucune règle définie à ce sujet. En réalité, il est rare de trouver un surfactant universel alors le choix du détergent et du lipide est souvent une question de chance où l'on doit considérer les propriétés de la protéine à étudier et des expériences à réaliser.

Malgré cela, les détergents restent les surfactants les plus utiles pour étudier la structure des protéines membranaires par RMN en solution considérant leur versatilité à solubiliser, purifier, transférer, renaturer et reconstituer les PM. Pour choisir les détergents qui serviront à développer de nouvelles membranes modèles, on va surtout viser des détergents qui sont doux, donc préféablement non chargés ou zwitterioniques, afin de favoriser le bon repliement et le maintien de l'activité de la protéine d'intérêt²⁴⁴. De même, un détergent qui peut rendre la membrane plus élastique peut être avantageux en RMN à l'état solide, tel que démontré avec le Tween 80 au chapitre V. Les propriétés moléculaires des détergents (Tableau 6.1) aideront à choisir un modèle prometteur.

Tableau 6.1 Propriétés moléculaires de détergents couramment utilisés dans les transférosomes et pour l'étude de protéines membranaires^{90, 273}.

Surfactant	Classe	CMC (mM)	Nombre d'agrégation	Masse moléculaire monomérique (g)
SDS	Ionique	3	80	288
DPC	Zwitterionique	1.5	70	352
DHPC (C6-PC)	Zwitterionique	15	35	454
DDM	Non-ionique	0.2	140	528
OG	Non-ionique	25	27	292
CHAPS	Zwitterionique	5	-	615
Brij 35	Non-ionique	0.09	40	1200
Tween 80	Non-ionique	0.01	60	1310
Tween 20	Non-ionique	0.06	-	1228
C ₁₂ E ₈	Non-ionique	0.09	120	538
Triton X-100	Non-ionique	0.3	140	625
Acide cholique, sel sodique	Non-ionique	9 à 15	3	178
Span 80	Non-ionique	-	-	428

SDS: dodécylsulfate de sodium, DPC: dodécylphosphocholine, DHPC: dihexanoylphosphocholine, DDM: dodecyl- β -maltoside, OG: Octyl β -D-glucoside, CHAPS: 3-[diméthylammonio]-1-propanesulfonate, Brij 35: éther lauryl polyoxyéthylène, Tween 80: monooléate sorbitane de polyoxyéthylène 80, Tween 20: monolaurate sorbitane de polyoxyéthylène 20, C₁₂E₈: octaéthylène glycol monododécyl éther, Triton X-100: éther de polyéthylène glycol et d'octylphénol, Span 80: monooléate sorbitane

L'étude des PM par RMN requiert une concentration importante de protéines, relativement à celle des surfactants, afin d'obtenir un signal suffisamment élevé. Il est donc favorable d'utiliser un détergent ayant un nombre d'agrégation faible, comme l'acide cholique à sel sodique, la DHPC, l'OG et le Brij 35 (Tableau 6.1). Les détergents ayant un nombre d'agrégation faible favorisent les petits complexes

surfactants/protéines qui se réorientent rapidement en solution, ce qui est idéal pour la RMN en solution. De plus, les PM ont tendance à précipiter lorsqu'elles sont appariées à des détergents ayant des CMC trop élevées. Il est donc préférable d'utiliser des détergents ayant des CMC basses, tels que le Brij 35, le Tween 20 et C₁₂E₈, ou simplement de rester largement au dessus de la CMC. Certains détergents, tels que la famille des Span, augmentent l'élasticité des liposomes pour les rendre plus flexibles (transfersomes) afin qu'ils puissent franchir la couche externe de l'épiderme, le *stratum corneum*^{274, 275}. Ces détergents sont potentiellement utiles pour former des membranes modèles qui s'orientent dans le champ magnétique. Lorsque l'on emploie des membranes modèles mixtes (à plus d'un surfactant) il est aussi important de vérifier la miscibilité entre les surfactants.

De la même manière, le choix du lipide peut aussi être optimisé. Il pourrait être intéressant de travailler avec des lipides qui ont des températures de transition basses pour l'étude structurale des PM, comme la palmitoyl-PC (POPC) et la dioleoyl-PC (DOPC) qui ont des T_m de -2 °C et -17 °C (Avanti Polar Lipids, Inc.), respectivement. Travailler à basse température permet de ralentir la dynamique des protéines, simplifiant leurs mouvements, ce qui augmente la sensibilité (signal/bruit) en RMN à l'état solide tout en maintenant la phase liquide cristalline^{276, 277}. Le point de Krafft, étant la température minimale à laquelle les surfactants forment des micelles, est un paramètre qu'il faut aussi considérer en travaillant à basse température, car en dessous de cette température la CMC n'existe plus.

Les efforts mis ces dernières décennies sur le développement de nouveaux modèles membranaires ont porté fruit en RMN en solution et à l'état solide. Parmi les structures des PM obtenues, la taille est passée de 4 kDa²⁷⁸ jusqu'à 43 kDa²⁷⁹ par RMN en solution ainsi que de 4 kDa²⁸⁰ à 83 kDa²⁶³ par RMN de l'état solide. Il y a plus de 30 ans, le SDS²⁸¹ et la DMPC²⁸² étaient le détergent et le lipide, respectivement, les plus employés. De nos jours, la disponibilité de nouveaux

modèles membranaires est en pleine croissance. Notre équipe a publié un article de revue extensif détaillant les modèles membranaires disponibles jusqu'à présent pour l'étude des protéines membranaires par RMN, auquel j'ai participé (Annexe B), permettant d'étudier des protéines de plus en plus grosses et ouvrant donc des perspectives pour l'étude structurale du hERG par RMN.

6.3.3 Le hERG, une cible thérapeutique et son rôle dans le cancer

Dans cette thèse, on focalise principalement sur les effets indésirables du blocage du hERG (prolongation du QT, TdP, arythmies fatales). Étant donné les progrès récents sur la caractérisation de la fonction du hERG, celui-ci pourrait aussi être exploité comme cible thérapeutique. Par exemple, le hERG est la cible primaire des agents antiarythmiques de classe III²⁵⁷. Cette catégorie de médicaments perturbe le courant potassique du hERG en prolongeant la repolarisation, donc l'intervalle QT. Ces médicaments pourraient donc servir comme stratégie thérapeutique pour les gens atteints de la maladie génétique du syndrome du QT court (*short QT syndrome*; SQTS) pour empêcher les arythmies liées aux courants réentrants causés par ce syndrome²⁵⁷.

Le hERG est surtout exprimé dans les cardiomyocytes mais se retrouve aussi dans d'autres tissus, tels que les cellules neuronales, pancréatiques, chromaffines et dans les muscles lisses du tube digestif¹⁹⁹. La présence du hERG dans les cellules tumorales a encouragé son utilisation comme cible thérapeutique afin de diagnostiquer, traiter et classer plusieurs types de cancers²⁵⁷.

En oncologie, énormément d'efforts sont mis pour cibler spécifiquement les cellules cancéreuses. Le hERG est exprimé constitutivement dans plusieurs lignées cellulaires tumorales^{199, 283} où son expression est plus fréquente que dans les tissus non cancéreux^{284, 285}. Plusieurs groupes de recherche ont tenté de déterminer le rôle du

hERG dans le cancer. Certains ont démontré que l'expression du hERG facilitait la prolifération des cellules tumorales²⁸⁶ et qu'en utilisant des médicaments qui le bloquent ils pouvaient inhiber la prolifération^{61, 287-289}. De plus, l'expression du hERG dans des lignées cellulaires cancéreuses peut aussi faciliter la propagation du cancer (migration) puisqu'elles perdent l'inhibition de contact^{287, 290}. De plus, le hERG semble réguler l'invasion des tumeurs, car il est souvent retrouvé dans les cancers métastatiques²⁹¹. Son rôle dans l'angiogenèse des tumeurs serait aussi mis en évidence, car son ouverture et sa fermeture sont modulées par l'hypoxie²⁹². Les tumeurs sont souvent caractérisées par un manque d'oxygène, car la croissance des tissus cancéreux devance souvent la néovascularisation. Or, la surexpression du hERG modulerait la sécrétion de VEGF, un facteur de croissance de l'endothélium vasculaire²⁹³.

En résumé, l'identification et la caractérisation de la fonction du hERG dans plusieurs tissus est prometteur pour exploiter le hERG dans la pathologie du cancer. Le hERG pourrait donc servir de marqueur pour dépister le cancer, et de cible thérapeutique. Par exemple, l'astémizole, un antihistaminique ayant une capacité d'inhibition du hERG, serait un bon candidat de médicament anticancéreux. Les histamines sont connues pour favoriser la prolifération des cellules normales et malignes. Il a été démontré de manière *in vivo* et *in vitro* que l'astémizole bloque les canaux K_v11.1, comme plusieurs autres antihistaminiques, et inhibe la prolifération des cellules cancéreuses²⁹⁴. Les effets secondaires cardiovasculaires sont rares, donc l'utilisation de médicaments qui bloquent le hERG serait une stratégie innovatrice pour combattre le cancer.

Le canal hERG a longtemps été la cible la plus redoutée puisqu'il a toujours été un grand défi de prédire l'interaction de celui-ci avec les médicaments. Poursuivre les études structurales et mécanistiques du canal K_v11.1 nous permettra de mieux comprendre le processus par lequel les médicaments anti-hERG l'inactivent et

éventuellement de surmonter la complexité de la nocuité des médicaments. Dans ce contexte, tout progrès, y compris le développement de nouveaux modèles membranaires, tels que le PC/TW80, est appréciable pour aider à répondre à ces questions cruciales du point de vue de la santé publique.

La détermination structurale et dynamique d'une protéine membranaire entière, telle que le hERG, est motivée par ces enjeux capitaux pour la société, mais en l'état actuel des possibilités apportées par la science, cette tâche est très difficile et nous avançons progressivement. La cristallographie de rayons X et la RMN sont sollicitées pour résoudre ces problèmes, et bénéficient également des progrès considérables réalisés en biochimie des protéines membranaires. Dans le but d'utiliser au mieux la RMN des solides pour franchir ces obstacles, nous nous sommes d'abord limités à l'étude structurale des zones les plus cruciales de cette protéine. Mais nous avons également préparé l'avenir en développant de nouvelles membranes modèles qui pourront être utiles à des études plus complètes et espérer enfin, un jour, connaître la structure et le mécanisme de cette protéine littéralement au cœur de l'organisme humain.

ANNEXE A

POTENTIAL ROLE OF THE MEMBRANE IN HERG CHANNEL FUNCTIONING AND DRUG-INDUCED LONG QT SYNDROME

Étienne Chartrand, Alexandre A. Arnold, Andrée Gravel, Sarah Jenna et Isabelle
Marcotte

Biochimica et Biophysica Acta 1798 (2010) 1651–1662

A.1 Résumé

Les canaux potassiques human ether-à-go related gene (hERG) se trouvent dans les membranes des cellules du myocarde où ils assurent une activité cardiaque normale. L'interaction de médicaments avec ce canal, un effet secondaire que l'on nomme le syndrome du QT long acquis (ALQTS), peut mener à des arythmies et même à l'arrêt cardiaque. Le canal hERG est un membre unique de la famille des canaux potassiques voltages dépendants, car la boucle extracellulaire du domaine du pore reliant l'hélice transmembranaire S5 à l'hélice du pore est particulièrement longue. Considérant la proximité du segment S5-P à la surface de la membrane, nous étudions l'interaction du segment central I583-Y597 avec des bicelles. Les expériences de RMN en solution et à l'état solide, ainsi que les résultats de dichroïsme circulaire démontrent la forte affinité entre le segment I583-Y597 et la membrane dans laquelle le segment S5-P interagirait principalement avec la surface de la membrane de manière non structurée. On a observé que la structure de ce segment dépendait de la composition des membranes modèles. La présence de micelles de détergent et de charges négatives favorise la conformation hélicoïdale. Nos résultats suggèrent que l'interaction entre le S5-P et la membrane pourrait participer à stabiliser des conformations transitoires du canal, mais que la structure en hélice serait déclenchée par des interactions avec d'autres domaines du hERG. Puisque des sites de liaison de médicaments ont été identifiés sur le segment S5-P,

nous avons vérifié son rôle dans le ALQTS. Les quatre médicaments ALQTS-actifs qui ont été étudiés ont démontré plus d'affinité avec la membrane qu'avec le segment S5-P. Nos résultats indiquent donc deux rôles possibles de la membrane quant au fonctionnement du canal hERG et dans le ALQTS.



Contents lists available at ScienceDirect

Biochimica et Biophysica Acta

journal homepage: www.elsevier.com/locate/bbamem

Potential role of the membrane in hERG channel functioning and drug-induced long QT syndrome

Étienne Chartrand, Alexandre A. Arnold, Andrée Gravel, Sarah Jenna, Isabelle Marcotte *

Department of Chemistry, Pharmaqam/NanaQAM, Université du Québec à Montréal, P.O. Box 8888, Downtown Station, Montreal, Canada H3C 3P8

ARTICLE INFO

Article history:

Received 2 November 2009

Received in revised form 21 April 2010

Accepted 17 May 2010

Available online 25 May 2010

Keywords:

NMR spectroscopy

Bicelles

Membrane-protein interaction

Drug-protein interaction

Cardiotoxic drugs

Voltage-gated potassium channel

ABSTRACT

The human ether-à-go-go related gene (hERG) potassium channels are located in the myocardium cell membrane where they ensure normal cardiac activity. The binding of drugs to this channel, a side effect known as drug-induced (acquired) long QT syndrome (ALQTS), can lead to arrhythmia or sudden cardiac death. The hERG channel is a unique member of the family of voltage-gated K⁺ channels because of the long extracellular loop connecting its transmembrane S5 helix to the pore helix in the pore domain. Considering the proximal position of the S5-P linker to the membrane surface, we have investigated the interaction of its central segment ⁵⁸³Y⁵⁹⁷ with bicelles. Liquid and solid-state NMR experiments as well as circular dichroism results show a strong affinity of the ⁵⁸³Y⁵⁹⁷ segment for the membrane where it would sit on the surface with no defined secondary structure. A structural dependence of this segment on model membrane composition was observed. A helical conformation is favoured in detergent micelles and in the presence of negative charges. Our results suggest that the interaction of the S5-P linker with the membrane could participate in the stabilization of transient channel conformations, but helix formation would be triggered by interactions with other hERG domains. Because potential drug binding sites on the S5-P linker have been identified, we have explored the role of this segment in ALQTS. Four LQTS-labile drugs were studied which showed more affinity for the membrane than this hERG segment. Our results, therefore, identify two possible roles for the membrane in channel functioning and ALQTS.

© 2010 Elsevier B.V. All rights reserved.

1. Introduction

HERG (*human ether-à-go-go-related-gene*) potassium channels are essential for the normal electrical activity of the heart. Located in the myocardium cell membrane, the structure of these voltage-gated K⁺ channels (VGK) has never been determined experimentally. Homology models of the hERG K⁺ channel have been proposed based on its primary sequence and the X-ray structure of various bacterial K⁺ channels [1–3]. The predicted structure consists of four monomeric subunits, each containing six transmembrane spanning helices S1–S6 [4]. The first four helices (S1–S4) comprise the primary voltage sensor while S5 and S6 form the pore domain. The K⁺ selectivity filter and a small pore helix (P) involved in inter-subunits contacts are found on the extracellular loop that links S5 to S6. The loops from each monomer meet into the pore to form the selective K⁺ doorway of the channel [5].

Inherited mutations in the hERG gene can cause the long QT syndrome (LQTS), a cardiac repolarization disorder that predisposes individuals to ventricular arrhythmia that can lead to sudden death. However, A(cquired)LQTS can also be induced by the blockage of the

hERG channels by prescription drugs. This side effect has resulted in significant labelling restrictions or drug withdrawal from the market by regulatory agencies worldwide [6,7]. It is now routine practice in the pharmaceutical industry to test compounds for hERG-channel activity, and LQTS is a common reason for drug failure in early preclinical safety trials [8].

The problem of ALQTS is correlated with the wide spectrum of hERG blockers. Several classes of structurally different therapeutic molecules such as antibiotics, antihistamines, antipsychotics and antiarrhythmics have LQTS side effects [9–12]. Electrophysiology and *in silico* studies show that most hERG-channel blockers would exert their activity by binding one or several sites located in the pore domain. This region is composed of S5 and S6 which inner cavity is lined by aromatic and polar residues that permit hydrophobic, electrostatic and polar interactions with a wide range of compounds [1,4,13–16]. Tyr⁶⁵² and Phe⁶⁵⁶ located on S6 are especially important for the binding of many drugs [1,15–19]. The role of the extracellular S5-P linker has also been pointed out with residues such as Ser⁶²⁰ [14], Thr⁶²³, Ser⁶²⁴ and Val⁶²⁵ [16] being involved in the binding of LQTS-prone drugs. Toxins such as ErgToxin and BeKm-1 are known to bind to this region of hERG while they do not bind to other members of the VGK family [20,21]. However, some toxins such as agitoxin and charybdotoxin are known to bind the S5-P loop of VGK channels but not the hERG.

* Corresponding author. Department of Chemistry, Université du Québec à Montréal, P.O. Box 8888, Downtown Station, Montreal (Qc), Canada H3C 3P8. Tel.: +1 514 987 3000 #5015; fax: +1 514 987 4054.

E-mail address: marcotte.isabelle@uqam.ca (I. Marcotte).

The hERG channel is a unique member of the VGK family because of its long extracellular loop connecting S5 to the pore helix, i.e. 43 amino acid residues vs. 12–23 residues in most K⁺ channels [22,23]. Liu et al. [24] showed that mutations in the 15 amino-acid residue central segment I⁵⁸³–Y⁵⁹⁷ of the S5-P linker lead to hERG channel dysfunction. They thus suggested its role in the degree of inactivation and K⁺ selectivity [25]. Their analysis of these mutations also suggested a helical periodicity of I⁵⁸³–Y⁵⁹⁷ [24]. Recent nuclear magnetic resonance (NMR) structural work performed on this segment also showed a helical conformation in sodium dodecylsulfate (SDS) and dodecylphosphocholine (DPC) micelles [23,26]. A model was proposed in which the NH₂-terminal would be located close to the pore entrance, with a 20 Å 583–597 helix that would be sufficiently long to interact with the voltage-sensing domain [24]. From these studies, it was suggested that the I⁵⁸³–Y⁵⁹⁷ extracellular segment of the hERG would undergo dynamical structural changes, approaching the pore entrance to participate to the function of the channel outer mouth [23,25]. It is clear that this long hERG S5-P linker is a critical region of the channel, therefore it is of great importance to identify its dynamic and structural role in the channel function.

Considering the proximal position of the S5-P linker to the membrane surface, the aim of this work was to investigate the interaction of the I⁵⁸³–Y⁵⁹⁷ segment of hERG with model phospholipid membranes. To the best of our knowledge, no information regarding its interactions with membrane has been published. Moreover, to explore the role of this S5-P linker moiety on the drug-induced LQTS, we have also studied its interaction with LQTS-labile drugs. This was done by combining liquid- and solid-state NMR and using bicelles as model biomembranes. Bicelles are generally composed of dimyristoylphosphatidylcholine (DMPC) and dihexanoylphosphatidylcholine (DHPC) in a molar ratio (*q*) which determines the membrane size, shape and properties [27–29]. By adjusting the *q* ratio, fast-tumbling and magnetically aligned bicelles (*q* > 2.3) can be prepared, therefore these membranes are tunable for liquid- and solid-state NMR experiments, respectively. Similarly to natural membranes, bicelles have a planar surface and their lipids are in the liquid-crystal phase.

Four drugs with reported QT prolongation effect were selected for this study because of their different structures, octanol–water partition coefficients (logP), and pharmacological classes, as shown in Table 1. Bepridil, a calcium antagonist initially developed as an

antianginal agent, was withdrawn from the market for causing Torsades de Pointes (TdP) [30–32]. Diphenhydramine and cetirizine are respectively first- and second generation antihistamines that showed inhibition of hERG channels [33–35], while pentamidine is an antiprotozoal agent reported to cause QT prolongation and TdP when given in intravenous form [36–38].

Using ¹H liquid-state NMR with Pulsed Field Gradient (PFG) self-diffusion measurements, the membrane affinity of I⁵⁸³–Y⁵⁹⁷ and the drugs, as well as the drug/segment association are evaluated. Saturation transfer difference (STD) ¹H NMR experiments are used to determine the location of the hERG segment in the membrane. Two-dimensional ¹H NMR and circular dichroism spectra provide structural data on the peptide in water, bicelles and various detergent micelles. Finally, solid-state ³¹P and ²H NMR are employed to probe the effect of the peptide and the cardiotoxic drugs on the polar and hydrophobic regions of the membrane, respectively.

2. Materials and methods

2.1. Materials

The hERG extracellular linker segment with sequence IGWLHNLGDQIGKPY was synthesized by GenScript Corporation (Piscataway, NJ, USA) with >95% purity. Protonated and deuterated dimyristoyl- and dihexanoylphosphatidylcholine (DMPC, DMPC-d₅₄, DHPC, DHPC-d₂₂), dimyristoylphosphatidylserine (DMPS), dodecylphosphocholine (DPC), 1-myristoyl-2-hydroxy-sn-glycero-3-phosphocholine (lyso-myristoylphosphatidylcholine, LMPG) and 1-myristoyl-2-hydroxy-sn-glycero-3-phosphoglycerol sodium salt (lyso-myristoylphosphatidylglycerol, LMPG) were purchased from Avanti Polar Lipids (Alabaster, AL, USA) while hexamethyldisilane (HMDS) and deuterium-depleted water, deuterated sodium dodecylsulfate (SDS-d₂₅), pentamidine isothionate, bepridil, cetirizine and diphenhydramine hydrochlorides were obtained from Sigma Aldrich (Oakville, ON, Canada) and used without further purification. Deuterium oxide (D₂O) was purchased from CDN Isotopes (Pointe-Claire, QC, Canada).

2.2. Sample preparation

2.2.1. Nuclear magnetic resonance

Bicelles were prepared by mixing freeze-dried DMPC and DHPC with the desired long-to-short-chain (*q*) ratio in aqueous solution, with or without hERG segment, and submitted to a series of three freeze (liquid N₂)/thaw (50 °C)/vortex shaking cycles until a transparent non-viscous solution was obtained. Hydration percentages (weight/weight) were 96% for high-resolution NMR and 80% for solid-state NMR, and *q* ratios were as follows: *q* = 0.5 for both translational diffusion and saturation transfer difference measurements, *q* = 1 for chemical shift assignment and analysis, and *q* = 3.5 for solid-state NMR experiments. Total lipid/peptide (L/P) molar ratios of 25:1 and 100:1 were used for solid-state NMR, and 50:1 for high-resolution ¹H NMR. In all NMR experiments the peptide concentration was 5 mM and the surfactant concentration was, thus, maintained well above the critical micelle concentration (CMC) of DHPC in the bicelle mixture (15 mM) [39]. The same sample preparation was applied to SDS micelles. Because this segment is believed to be dynamic and possibly involved in the K⁺ channel function, deionized water (pH = 5.5) was used to avoid salt interference [23]. ¹H diffusion NMR experiments were carried out in D₂O while all high-resolution NMR experiments were done using 10% D₂O. All two-dimensional NMR experiments were carried out using lipids and SDS with deuterated acyl chains to minimize the contribution of the lipid resonances to the ¹H NMR spectra. Oriented bicelles for solid-state ²H NMR were prepared with DMPC-d₅₄ in deuterium-depleted H₂O.

Table 1
Structures and logP values of the studied cardiotoxic drugs.

Drug	logP	Structure
Bepridil	5.33	
Cetirizine	2.98	
Diphenhydramine	3.44	
Pentamidine	1.32	

2.2.2. Circular dichroism

Bicelles and micelles were prepared as described above. Bicelles containing DMPS (Bicelles/PS) were made by substitution of 25% of DMPC with the negatively charged DMPS. For all samples, a hydration percentage of 99% was employed. The concentration of hERG I⁵⁸³–Y⁵⁹⁷ segment was kept to 0.13 mg/ml (76 μM) while lipid or surfactant concentrations were 33 mM (bicelles), 22 mM (Bicelles/PS), 30 mM (DHPC), 15 mM (DPC, LMPC, LMPG). All lipid or surfactant concentrations were thus kept above their CMC [39,40]. The surfactant/peptide molar ratio was 200:1 to provide an appropriate micelle:peptide stoichiometry that limits possible peptide aggregation. In the case of bicelles ($q = 1$), a total lipid-to-peptide molar ratio of 600:1 was employed to ensure that at least two bicelles were available per I⁵⁸³–Y⁵⁹⁷ segment in the sample. This can be assessed knowing concentration of DMPC and DHPC, the q ratio and the surface area of phosphatidylcholines [41].

2.3. Solution and solid-state NMR

All spectra were recorded on a hybrid liquid/solid-state Varian Inova Unity 600 (Varian, Walnut Creek, CA, USA) spectrometer operating at frequencies of 599.95 MHz for ¹H, 246.86 MHz for ³¹P and 92.125 MHz for ²H. The ¹H chemical shifts were internally referenced by adding a small amount of 2,2-dimethyl-2-silapentane-5-sulfonic acid (DSS) set to 0.0 ppm. All ³¹P NMR spectra were externally referenced with respect to the signal of 85% phosphoric acid set to 0 ppm.

2.3.1. Pulsed-field gradient (PFG) diffusion experiments

¹H NMR self-diffusion measurements at 25 °C were performed with a double-resonance 3-mm indirect z-gradient probe using the water-suppressed LED pulse sequence (water-sLED) [42]. A hard 90° pulse of 5.5 μs was used. The gradient pulse duration δ was 6 ms and diffusion times (Δ) were varied between 100 and 150 ms to ensure that the echo intensities were attenuated by at least 80%. 24000 data points were obtained and typically 48 scans were acquired for each selected gradient strength with a recycle delay of 5.0 s. A complete attenuation curve was obtained by measuring 15 gradient strengths which were linearly incremented between 2.1 and 31.5 G/cm.

Translational diffusion coefficients (D_s) were calculated using the following equation [42]:

$$A(G) = A(0) \exp \left[-(\gamma \delta G)^2 (\Delta - \delta / 3) D_s \right] \quad (1)$$

where $A(G)$ is the echo amplitude, γ is the ¹H gyromagnetic ratio. The gradient strength was calibrated using back calculation of the coil constant from a measurement of the diffusion constant of H₂O traces in D₂O using $D_s = 1.9 \times 10^{-5} \text{ cm}^2/\text{s}$ at 25 °C [43].

2.3.2. Saturation transfer difference (STD) experiments

The STD experiments consisted of a train of 50 ms Gaussian selective pulses separated by 1 ms delays and followed by a WET water suppression and detection [44–46]. The saturation frequencies were alternated between the resonance to be saturated and –25 ppm. The Gaussian pulses were applied with radio-frequency field strength of 120 Hz and saturation times were varied between 250 ms and 5 s. The recycle delay was 3 s.

2.3.3. High-resolution ¹H two-dimensional experiments

¹H total correlation spectroscopy (TOCSY) spectra were recorded with a 90° pulse of 5.5 μs, and spin-lock times of 25, 50 and 100 ms with MLEV17 spin-lock fields of 15 kHz [47]. A spectral width of 8 kHz was used in both dimensions with 512 and 1024 complex data points in the indirect and direct dimensions, respectively. 16 transients were accumulated with a repetition delay of 1 s. Two-dimensional nuclear Overhauser spectroscopy (NOESY) spectra [48,49] were recorded

using a pulse length of 5.5 μs with mixing times varying from 100 to 750 ms. A spectral width of 8 kHz was used in both dimensions with 1024 data points in F2 and 512 increments in F1. A total of 16 transients were recorded with a repetition delay of 1 s.

2.3.4. Solid-state NMR experiments (SS-NMR)

Solid-state NMR experiments were carried out using a 4-mm broadband/¹H dual-frequency magic-angle-spinning probehead. ³¹P NMR spectra were recorded using a phase-cycled Hahn echo pulse sequence with gated broadband proton continuous wave decoupling at a field strength of 50 kHz [50]. The 90° pulse length was 5 μs, the interpulse delays were 30 μs and typically 4800 scans were acquired with a recycle delay of 3 s. ²H NMR spectra were obtained using a solid echo pulse sequence [51] with a 90° pulse length of 3 μs, an interpulse delay of 45 μs and repetition delay of 500 ms. At least 8000 data points were obtained and typically 5000 scans were acquired. The quality of the bicelles' magnetic orientation with or without the peptide was sufficient to enable the direct measurement of quadrupolar splittings on the ²H spectra with no de-Pakeing.

2.3.5. Data processing

Diffusion, STD and SS-NMR data were processed using matNMR [52]. High-resolution 2D NMR spectra were processed using the NMRPipe package [53] and analyzed with the software NMRView for chemical shift assignment and NOE calibrations [54].

2.3.6. Circular dichroism (CD) spectropolarimetry

CD analyses were performed on a JASCO J-815 spectrometer (Jasco Inc., Easton, MD, USA) at ~23 °C. Data were collected using a 1-mm 100 QS cuvette over the wavelength range 190–250 nm and with a resolution of 0.2 nm, a bandwidth of 1 nm, and a response time of 0.5 s. The signal was averaged over 5 scans with blank subtraction of the lipid or surfactant suspension. In order to estimate the contributions of different structural elements, CD spectra were deconvoluted using DICHROWEB and the SELCON3 or CONTIN-LL algorithms [55].

3. Results

3.1. Interaction of I⁵⁸³–Y⁵⁹⁷ with model membranes

3.1.1. Does this extracellular linker segment bind even weakly to the membrane?

The central segment I⁵⁸³–Y⁵⁹⁷ of the S5-P linker of the hERG channel displays a strong amphipathicity, therefore its potential binding to the membrane needs to be addressed. As a first step, we have recorded ¹H NMR spectra of this peptide in water and in the presence of membrane mimetic milieus. Initially, TOCSY spectra (not shown) were acquired to assign the ¹H chemical shifts of the hERG segment in water, bicelles and SDS micelles. The chemical shift values are shown as supplementary material.

The 1D ¹H NMR spectra show major changes for the amide and aromatic regions when I⁵⁸³–Y⁵⁹⁷ is in deuterated bicelles (Fig. 1B) and SDS-d₂₅ micelles (Fig. 1C). In these conditions resonances are shifted and considerably broadened as compared to the peptide in water (Fig. 1A). This most likely results from a reduced mobility of the peptide upon binding to large bicellar or micellar objects.

In order to quantify the affinity of this hERG segment for the membrane, we have determined the fraction of peptide bound to the membrane. This was done by measuring the self-diffusion coefficients of the peptide in H₂O and in the presence of bicelles ($q = 0.5$) by ¹H NMR using pulsed field gradient stimulated echo (PFGSTE) experiments [46,56–58]. If the hERG segment is in rapid exchange on the NMR timescale between the free and the bound states and assuming a two-site model as proposed by Stilbs [59], the diffusion coefficient (D_{obs}) of the bicelle-associated peptide will be an average of diffusion coefficients for the free (D_{free}) and bound (D_{bound}) states. In our study,

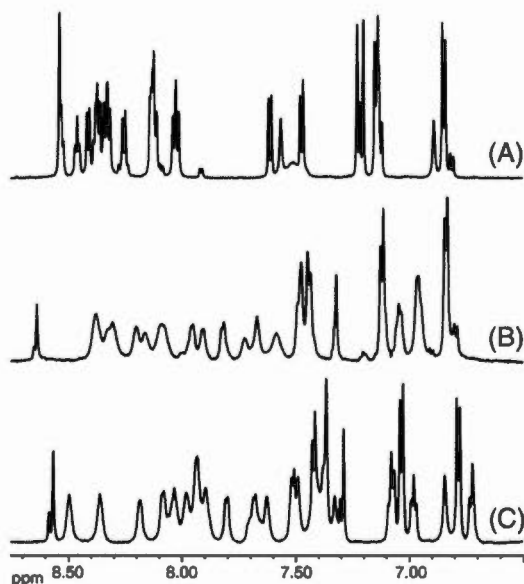


Fig. 1. Amide and aromatic regions of the ^1H NMR spectra of hERG $I^{583}\text{--}Y^{597}$ in (A) water, (B) bicelles (DMPC- d_{54} /DHPC- d_{22} , $q = 1$), and (C) SDS- d_{25} micelles (lipid or surfactant-to-peptide molar ratio of 50:1).

D_{free} refers to the diffusion coefficient of the peptide in water and D_{bound} to the diffusion coefficient of the bicelles in water. Following such a model, the percentage of peptide bound to the membrane can be calculated as follows:

$$\frac{D_{\text{obs}} - D_{\text{free}}^{\phi}}{D_{\text{bound}} - D_{\text{free}}^{\phi}} \times 100 \quad (2)$$

This model can also be applied to assess the binding of a drug with a membrane or a peptide.

D_{free}^{ϕ} is the corrected free diffusion coefficient because in a bicelle environment, the diffusion of the free hERG peptide (or drug) in the aqueous solution can be hindered by the actual presence of the bicelles. It is thus essential to correct D_{free} by introducing an obstruction factor A that can be defined, for spherical objects, according to the following equation:

$$A = 1 / (1 + 0.5\phi) \quad (3)$$

where ϕ is the volume fraction of the obstructing particles. A factor A of 0.935 can be calculated for a 14% w/w bicelle solution at 20 °C using a spherical model as proposed by Gaemers and Bax [60]. Because a radius of 43 Å is predicted for bicelles with $q = 0.5$ and a bilayer thickness of ~40 Å [61], we have approximated the bicelles as spherical objects and used this correction factor in our diffusion measurement calculation as was done for the neuropeptide met-enkephalin [57]. Since there are no analytical expressions to calculate obstruction factors for discoidal objects, the best approximation for which an analytical expression exists would be spheroids [60,62], leading to an obstruction factor of 0.925. The commonly used spherical approximation, thus, appears to be excellent for isotropic bicelles with $q = 0.5$ as used in our study.

The value of D_{obs} used in the calculations was the average of the diffusion coefficients obtained for three peptide resonances. Although the diffusion coefficient of bicelles can be measured with the PFGSTE experiment from the signals of DMPC/DHPC directly, it can also be

measured more accurately and conveniently from the signal of a small amount of a hydrophobic probe molecule known to be completely partitioned within the hydrophobic core of the bicelles. Indeed, in the case of bicelles with low q ratios, the lipids are rapidly exchanging between the solution and the micelle-like object [63]. As a consequence, the apparent diffusion coefficient obtained directly from lipid signals is usually from 5% to 10% higher than the actual diffusion coefficient of bicelles determined from the diffusion of the probe molecule [56]. In this work, a small amount of hexamethyldisilane (HMDS) was added to the bicellar samples and its resonance used to measure the diffusion of the whole bicelle. HMDS has been widely used for this purpose in diffusion studies of micellar and bicellar systems [56,59].

Table 2 presents the diffusion coefficients measured for pure bicelles, free and membrane-associated $I^{583}\text{--}Y^{597}$ peptide as well as its percentage of association to the bicelles as calculated from equation (2). All the plots of the normalized natural log signal intensity versus squared gradient strength G^2 were linear (not shown), consistent with a fast-exchange scenario (or a single-state case). This also indicates that there is no influence of intermolecular NOEs on the diffusion results [64,65]. The translational diffusion coefficients for the bicelles are in good agreement with the values reported in the literature [46,63]. Our results show that 98% of the peptide would bind to the model membranes at the lipid/peptide (L/P) molar ratio studied (100:1). This constitutes the extreme case of the model presented in equation (2) in which the association equilibrium is displaced towards a bound state, i.e. a single-state model.

3.1.2. Is the membrane perturbed by the hERG segment?

Considering the strong affinity of the $I^{583}\text{--}Y^{597}$ segment of the extracellular hERG loop, we have examined its effect on the phospholipid membrane. ^{31}P and ^2H SS-NMR experiments are well-established techniques to study the effect of peptides or drugs on model and natural membranes. The high NMR sensitivity and 100% natural abundance of the ^{31}P isotope as well as the presence of a single phosphorus nucleus in the phospholipid headgroup allow exploiting ^{31}P NMR to obtain valuable information on the polar region of lipid membranes [66]. The hydrophobic region on the other hand can be studied by ^2H SS-NMR using phospholipids with deuterated acyl chains. The quadrupolar interaction is highly sensitive to motions in the bilayer, thus perturbations of the hydrophobic core can be probed [67,68].

Fig. 2A presents the ^{31}P SS-NMR spectra of DMPC- d_{54} /DHPC bicelles with and without the hERG peptide at 37 °C. These spectra are typical of well-oriented bilayers with the normal perpendicular to the direction of the magnetic field. As assigned in previous work [27], the upfield resonance corresponds to the long-chain DMPC whereas DHPC resonance appears at the downfield side of the spectrum. This can be explained by the reorientation or fast lateral diffusion of the short-chain phospholipids on the highly curved region formed by the

Table 2
Translational diffusion coefficients of bicelles ($q = 0.5$), hERG $I^{583}\text{--}Y^{597}$ and cardiotoxic drugs used to calculate the fraction of bound peptide and drugs.

System	$D_{\text{obs}} (\times 10^{-10} \text{ m}^2 \cdot \text{s}^{-1})$			
	in water	with Bicelles	with $I^{583}\text{--}Y^{597}$	with Bicelles/ $I^{583}\text{--}Y^{597}$
Bicelles	0.29	–	–	–
hERG $I^{583}\text{--}Y^{597}$	1.72	0.31 98%	–	–
Bepridil	3.82	0.28 100%	3.43 18%	–
Cetirizine	3.97	0.33 99%	3.70 13%	–
Pentamidine	3.57	0.37 97%	3.27 16%	–
Diphenhydramine	4.94	0.42 97%	4.68 9%	0.38 98%

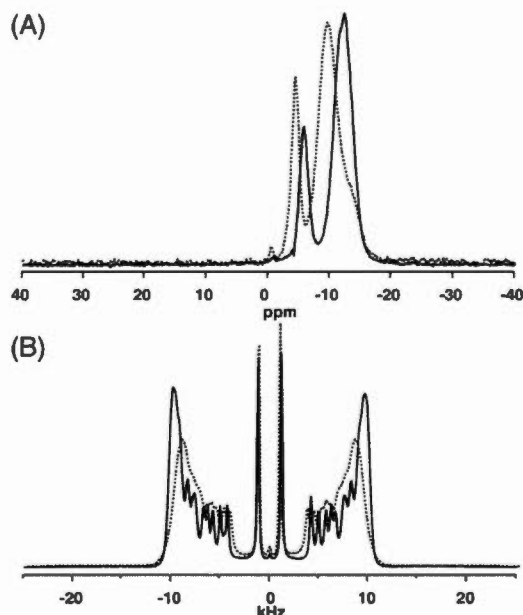


Fig. 2. (A) ^{31}P and (B) ^2H SS-NMR spectra of DMPC/DHPC bicelles ($q = 3.5$) without (solid line) and with (dashed line) hERG $^{583}\text{-Y}^{597}$ at 37°C with a lipid-to-peptide molar ratio of 100:1.

bicelle rim [69,70] or DHPC-rich defects of a perforated lamellae [71]. Fig. 2A shows that the hERG peptide has an effect on both DMPC and DHPC resonances in bicelles at a L/P ratio of 100:1 as seen by changes in the phospholipid chemical shifts, i.e. -5.91 to -4.53 ppm for DHPC and -12.47 to -9.75 ppm for DMPC. These changes could be explained by an effect of Ile 583 -Tyr 597 on the lipid bicelle dynamics, to which could be superimposed a deshielding effect of charged or aromatic moieties in the phosphorus atom vicinity. A broadening of the phospholipid resonances is also observed when the hERG segment is added to the bicelles, with an additional upfield shoulder on the DMPC resonance. This peak broadening could result from a greater distribution in bicelle orientation in the presence of the peptide (mosaic spread) [72]. A strong perturbation of the headgroup region of the membrane is thus evidenced and this effect was even more substantial at an L/P ratio of 25:1 where the bicelle morphology appeared to be destroyed (data not shown).

The ^2H spectra of DMPC- d_{54} bicelles at 37°C with and without the Ile 583 -Tyr 597 are shown in Fig. 2B. Again, these spectra are typical of bicelles with their lipid bilayer normal oriented perpendicularly to the magnetic field direction [27,28]. Well-defined doublets can be attributed to most of the deuterons along the lipid acyl chain, with the innermost doublet ascribed to the terminal CD_3 and the largest quadrupolar splitting to CD_2 attached to the glycerol backbone near the polar-apolar interface. The bicelle orientation is preserved when the hERG peptide is incorporated in an L/P ratio of 100:1. This is not the case for high segment proportions (L/P = 25:1) where the bicelle orientation is totally lost (not shown). The resolution of the doublet for the various deuterium positions is decreased when the hERG peptide interacts with the bicelles. This could be attributed to an increase in mosaic spread of bicelle orientation, as possibly suggested by ^{31}P NMR, or changes in transverse relaxation.

To better understand the effect of the hERG segment on the hydrophobic core of the bilayer, we have plotted the quadrupolar splitting ($\Delta\nu_Q$) values along DMPC acyl chains. Changes in $\Delta\nu_Q$ values allows determination of variations in the lipid chain order [67]. The

measured $\Delta\nu_Q$ values shown in Fig. 3 display significant changes upon addition of the hERG segment to the bicelles. On average, this peptide decreases $\Delta\nu_Q$ values by $\sim 10\%$ in the characteristic plateau region closer to the headgroup for an L/P ratio of 100:1, while C- D_2 bonds deeper in the bilayer are weakly affected. Although this difference of perturbation along the acyl chains suggests a non-transmembrane orientation of the peptide, the center of the bilayer is intrinsically disordered, thus less sensitive to perturbations. Therefore the orientation of hERG $^{583}\text{-Y}^{597}$ in the bicelles has been ascertained by conducting additional NMR experiments described in the next section.

3.1.3. Does the hERG $^{583}\text{-Y}^{597}$ adopt a preferred orientation with respect to the membrane?

Both the liquid-state NMR translational diffusion measurements and SS-NMR experiments presented in the preceding sections indicate a strong interaction of the hERG extracellular linker segment with the membrane. The ^{31}P and ^2H SS-NMR experiments show that the membrane is strongly perturbed and it is worthwhile to examine whether the peptide adopts a preferred orientation in the bilayer. For this purpose, we have carried out STD experiments [44] on bicelles in the presence of hERG Ile 583 -Tyr 597 . In these experiments, specific lipid resonances are saturated and the effect of this saturation on the hERG segment resonances is monitored. More specifically, we have saturated lipid signals from the headgroup (choline), interface (glycerol) and hydrophobic regions (terminal methyl) and monitored the variations in the saturation transfer build up and maximum values for different residues along the peptide. It was thus possible to assess its position inside the membrane, as was done by Wang, Lind and colleagues [46,73]. DMPC/DHPC- d_{22} bicelles were employed for STD experiments in order to probe the peptide penetration in the planar section of the bilayer and minimize contacts with high-curvature regions.

Fig. 4 shows the saturation transfer curves of the H_N protons for Trp 585 , Asn 588 , Asp 591 , Ile 593 , Lys 595 and Tyr 597 when the choline, glycerol and terminal methyl groups are saturated. These residues were chosen so as to span the complete length of the peptide. In all cases, the saturation transfers are efficient with maximum plateau values close to 0.3. These results are consistent with the previously determined scenario in which the peptide is strongly bound to the bilayer [45]. In effect, the saturation transfer will increase as the equilibrium between the bound and free states is displaced towards

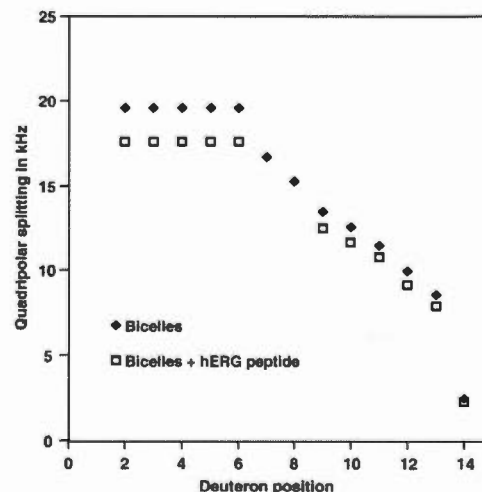


Fig. 3. Quadrupolar splitting for different deuterium positions along DMPC- d_{54} acyl chains in bicelles with and without hERG $^{583}\text{-Y}^{597}$ segment ($q = 3.5$, lipid-to-peptide molar ratio of 100:1).

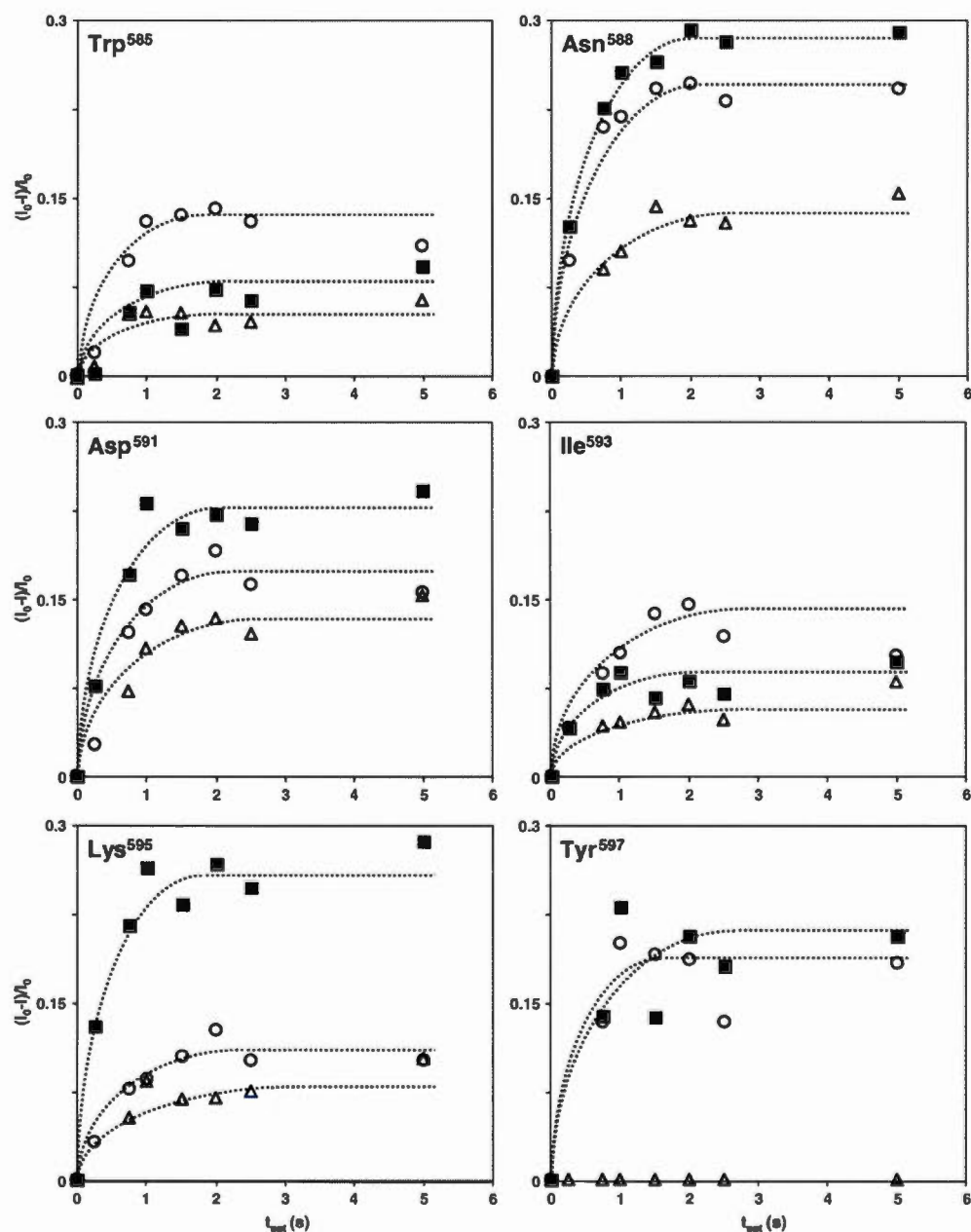


Fig. 4. Observed STD curves of amide protons for selected residues of hERG ⁵⁸³–⁵⁹⁷ segment in bicelles when choline (○), glycerol (■) or terminal methyl (Δ) resonances of DMPC are saturated.

the bound form [45]. For residues close to the segment extremities (Trp⁵⁸⁵ and Tyr⁵⁹⁷), the transfer from the lipid terminal methyl group is very weak or null and maximum to the choline protons. Note that for both these residues, the choline resonance at 3.25 ppm falls close to the H_β resonances which could be directly saturated. Therefore, it is important to assess the penetration of the residue in the membrane by comparing saturation transfers from three different lipid sites. Should one of these saturation curves be overestimated, the two other would

hold. For the amide proton of residues 588, 591, 595 and 597 the maximum saturation transfer takes place with the glycerol position, whereas the transfer from the lipid choline group decreases when going from Asn⁵⁸⁸ to Lys⁵⁹⁵ then increases for Tyr⁵⁹⁷. Ile⁵⁹³ shows the highest saturation transfer from the choline headgroup. The saturation transferred from the lipid methyl groups remains constant for central residues 588 and 591, decreases for Ile⁵⁹³ and is null for the terminal Tyr⁵⁹⁷.

The trends extracted from the analysis of Fig. 4 indicate that the peptide does not span the membrane and remains in the headgroup region in the vicinity of the glycerol interface. It can be tentatively proposed that the central part of the peptide is buried deeper in the membrane than the terminal parts, however, the interpretation of this data in terms of accurate distances is difficult as spin diffusion effects cannot be ruled out [46,73], in particular for such large objects as peptide/bicelle systems with slow correlation times. Spin diffusion can take place within the phospholipids, leading to an indirect saturation transfer to the peptide from a part of the lipid that is not directly in contact with the saturated lipid moiety. To quantify this possible effect, we have measured spin diffusion within DMPC by monitoring the STD signal of the terminal methyl group when the choline protons were saturated and vice versa. Our data (not shown) indicate that this saturation transfer is negligible since it is less than 3% of the maximum lipid-peptide saturation transfer. It should be noted that no peptide-lipid cross peaks could be detected in the 2D NOESY spectra with mixing times up to 750 ms (data not shown). We suggest that fast dynamics and longitudinal relaxation during the NOE mixing time could result in cross peaks too weak to be detected.

3.1.4. Does the membrane environment influence $I^{583-597}$ structure?

Clearly, the previous interpretation of the STD experiments raises the question as to what structure this hERG extracellular loop segment adopts when interacting with the membrane. The structure of the Ile⁵⁸³-Tyr⁵⁹⁷ segment, as part of longer hERG segments, has recently been elucidated in water and SDS micelles by Torres et al. [26], and in water, DPC and SDS micelles by Jiang et al. [23]. Using CD and NMR, both studies determined that the hERG S5-P loop was unstructured in water and formed an α -helix from residues 585 to 593 [26] or an α -helix from residues 583 to 590 and a 3_{10} -helix from positions 591 to 593 [23]. These differences hint to potential structural changes as a function of the membrane milieu. In order to verify any particular structural behaviour of the S5-P segment in membranes, CD studies were carried out with hERG $I^{583-597}$ segment in various membrane mimetic environments frequently used in membrane protein structure determination [74]. Negatively charged SDS and LMPG micelles, zwitterionic DPC, LMPC and DHPC micelles as well as DMPC/DHPC bicelles were evaluated. LMPC, LMPG and DHPC are the most lipid-like surfactants [74]. Because a helical structure of the S5-P segment was reported in SDS micelles, bicelles with 25% (Bicelles/PS25%) and 50% of negatively charged DMPS were also used to verify the effect of negative charges on the segment structure.

Our CD results (Fig. 5) clearly demonstrate that the membrane mimetic environment can influence the structure of the hERG peptide $I^{583-597}$. First, an α -helical structure is favoured in SDS (data not shown), DPC, LMPG and LMPC micelles as suggested by the positive ellipticity seen between 190 and 195 nm and a negative minimum at ~205 and 222 nm. In order to quantify the contributions of different structural elements, CD spectra were analyzed with the DichroWeb program [55]. According to this analysis, the hERG peptide would be 57% α -helical in SDS and LMPG, 54% in DPC and 61% in LMPC micelles. These results are consistent with previous work published [23,26]. Fig. 5 shows that the hERG loop segment does not adopt a well-defined structure in water or DHPC micelles. A maximum at ~225 nm is seen in the CD spectra of the peptide in water and DHPC micelles. Because of the presence, in the hERG segment, of a glutamine residue which can have propensity to adopt a polyproline II conformation, the possibility of such secondary structure cannot be excluded, albeit the absence of a negative band centered at ~205 nm [75]. The CD spectra measured in bicelles shows a higher residual molar ellipticity between 190 and 195 nm and a decrease of intensity between 210 and 220 nm as compared to the pure random coil signature. This could be attributed to a small proportion of α -helices. These spectra are therefore not characteristic of a purely unstructured peptide. DichroWeb deconvolution of $I^{583-597}$ CD spectrum in bicelles

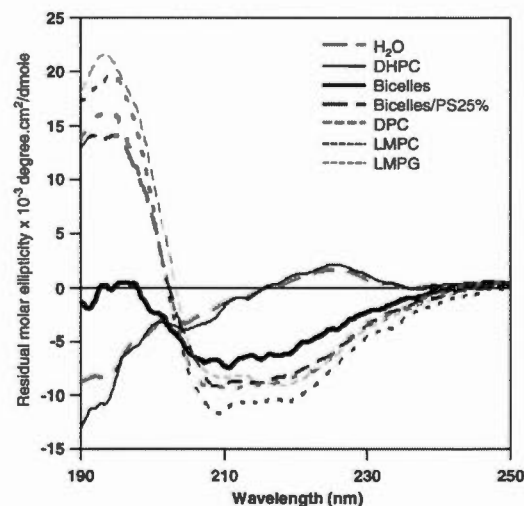


Fig. 5. Circular dichroism spectra of hERG $I^{583-597}$ in H₂O (pH=5.5) and in various membrane mimetic environments: DMPC/DHPC bicelles and bicelles with 25 mol% DMPS ($q=1$), DHPC, DPC, LMPC and LMPG micelles.

indicates an increased contribution of helices (30%), strands (20%) and turns (20%) while the "unordered" contribution is smaller as compared to the peptide spectrum recorded in water or DHPC. Interestingly, spectra obtained in negatively charged bicelles made of 25% DMPS display the characteristic signature of an α -helical structure. The α -helical content increases to 54% and 65% for bicelles comprising 25 and 50 mol% (not shown) of DMPS, respectively.

Because phosphatidylcholines are highly abundant in cardiomyocytes [75,76], we have further investigated the structure of the hERG $I^{583-597}$ segment in zwitterionic DMPC/DHPC bicelles using 2D ¹H NMR experiments. In contrast to surfactant micelles, bicelles display a planar bilayer region that is similar to that of biomembranes. H_α secondary chemical shifts can be used as a first step for structural characterization. As was shown by Wishart et al. [77], a negative deviation of the H_α chemical shift value from random coil values is indicative of an α -helical structure. Fig. 6A compares the H_α secondary chemical shifts of the Ile⁵⁸³-Tyr⁵⁹⁷ in bicelles, SDS micelles and water obtained from TOCSY spectra. All backbone resonances could be assigned except HN of Ile⁵⁸³ and Gly⁵⁸⁴ and H_α resonances of Gly⁵⁸⁴ and Leu⁵⁸⁹, possibly due to signal overlap within the peptide or from the protonated phospholipid headgroups. Virtually all sidechain resonances (96%) could be assigned (supplementary data). Examination of Fig. 6A shows that the H_α chemical shifts of the hERG segment in bicelles follow the same trend as those obtained in SDS micelles, with similar although generally smaller deviations from random coil values. Although the H_α secondary chemical shifts indicate a propensity towards a helical structure, no contacts indicative of a defined secondary structure could be detected by 2D NOESY experiments with mixing times up to 250 ms, as shown in Fig. 6B. Our CD and NMR results indicate that the peptide, despite adopting an α -helical conformation in strong surfactants such as SDS or DPC and displaying a helical propensity in bicelles, does not adopt a defined conformation when bound to these model membranes.

3.2. Interaction of cardiotoxic drugs with $I^{583-597}$ and model membranes

Previous work has demonstrated that drugs such as dofetilide and vesmarinone can induce LQTS by binding sites on the S5-P extracellular loop of the hERG channel [14,16]. Therefore, we have investigated the potential role of the central segment $I^{583-597}$ in

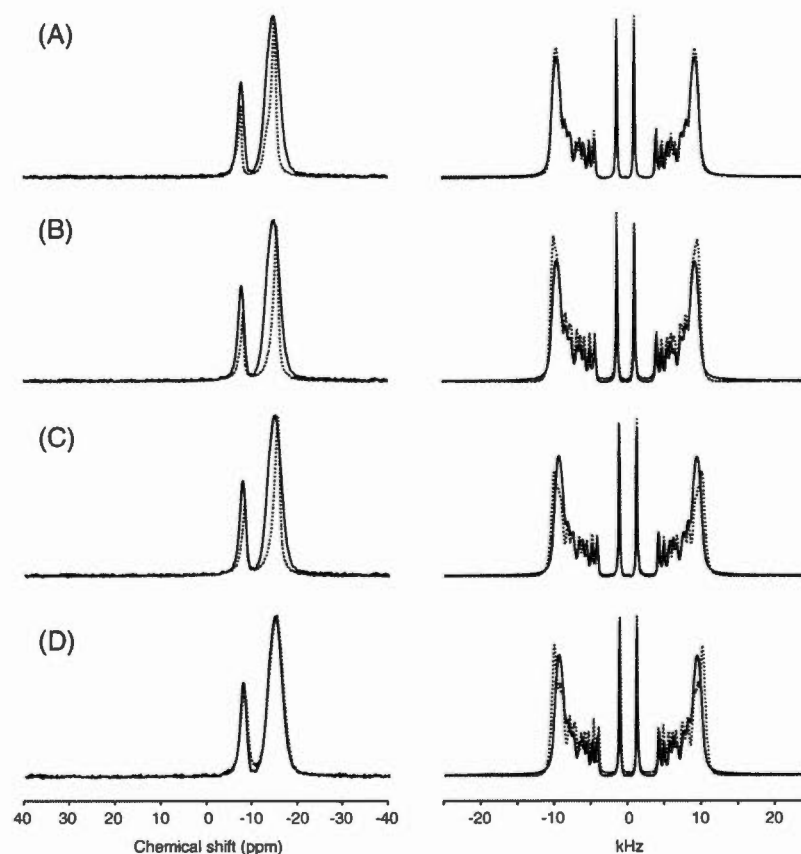


Fig. 7. ^{31}P (left) and ^2H (right) SS-NMR spectra of DMPC/DHPC bicelles ($q=3.5$) at 37°C in the presence of (A) pentamidine, (B) diphenhydramine, (C) cetirizine and (D) bepridil (dotted lines) with a drug-to-lipid ratio of 100:1. The reference spectra of bicelles are superimposed for comparison (solid line).

Bicelles were used as model membranes because they are amenable to both liquid- and solid-state NMR. In addition, their composition and morphology provide a good mimic of natural membranes. Lipids are determinants for channel function and their composition greatly influences membrane structural and physical properties, such as curvature and fluidity that are involved in the regulation of the gating of K^+ channels [75,85,86]. Mammalian plasma membranes are composed of diverse lipids comprising cholesterol, sphingolipids and phospholipids, with phosphatidylcholines the most abundant [87]. Furthermore, phospholipids are not symmetrically distributed within the bilayer of the plasma membrane. Zwitterionic phosphatidylcholines are more concentrated in the outer leaflet while negatively charged phosphatidylserines are found in the inner leaflet [76]. This further explains the choice of a zwitterionic DMPC/DHPC bicellar system for our NMR work.

The combination of liquid- and solid-state NMR experiments showed that the studied hERG segment interacts strongly with the membrane where it would most likely lie on the surface. This interaction perturbs the lipid headgroups dynamics and increases the acyl chain mobility close to the interface. The bilayer integrity is however preserved. The interaction of the ^{583}Ile – ^{597}Tyr peptide with the model membrane is consistent with a “floppy” outer mouth, as proposed by Liu et al. [24]. Based on secondary structure analyses and cysteine-scanning mutagenesis, they demonstrated that the conformational flexibility of the outer mouth plays a key role in the hERG

channel function. This flexibility and significant length of the S5-P linker could allow it to reach the membrane surface where its strong affinity might allow the stabilization of certain channel conformations during the gating process [5].

We have then determined the structure of ^{583}Ile – ^{597}Tyr in zwitterionic bicelles. This step was important as previous NMR studies were performed in detergent (SDS and DPC) micelles [23,26]. Our multidimensional ^1H NMR experiments and chemical shift analysis indicate that the ^{583}Ile – ^{597}Tyr segment shows no defined secondary structure. These findings are confirmed by CD spectroscopy which also shows that the hERG linker segment is unstructured in water while it is structured in most of the detergents used in membrane structure determination, including SDS [74,88]. It thus appears that the membrane environment strongly influences the structure of this hERG loop segment.

Interestingly, the CD spectra of negatively charged bicelles containing 25% and 50 mol% (not shown) of DMPS display the characteristic signals of an α -helical structure, and the helical content increases with surface charge. It is thus clear that the charge of the model membrane has an effect on the ^{583}Ile – ^{597}Tyr structure. The membrane potential in the cardiomyocytes changes rapidly during the gating process. Therefore, according to our results, we can hypothesize that this rapid change in surface charge could possibly result in a modification of the conformation of the extracellular segment (^{583}Ile – ^{597}Tyr) of the hERG channel.

We believe that the apparent contradiction between the structure of the peptide in DMPC bilayers or in surfactant micelles might be of functional importance. Torres et al. [26] and Jiang et al. [23] have shown, using electrophysiology experiments, that the S5-P linker interacts with other parts of the channel. It is thus possible that hydrophobic regions of the hERG channel might provide an additional driving force that would enable the structuring of the region from W⁵⁸⁵ to I⁵⁹³ the segment that has been shown to adopt an alpha helical conformation in SDS or DPC micelles [23,26]. According to our results, an interaction with the membrane bilayer would not be sufficient for this segment to adopt a helical structure. Thus, should the functional structure of W⁵⁸⁵–I⁵⁹³ actually be an alpha-helix, it would result from protein-protein interactions rather than protein-membrane interactions. For lack of structural data on the complete hERG pore in a membrane milieu, the question of the *in vivo* structure of segment I⁵⁸³–Y⁵⁹⁷ remains open.

Considering the structural flexibility of the S5-P linker, a model in which segment I⁵⁸³–Y⁵⁹⁷ would bind competitively (or at different stages of the gating process) to other parts of the pore channel or the membrane can be hypothesized. The concomitant structural changes could provide additional conformational flexibility to the outer mouth region. This is consistent with the role of the extracellular pore loops in the pore domain of ion channels, i.e. to provide architectural versatility [5].

The results obtained by ¹H NMR diffusion experiments show that the four hERG-active drugs studied in this work have a weak affinity for the I⁵⁸³–Y⁵⁹⁷ segment. The experiments were done at a drug/peptide molar ratio of 1:1, well above what could be expected biologically. This segment would, thus, most likely not be targeted by bepridil, cetirizine, diphenhydramine and pentamidine in the ALQTS mechanism. Previous studies on bepridil suggest that this antiangine medicine would bind sites close to the pore helix (Thr⁶²³, Ser⁶²⁴, and Val⁶²⁵) and Phe⁶⁵⁶ on S6. However, these drugs showed a marked affinity for the membrane environment of the hERG channel. It is thus conceivable that the partition of these drugs in the membrane could change its local properties, thus affecting the channel function. For example, voltage-gated K⁺ channels such as the Shaker are known to be mechanosensitive and can respond to membrane stretch [76]. Therefore the movement of VGK channels during the gating can be altered by the lipid-protein interface [76]. Studies have shown that the conformation of channels such as the MscL can be changed by deformation of the lipid bilayer [89]. The lipid annulus composition around membrane proteins such as ion channels plays a role in its conformation and could be involved in triggering events [86]. Therefore, perturbation of this annular shell by drugs is a possible drug action mechanism as suspected with anaesthetics [90]. A similar mechanism of action has been evidenced with the voltage-sensor toxin Vstx1 with the Kv2.1 channel [91]. Finally, the QT prolongation induced by these drugs would most likely be explained by a preference for other binding sites on other hERG domains. They could, for example, traverse the membrane to access putative LQTS-provoking target residues which lie in the cytosolic (intracellular) parts of the hERG channel, as was observed for tetracaine which interaction with membrane lipids enhanced its access to the transmembrane pore [92]. Therefore, our drug-membrane interaction results open the possibility of a membrane catalysis model for drugs involved in the ALQTS, as can be observed for receptor ligands [93].

5. Conclusion

Using a liquid- and solid-state NMR approach, we have shown that extracellular S5-P linker segment I⁵⁸³–Y⁵⁹⁷ of the hERG channel strongly interacts with model PC membranes where it would rest in the polar region. This segment does not adopt a well-defined secondary structure despite its strong interaction with this specific membrane bilayer, as confirmed by circular dichroism analysis. Its conformation, however, was shown to vary as a function of the

membrane nature and charge, thus proving its strong structural flexibility. These results show that the membrane is likely to play an important role in hERG channel functioning, possibly by stabilizing transient conformations during the gating process. The interaction with this hERG segment of four cardiotoxic drugs, namely bepridil, cetirizine, diphenhydramine and pentamidine, was shown to be negligible. However, these drugs proved to have a strong affinity for the membrane, thus opening the possibility for a membrane-mediated ALQTS mechanism or membrane catalysis.

Acknowledgments

É.C. and A.G. wish to thank the *Groupe de Recherche Axé sur la Structure des Protéines* (GRASP), the *Faculté des Sciences* of UQAM and the Natural Sciences and Engineering Research Council (NSERC) of Canada for the award of scholarships. We would like to thank J. Kornblatt (Concordia University), T. Sprules (Quebec/Eastern Canada NMR Centre) and M.R.R. de Planque (University of Southampton) for technical assistance and insightful discussions. This work was supported by the NSERC, the *Fonds Québécois de la Recherche sur la Nature et les Technologies* (FQRNT), and by the Canadian Foundation for Innovation (CFI).

Appendix A. Supplementary data

Supplementary data associated with this article can be found, in the online version, at doi:10.1016/j.bbmem.2010.05.019.

References

- [1] J.S. Mitcheson, J. Chen, M. Lin, C. Culberson, M.C. Sanguinetti, A structural basis for drug-induced long QT syndrome, *Proc. Natl. Acad. Sci. USA* 97 (2000) 12329–12333.
- [2] Y. Jiang, A. Lee, J. Chen, M. Cadene, B.T. Chait, R. MacKinnon, Crystal structure and mechanism of a calcium-gated potassium channel, *Nature* 417 (2002) 515–522.
- [3] M.C. Trudeau, J.W. Warmke, B. Ganetzky, G.A. Robertson, hERG, a human inward rectifier in the voltage-gated potassium channel family, *Science* 269 (1995) 92–95.
- [4] M. Recanatini, E. Poluzzi, M. Masetti, A. Cavalli, F. De Ponti, QT prolongation through hERG K(+) channel blockade: current knowledge and strategies for the early prediction during drug development, *Med. Res. Rev.* 25 (2005) 133–166.
- [5] R. MacKinnon, Pore loops: an emerging theme in ion channel structure, *Neuron* 14 (1995) 889–892.
- [6] D.M. Roden, R. Temple, The US Food and Drug Administration cardiorenal advisory panel and the drug approval process, *Circulation* 111 (2005) 1697–1702.
- [7] R.R. Shah, Drug-induced QT interval prolongation - regulatory guidance and perspectives on hERG channel studies, in: D.J. Chadwick, J. Goode (Eds.), *The hERG cardiac potassium channel: structure, function and long QT syndrome*, John Wiley & Sons Ltd, Chichester, 2005, pp. 251–285.
- [8] M.C. Sanguinetti, M. Tristani-Firouzi, hERG potassium channels and cardiac arrhythmia, *Nature* 440 (2006) 463–469.
- [9] A.M. Brown, D. Rampe, Drug-induced long QT syndrome: is hERG the root of all evil, *Pharmaceutical News* 7 (2000) 15–20.
- [10] F. De Ponti, E. Poluzzi, A. Cavalli, M. Recanatini, N. Montanaro, Safety of non-antiarrhythmic drugs that prolong the QT interval or induce torsade de pointes: an overview, *Drug Saf.* 25 (2002) 263–286.
- [11] H. Abriel, J. Schläpfer, D.J. Keller, B. Gavillet, J. Biollaz, R. Stollé, L. Kappenberger, Molecular and clinical determinants of drug-induced long QT syndrome an iatrogenic channelopathy, *Swiss Med. Wkly* 134 (2004) 685–694.
- [12] S. Ekins, Predicting undesirable drug interactions with promiscuous proteins *in silico*, *Drug Discov. Today* 9 (2004) 276–285.
- [13] A.M. Aronov, Predictive *in silico* modeling for hERG channel blockers, *Drug Discov. Today* 10 (2005) 149–155.
- [14] E. Ficker, W. Jarolimek, J. Kiehn, A. Baumann, A.M. Brown, Molecular determinants of dofetilide block of hERG K⁺ channels, *Circ. Res.* 82 (1998) 386–395.
- [15] J.P. Lees-Miller, Y. Duan, G.Q. Teng, H.J. Duff, Molecular determinant of high-affinity dofetilide binding to hERG1 expressed in *Xenopus* oocytes: involvement of S6 sites, *Mol. Pharmacol.* 57 (2000) 367–374.
- [16] K. Kamiya, J.S. Mitcheson, K. Yasui, I. Kodama, M.C. Sanguinetti, Open channel block of hERG K(+) channels by vesnarinone, *Mol. Pharmacol.* 60 (2001) 244–253.
- [17] J.A. Sanchez-Chapula, T. Ferrer, R.A. Navarro-Polanco, M.C. Sanguinetti, Voltage-dependent profile of human ether-a-go-go-related gene channel block is influenced by a single residue in the S6 transmembrane domain, *Mol. Pharmacol.* 63 (2003) 1051–1058.

- [18] J.A. Sanchez-Chapula, R.A. Navarro-Polanco, C. Culberson, J. Chen, M.C. Sanguinetti, Molecular determinants of voltage-dependent human ether-a-go-go related gene (HERG) K⁺ channel block, *J. Biol. Chem.* 277 (2002) 23587–23595.
- [19] M.C. Sanguinetti, J. Chen, D. Fernandez, K. Kamiya, J. Mitcheson, J.A. Sanchez-Chapula, Physicochemical basis for binding and voltage-dependent block of hERG channels by structurally diverse drugs: in The hERG cardiac potassium channel: structure, function and long QT syndrome, John Wiley & Sons Ltd, Chichester, 2005 pp. 159–170.
- [20] G.B. Gurrrola, B. Rosati, M. Rocchetti, G. Pimienta, A. Zaza, A. Arcangeli, M. Olivetto, L.D. Possani, E. Wanke, A toxin to nervous, cardiac, and endocrine ERG K⁺ channels isolated from *Centruroides noxius* scorpion venom, *FASEB J.* 13 (1999) 953–962.
- [21] Y.V. Korolkova, S.A. Kozlov, A.V. Lipkin, K.A. Pluzhnikov, J.K. Hadley, A.K. Filippov, D.A. Brown, K. Angelo, D. Strobaek, T. Jespersen, S.P. Olesen, B.S. Jensen, E.V. Grishin, An ERG channel inhibitor from the scorpion *Buthus eupeus*, *J. Biol. Chem.* 276 (2001) 9868–9876.
- [22] L. Pardo-Lopez, M. Zhang, J. Liu, M. Jiang, L.D. Possani, G.-N. Tseng, Mapping the binding site of a human ether-a-go-go-related gene-specific peptide toxin (ErgTx) to the channel's outer vestibule, *J. Biol. Chem.* 277 (2002) 16403–16411.
- [23] M. Jiang, M. Zhang, I.V. Maslennikov, J. Liu, D.-M. Wu, Y.V. Korolkova, A.S. Arseniev, E.V. Grishin, G.-N. Tseng, Dynamic conformational changes of extracellular S5-P linkers in the hERG channel, *J. Physiol.* 569 (2005) 75–89.
- [24] J. Liu, M. Jiang, G.-N. Tseng, Structural and functional role of the extracellular S5-P linker in the hERG potassium channel, *J. Gen. Physiol.* 120 (2002) 723–737.
- [25] M. Zhang, J. Liu, G.-N. Tseng, Gating changes in the activation and inactivation processes of the hERG channel, *J. Gen. Physiol.* 124 (2004) 703–718.
- [26] A.M. Torres, P. Bansal, M. Sundé, C.E. Clarke, J.A. Bursill, D.J. Smith, A. Bauskin, S.N. Breit, T.J. Campbell, P.F. Alewood, P.W. Kuchel, J.I. Vandenberg, Structure of the HERG K⁺ channel S5P extracellular linker, *J. Biol. Chem.* 278 (2003) 42136–42148.
- [27] C.R. Sanders, J.P. Schwonek, Characterization of magnetically orientable bilayers in mixtures of dihexanoylphosphatidylcholine and dimyristoylphosphatidylcholine by solid-state NMR, *Biochemistry* 31 (1992) 8898–8905.
- [28] I. Marcotte, M. Auger, Bicelles as model membranes for solid- and solution-state NMR studies of membrane peptides and proteins, *Concepts Magn. Res.* 24A (2005) 17–37.
- [29] M.N. Triba, D.E. Warschawski, P.F. Devaux, Reinvestigation by phosphorus NMR of lipid distribution in bicelles, *Biophys. J.* 88 (2005) 1887–1901.
- [30] P. Coumel, Safety of bepridil: from review of the European data, *Am. J. Cardiol.* 69 (1992) 75D–78D.
- [31] A. Gill, S.F. Flaim, B.P. Damiano, S.P. Sit, M.D. Brannan, Pharmacology of bepridil, *Am. J. Cardiol.* 69 (1992) 11D–16D.
- [32] C. Chouabe, M.D. Drici, G. Romey, J. Barhanin, Effects of calcium channel blockers on cloned cardiac K⁺ channels IKr and IKs, *Thérapie* 55 (2000) 195–202.
- [33] H. Choe, K.H. Nah, S.N. Lee, H.S. Lee, S.H. Jo, C.H. Leem, Y.J. Jang, A novel hypothesis for the binding mode of hERG channel blockers, *Biochim. Biophys. Res. Commun.* 344 (2006) 72–78.
- [34] J.D. Gilbert, S.A. Cahill, D.G. McCartney, A. Lukas, G.J. Gross, Predictors of torsades de pointes in rabbit ventricles perfused with sedating and nonsedating histamine H1-receptor antagonists, *Can. J. Physiol. Pharmacol.* 78 (2000) 407–414.
- [35] W. Zareba, A.J. Moss, S.Z. Rosero, R. Haji-Ali, J. Konecki, M. Andrews, Electrocardiographic findings in patients with diphenhydramine overdose, *Am. J. Cardiol.* 80 (1997) 1168–1173.
- [36] J.M. Wharton, P.A. Demopoulos, N. Goldschlager, Torsade de pointes during administration of pentamidine isethionate, *Am. J. Med.* 83 (1987) 571–576.
- [37] M. Pujol, J. Carratala, J. Mauri, P.F. Viladrich, Ventricular tachycardia due to pentamidine isethionate, *Am. J. Med.* 84 (1988) 980.
- [38] Y.A. Kuryshv, E. Ficker, L. Wang, P. Hawryluk, A.T. Dennis, B.A. Wible, A.M. Brown, J. Kang, X.-L. Chen, K. Sawamura, W. Reynolds, D. Rampe, Pentamidine-induced long QT syndrome and block of hERG trafficking, *J. Pharmacol. Exp. Ther.* 312 (2005) 316–323.
- [39] D. Marsh, CRC Handbook of lipid bilayers, CRC Press Inc., Boca Raton, 1990.
- [40] D. Schwarz, F. Junge, F. Durst, N. Frölich, B. Schneider, S. Reckel, S. Sobhanifar, V. Dotsch, F. Bernhard, Preparative scale expression of membrane proteins in *Escherichia coli*-based continuous exchange cell-free systems, *Nat. Protoc.* 2 (2007) 2945–2957.
- [41] R.R. Vold, R.S. Prosser, Magnetically oriented phospholipid bilayered micelles for structural studies of polypeptides. Does the ideal bicelle exist? *J. Magn. Reson.* 113 (1996) 267–271.
- [42] A.S. Altieri, D.P. Hinton, R.A. Byrd, Association of biomolecular systems via pulsed field gradient NMR self diffusion measurements, *J. Am. Chem. Soc.* 117 (1995) 7566–7567.
- [43] M. Holz, Temperature-dependent self-diffusion coefficients of water and six selected molecular liquids for calibration in accurate ¹H NMR PFG measurements, *Phys. Chem. Chem. Phys.* 2 (2000) 4740–4742.
- [44] M. Mayer, B. Meyer, Characterization of ligand binding by saturation transfer difference NMR spectroscopy, *Angew. Chem. Int. Ed.* 38 (1999) 1784–1788.
- [45] M. Mayer, B. Meyer, Group epitope mapping by saturation transfer difference NMR to identify segments of a ligand in direct contact with a protein receptor, *J. Am. Chem. Soc.* 123 (2001) 6108–6117.
- [46] J. Wang, J.R. Schnell, J.J. Chou, Amantadine partition and localization in phospholipid membrane: a solution NMR study, *Biochim. Biophys. Res. Commun.* 324 (2004) 212–217.
- [47] A. Bax, D.G. Davis, MLEV-17-based two-dimensional homonuclear magnetization transfer spectroscopy, *J. Magn. Reson.* 65 (1985) 355–360.
- [48] J. Jeener, B.M. Meier, P. Bachmann, R.R. Ernst, Investigation of exchange processes by two-dimensional NMR spectroscopy, *J. Chem. Phys.* 71 (1979) 4546–4553.
- [49] S. Macura, R.R. Ernst, Elucidation of cross relaxation in liquids by two-dimensional NMR spectroscopy, *Mol. Phys.* 41 (1980) 95–117.
- [50] M. Rance, R.A. Byrd, Obtaining high-fidelity spin-1/2 powder spectra in anisotropic media: phase-cycled Hahn echo spectroscopy, *J. Magn. Reson.* 52 (1983) 221–240.
- [51] J.H. Davis, K.R. Jeffrey, M. Bloom, M.I. Valic, T.P. Higgs, Quadrupolar echo deuteron magnetic resonance spectroscopy in ordered hydrocarbon chains, *Chem. Phys. Lett.* 42 (1976) 390–394.
- [52] J.D. van Beek, matNMR: A flexible toolbox for processing, analyzing and visualizing magnetic resonance data in Matlab®, *J. Magn. Reson.* 187 (2007) 19–26.
- [53] F. Delaglio, S. Grzesiek, G.W. Vuister, G. Zhu, J. Pfeifer, A. Bax, NMRPipe: a multidimensional spectral processing system based on UNIX pipes, *J. Biomol. NMR* 6 (1995) 277–293.
- [54] B.A. Johnson, R.A. Blevins, NMRView: a computer program for the visualization and analysis of NMR data, *J. Biomol. NMR* 4 (1994) 603–614.
- [55] L. Whitmore, B.A. Wallace, DICHROWEB, an online server for protein secondary structure analyses from circular dichroism spectroscopic data, *Nucleic Acids Res.* 32 (2004) W668–W673.
- [56] X. Gao, T.C. Wong, Studies of the binding and structure of adrenocorticotropin peptides in membrane mimics by NMR spectroscopy and pulsed-field gradient diffusion, *Biophys. J.* 74 (1998) 1871–1888.
- [57] I. Marcotte, F. Separovic, M. Auger, S.M. Gagné, A multidimensional ¹H NMR investigation of the conformation of methionine-enkephalin in fast-tumbling bicelles, *Biophys. J.* 86 (2004) 1587–1600.
- [58] T.L. Whitehead, L.M. Jones, R.P. Hicks, Effects of the incorporation of CHAPS into SDS micelles on neuropeptide-micelle binding: separation of the role of electrostatic interactions from hydrophobic interactions, *Biopolymers* 58 (2001) 593–605.
- [59] P. Stibbs, Fourier transform pulsed-gradient spin-echo studies of molecular diffusion, *Prog. Nucl. Magn. Reson. Spectrosc.* 19 (1987) 1–45.
- [60] S. Gaemers, A. Bax, Morphology of three lyotropic liquid crystalline biological NMR media studied by translational diffusion anisotropy, *J. Am. Chem. Soc.* 123 (2001) 12343–12352.
- [61] P.A. Luchette, T.N. Vetman, R.S. Prosser, R.E.W. Hancock, M.-P. Nieh, C.J. Glinka, S. Krueger, J. Katsaras, Morphology of fast-tumbling bicelles: a small angle neutron scattering and NMR study, *Biochim. Biophys. Acta* 1513 (2001) 83–94.
- [62] H. Johannesson, B. Halle, Solvent diffusion in ordered macrofluids: A stochastic simulation study of the obstruction effect, *J. Chem. Phys.* 104 (1996) 6807–6817.
- [63] A. Andersson, L. Måler, Size and shape of fast-tumbling bicelles as determined by translational diffusion, *Langmuir* 22 (2006) 2447–2449.
- [64] A. Chen, M. Shapiro, Nuclear Overhauser effect on diffusion measurements, *J. Am. Chem. Soc.* 121 (1999) 5338–5339.
- [65] L.H. Lucas, J. Yan, C.K. Larive, E.R. Zartler, M.J. Shapiro, Transferred nuclear overhauser effect in nuclear magnetic resonance diffusion measurements of ligand-protein binding, *Anal. Chem.* 75 (2003) 627–634.
- [66] J. Seelig, ³¹P nuclear magnetic resonance and the head group structure of phospholipids in membranes, *Biochim. Biophys. Acta* 515 (1978) 105–140.
- [67] J. Seelig, Deuterium magnetic resonance: theory and application to lipid membranes, *Q. Rev. Biophys.* 10 (1977) 353–418.
- [68] J.H. Davis, The description of membrane lipid concentration, order and dynamics by ²H-NMR, *Biochim. Biophys. Acta* 737 (1983) 117–171.
- [69] F. Picard, M.-J. Paquet, J. Levesque, A. Bélanger, M. Auger, ³¹P NMR first spectral moment study of the partial magnetic orientation of phospholipid membranes, *Biophys. J.* 77 (1999) 888–902.
- [70] E. Sternin, D. Nizza, K. Gawrish, Temperature dependence of DMPC/DHPC mixing in a bicellar solution and its structural implications, *Langmuir* 17 (2001) 2610–2616.
- [71] M.P. Nieh, C.J. Glinka, S. Krueger, R.S. Prosser, J. Katsaras, SANS study on the effect of lanthanide ions and charged lipids on the morphology of phospholipid mixtures. Small-angle neutron scattering, *Biophys. J.* 82 (2002) 2487–2498.
- [72] A. Arnold, T. Labrot, R. Oda, E.J. Dufourc, Cation modulation of “bicelle” size and magnetic alignment as revealed by solid state NMR and electron microscopy, *Biophys. J.* 82 (2002) 2667–2680.
- [73] J. Lind, A. Graslund, L. Måler, Membrane interactions of dynorphins, *Biochemistry* 45 (2006) 15931–15940.
- [74] C.R. Sanders, F. Sönnichsen, Solution NMR of membrane proteins: practice and challenges, *Magn. Reson. Chem.* 44 (2006) S24–S40.
- [75] J. Abi-Char, A. Maguy, A. Coulombe, E. Balse, P. Ratajczak, J.-L. Samuel, S. Nattel, S. N. Hatem, Membrane cholesterol modulates Kv1.5 potassium channel distribution and function in rat cardiomyocytes, *J. Physiol.* 582 (2007) 1205–1217.
- [76] L.M. Boland, Drzewiecki, Polyunsaturated fatty acid modulation of voltage-gated ion channels, *Cell Biochem. Biophys.* 52 (2008) 59–84.
- [77] D.S. Wishart, B.D. Sykes, F.M. Richards, The chemical shift index: a fast and simple method for the assignment of protein secondary structure through NMR spectroscopy, *Biochemistry* 31 (1992) 1647–1651.
- [78] G. Bazzoni, M. Rasia, Effects of amphipathic drug on the rheological properties of the cell membrane, *Blood Cells* 24 (1998) 552–559.
- [79] I. Marcotte, E.J. Dufourc, M. Ouellet, M. Auger, Interaction of the neuropeptide met-enkephalin with zwitterionic and negatively charged bicelles as viewed by ³¹P and ²H solid-state NMR, *Biophys. J.* 85 (2003) 328–339.
- [80] J. Wang, M.C. Trudeau, A.M. Zappia, G.A. Robertson, Regulation of deactivation by an amino terminal domain in human ether-a-go-go-related gene potassium channels, *J. Gen. Physiol.* 112 (1998) 637–647.
- [81] J. Wang, C.D. Myers, G.A. Robertson, Dynamic control of deactivation gating by a soluble amino-terminal domain in HERG K⁺ channels, *J. Gen. Physiol.* 115 (2000) 749–758.

- [82] E.C. Roti Roti, C.D. Myers, R.A. Ayers, D.E. Boatman, S.A. Delfosse, E.K.L. Chan, M.J. Ackerman, C.T. January, G.A. Robertson, Interaction with GM130 during HERG ion channel trafficking, *J. Biol. Chem.* 277 (2002) 47779–47785.
- [83] G.-N. Tseng, K.D. Sonawane, Y.V. Korolkova, M. Zhang, J. Liu, E.V. Grishin, H.R. Guy, Probing the outer mouth structure of the hERG channel with peptide toxin footprinting and molecular modeling, *Biophys. J.* 92 (2007) 3524–3540.
- [84] P. Ju, G. Pages, R.P. Riek, P.-C. Chen, A.M. Torres, P. Bansal, S. Kuyucak, P.W. Kuchel, J.I. Vandenberg, The pore domain outer helix contributes to both activation and inactivation of the hERG K⁺ channel, *J. Biol. Chem.* 284 (2009) 1000–1008.
- [85] J.A. Lundbaek, P. Birn, J. Girshman, A.J. Hansen, O.S. Andersen, Membrane stiffness and channel function, *Biochemistry* 35 (1996) 3825–3830.
- [86] A.G. Lee, Lipid-protein interactions in biological membranes: a structural perspective, *Biochim. Biophys. Acta* 1612 (2003) 1–40.
- [87] G. van Meer, D.R. Voelker, G.W. Feigenson, Membrane lipids: where they are and how they behave, *Nat. Rev. Mol. Cell Biol.* 9 (2008) 112–124.
- [88] R.D. Krueger-Koplin, P.L. Sorgen, S.T. Krüeger-Koplin, I.O. Rivera-Torres, S.M. Cahill, D.B. Hicks, L. Grinius, T.A. Krulwich, M.E. Girvin, An evaluation of detergents for NMR structural studies of membrane proteins, *J. Biomol. NMR* 17 (2004) 43–57.
- [89] E. Perozo, A. Kloda, D.M. Cortes, B. Martinac, Physical principles underlying the transduction of the bilayer deformation forces during mechanosensitive channel gating, *Nat. Struct. Biol.* 9 (2002) 696–703.
- [90] O.G. Mouritsen, K. Jorgensen, A new look at lipid-membrane structure in relation to drug research, *Pharm. Res.* 15 (1998) 1507–1519.
- [91] D. Schmidt, R. MacKinnon, Voltage-dependent K⁺ channel gating and voltage sensor toxin sensitivity depend on the mechanical state of the lipid membrane, *Proc. Natl Acad. Sci. USA* 105 (2008) 19276–19281.
- [92] J.E. Baenziger, S.E. Ryan, M.M. Goodfried, V. N.Q., R.M. Sturgeon, C.J.B. daCosta, Lipid composition alters drug action at the nicotinic acetylcholine receptor, *Mol. Pharmacol.* 73 (2008) 880–890.
- [93] D.F. Sargent, R. Schwyzer, Membrane lipid phase as catalyst for peptide-receptor interactions, *Proc. Natl Acad. Sci. USA* 83 (1986) 5774–5778.

Tableau A.S1 Proton chemical shifts of the hERG peptide in water at pH 5.5 and 25 °C and in bicelles DMPC/DHPC $q=1$ at pH 5.5 and 25 °C (grey color).

Residue	NH	CaH	C β H	C γ H	Others
Ile1	8.1	3.82	1.88	C γ H ₃ 0.91 C γ H ₂ 1.18, 1.45	C δ H ₃ 0.88
Ile1	-	3.81	1.83	C γ H ₃ 0.80 C γ H ₂ 1.17, 1.50	C δ H ₃ 0.70
Gly2	8.52	3.91			
Gly2	-	3.92			
Trp3	8.13	4.7	3.17, 3.26		C(2)H 7.22; N(1)H 10.14 C(7)H 7.46; C(6)H 7.21 C(5)H 7.12; C(4)H 7.60
Trp3	7.63	4.55	3.31, 3.38		C(2)H - ; N(1)H 10.37 C(7)H 7.42; C(6)H 7.03 C(5)H 6.94; C(4)H 7.47
Leu4	8.13	4.22	1.45	1.39	C δ H ₃ 0.77, 0.83
Leu4	8.10	4.07	1.30	1.57	C δ H ₃ 0.91, 0.95
His5	8.33	4.53	3.03, 3.16		C(2)H 8.53; C(4)H 7.19
His5	8.10	4.39	3.28, 3.31		C(2)H 8.61; C(4)H 7.29
Asn6	8.24	4.68	2.82, 2.88		N δ H ₂ 6.88, 7.56
Asn6	8.36	4.56	2.79, 2.92		N δ H ₂ 6.95, 7.66
Leu7	8.31	4.28	1.61	1.60	C δ H ₃ 0.83, 0.90
Leu7	7.83	-	1.69	-	C δ H ₃ 0.93
Gly8	8.45	3.88			
Gly8	8.35	3.83, 3.93			
Asp9	8.41	4.65	2.72, 2.81		
Asp9	8.03	4.61	2.89		
Gln10	8.36	4.32	1.95, 2.08	2.30	N ϵ H ₂ 6.84, 7.46
Gln10	8.13	4.36	2.04, 2.17	2.78	N ϵ H ₂ 6.93, 7.45
Ile11	8.11	4.12	1.85	C γ H ₃ 0.84 C γ H ₂ 1.17, 1.44	C δ H ₃ 0.88
Ile11	7.85	4.11	1.94	C γ H ₃ 0.92 C γ H ₂ 1.21, 1.56	C δ H ₃ 0.85
Gly12	8.37	3.88			
Gly12	8.23	3.88, 3.92			
Lys13	8.02	4.58	1.72	1.38	C δ H ₂ 1.64; C ϵ H ₂ 2.95 N ζ H ₃ ⁺ 7.50
Lys13	7.92	4.56	1.64, 1.70	1.40, 1.36	C δ H ₂ 1.65; C ϵ H ₂ 2.96 N ζ H ₃ ⁺ 7.55
Pro14		4.36	1.86, 1.94	2.17	C δ H ₂ 3.57, 3.73
Pro14		4.44	1.88, 1.92	2.15	C δ H ₂ 3.54, 3.75
Tyr15	7.97	4.50	3.02		C(3,5)H 6.84; C(2,6)H 7.13
Tyr15	7.75	4.54	3.00, 3.04		C(3,5)H 6.81; C(2,6)H 7.10

ANNEXE B

CHOOSING MEMBRANE MIMETICS FOR NMR STRUCTURAL STUDIES OF TRANSMEMBRANE PROTEINS

Dror E. Warschawski, Alexandre A. Arnold, Maïwenn Beaugrand, Andrée Gravel, Étienne Chartrand et Isabelle Marcotte

Biochimica et Biophysica Acta 1808 (2011) 1957–1974

B.2 Résumé

L'environnement natif des protéines membranaires est complexe et les scientifiques ont ressenti le besoin de le simplifier afin de réduire le nombre de variables. Toutefois, la simplification excessive peut engendrer des problèmes expérimentaux, ce qui pourrait contribuer au fait que les protéines membranaires ne soient représentées que faiblement dans la base de données structurale et c'est la raison qu'elles sont difficilement étudiées par spectroscopie de résonance magnétique nucléaire (RMN). Les progrès technologiques permettent l'utilisation de modèles plus complexes et, dans le contexte de la RMN, une grande variété de mimétiques membranaires sont maintenant disponibles. Cet article de revue fournit un guide pour la sélection de systèmes de membranes modèles appropriés pour l'étude RMN des protéines membranaires, en fonction de la protéine et de l'information recherchée. À part les bicouches (de tailles, morphologies et lamellarités variables), les bicelles (orientées et isotropes) et des micelles de détergent, cet article de revue va aussi décrire les mimétiques membranaires les plus récents, tels que les amphipols, les nanodisques et les micelles inversées. La RMN en solution et à l'état solide, ainsi que des techniques moins communes, telles que la DNP et la MAOSS, y seront abordées.



Contents lists available at ScienceDirect

Biochimica et Biophysica Acta

journal homepage: www.elsevier.com/locate/bbamem

Review

Choosing membrane mimetics for NMR structural studies of transmembrane proteins

Dror E. Warschawski^{a,b,*}, Alexandre A. Arnold^a, Maiwenn Beaugrand^a, Andr  e Gravel^a,
  tienne Chartrand^a, Isabelle Marcotte^{a,**}

^a Department of Chemistry, Pharmaqam/NanoQAM, Universit   du Qu  bec    Montr  al, P.O. Box 8888, Downtown Station, Montr  al, Canada H3C 3P8

^b Institut de Biologie Physico-Chimique, CNRS - Universit   Paris Diderot, 13 rue Pierre et Marie Curie, F-75005 Paris, France

ARTICLE INFO

Article history:

Received 26 October 2010

Received in revised form 28 March 2011

Accepted 29 March 2011

Available online 6 April 2011

Keywords:

Membrane protein

NMR

Membrane mimetics

Detergents

Lipids

Protein structure

ABSTRACT

The native environment of membrane proteins is complex and scientists have felt the need to simplify it to reduce the number of varying parameters. However, experimental problems can also arise from oversimplification which contributes to why membrane proteins are under-represented in the protein structure databank and why they were difficult to study by nuclear magnetic resonance (NMR) spectroscopy. Technological progress now allows dealing with more complex models and, in the context of NMR studies, an incredibly large number of membrane mimetics options are available. This review provides a guide to the selection of the appropriate model membrane system for membrane protein study by NMR, depending on the protein and on the type of information that is looked for. Beside bilayers (of various shapes, sizes and lamellarity), bicelles (aligned or isotropic) and detergent micelles, this review will also describe the most recent membrane mimetics such as amphipols, nanodiscs and reverse micelles. Solution and solid-state NMR will be covered as well as more exotic techniques such as DNP and MAOSS.

   2011 Elsevier B.V. All rights reserved.

Contents

1. Introduction	1958
2. Parameters dictating the choice of a model membrane	1959
2.1. Biological requirements	1959
2.2. Experimental requirements	1960
3. Slow-tumbling objects	1961
3.1. Isotropic membrane systems	1961
3.1.1. Multilamellar vesicles	1961
3.1.2. Giant and large unilamellar vesicles	1962

Abbreviations: AAO, anodic aluminium oxide; c7-DHPC, 1,2-heptanoyl-1-*sn*-glycero-3-phosphocholine; CMC, critical micelle concentration; CMT, critical micelle temperature; CTAB, cetyl trimethylammonium bromide; DBBPC, 1-dodecanoyl-2-(4-(4-biphenyl)butanoyl)-*sn*-glycero-3-phosphocholine; DDM, dodecylmaltoside; DHAB, dihexadecyldimethylammonium bromide; DHPC, 1,2-hexanoyl-1-*sn*-glycero-3-phosphocholine; DLPC, 1,2-dilauroyl-*sn*-glycero-3-phosphocholine; DM, decylmaltoside; DMPA, 1,2-dimyristoyl-*sn*-glycero-3-phosphate; DMPC, 1,2-myristoyl-1-*sn*-glycero-3-phosphocholine; DMPC, 1,2-dimyristoyl-*sn*-glycero-3-phospho-(1'-*rac*-glycerol); DMPE, 1,2-myristoyl-1-*sn*-glycero-3-phosphoethanolamine; DMPS, 1,2-dimyristoyl-*sn*-glycero-3-phospho-L-serine; DMSO, dimethyl sulfoxide; DNP, dynamic nuclear polarization; DOPC, 1,2-dioleoyl-*sn*-glycero-3-phosphocholine; DOPG, 1,2-dioleoyl-*sn*-glycero-3-phospho-(1'-*rac*-glycerol); DOPE, 1,2-oleoyl-*sn*-glycero-3-phosphoethanolamine; DOPS, 1,2-dioleoyl-*sn*-glycero-3-phospho-L-serine; DOTAP, 1,2-dioleoyl-3-trimethylammonium-propane; DPC, *n*-dodecylphosphocholine; DPPC, 1,2-dipalmitoyl-*sn*-glycero-3-phosphocholine; DPPG, 1,2-dipalmitoyl-*sn*-glycero-3-phospho-(1'-*rac*-glycerol); DSPC, 1,2-distearoyl-*sn*-glycero-3-phosphocholine; GUV, giant unilamellar vesicle; HDL, high-density lipoprotein; HIMSELF, heteronuclear isotropic mixing leading to spin exchange via the local field; HSQC, heteronuclear single quantum coherence; LOPG, 1-oleoyl-2-hydroxy-*sn*-glycero-3-phospho-(1'-*rac*-glycerol); LPPG, 1-palmitoyl-2-hydroxy-*sn*-glycero-3-phospho-(1'-*rac*-glycerol); LUV, large unilamellar vesicle; MAOSS, magic angle oriented sample spinning; MAS, magic-angle spinning; MLV, multilamellar vesicle; MP, membrane protein; MSP, membrane scaffold proteins; NLP, nanopore protein; NMDA, *N*-methyl-D-aspartate; NMR, nuclear magnetic resonance; NOESY, nuclear overhauser effect spectroscopy; OG, octylglucoside; PDC, protein-detergent complex; PEEK, polyetheretherketone; PET, polyethylene terephthalate; PISEMA, polarization inversion spin exchange at magic angle; POPC, 1-palmitoyl-2-oleoyl-*sn*-glycero-3-phosphocholine; POPG, palmitoyl-2-oleoyl-*sn*-glycero-3-phospho-(1'-*rac*-glycerol); PSC, protein-surfactant complex; PSPC, 1-palmitoyl-2-stearoyl-1-*sn*-glycero-3-phosphocholine; R², rotational resonance; REDOR, rotational echo double resonance; SDS, sodium dodecylsulfate; SUV, small unilamellar vesicle; TBBPC, 1-tetradecanoyl-2-(4-(4-biphenyl)butanoyl)-*sn*-glycero-3-phosphocholine; TFE, 2,2,2-trifluoroethanol; T_m, melting temperature; TROSY, transverse relaxation optimized spectroscopy

* Correspondence to: D.E. Warschawski, UMR 7099, CNRS and Universit   Paris Diderot, IBPC, 13 rue Pierre et Marie Curie, F-75005 Paris, France. Tel.: +33 1 58 41 51 11; fax: +33 1 58 41 50 24.

** Correspondence to: I. Marcotte, Department of Chemistry, Universit   du Qu  bec    Montr  al, P.O. Box 8888, Downtown Station, Montreal (Qc) H3C 3P8 Canada. Tel.: +1 514 987 3000#5015; fax: +1 514 987 4054.

E-mail addresses: Dror.Warschawski@ibpc.fr (D.E. Warschawski), marcotte.isabelle@uqam.ca (I. Marcotte).

3.2. Oriented membrane systems	1963
3.2.1. Mechanically aligned bilayers	1963
3.2.2. Magnetically aligned bicelles	1963
3.2.3. Spinning oriented systems	1965
4. Fast-tumbling objects	1966
4.1. Micelles	1966
4.2. Isotropic bicelles	1967
4.3. Small unilamellar vesicles	1968
4.4. Other systems	1968
4.4.1. Organic solvents	1968
4.4.2. Reverse micelles	1968
4.4.3. Amphipols	1968
4.4.4. Nanolipoproteins (nanodiscs)	1969
5. Conclusion	1970
Acknowledgments	1970
References	1970

1. Introduction

Biological membranes are complex natural barriers which isolate the content of the cells from the extracellular environment while controlling exchanges with the external milieu. They also compartmentalize a variety of cellular organelles such as the endoplasmic reticulum (ER), mitochondria, chloroplast, Golgi apparatus, lysosome and nucleus. The total surface area of internal eukaryote cell membranes is of 7000 μm^2 , i.e., ten times that of the plasma membrane, highlighting the important biological role of organelle membranes [1]. Biomembranes consist of phospholipid bilayers (mostly replaced by glycolipids in algae and plant chloroplasts), which may also contain cholesterol and are spanned by membrane proteins (MPs). Cholesterol is not found in prokaryotes and is replaced in yeasts, fungi, algae and plants by ergosterol, sitosterol and lanosterol [2]. The lipid composition of biomembranes varies in the different cell types, organelles and organisms as illustrated in Table 1. These differences can be explained by the functions of the membranes and organelles. For example, cholesterol and phospholipids are synthesized in the ER, explaining its high membrane phospholipid content [3]. The lipid composition may even vary between two monolayers of a bilayer and within different regions of a bilayer as evidenced by the hypothesized "lipid rafts" [4].

The variability in membrane composition is also observable between Gram (–) and Gram (+) bacteria. While both bacteria have an inner phospholipid membrane with comparable composition, Gram (–) have an additional outer membrane, of which the external monolayer is enriched in lipopolysaccharides [5]. Although not entirely understood, the incredible diversity of lipids in membranes, and its conservation, is an indication that they must play specific roles in biological processes.

The membrane and its constituents are involved in essential biochemical processes such as molecular transport, signalling, catalysis, cell–cell interactions and fusion. The protein content of membranes is variable and depends on the cell type and activity. For instance, human erythrocytes contain 40% of lipids and 60% of proteins while myelin is composed of 80% of lipids and 20% of proteins in weight [6,7]. MPs are divided into three classes according to their interaction with the membrane, namely intrinsic transmembrane proteins spanning the membrane, peripheral proteins which do not interact with the membrane core, and lipid-anchored proteins covalently bound to one or several lipid molecules [1].

Because one-third of the human genes codes for MPs [8], their structure–function relationship is of great interest considering their involvement in many pathologies. For example, mutations in the vasopressin receptor and cystic fibrosis transmembrane conductance

Table 1

Lipid composition of selected biomembranes expressed in average weight% of total lipids except for Peas, *Chlamydomonas reinhardtii* and *Aspergillus niger* membranes where the composition is in mol% of total lipids.

Cell/Organelle	PC	PE	PS	PG	PI	SM	CL	Ste	Other
Eukaryotes									
Erythrocyte (human) [7,31,262]	20	16	5	0	0	20	0	23	
Erythrocyte (rat) [262]	34	11	1	0	0	16	0	28	
Myelin (rat brain) [263]	11	14	7	0	0	6	0	22	
Rough endoplasmic reticulum (rat liver) [262,263]	58	18	3	0	9	4	0	5	
Mitochondria (rat liver) [262,263]									
Inner	43	25	1	2	6	3	17	3	
Outer	47	22	3	3	12	6	4	3	
Golgi apparatus (rat liver) [262,263]	43	16	5	0	8	11	0	8	
Nuclear membranes (rat liver) [262,263]	55	20	4	0	9	3	0	9	
Pea root plasma membranes (plant) [264]	57	38	0	0	0	0	0	5 ^a	
Pea leave chloroplast membranes (plant) [265]	7	0	0	6	1	0	0	2	84 (GL)
<i>Chlamydomonas reinhardtii</i> (alga) [266]	0	0	0	3	0	0	0	3 ^b	56 (GL)
<i>Aspergillus niger</i> (fungus) [267]	37	32	4	0	3	4	6	7 ^b	
<i>Candida albicans</i> (yeast) [268]	32	21	3	0	4	0	0	13 ^b	
Prokaryotes									
<i>Escherichia coli</i> (Gram-negative bacteria) [5,269]									
Inner	0	60	0	33	0	0	7	0	
Outer	0	61	0	13	0	0	1	0	25 (LPS)
<i>Bacillus subtilis</i> (Gram-positive bacteria) [270]	0	13	0	77	0	0	4	0	6 (GL)

PC = phosphatidylcholine, PE = phosphatidylethanolamine, PS = phosphatidylserine, PG = phosphatidylglycerol, PI = phosphatidylinositol, SM = sphingomyelin, CL = cardiolipin, GL = galactolipids (monogalactosyldiacylglycerol digalactosyldiacylglycerol, sulfoquinovosyldiacylglycerol), LPS = lipopolysaccharides, Ste = sterols (mostly cholesterol).

^a Mostly sitosterol.

^b Mostly ergosterol.

regulator (CFTR) protein are respectively responsible for X-linked nephrogenic diabetes insipidus (NDI) [9] and cystic fibrosis [10]. A defect on aquaporin AQPO in lens fiber cells is involved in congenital cataracts [11], and there is evidence that channels of the TRP (transient receptor potential) superfamily are involved in kidney disorders, cancer and hypertension [12–14]. Sometimes, a single mutation in the transmembrane part of a protein prevents dimerization and causes various cancers as in the case of the tyrosine kinase receptor family [15]. Therefore, several MPs garner the attention of the pharmaceutical industry. For example the transactivation of the epidermal growth factor receptor (EGFR) is being studied in order to prevent the progression of chronic kidney disease [16], and the calcitonin gene related peptide (CGRP) receptor is targeted to treat migraine headaches [17]. Since voltage-gated sodium channels are expressed in different cancers, they are becoming targets for drug design [18], and so are G-protein-coupled receptors (GPCRs) [19].

The arduous crystallization as well as the difficulty to obtain enough quantities of pure and active MPs has limited the number of known three-dimensional structures which account for only 3% of the identified three-dimensional (3D) structures of proteins [20]. Nuclear magnetic resonance (NMR) is a unique tool to determine MP structure and dynamics in native-like conditions [21]. NMR can tackle samples that are solid or liquid, viscous or fluid, oriented or isotropic, static or spinning, cold or warm, etc. It is a non-invasive technique that can give access to very accurate local distances, orientations or dynamics, the docking of biomolecules, but also the full high-resolution 3D structure of a protein by measuring a wealth of structural constraints through 2D or 3D spectra. Beside protons, NMR mostly exploits ^{13}C , ^{15}N and ^2H when studying MPs. Since those isotopes are not naturally abundant, proteins have to be isotopically enriched, either uniformly or specifically [22–24].

The structural complexity of biological membranes, however, constitutes a challenge for NMR. This obliges the reconstitution of MPs in membrane mimetics which are generally prepared using lipids or detergents. The composition of these mimetics needs to be chosen carefully as it strongly influences several physical properties such as shape, curvature, thickness, lateral pressure, dielectric constant and hydration [25]. It can also modulate the structure and activity of MPs including ion channels [26–28]. A variety of membrane mimetics are available for NMR studies of MPs which can be selected according to the experiment to be performed. This review article first describes crucial parameters that should be examined in order to choose the suitable model. It then presents the numerous options available depending on the type of NMR study to be performed. For each membrane mimetic, a thorough description of the surfactant and of the protein–surfactant complex (PSC) will be given, as well as general guidelines for making the complex, a discussion on the advantages and drawbacks of each approach, and several recent examples of successful NMR applications in the study of MPs. The reader is referred to the list of abbreviations for complete nomenclature of the lipids and detergents.

2. Parameters dictating the choice of a model membrane

Because MPs are very hydrophobic molecules and peptide chemical synthesis yields decrease with length, larger proteins must be over-expressed in host organisms such as *Escherichia coli* or yeasts, or by the newly designed cell-free expression system, preferably with an affinity tag for purification [24,29–31]. During its expression, an MP is either targeted to the membranes of the expressing organism or into inclusion bodies (or protein precipitates). Subsequently, these proteins need to be purified, re-natured and reconstituted so they can regain a native and active structure. Because MPs are hydrophobic molecules they need to be transferred to membrane mimetics in order to be manipulated in solution, which is a very delicate step. The membrane mimetics should meet two criteria: first, it should reflect as closely as possible the natural environment of the protein to reproduce the MP–environment interactions and allow the protein to achieve its

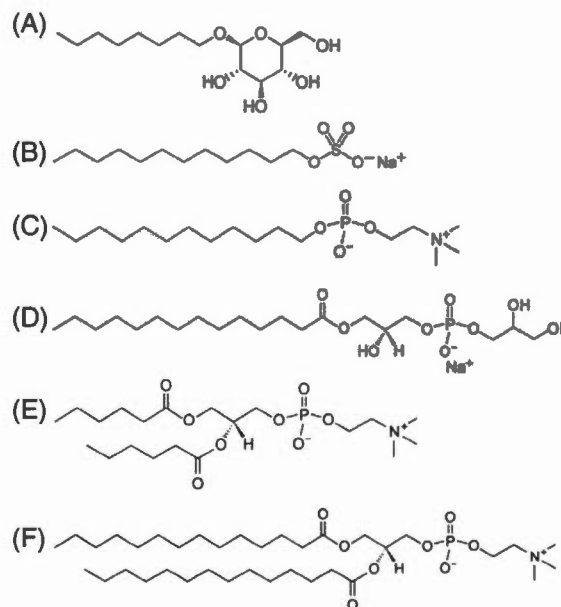


Fig. 1. Molecular structure of commonly used surfactants for the preparation of membrane mimetics: (A) octylglucoside (OG), (B) sodium dodecylsulfate (SDS), (C) n-dodecylphosphocholine (DPC), (D) lyso-myristoylphosphatidylglycerol (LMPG), (E) dihexanoylphosphatidylcholine (DHPC), (F) dimyristoyl-phosphatidylcholine (DMPC).

native state and, at the same time, it must lead to well-resolved NMR spectra. The parameters to be considered when choosing a membrane mimetic for the NMR study of a MP can therefore be divided into biological and technical requirements that will be examined below.

2.1. Biological requirements

Membrane mimetics are prepared by self-association of surfactants in aqueous solution. Surfactants can be divided into two large classes, i.e., those which form micelles (called detergents) and those which form bilayers (i.e., lipids). While detergents can be used to solubilize MPs by extracting them directly from their native membrane, the incorporation of MPs into lipid bilayers requires an additional reconstitution step. To some extent, a detergent micelle will never fully mimic a biomembrane which is primarily a lipid bilayer [25]. Nevertheless, the selection of surfactants should as much as possible take into account the physical characteristics of the biomembrane to be mimicked. To begin with, biological membranes are lipid bilayers ~4 nm thick in a liquid crystalline phase. Therefore an ideal model should be morphologically similar at accessible temperatures since changes in the membrane fluidity will affect the equilibrium distribution of the different conformers [25]. The structures of commonly used surfactants are shown in Fig. 1.

As discussed previously, inter-specific and inter-organelle membrane compositions vary. Cholesterol, for example, is not found in prokaryote membranes, and PC is the most abundant phospholipid in eukaryote cell membranes while PE is dominant in many bacterial strains. The nature of the lipids (charge, acyl chain length, insaturations) composing a biological membrane is important because it dictates the propensity to form a bilayer, as well as the membrane thickness, curvature, fluidity or stiffness [32,33]. For instance, cholesterol, which rigidifies the lipid acyl chains, tunes the membrane fluidity. The balance between the mechanical properties of the biomembrane as determined by the nature of its lipid content can

also have a significant importance on protein structure and function [26,34]. In consequence, the model membrane thickness, curvature and stiffness can modulate the folding, function and equilibrium of MPs [34–36]. For example, the presence of sphingomyelin is required by the pore forming equinatoxin II [37]. The function of the mechanosensitive channel of large conductance (MscL) from *E. coli* was shown to be dictated by its interaction with surrounding lipids depending on their chain lengths or headgroups [38,39]. Similarly, the charge of the membrane constituents counts when studying MPs and peptides which have an affinity for charged lipids, as it is the case for a variety of antimicrobial peptides [40–43]. Likewise, lipid composition can affect the orientation of transmembrane helices in a membrane. Studies show that the tilt of such helices is affected when the model membrane phospholipid chain lengths do not match the hydrophobic length of the protein [44,45]. A review on the interaction of helical transmembrane proteins with membrane lipids can be consulted [46].

The literature shows examples where MP structures differed depending on the composition of the membrane mimetics used in NMR. This stresses the importance of knowing the physico-chemical properties of the mimetics discussed in this review, in order to explain their effect on the protein structure. It should be remembered that biological molecules are dynamic and that sample preparation can trap a molecule in a variety of states that may be “native” or not. Current efforts in structural biology focus on trying to determine the lower populated intermediate states that are thought to be more informative than the more stable, low-energy states that proteins take along a specific mechanism pathway [47]. For example, the structure of phospholamban was studied by NMR in different conditions and gave various 3D structures in bilayers with different thickness and fluidity such as pure POPC bilayers, POPC/POPG bilayers, mechanically aligned DOPE/DOPC bilayers or DPC micelles [48–51]. In such a case, as discussed below, all structures were considered “active” in different relevant states. Similarly, the structure of membrane-bound α -synuclein was shown to be modulated in presence of curved vesicles and micelles or flat bicelles, confirming the importance of the environment upon protein folding into its final structure [52]. The challenge of finding the best membrane mimetics is not specific to NMR structure determination. For example, the influenza virus M2 proton channel was studied in bilayers made of pure lipids of various lengths (DLPC, DMPC, DOPC) as well as in mechanically aligned DOPC/DOPE bilayers and DHPC micelles and gave different results by solution, oriented and magic-angle spinning solid-state NMR techniques [53–58] but also by X-ray crystallography in OG micelles [59]. In this particular case, the structures were not all considered “native-like”. Cross and co-workers recently discussed the bias introduced by the crystal packing on the one hand (high pressure and presence of PEG that resulted in an artificial dimer and no pore) and the extremely high curvature of the detergent micelle that left the solid-state NMR structure the most relevant one [25].

The assessment of MP activity, especially in detergent solution, is a challenge for NMR as well as for 2D and 3D crystallization methods [60]. In favorable cases, protein activity could be assessed *in situ* using complementary studies, e.g., by measuring the binding, by isothermal titration calorimetry, of a known ligand requiring a specific protein conformation [61]. In other instances, it is essential to ascertain that the membrane mimetic did not irreversibly denature the protein. To exclude such mimetics, it is often possible to reconstitute the MP in a native-like environment and verify the loss of activity.

2.2. Experimental requirements

The choice of membrane mimetics to study MPs should also be dictated by the type of information that is searched for and by the NMR experiment to be performed. Parameters such as experiment time, temperature, pH, hydration and surfactant-to-MP ratio must be considered.

The structure determination of MPs requires 2D NMR experiments that are usually performed over long periods of time. Therefore, the stability of membrane mimetics is of great importance as they should maintain the functional state of the protein and limit its conformational flexibility [34]. In solution NMR, for example, Krueger-Koplin et al. [62] have evaluated 25 detergents such as SDS and lyso-phospholipids using ^1H – ^{15}N HSQC experiments. Their study showed that LPPG generally produced high-quality spectra with sample lifetimes greater than 1 month for five proteins tested. Nevertheless, other detergents were also favorable depending on the MP studied. However, the presence of multiple conformations was suspected for certain test proteins in SDS micelles, as suggested by an abnormally high number of cross peaks.

An appropriate membrane mimetic should also have a temperature range of stability covering that of the experiment to be performed – which can be up to 37 °C in some cases while certain solid-state NMR experiments are carried out at sub-zero temperatures [63]. The temperature can affect the quality of the NMR spectra as well as sample life time. In solution NMR, Krueger-Koplin et al. [62] report that the spectral intensities and linewidths of subunit c from *B. pseudofirmus* observed by ^1H – ^{15}N HSQC varied between 22 and 48 °C when studied in LOPG and LPPG micelles. Surfactant stability with respect to pH is also desired to avoid potential hydrolysis of ester links (in the case of phospholipids, for example) and subsequent membrane disruption. Models using ether-linked phospholipids have shown improved stability at low pH although with a different phase behaviour [64].

Membranes are hydrated systems, and a minimum hydration value must be maintained in order to ensure that the structure survives. The primary hydration shell of a lipid is composed of about 20 water molecules [65], which imposes a water content of around 50% in weight and no less than 30% for correct swelling. In addition, a high lipid-to-MP ratio should be achieved to provide sufficient hydrophobic environment. A typical ratio used in NMR is between 4:1 and 1:1 (in weight) [24,56,63,66–69]. A ratio of 1:1 is close to the one found in biomembranes and guarantees a high NMR sensitivity and, at the same time, that each protein is surrounded by at least one layer of lipids. Standard functional reconstitutions, on the other hand, are typically done a ratio of 80:1 in weight [70]. In all instances, NMR tubes are filled with large amounts of water and lipids or detergents and very low quantities of protein material.

As was mentioned previously, membrane mimetics can be divided into micelles and bilayers. They can also be classified as oriented vs. isotropic systems or according to other physical parameters (size, composition, charge etc.). Since the nature of the sample will dictate the NMR experiment (and *vice versa*), the following sections will be presented according to the most important of the parameters: the correlation time of the protein–surfactant complex (PSC). PSCs are highly dynamic structures with slow, intermediate, and fast local and global dynamics depending on the overall molecular weight of the complex [71]. The weight and shape of this complex, the temperature and viscosity of the milieu will mostly affect the global correlation time τ_c of the system. Fast-tumbling small PSCs (<100 kDa) can be studied by solution NMR [62,72–77], while slow reorienting aggregates are more amenable to solid-state NMR [78,79]. Protein size and PSC tumbling rate are related but not directly proportional. First, the surfactant molecules contribute to at least half of the molecular weight of a PSC. Second, while a protein such as the light-harvesting complex 2 (LH2) is only 16 kDa small, it organizes in the membrane as a nonamer of 150 kDa and can only be studied by solid-state NMR [80]. While protein size is generally inversely proportional to spectral sensitivity, the LH2 nonamer of 150 kDa is actually nine times more sensitive than the 16 kDa monomer since the signals of each monomer add up. In the following section, slow-tumbling membrane systems will be divided into two sections depending on their ability to align in the magnetic field B_0 of the NMR spectrometer.

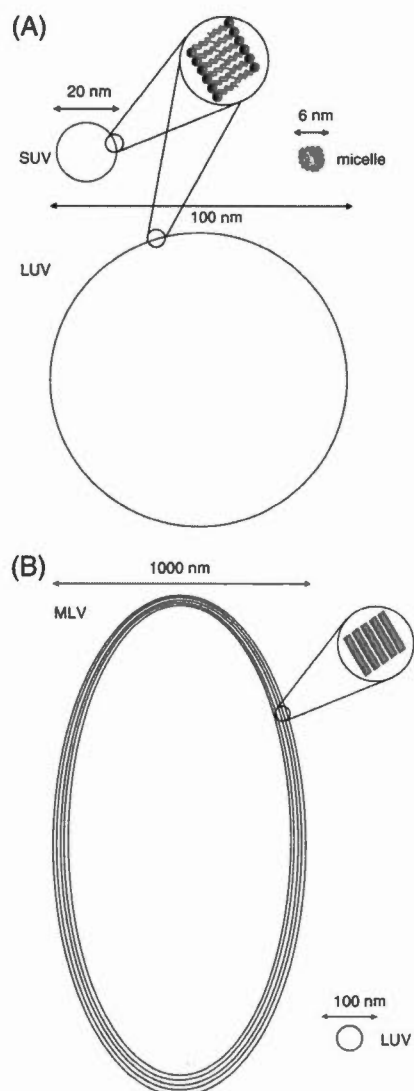


Fig. 2. Cartoons depicting several membrane mimetics described in the text. (A) detergent micelle, small unilamellar vesicle (SUV) and large unilamellar vesicle (LUV). (B) large unilamellar vesicle (LUV) and multilamellar vesicle (MLV).

3. Slow-tumbling objects

NMR spectroscopy and spectral resolution respectively rely and depend on magnetic interactions that are often orientation-dependent. With objects that are fast-tumbling (under 50 ns correlation time), the effect of such interactions is suppressed and high-resolution spectra can be obtained. In the case of slow-tumbling objects that we will examine in this section, other approaches have to be followed to regain the high spectral resolution—this is the field of solid-state NMR. One such approach is magic-angle spinning (MAS) where the “solid” sample is spun at high rates at an angle of 54.7° with respect to the magnetic field, yielding spectra alike to those obtained in the presence of fast molecular tumbling in solution. A second approach is sample orientation, if possible, where the orientation dependence of

the magnetic interactions is fixed to a single value rather than averaged out. Finally, another option for slow-tumbling objects is to retain the orientation dependence of magnetic interactions and extract meaningful data from poorly resolved NMR spectra.

3.1. Isotropic membrane systems

3.1.1. Multilamellar vesicles

Lipids in water organize as closed bilayers called vesicles or liposomes. Depending on their preparation, they can have various sizes and lamellarity. Spontaneously, lipids in water form large multilamellar vesicles (MLVs) that are inhomogeneous in composition, but on the order of $1\ \mu\text{m}$ diameter and up to a dozen bilayers [81] (Fig. 2). Very easy to prepare, MLVs can incorporate any type of lipids and can be tailor-made to mimic any biological membrane composition. Nevertheless, MPs do not insert spontaneously into lipid membranes and an additional reconstitution step is necessary [24,82]. Whether produced chemically or biologically, in biomembranes or in inclusion bodies, MPs have to be solubilized to facilitate their manipulation. Some MPs, usually small peptides, are very resistant and can be dissolved in organic solvents with the appropriate lipid mixture and even dried out entirely without losing their ability to fold back to an active structure [42,49,66,83–88]. MLVs containing MPs are obtained by rehydration of such a mixture.

More fragile MPs have to be solubilized using detergent molecules. They can either be studied in detergents (Section 4.1) or be transferred to another environment such as vesicles, supported membranes (Section 3.2.1), bicelles (Section 3.2.2), nanodiscs or amphipols (Section 4.4). The general procedure consists in making ternary complexes of MP, detergent molecules and the new surfactant in which the MP will be reconstituted. The detergent is subsequently removed by one of several methods, the most popular ones being the use of polystyrene beads (biobeads) or simple dialysis until the detergent concentration is below the critical micelle concentration [70].

Although the vesicle multilamellarity is not biologically relevant, the local constraints in the MLV membrane are that of a cell because of the vesicle size and curvature. In addition, this type of sample is advantageous for NMR analysis because it is highly concentrated in lipids and embedded proteins. A typical sample may contain a ratio of 1:1 (in weight) of lipids-to-water, and 4:1 of lipids-to-protein [24]. The multilamellar nature of these objects makes them improper for the study of lipid asymmetry or transport across the membrane since it is difficult to define an exterior and an interior of the vesicle and because of inter-bilayer effects. The large size of these objects and the resulting slow tumbling also make them unsuitable for solution NMR, but they are appropriate for solid-state NMR applications.

NMR spectra of static solids are poorly resolved, but focusing on specifically labelled parts of the molecule, one can still obtain crucial dynamic or structural information. Solid-state ^2H and ^{31}P NMR can be employed to study lipid/protein interactions in MLVs incorporating deuterated lipids [85,89]. Using ^2H NMR, Jones et al. [66] have measured the orientation and local dynamics of the protein EGF receptor containing deuterated alanines in POPC MLVs, with and without cholesterol.

Spectral resolution can be increased by spinning the sample at the magic angle. In the 1990s, the technology was insufficient for resolving all atoms of a protein in a sample, but by specifically labelling some ^{13}C and ^{15}N atoms, one could measure very accurate distances in a protein. With a technique called Rotational Resonance (R2) and only two ^{13}C atoms, Griffin and co-workers could determine the conformation of the small retinal molecule inside a macromolecular complex formed by the 26-kDa MP bacteriorhodopsin, lipids from the bacterial membrane and water [90]. With a similar technique called REDOR, two ^{13}C and one ^{15}N atoms, Schaefer and co-workers could determine the secondary structure and orientation of the antibacterial peptide magainin in DPPG or DPPG/DPPC MLVs [83]. With three ^{13}C and one ^{15}N atoms, Separovic and co-workers could

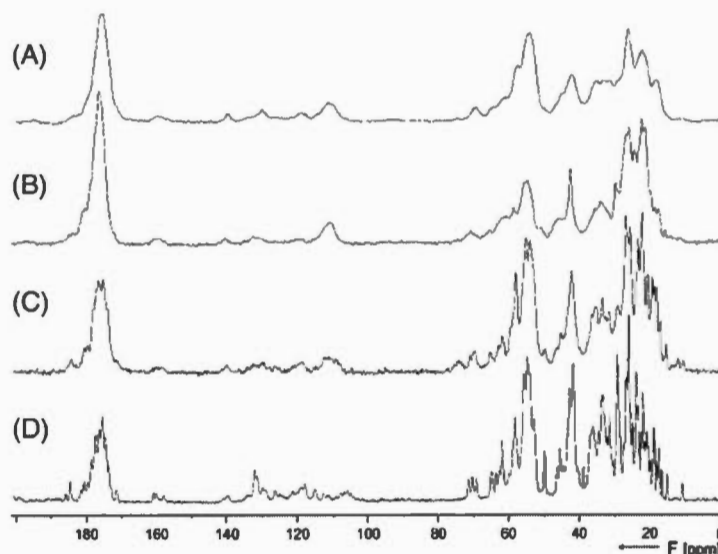


Fig. 3. 1D ^{13}C solid-state NMR spectra of differently prepared α -spectrin SH3 samples. Sample (A) was entirely lyophilized from aqueous low-salt buffer. Sample (B) was partly lyophilized from aqueous low-salt buffer. Sample (C) was lyophilized from a solution containing poly-ethylene glycol and sucrose. Sample (D) was precipitated from a $(\text{NH}_4)_2\text{SO}_4$ -rich solution. Remark: the proteins in sample (D) are micro-crystallized. Adapted from [92] with permission.

locate the conformational flexibility of an α -helix of the nicotinic acetylcholine receptor in DSPC or POPC MLVs [86].

Since the seminal work of Oschkinat and co-workers [91], magic-angle spinning NMR has become an important technique that provides new protein structures itemized in the Protein Data Bank (PDB) [21]. MAS-NMR is now tackling samples made of uniformly labelled proteins embedded into hydrated MLVs and has helped to determine a number of 3D structures such as proteogrin in POPC MLVs [87] or the Influenza M2 channel in DLPC or DMPC MLVs [56,67]. The membrane environment should provide a native/active conformation for the protein, which would also be an advantage for NMR since a single conformation would give a highly resolved spectrum, whereas any other preparation that may result in a distribution of conformations would compromise the quality of the spectra, as illustrated by Fig. 3 on a soluble protein [92]. Nevertheless, membranes are also rich in slow dynamics and spectra may still suffer from a distribution of active conformations. Temperature is a parameter that can be used to either slow down or accelerate conformational exchange [67,68,93]. Resolution and sensitivity in solid-state NMR is currently insufficient for routine 3D structure determination of uniformly labelled MPs in MLVs. Nevertheless, this area is constantly evolving, especially with the development of Dynamic Nuclear Polarization (DNP) [94] or new isotopic labelling techniques [95].

Several large transmembrane proteins are being assigned in a membrane environment, and the structure is on the way, such as for the phospholamban pentamer in DMPC or DOPC/DOPE MLVs [69], the outer membrane protein G in MLVs made of *E. coli* lipid extracts [68], the potassium channel KcsA in asolectin MLVs [63], the cytochrome bo3 oxidase in MLVs made of endogenous *E. coli* lipids [93], the sensory rhodopsin in purple membrane lipids MLVs [96] or the mechano-sensitive channel Mscl in DOPC MLVs [24]. DNP is one of the most fascinating recent developments in solid-state NMR for signal enhancement, and one obvious application is the study of MPs. Such an approach is currently being followed by the group of Griffin on frozen bacteriorhodopsin in MLVs with deuterated lipids, water and glycerol used for cryoprotection [94].

3.1.2. Giant and large unilamellar vesicles

Several methods exist to make unilamellar vesicles, the most popular ones being reverse-phase evaporation of organic solvents, extrusion through polycarbonate filters or sonication [81]. Most vesicles can be prepared with almost any type of lipids. The major advantage, as mentioned before, is that the inner layer, the outer layer, the interior and the exterior of the liposome are easily defined, and the transport of solutes through a protein can be measured across the membrane. Other properties depend on the liposome diameter that can range from 10 μm (Giant Unilamellar Vesicles or GUVs) down to 100 nm for typical Large Unilamellar Vesicles (LUVs), or even 20 nm for Small Unilamellar Vesicles (SUVs) obtained by sonication.

GUVs and LUVs have a small curvature and, hence, provide a native-like local environment for MPs. They also have large interior volume and, thus, a low membrane concentration in the sample rendering them unfavorable for NMR which is an insensitive technique. For these reasons, GUVs are never used in NMR and LUVs are mostly studied for looking at lipids, but not at MPs. The use of SUVs for the study of MPs by solution NMR will be reviewed below in Section 4.3.

The combined effect of vesicle tumbling (radius R , viscosity η and rate $1/t_r$) and lateral diffusion (constant D and rate $1/t_d$) can lead to partial or complete averaging of NMR interactions. Assuming that the effective correlation time t_v is described by the following equation [97]:

$$\frac{1}{t_v} = \frac{1}{t_r} + \frac{1}{t_d} = \frac{3kT}{4\pi\eta R^3} + \frac{6D}{R^2} \quad (1)$$

Bloom et al. [97] have shown that lipid diffusion around the vesicle was independent of vesicle size and that high-resolution ^1H NMR spectra were obtained when the vesicle tumbling was fast enough, i.e., when the vesicles were sufficiently small.

3.2. Oriented membrane systems

Orienting all molecules of a sample in the same direction can be difficult. Luckily, in the case of lipids, there are several cases where they spontaneously align in a given direction. Peptides or proteins embedded in the lipid membrane can therefore be oriented as well. We will examine two different types of oriented membrane systems: supported on glass plates or non-supported magnetically aligned bicelles. We will also consider the emerging field of MAOSS which combines orienting and spinning of the sample.

3.2.1. Mechanically aligned bilayers

When hydrated with the adequate amount of water, almost all lipids spontaneously align on glass plates with the bilayer normal perpendicular to the plates' plane. Furthermore, when introduced in the magnetic field, additional magnetic alignment significantly improves the lipid mosaic spread (deviation from perfect orientation) to be down to 0.3° [98]. The mechanical alignment of lipid bilayers supported on glass plates is, therefore, a very convenient way to orient a MP in the magnetic field.

Oriented samples are prepared by spreading a lipid/protein dispersion on glass plates. Typically, lipids and proteins are dissolved in an organic solvent but if necessary, proteins can be reconstituted in a hydrated lipid membrane without using solvents. In both cases, the dispersion first has to be significantly dehydrated and the plates are subsequently rehydrated in a chamber for a couple of days. Phospholipid alignment can easily be checked by ^2H or ^{31}P NMR which provide characteristic oriented lipid signals. Each plate is a square of $\sim 1\text{ cm}^2$, and about twenty such plates can be stacked into a sealed NMR tube [99,100].

With the appropriate NMR probe, any orientation of the supported bilayers can be achieved, whereas bicelles (see next section) can only adopt parallel or perpendicular orientations. Glass plate supported membranes can be aligned with almost any lipid, at almost any temperature, whereas bicelles only align in a specific temperature range depending on their composition. Nevertheless, lipid bilayers will align on a glass plate only within a specific hydration range (typically around 40% by weight [99]), which is low compared to native membranes and hardly permits the change of pH or solute concentration once the samples are made. Furthermore, a significant fraction of the sample volume is occupied by the glass plates, thus reducing the sensitivity of the NMR experiments since a typical sample will contain a weight ratio of lipids-to-protein between 3:1 [99] and 160:1 [100], and typically 20:1.

While this system was first used to study lipid dynamics (see, for example, [101]), solid-state NMR of mechanically aligned membranes has generated the first 3D structure of a MP by NMR [99]. This seminal

work by the group of Cross has resulted from a systematic ^{15}N NMR study of gramicidin A in DMPC membranes started in 1986 [102] where the peptide structure is deduced from each peptide plane orientation determined independently. This approach has been improved by the group of Opella with the development of PISEMA [103–106] and related sequences such as SAMMY [107] or HIMSELF [108] that can be applied to uniformly ^{15}N -labelled peptides. These sequences provide 2D spectra with patterns that directly depend on helix tilts in the membrane, as shown on Fig. 4 with the peptide tBd [106]. In solid-state NMR, the approach of using oriented membranes on glass plates has been the most efficient, as of today, for providing new MP structures [21]. Since 1993 over half a dozen membrane peptide structures have been determined to high resolution, such as several M2 channels (from the nicotinic acetylcholine receptor, NMDA receptor and influenza A virus), in DMPC or POPC/DOTAP 4:1 membranes, as well as the small Vpu channel from HIV-1 in DOPC/DOPG 9:1 membranes [54,100,109]. Finally, a combination of solid-state NMR on DOPC or DOPC/DOPE 4:1 (molar ratio) membranes aligned on glass plates and solution NMR on MPs solubilized in DPC detergents has allowed the determination of several dynamic and active structures of phospholamban, resting and active, compared to the static picture determined in solution only [48,51]. As discussed before regarding the structure determination of the influenza virus M2 proton channel [25], this combination of different NMR techniques – especially if performed in the same membrane environment – or NMR and crystallographic techniques, may well be the best approach to compensate for each technique pitfall.

3.2.2. Magnetically aligned bicelles

Bilayered micelles – or so-called *bicelles* – have been introduced in the 1990s as new membrane mimetics [110,111] and quickly gained popularity considering the numerous advantages they offer for studying membrane peptides and proteins. Their composition and local morphology resemble those of biomembranes – i.e., a planar bilayer of phospholipids – and they have proven their versatility as they can be used in both solution and solid-state NMR. Moreover, bicelles are transparent and, thus, amenable to optical spectroscopy such as circular dichroism [112–117].

Bicelles are composed of long- and short-chain phospholipids, generally DMPC and DHPC [111] although DMPC can be replaced by large fractions of other saturated or unsaturated long-chain lipids with various headgroups, as well as cholesterol, gangliosides and ceramides [118–133]. Thereby bicelles can mimic a variety of biomembranes such as prokaryote, mitochondria, erythrocyte, myelin, neurons and skin [134]. Both lipids can be replaced by PCs with chain length different by one or two carbons [130,135]. DMPC and DHPC can also be replaced by analogs with ether links in lieu of carboxy-ester

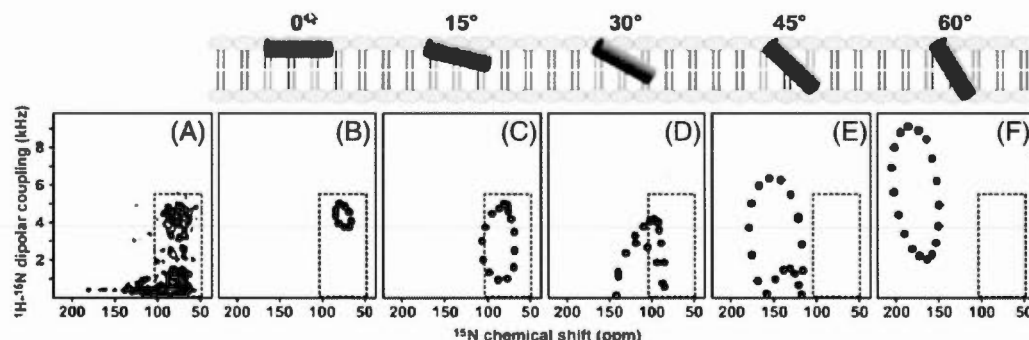


Fig. 4. 2D PISEMA NMR spectra (A) and simulations (B–F) of the uniformly ^{15}N -labeled tBd peptide in oriented lipid bilayers. The helical tilt angle is indicated above each simulation. The experimental spectra are best fitted for helix parallel to the membrane surface, or with a tilt under 20°. Adapted from [106] with permission.

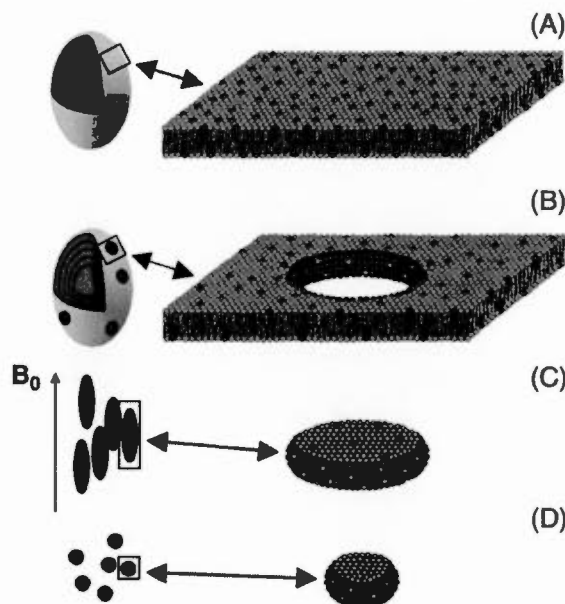


Fig. 5. The various morphologies of bicelles: (A) large mixed multilamellar vesicles, (B) perforated multilamellar vesicles, (C) large magnetically aligned bicelles and (D) small isotropic bicelles. Large bicelles align with the normal to their bilayer perpendicular to the external magnetic field B_0 , as shown on (C). Adapted from [141] with permission.

bonds to access acidic and basic pH and improve bicelle stability [64,136,137]. Recently, cholesterol sulfate was shown to improve the thermal stability of bicelles and broaden the interval of temperature at which they align [138]. It is also possible to prepare bicelles mixed with non-lipid surfactants such as bile salt analogues [110,139] or Triton X-100 [140].

The morphology of bicelles has been the object of much debate and was extensively studied by several research groups, as reviewed by

Marcotte and Auger [134]. However, recent ^{31}P solid-state NMR studies published by Triba et al. [141] support a model in which the shape is dictated by the long-to-short-chain phospholipid q ratio as well as temperature. Bicelles can thus be found as discs, vesicles or perforated vesicles as shown in Fig. 5, and therefore prepared according to the NMR experiment to be performed. Fast-tumbling discoid (isotropic) bicelles are characterized by a low q ratio and used in solution NMR studies of MPs, as will be described in Section 4.2, while high- q , magnetically self-aligning bicelles are prepared for the orientation measurements of MPs that will be described below. For detailed applications of isotropic and oriented bicelles for the NMR study of membrane-associated surfactants and proteins, the reader is referred to several reviews [134,142,143].

At temperatures above DMPC's gel-to-fluid phase transition (typically $>30^\circ\text{C}$), long-to-short-chain lipid ratios $q>2.3$, and lipid concentrations of 3–60% w/v in aqueous solution, bicelles are known to spontaneously align in the magnetic field [141,144–147] with their bilayer normal perpendicular to the direction of the magnetic field, as illustrated in Fig. 5C. The magnetic alignment of bicelles is attributed to the anisotropy of the magnetic susceptibility of the phospholipids, as detailed elsewhere [134]. Although the average bicelle orientation is determined, the distribution and oscillation around this position have an effect on the NMR data [141]. The mosaic spread affects the width and symmetry of resonances, and it is reported around 6° [148]. Oscillations partially average magnetic interactions in molecules embedded in bicelles and additional order parameters between 0.7 and 0.9 therefore have to be included to take this effect into account [114].

Aligned bicelles can be prepared by mixing the phospholipids in the appropriate buffer solution, followed by a series of freeze (liquid nitrogen)/thaw (37°C)/vortex shaking, leading to a transparent non-viscous sample. Proteins can be co-solubilized with the phospholipids in solvents such as 2,2,2-trifluoroethanol (TFE), followed by vacuum-drying prior to hydration [88,113]. In some cases proteins do not survive organic solubilization or full drying, thus reconstitution protocols have been optimized to incorporate MPs into bicelles without such damaging steps [114]. Typically, a q value of 3 to 3.5 is employed with 20–60% w/v lipids in aqueous solutions [44,84,108,114,120,149–154]. Details on the preparation of bicelles samples for solid-state NMR study of MPs can be found in De Angelis and Opella [155]. Proteins as big as 350 residues have been successfully incorporated into oriented bicelles, as demonstrated with the G-

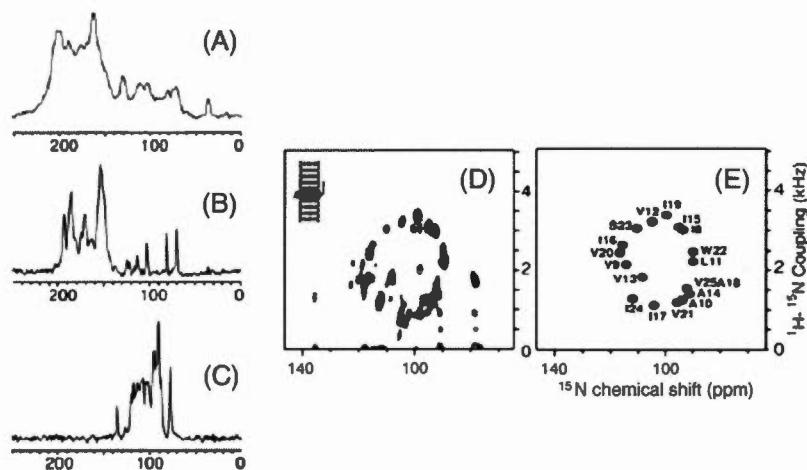


Fig. 6. Solid-state NMR spectra of the transmembrane domain of Vpu in lipid bilayers differently aligned: on glass plates (A), in "flipped" bicelles (B) or in "normal" bicelles (C–E). (A–C) are 1D ^{15}N NMR spectra while (D) is a 2D PISEMA NMR spectrum allowing for resonance assignment (shown in E) and helix tilt determination (determined here to be approximately 30° with respect to the bilayer normal). Adapted from [151] with permission.

protein-coupled receptor CXCR1 [156]. Fannucci et al. [157] observed that large bicelles preserved the folded structure of the Ton box motif of BtuB, and Czerski and Sanders [158] showed that the integral MP diacylglycerol kinase (DAGK) maintained its catalytic activity when incorporated into DMPC or DPPC bicelles.

DMPC/DHPC bicelles have a thickness of ~4 nm similar to a natural bilayer [159] as well as a planar surface. They are also stable over a wide extent of ionic strengths and pH [111,144], as opposed to acidic bicelles which are more fragile and subject to hydrolysis [120,122]. Aligned bicelles have several advantages over mechanically aligned bilayers: in the correct temperature range, bicelles tend to improve the resolution of ^{15}N and PISEMA spectra as compared to bilayers mechanically aligned on glass plates as illustrated in Fig. 6A and B with the transmembrane domain of Vpu [151]. The sample is easier to prepare, better hydrated and the volume is large because of the absence of glass in the sample. In addition, MPs expressed in bacteria can be purified either with the bicellar long- or short-chain lipid to which the lipid companion can then be added in order to obtain bicelles [114,156,160]. However, it should be noted that the presence of a protein may affect the orientation of bicelles, as was observed with gramicidin [88].

Aligned bicelles are frequently used to determine the orientation of transmembrane helices with respect to the bilayer normal such as that of antimicrobial peptides but also large transmembrane proteins such as the β -barrel tOmpA and OmpX, as long as their axial diffusion is fast [114,154]. This information – which is complementary to the structure that can be obtained by solid-state NMR, solution NMR, or any other method – can be provided by ^{15}N or ^2H NMR as the ^{15}N chemical shift value or the ^2H quadrupolar splitting of specifically labelled residues are indicative of the chemical bond orientation with respect to B_0 direction [108,120,150]. Improvement over this approach with PISEMA related sequences has allowed the resonance assignment and helix tilt determination of the Vpu channel from HIV-1, as shown on Fig. 6C–E [151]. Similar approaches have provided the structure of a truncated construct of the mercury transport membrane protein MerF-t [151], as well as the orientation of several proteins such as the cytochrome *b5* [108], TatAd from *B. subtilis* [153] or the p7 protein of hepatitis C virus [161] in lipid bilayers. Although aligned bicelles are slow-tumbling objects used in solid-state NMR, large bicelles can also be employed in solution NMR to induce residual alignment in water-soluble proteins and obtain residual dipolar couplings used in structure determination, as thoroughly detailed elsewhere [162,163].

Due to their large magnetic susceptibility, the addition of paramagnetic lanthanides flips the orientation of the bicelle normal from

perpendicular to parallel to the static magnetic field direction. This effect achieved at very small lanthanides/lipids molar ratios (<0.1) is well detailed by Prosser et al. [164] and will not be discussed further here. The advantage of this method is to double the NMR frequency range of ^{15}N chemical shifts (Fig. 6B compared to 6C), thus improving the resolution of the amide spectral region, as demonstrated with the fd coat and Vpu proteins [84]. The same effect is observed on ^2H NMR spectra. Another advantage of the parallel alignment is that protein orientation in the membrane becomes independent of its azimuthal orientation and axial diffusion rate. Spectra obtained at 0° and 90° alignments can also help confirming the orientation of proteins such as the large outer MPs from *E. coli* [114,154] or the small MerF-t and Vpu transmembrane α -helices [44,151,152]. The presence of paramagnetic ions may perturb protein activity, shift amino acid resonance frequencies or catalyze lipid hydrolysis, although lipids with chelating headgroups can be used to sequester the lanthanides away from the protein [165]. However the protein moieties within the hydrophobic core of the bicelles should not be affected [84].

In order to avoid the use of lanthanide ions altogether, it is possible to prepare parallel-aligned bicelles by replacing DMPC with phospholipids containing a biphenyl group on one acyl chain, such as DBBPC or TBBPC [166,167]. The large positive magnetic susceptibility of the biphenyl groups is responsible for flipping the bicelle orientation. Although the temperature range where “biphenylated” bicelles align is larger compared to DMPC/DHPC bicelles, the composition domain for which orientation occurs is reduced [166]. These new bicelles have yet to be proven general for the incorporation of MPs, but they have already been successfully applied to the study of the Pf1 coat protein [168].

3.2.3. Spinning oriented systems

Aligned bilayers can also be utilized in combination with MAS to improve the resolution, signal-to-noise ratio and sensitivity of the NMR measurement of orientation. This approach introduced as MAOSS (magic angle oriented sample spinning) was proposed by Glaubitz and Watts in 1998 [169]. The original membrane system consists of a series of lipid bilayers deposited on glass discs which are then stacked and placed in a MAS rotor to orient their bilayer normal parallel to the rotor axis, as shown in Fig. 7A. Purple membranes – an hexagonal crystalline lattice of the light-driven proton pump bacteriorhodopsin (BR) from *H. salinarum* – can also be oriented on glass plates and spun [170]. This strategy presents two assets from an NMR point of view. Firstly, high sensitivity in the orientation measurement is achieved since small deviations from the normal result in dramatic spectral changes. Secondly, this orientation allows anisotropic motions such as rotational diffusion to partially average interactions which are predominantly dipolar [71]. Residual interactions can easily be removed even at slow spinning speeds of up to 3 kHz. Mosaic spread values are reported below 20° [171]. Using this approach, high resolution for ^1H NMR resonances can be obtained [169]. MAOSS has also been employed for a ^2H NMR study of photointermediates of specifically deuterated bacteriorhodopsin [172] as well as for the study of the M13 coat protein by ^{13}C NMR [173]. Interestingly, this method can also be combined with standard solid-state NMR experiments such as REDOR where deviations from the non-oriented case can be analyzed in terms of the targeted molecule orientation [171].

Certain disadvantages are however also associated to this method. For example, under MAS conditions, centrifugal forces induce migration of the sample towards the edges of the plates, thus limiting the spinning rate. Likewise, the heftiness of the glass plates also makes it difficult to spin the sample at high rates, and since glass occupies most of the rotor's volume, only a small amount of protein is actually introduced [174]. More recently Sizun and Bechinger [175] suggested an alternative approach to obtain a bilayer with its normal oriented perpendicular to the magnetic field. In such a case, the bilayer alone or with reconstituted peptides is first dissolved in chloroform or TFE then adsorbed onto a thin polymer foil from which the solvent is

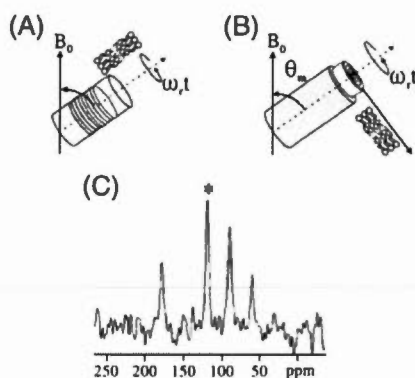


Fig. 7. (A) Arrangement of glass plates and rotor used in MAOSS. (B) Arrangement of polymer sheets and rotor used in the alternative MAOSS approach. (C) 1D ^{15}N MAOSS NMR spectrum of a peptide, obtained using the approach described in (B). Adapted from [175] with permission.

subsequently evaporated under vacuum. The resulting dry polymer sheet is then brought to desired humidity, rolled up and placed with its long axis parallel to the rotor axis (Fig. 7B and 7C) [170,174–177]. Major advantages of this approach are the ease of preparation, the low cost of the required materials, especially since this type of system can be prepared on various types of polymer foils such as polyetheretherketone (PEEK) [174–176], polycarbonate [174] and polyethylene terephthalate (PET) [170,177–179]. In addition, samples can fit in 4-mm rotors and reach high spinning rates of up to 10 kHz as opposed to the limited 3–5 kHz of conventional MAOSS [175]. The reported mosaic spread values are 3.7° [175], below 8° [178] and up to 22° in the case of short-chain lipids [170]. However, in all cases, spinning the sample should increase the quality of the orientation as a result of centrifugal forces [175,180].

Another approach exploits large magnetically aligned bicelles to determine the structure of MP segments in combination with MAS. The high-resolution ¹H NMR spectra obtained can be used to acquire 2D experiments such as NOESY and deduce structurally-relevant information [150].

4. Fast-tumbling objects

As mentioned before, high spectral resolution can be obtained in solution NMR with objects that have a correlation time below 50 ns which corresponds to an upper limit of approximately 100 kDa. In some favorable cases, especially with proteins under 30 kDa, a complete interaction map can be obtained and allow for the determination of a 3D molecular structure. With such approaches, solution NMR has elucidated the structures of some 6000 soluble proteins in the past 20 years [181]. In more challenging cases, partial structural and dynamic information can still be obtained, sometimes with the use of specific isotopic labelling schemes [182]. The most common way to study MPs by solution NMR is to solubilize them in detergent micelles [62,72,74,75] but new systems are being developed [73,76,77] and will be described below.

4.1. Micelles

Micelles are the most frequently used membrane mimetics for the structure determination of peptides and proteins by solution NMR and have helped in solving the structures of ca. 25 MPs in the past 15 years [21,62,74,76]. These aggregates are formed by self-assembly of amphiphilic molecules in solution in order to minimize the contact of their hydrophobic tails with the aqueous environment (Fig. 2A). Because they are small spherical monolayers with a rough surface, the micelle morphology differs from that of biomembranes. They can also adopt elliptical or rod-like shapes at high detergent concentrations or with weakly polar surfactants [183]. Micelles are formed at a specific detergent-dependent concentration – the critical micelle concentration (CMC). They are also characterized by an aggregation number (*N*) that can be as low as 4 and up to several hundred of molecules [76,183,184]. The molecular weight of a micelle is therefore *N* times the molecular weight of the detergent monomer. They are on the order of ~3 nm radius, corresponding to a correlation time of ca. 25 ns. The micelle concentration [*M*] is related to the detergent concentration [*D*] by the relation:

$$[M] = (D - \text{CMC}) / N \quad (2)$$

Micelle formation also occurs at a critical micelle temperature (CMT). SDS, for example, precipitates at temperatures below 4 °C. Therefore, the incorporation of an MP into micelles as well as the NMR experiments must be performed above the Kraft point, i.e., at the temperature at which a turbid detergent solution becomes clear due to micelle formation.

In the case of the ternary mixture of detergents, MPs and water, the detergent hydrophobic moieties often spontaneously cover the hydrophobic parts of the proteins to form protein–detergent complexes (PDCs) that remain water-soluble. When the protein is small, the complex resembles a micelle in which the protein is embedded. In other cases, the detergent may play the role of a lifebuoy around the MP. As discussed by Strandberg and Ulrich it is assumed that each micelle accommodates only one peptide [41]. The fast tumbling of micelles in solution often averages out orientation-dependent interactions in NMR such as dipolar coupling and chemical shift anisotropy, thus leading to high spectral resolution. Micelles are, thus, well indicated for structure determination of MPs by solution NMR. If possible, perdeuterated detergents should be employed to avoid overlap with the protein resonances on the ¹H NMR spectra. Nevertheless, most modern NMR experiments make use of ¹⁵N- or ¹³C-filtered experiments, thus removing the detergent contribution in the spectra, even if it is protonated [185–187].

After purification, the NMR sample needs to be concentrated to obtain a high protein concentration (on the order of 1 mM), but the final detergent concentration increases as well. Detergent concentration can then be reduced, more easily when its CMC is high. In addition to the micelles and PDCs, detergent monomers are present in the solution (at a concentration corresponding to their CMC), hence contributing to the solution viscosity and molecular tumbling rate. Since MPs may precipitate when solubilized at the CMC, it is advised to maintain them in solution with detergents above the CMC, especially for detergents with high aggregation numbers, so that the micelle concentration [*M*] exceeds the protein concentration [184]. Detergent concentration should be optimized on a case-by-case basis [188].

The properties of PDCs highly depend on the physicochemical properties of the detergents. DPC and SDS micelles are the most commonly used for structure determination of MPs and peptides [41,189,190] and references in [75]. It is important to favor detergents with small aggregation numbers to obtain small, fast-tumbling PDCs and increase the protein signal because of the reduced surfactant proportion. For example, although DDM is a mild detergent that tends to maintain the functionality of MPs, it forms large micelles (~60 kDa) that reduce protein signals in solution NMR both because the micelles tumble slowly – which broadens the protein signals – and because the protein-to-surfactant ratio is smaller [60]. Anionic detergents such as SDS can be more denaturing than the other types, non-ionic micelles being the mildest [191,192]. Zwitterionic detergent micelles such as DPC are used to mimic eukaryote membranes while the negatively charged SDS micelles would resemble bacterial membranes [41].

Unfortunately, no rules apply when searching for the right detergent; however Vinogradova et al. [72] reported that the catalytic activity of DAGK was higher in micelles of medium-chain length detergents such as DPC or DM which therefore should be considered as good models since their low molecular weight contributes little to the overall weight of the PDC. The use of a mild detergent does not guarantee that a protein will be properly folded, though. Mo et al. [193] showed that the helical proteins bacteriorhodopsin and Ste2p from *S. cerevisiae* are found in partially folded states in OG (octylglucoside) and DM micelles, respectively. Comparison with different detergent types reveals that the small multidrug-resistance pump (Smr) adopts a native conformation in bicelles and DM micelles, but not in LPPG and DPC micelles [76]. One risk is that the surfactant covers not only the hydrophobic part of the protein but also its active sites, thus affecting its activity [62,76]. As an illustration the *E. coli* enzyme PagP has no activity in OG and DPC micelles due to detergent binding in the active site, but recovers its activity in CYFOS-7 micelles (a DPC analogue with a chain terminal cyclohexyl group) [187,194]. LPPG micelles often lead to high-quality spectra [62,76]; however, as seen for the protein Smr, it is not necessarily the ideal detergent for a given protein. The spontaneous curvature of micelles does not always accommodate MPs and the activity of enzymes or ion channels can be compromised [25,52,76,194].

Table 2

Average characteristics of detergents frequently employed for structural NMR studies of proteins. Adapted from [31,74,76,183,188]. Details on the protein structure can be found in [21].

Detergent	Monomer MW (g/mol)	Monomer CMC (mM)	N	Micellar MW (kDa)	Typical NMR conditions	Some MP structures solved by solution NMR
Non-ionic (mild)						
DDM (C12-DM)	511	0.2	140	72		
DM (C10-DM)	483	2	80	39		
OG (C8-G)	292	20	90	26	200 mM/40 °C	PagP
Zwitterionic						
DPC (C12-PC or FOS-12)	352	1.5	70	25	200 mM/40 °C	GpA, OmpA, PagP, OmpX, OmpG, PLN, DsbB, i3, DAGK, Rv1761c, CD4
LDAO (C12-DAO)	229	1	75	17	300 mM/40 °C	VDAC
c7-DHPC (D7-PC)	482	1.5	25	12	100 mM/50 °C	SRII
DHPC (D6-PC)	454	15	35	16	300 mM/40 °C	M2, OmpA, kpOmpA, Pf1
Anionic						
LPPG (L16-PG)	507	0.02	160	81	200 mM/50 °C	DTF
LMPC (L14-PG)	479	0.2	55	26	80 mM/40 °C	KCNE1
SDS (C12-S)	288	3	80	23	500 mM/40 °C	MerF, FXVD1, FXVD4
Mixtures						
DPC/SDS 5:1 ^b	–	–	–	–	150 mM DPC/30 °C	ZZ
DHPC/DMPC 4:1 ^b (isotropic bicelles)	–	–	200 DHPC/50 DMPC	125	200 mM DHPC/40 °C	Bnip3, ErbB2, EphA1, α IIb- β 3

^a Protein abbreviations: α IIb- β 3 (Integrin α IIb- β 3); Bnip3 (Bnip3 transmembrane domain); CD4 (human CD4); DAGK (diacylglycerol kinase); DTF (G-protein-coupled receptor double transmembrane fragment); EphA1 (EphA1 transmembrane domain); ErbB2 (ErbB2 transmembrane segment); FXVD1 (human FXVD1, Na,K-ATPase regulatory protein); FXVD4 (human FXVD4, CHIF); GpA (human Glycophorin A transmembrane domain); i3 (i3 intracellular loop of the vasopressin V2 receptor); KCNE1 (human KCNE1); M2 (Influenza M2 proton channel); Pf1 (Pf1 major coat protein); PLN (human phospholamban); Rv1761c (Rv1761c from Mycobacterium tuberculosis); SRII (Sensory rhodopsin II); VDAC (human VDAC-1); ZZ (zetazeta transmembrane domain).

^b mol/mol ratio.

If possible, functional assays should be conducted to identify the best surfactant to be employed [60,72].

The challenge is to find the most appropriate detergent for the structural NMR study that also solubilizes the protein in a native conformation—and no such universal detergent exists. Recently the group of Nietispach [186] solved the structure of sensory Rhodopsin in c7-DHPC micelles after trying over 15 different detergent molecules and several samples conditions (concentration, temperature, isotopic labelling scheme etc.), showing that NMR of MPs is not yet a routine technique. We have reviewed in Table 2 the main characteristics of commonly used detergents for solution NMR studies of MPs and peptides and typical conditions at which they have been used in structural determination of MPs (detergent concentration and sample temperature). The reader should refer to these conditions for initial screening.

With the progress that has allowed solution NMR to tackle larger objects in solution, a greater number and diversity of structures have recently been solved for MPs solubilized in detergents [21]. Among

the ca. 25 MP structures determined this way, over half were obtained on MP solubilized in DPC. SDS was mostly used for small peptides whereas DPC and DHPC were used for larger proteins. From small α -helical proteins [189] and large β -barrels [185,187,195–197], applications have now extended to larger α -helical complexes such as the 30 kDa pentamer of human phospholamban [48], the 20 kDa tetramer of the Influenza M2 proton channel [55], the 18 kDa enzyme DsbB [198], the 43 kDa trimer of diacylglycerol kinase [199] and the 26 kDa sensory rhodopsin II [186]. This last example shows the potential to determine structures of other 7 α -helix complexes such as GPCRs. Because of the potential pharmaceutical applications of GPCRs and the extreme difficulty to crystallize them in an active form, this is the current Holy Grail for solution NMR.

4.2. Isotropic bicelles

The composition and preparation of isotropic and aligned bicelles are very similar and the insertion of a MP in bicelles is usually

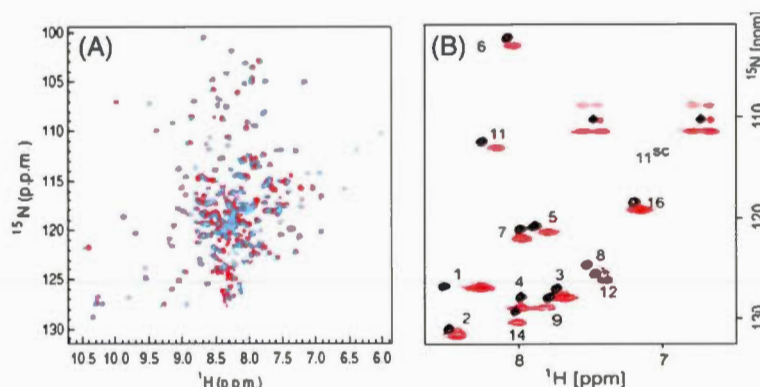


Fig. 8. 2D ^1H - ^{15}N NMR spectra of membrane proteins differently solubilized. (A) Overlay of the phototaxis receptor sensory rhodopsin II in DHPC micelles (cyan) and in isotropic bicelles (red). (B) Overlay of the anti-tamoxifen I in isotropic bicelles (black) and in nanodiscs (red). Adapted from [186,232] with permission.

performed by co-dissolution of the lipids and protein in aqueous solution when bicelles systems are prepared [112,133,200–203], or in solvents such as chloroform/methanol before evaporation (under a stream of inert gas or vacuum oven) and rehydration [137,204]. For isotropic bicelles, a typical q ratio of 0.25–0.5 is used with a hydration of 85–95% and lipid-to-peptide molar ratios between 25:1 and 100:1. Chain-perdeuterated lipids are usually employed to limit their contribution to the ^1H signals [112,117,159,200,202,203,205].

Because they offer a small lipid bilayer domain, isotropic bicelles (Fig. 5D) frequently prove advantageous over micelles for the study of MPs or MP segments. Lau et al. [133] showed a distortion of the α -helical conformation of integrin $\beta 3$ transmembrane domain in micelles as compared to bicelles, while Lindberg et al. [201] observed a different position of penetratin in SDS micelles vs. bicelles, which could be forced by the curvature and size of the micelle. Poget et al. [137] showed that bicelles preserve the ligand-binding activity of Smr. They also found that bicelles, over a series of detergent micelles, were the best membrane mimetics for the solution NMR structure determination of Smr and other proteins that must retain their native conformation [76]. Although about twice as large as micelles because they comprise approximately 200 DHPC and 50 DMPC molecules for a total of approximately 125 kDa (for $q=0.25$) [137,159], isotropic bicelles are very promising mimetics as shown in Fig. 8A which compares 2D spectra of pSRII in bicelles and DHPC micelles. In the future, they should often replace micelles in the study of MPs, helped by progress in solution NMR spectroscopy such as TROSY experiments which have extended the weight limit of protein study to above 100 kDa [47,182,206]. Actually, isotropic bicelles could be seen as just another detergent (DHPC) solubilizing a complex made of a MP and lipids, and we have added this particular mixture to the list of frequently used detergents in solution NMR of MPs (Table 2).

The reader is referred to Prosser et al. [143] for detailed applications of isotropic bicelles for the NMR study of membrane-associated amphiphiles and proteins. Briefly, typical 2D and 3D NMR experiments used for structure determination can be carried out on bicelle-inserted proteins [112,132,133,137,200,203,205,207]. The structure of a variety of MPs or protein transmembrane domains has been elucidated so far in isotropic bicelles, such as integrin $\beta 3$ transmembrane segment [133,208], the third helix of the *Antennapedia* homeodomain protein of *Drosophila* [201], Smr [137], the transmembrane domain of the apoptotic protein BNip3 [209], the dimeric transmembrane domain of the growth factor receptor ErbB2 [210], and of the receptor tyrosine kinase EphA1 [211], to name a few.

4.3. Small unilamellar vesicles

SUVs are the smallest possible vesicles with a diameter of around 30 nm—which is still an order of magnitude larger than a detergent micelle (Fig. 2A). They are formed by sonicating lipid dispersion in water while cooling the sample to avoid degradation from heating. Almost any type of lipids can be used – egg yolk phosphocholine is often preferred – except that vesicle fusion and aggregation occur more slowly with an addition of 10% (molar) of charged lipids (serine headgroup for example). SUVs containing MPs are obtained by sonicating lipid dispersions with MPs reconstituted into them, but only resistant proteins – usually small and globular – will stand such a procedure.

The properties of SUVs are opposite to those of LUVs: while their curvature is very high – imposing an asymmetrical distribution of lipids in the outer and inner monolayers and a strong pressure on MPs – their intermediate size provides very concentrated and moderately fast-tumbling samples, suited for solution NMR. A typical MP sample in SUVs may contain a ratio of 1:10 (in weight) of lipids to water, and 30:1 (molar) of lipids to proteins [212]. Although SUVs combine the advantages of a real lipid bilayer and a system amenable to solution NMR, they also have the inconvenient of being large, diluted and unstable. They have, therefore, seldom been used for MP structure

determination by NMR [212]. However, SUVs are often employed in NMR to study water-soluble proteins that are known to interact with lipid membranes [213].

4.4. Other systems

4.4.1. Organic solvents

Since MPs are not soluble in water, this whole article reviews membrane mimetics that can surround a protein to make it soluble while retaining its activity. Membrane mimetics and solvent viscosity are two factors that slow down PSC tumbling and, thereby, reduce the spectral resolution and sensitivity in solution NMR. Hydrophobic molecules such as MPs are often soluble in low viscosity organic solvents without the need of additional surfactants, and their correlation time is much smaller in such environment. Pure or mixtures of organic solvents such as methanol, isopropanol, chloroform, TFE or DMSO have been employed. NMR spectra of small membrane peptides in TFE have given results comparable to those solubilized in SDS [214,215]. Other small integral MPs have been studied in mixtures of methanol/chloroform/water which were shown to mimic the membrane environment [216–218]. However, interactions in membranes are a subtle balance between hydrophobic and hydrophilic contacts, and this subtlety is lost in organic solvents. While such milieu will trigger and stabilize helices, it will also disrupt helix–helix contacts and, in most cases, MPs will not retain significant native structure in organic solvents. Often limited to small and helical membrane peptides, this approach has to be carefully validated case by case.

4.4.2. Reverse micelles

As stated before, spectral resolution in solution NMR depends on molecular correlation time which is function of size but also of viscosity. Using apolar low-viscosity fluids (alkanes for example) is an attractive option that requires some optimization of the sample preparation. For instance, if the biological molecule structure is not retained in such an apolar solvent, it first requires to be encapsulated with water in an appropriate reverse micelle [219]. Micelle surfactants have to be screened in order to minimize the volume of the complex. The reverse micelle encapsulation approach for NMR study of MPs is also being developed by the Wand group [220]. The current best option, which was used to assign the NMR spectra of the potassium channel KcsA [220], is to encapsulate the protein in CTAB/DHAB:1/1 and to solubilize the complex in ethane and hexanol under high pressure (300 bar), requiring a specialized commercially available apparatus (Daedalus Innovations). This assembly is shown on Fig. 9A where the protein is surrounded by water (in blue), CTAB and DHAB surfactants (in red), hexanol (in green) and ethane (in grey). This approach is also used to study lipid-anchored proteins that bind to membranes via a covalently attached lipid or fatty acid, such as recoverin or the HIV-1 matrix protein, in their myristoylated form [221]. The development of this complex procedure is motivated by the possibility to push the size limit of proteins that could be studied by solution NMR. Nevertheless, in the case of MPs, reverse micelles suffer from the same problem as detergent micelles, i.e., the non-native environment which may affect their function and stability.

4.4.3. Amphipols

Detergent molecules are used both to extract MPs from their membrane environment and to keep them in solution by covering their hydrophobic parts. Alternative molecules have been designed to keep MPs in solution while preventing detergents to disrupt subunits or cofactors of the protein, occupy its active site, or affect its function [191,222,223]. Developed by the group of Popot, amphipols are among the most promising new membrane mimetics for NMR [222]. They are a family of short amphipathic polymers carrying a large number of hydrophobic chains that can replace detergent molecules as a lifebuoy around the MP with a very low rate of spontaneous

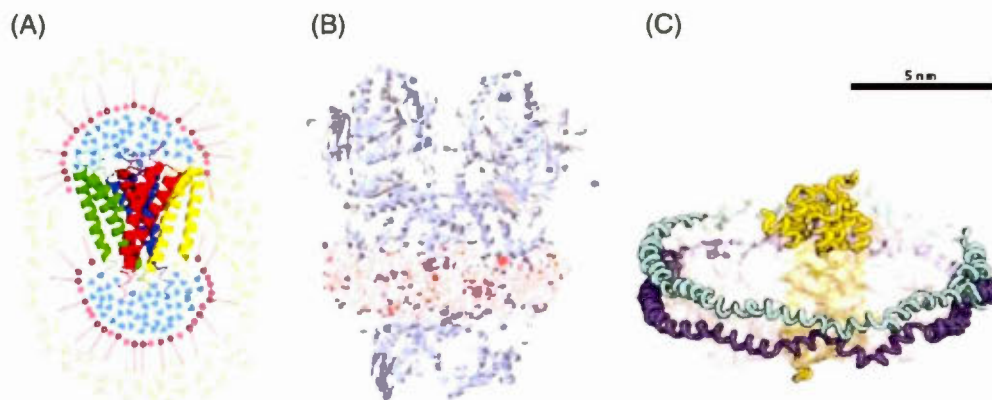


Fig. 9. Models of (A) potassium channel KcsA in reverse micelles, (B) cytochrome bcl amphipol complex and (C) rhodopsin nanodisc complex. The models are represented approximately to the scale given on the top right corner. Adapted from [220,224] with permission.

desorption and a high affinity for protein transmembrane surfaces (Fig. 9B). The length and charge of amphipols are tunable, but the most common version is composed of a ~70 residue polyacrylate chain in which some (~17) of the carboxylates have been randomly grafted octylamine, and some (~28) with isopropylamine. Carboxylates can also be changed to obtain a zwitterionic, sulfonated or non-ionic version [224]. Since amphipols cannot extract a MP from its membrane, the protein is usually transferred to them from a PDC, just like a reconstitution in lipid membranes: amphipols are added to the PDC and the detergent is removed through the usual procedure (see Section 3.1.1).

The quasi absence of free amphipols reduces the viscosity of the solution and the protein correlation time as compared to the detergent option. Amphipols have also been shown to maintain solubility of a very broad range of MPs such as the mitochondrial complex I, human GPCRs BLT1 and BLT2, bacterial outer MPs OmpA and OmpX, bacteriorhodopsin, the SR calcium ATPase, the nicotinic acetylcholine receptor and, more importantly, to biochemically stabilize them, as compared to detergent solutions [73,224,225]. Deuterated amphipols have been devised for NMR and although the complexes still tumble more slowly than in detergent solutions, they are amenable to solution NMR studies [226–228]. Fig. 10 compares 2D [^{15}N , ^1H]-TROSY spectra of OmpX in DHPC micelles and amphipols and shows that the

dispersion is identical [227]. While the resolution is slightly worse in amphipols, it was enough for unambiguous resonance assignment of about 60% of the protein residues. An amphipol-trapped GPCR (human BLT2) was also used to determine the structure of its bound ligand (leukotriene B4) [226]. Under these conditions, functional folding yields of 70% were achieved for the GPCR which was shown to be active for over 3 weeks—a duration sufficient to perform all relevant NMR experiments. Comparatively in detergents, BLT2 folding yield never exceeded 4% and its receptor binding capacity dropped after only 10 days [229].

4.4.4. Nanolipoproteins (nanodiscs)

Nanolipoproteins (NLPs) are new membrane systems for MP reconstitution [230–233]. As shown in Fig. 9C, NLPs are phospholipid bilayers encircled by stabilizing amphipathic helical membrane scaffold proteins (MSPs) leading to nanoscale disc-shaped objects also known as *nanodiscs*. A little larger than isotropic bicelles, these water-soluble assemblies have a diameter of ~10 nm and a thickness of ~4 nm equivalent to that of biomembranes. NLPs have several advantages for the NMR structural study of MPs: their size can be varied between 9.5 and 15 nm diameter [233–236] but there is only one protein per particle, they are monodisperse, stable and can be easily diluted, concentrated or dialysed if a change of buffer is required. Because of their flat lipid bilayer, NLPs are a better membrane mimetics compared to micelles which have a strong curvature [232,233]. Because of the stability of the MSP/lipid interaction with temperature, NLPs are also better membrane models, compared to bicelles which are stable only in a small temperature range. A thorough review on NLPs has been recently published [233].

Nanodiscs are prepared by sonicating a purified MSP such as apolipoprotein A-1 (apoA-1) with phospholipid vesicles (such as DMPC, DOPC, DPPC, POPC, DMPC, DOPG or gangliosides) at the gel–liquid crystal phase transition of the lipid. They can also be made by mixing phospholipids, with or without cholesterol, with the MSP in a detergent solution (like cholate or deoxycholate) followed by a slow detergent removal via dialysis or biobeads [230,233,237,238]. The detergent solution can also be used to solubilize the integral MP to be incorporated into the discs. Cell-free expression systems containing nanodiscs are commercially available [239] and more technical details on the preparation can be found in Ref. [233]. To avoid signal from the apolipoprotein and considering the size of the MP normally studied, isotopically labelled proteins of interest can be employed [240].

A variety of MPs have been reconstituted in a functional form and studied into nanodiscs, including cytochrome P450s [237,241,242],

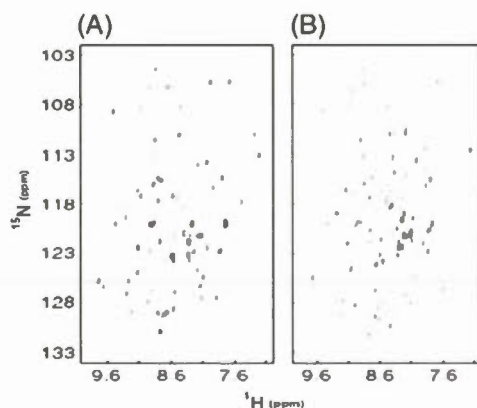


Fig. 10. 2D [^{15}N , ^1H] NMR spectra of OmpX in (A) amphipols and (B) in DHPC micelles. Adapted from [227] with permission.

bacteriorhodopsin [243], human CD4 [240] and G-protein-coupled receptors [244]. The size of NLPs makes them amenable to solution NMR studies since their correlation time is equivalent to an isotropic rotation of a globular protein of ca. 200 kDa [232]. A ^1H - ^{15}N -TROSY spectrum was collected for the antibiotic peptaibol anti-moebin with amide proton resonances shown to be a little broader to those obtained in isotropic bicelles (Fig. 8B) [232]. The voltage-sensing domain of the KvAP channel (four transmembrane helices) could also be reconstituted into nanodiscs and gave solution NMR fingerprint spectra with broad resonances but with a large amide proton signal dispersion, indicative of a native-like folding [245]. For large nanodisc-MP complexes, MAS solid-state NMR is an alternative as exemplified by the precipitation of the nanodisc/CYP3A4 complex with polyethylene glycol (PEG) that yielded high-quality 2D solid-state NMR spectra of the folded, active protein [246].

5. Conclusion

The biomembrane complexity is a challenge for the NMR structural study of MPs; however this review shows that a variety of artificial membranes are available for applications in both the solution and solid states. Systems of almost any size and lamellarity exist, either lipid- or detergent-based, self-orienting or mechanically aligned, and even tunable to experimental requirements such as bicelles. Detergents are most useful in structural studies because of their multiple roles in protocols such as solubilization, purification, transfer, renaturation and reconstitution of MPs. New techniques have been proposed to help the study of MPs such as MAS or reverse micelles at high pressure. Likewise, new molecules like amphipathic polymers and lipid/protein nanoparticles have been developed with the same objective. In search of additional oriented membrane systems with a large surface area, single bilayered nanotubes formed by adsorption into the pores of anodic aluminium oxide discs have been proposed [247–250]. In the recent years, a variety of new membrane mimetics have been used in NMR and protein crystallization such as lipid cubic phases [251–253], bola-amphiphile and diamine hollow cones [254], and porous phospholipid nanoshells [255], to name a few. Their application in structural study of proteins can be expected in a near future.

These efforts for identifying new membrane mimetics have been fruitful in solution NMR since, among the ~30 MP structures solved in the past 15 years, the maximum protein size has raised from around 6 kDa in the first decade, to 43 kDa in the last 2 years. These developments have contributed to solid-state NMR as well since, among the 20 protein structures solved in the last decade, 12 were solved in the past 2 years. Most of them were not MPs, though, but this is clearly the next goal to pursue since solid-state NMR is the only technique that can solve the atomic structure of a MP inside a native-like environment.

Thirty years ago in structural NMR laboratories, SDS was almost the only detergent [256], DMPC almost the only lipid [257], and solid-state NMR could only tackle small peptides [258,259]. Designing new membrane mimetics has not only helped us to better understand the interactions between MPs and their environment but has also allowed to push the limits of NMR in terms of size and complexity of the samples amenable to study. Current samples are often made of mixtures of MPs and several lipids and/or detergents, each providing essential properties to the complex. Consequently, NMR now solves structures of MPs made of several helices, barrels, multimers or protein–drug complexes.

We have often described membrane mimetics as “native like”. The next step will probably be the development of techniques that will allow the study of MPs in their native environment, i.e., *in vivo* biomolecular NMR and structural determination. As always, the first application has come out in the field of soluble proteins [260,261]. The goal is now to also transpose this approach to MPs.

Acknowledgments

This work was supported by the Natural Science and Engineering Research Council (NSERC) of Canada (I.M.) as well as CNRS and ANR-05-BLAN-0255 (D.E.W.). A.G. and É.C. are grateful to the NSERC, the Groupe de Recherche Axé sur la Structure des Protéines (GRASP) and the Université du Québec à Montréal (UQAM) for the award of M.Sc. scholarships. M.B. also wishes to thank UQAM for the award of a PhD scholarship. A.A.A. and I.M. are members of the CQMF (Centre Québécois des Matériaux Fonctionnels) and I.M. is a member of the GRASP.

References

- [1] H. Lodish, A. Berk, P. Matsudaira, C.A. Kaiser, M. Krieger, M.P. Scott, *Molecular Cell Biology*, 3rd ed. W. H. Freeman, New York, 2005.
- [2] J.K. Vollman, Sterols in microorganisms, *Appl. Microbiol. Biotechnol.* 60 (2003) 495–506.
- [3] G. van Meer, D.R. Voelker, G.W. Feigenson, Membrane lipids: where they are and how they behave, *Nat. Rev. Mol. Cell Biol.* 9 (2008) 112–124.
- [4] P.F. Devaux, R. Morris, Transmembrane asymmetry and lateral domains in biological membranes, *Traffic* 5 (2004) 241–246.
- [5] C.R.H. Raetz, C. Whitfield, Lipopolysaccharides endotoxins, *Annu. Rev. Biochem.* 71 (2002) 635–700.
- [6] P.F. Devaux, M. Seigneuret, Specificity of lipid–protein interactions as determined by spectroscopic techniques, *Biochim. Biophys. Acta* 822 (1985) 63–125.
- [7] W. Dowhan, M. Bogdanov, Functional roles of lipids in membranes, in: D.E. Vance, J.E. Vance (Eds.), *Biochemistry of Lipids, Lipoproteins, and Membranes*, Elsevier, New York, 2002, pp. 1–36.
- [8] L. Fagerberg, K. Jonasson, G. von Heijne, M. Uhlen, L. Berglund, Prediction of the human membrane proteome, *Proteomics* 10 (2010) 1141–1149.
- [9] D.G. Bichet, Vasopressin receptor mutations in nephrogenic diabetes insipidus, *Semin. Nephrol.* 28 (2008) 245–251.
- [10] M.T. Clunes, R.C. Boucher, Cystic fibrosis: the mechanisms of pathogenesis of an inherited lung disorder, *Drug Discov. Today Dis. Mech.* 4 (2007) 63–72.
- [11] A.S. Verkman, J. Ruiz-Ederra, M.H. Levin, Functions of aquaporins in the eye, *Prog. Retin. Eye Res.* 27 (2008) 420–433.
- [12] A.L. Firth, C.V. Remillard, J.X. Yuan, TRP channels in hypertension, *Biochim. Biophys. Acta* 1772 (2007) 895–906.
- [13] Y.-J. Hsu, J.G.J. Hoenderop, R.J.M. Bindels, TRP channels in kidney disease, *Biochim. Biophys. Acta* 1772 (2007) 928–936.
- [14] N. Prevarskaya, L. Zhang, G. Barritt, TRP channels in cancer, *Biochim. Biophys. Acta* 1772 (2007) 937–946.
- [15] M.A. Lemmon, J. Schlessinger, Cell signaling by receptor tyrosine kinases, *Cell* 141 (2010) 1117–1134.
- [16] F. Terzi, A central role of EGFR transactivation in chronic kidney diseases, *Drug Discov. Today Dis. Mech.* 4 (2007) 47–53.
- [17] S. Just, K. Arndt, T. Weiser, H. Doods, Pathophysiology of migraine: a role for neuropeptides, *Drug Discov. Today Dis. Mech.* 3 (2006) 327–333.
- [18] S. Roger, M. Potier, C. Vandier, P. Besson, J.Y. Le Guennec, Voltage-gated sodium channels: new targets in cancer therapy? *Curr. Pharm. Des.* 12 (2006) 3681–3695.
- [19] M.C. Lagerström, H.B. Schiöth, Structural diversity of G protein-coupled receptors and significance for drug discovery, *Nat. Rev. Drug Discov.* 7 (2008) 339–357.
- [20] S. White, Membrane proteins of known 3D structure, http://blanco.biomed.uci.edu/Membrane_Proteins_xtal.html Feb. 9, 2011.
- [21] D.E. Warschawski, Membrane proteins of known structure determined by NMR, <http://www.drorlist.com/nmr/MPNMR.html> Feb. 9, 2011.
- [22] N.K. Goto, L.E. Kay, New developments in isotope labeling strategies for protein solution NMR spectroscopy, *Curr. Opin. Struct. Biol.* 10 (2000) 585–592.
- [23] M. Kainosho, T. Torizawa, Y. Iwashita, T. Terauchi, A.M. Ono, P. Güntert, Optimal isotope labelling for NMR protein structure determinations, *Nature* 440 (2006) 52–57.
- [24] A. Abdine, M.A. Verhoeven, K.-H. Park, A. Ghazi, E. Guitter, C. Berrier, C. Van Heijenoort, D.E. Warschawski, Structural study of the membrane protein MscL using cell-free expression and solid-state NMR, *J. Magn. Reson.* 204 (2010) 155–159.
- [25] T.A. Cross, M. Sharma, M. Yi, H.-X. Zhou, Influence of solubilizing environments on membrane protein structures, *Trends Biochem. Sci.* 36 (2011) 117–125.
- [26] J.A. Lundbaek, P. Birn, J. Girshman, A.J. Hansen, O.S. Andersen, Membrane stiffness and channel function, *Biochemistry* 35 (1996) 3825–3830.
- [27] X. Wang, M. Bogdanov, W. Dowhan, Topology of polytopic membrane protein subdomains is dictated by membrane phospholipid composition, *EMBO J.* 21 (2002) 5673–5681.
- [28] J. Abi-Char, A. Maguy, A. Coulombe, E. Balse, P. Ratajczak, J.-L. Samuel, S. Nattel, S. N. Hatem, Membrane cholesterol modulates Kv1.5 potassium channel distribution and function in rat cardiomyocytes, *J. Physiol.* 582 (2007) 1205–1217.
- [29] B. Schneider, F. Junge, V.A. Shirokov, F. Durst, D. Schwarz, V. Dötsch, F. Bernhard, Membrane protein expression in cell-free systems, *Methods Mol. Biol.* 601 (2010) 165–186.
- [30] S. Wagner, M.L. Bader, D. Drew, J.-W. de Gier, Rationalizing membrane protein overexpression, *Trends Biotechnol.* 24 (2006) 364–371.
- [31] S. Reckel, S. Sobhanifar, F. Durst, F. Lohr, V. Shirokov, V. Dötsch, F. Bernhard, Strategies for the cell-free expression of membrane proteins, *Methods Mol. Biol.* 607 (2010) 187–212.

- [32] P.R. Cullis, D.B. Fenske, M.J. Hope, Physical properties and functional roles of lipids in membranes, in: D.E. Vance, J.E. Vance (Eds.), *Biochemistry of Lipids, Lipoproteins and Membranes*, Elsevier, Amsterdam, 1996, pp. 1–33.
- [33] O.G. Mouritsen, *Life as a Matter of Fat: The Emerging Science of Lipidomics*, Springer-Verlag, Berlin, 2005.
- [34] O.S. Andersen, R.E. Koeppe, Bilayer thickness and membrane protein function: an energetic perspective, *Annu. Rev. Biophys. Biomol. Struct.* 36 (2007) 107–130.
- [35] M. Carrillo-Tripp, S.E. Feller, Evidence for a mechanism by which ω -3 polyunsaturated lipids may affect membrane protein function, *Biochemistry* 44 (2005) 10164–10169.
- [36] H. Hong, L.K. Tamm, Elastic coupling of integral membrane protein stability to lipid bilayer forces, *Proc. Natl. Acad. Sci. USA* 101 (2004) 4065–4070.
- [37] G. Anderlüh, A. Razpotnik, Z. Podlesek, P. Macek, F. Separovic, R.S. Norton, Interaction of the eukaryotic pore-forming cytotoxin equinatoxin II with model membranes: 19F NMR studies, *J. Mol. Biol.* 347 (2005) 27–39.
- [38] E. Perozo, D. Cortes, P. Sompompisut, A. Kloda, B. Martinac, Open channel structure of MscL and the gating mechanism of mechanosensitive channels, *Nature* 418 (2002) 942–948.
- [39] A.M. Powl, J.M. East, A.G. Lee, Importance of direct interactions with lipids for the function of the mechanosensitive channel MscL, *Biochemistry* 47 (2008) 12175–12184.
- [40] J.J. Buffy, T. Hong, S. Yamaguchi, A.J. Waring, R.L. Lehrer, M. Hong, Solid-state NMR investigation of the depth of insertion of proteogrin-1 in lipid bilayers using paramagnetic Mn^{2+} , *Biophys. J.* 85 (2003) 2363–2373.
- [41] E. Strandberg, A.S. Ulrich, NMR methods for studying membrane-active antimicrobial peptides, *Concepts Magn. Reson.* 23A (2004) 89–120.
- [42] J.X. Lu, K. Damodaran, J. Blazys, G.A. Lorigan, Solid-state nuclear magnetic resonance relaxation studies of the interaction mechanism of antimicrobial peptides with phospholipid bilayer membranes, *Biochemistry* 44 (2005) 10208–10217.
- [43] P.J. Sherman, R.J. Jackway, J.D. Gehman, S. Praporski, G.A. McCubbin, A. Mechler, L.L. Martin, F. Separovic, J.H. Bowie, Solution structure and membrane interactions of the antimicrobial peptide falixadin 4.1a: an NMR and QCM study, *Biochemistry* 48 (2009) 11892–11901.
- [44] S.H. Park, A.A. De Angelis, A.A. Nevzorov, H.-C. Wu, S.J. Opella, Three-dimensional structure of the transmembrane domain of Vpu from HIV-1 in aligned phospholipid bilayers, *Biophys. J.* 91 (2006) 3032–3042.
- [45] E. Strandberg, S. Özdirekcan, D.T.S. Rijkers, P.C.A. van der Wel, R.E. Koeppe, R.M.J. Liskamp, J.A. Killian, Tilt angles of transmembrane model peptides in oriented and non-oriented lipid bilayers as determined by 2H solid-state NMR, *Biophys. J.* 86 (2004) 3709–3721.
- [46] T.K.M. Nyholm, S. Özdirekcan, J.A. Killian, How protein transmembrane segments sense the lipid environment, *Biochemistry* 46 (2007) 1457–1465.
- [47] C. Wang, M. Rance, A.G. Palmer, Mapping chemical exchange in proteins with $MW > 50$ kD, *J. Am. Chem. Soc.* 125 (2003) 8968–8969.
- [48] K. Oxeño, J. Chou, The structure of phospholamban pentamer reveals a channel-like architecture in membranes, *Proc. Natl. Acad. Sci. USA* 102 (2005) 10870–10875.
- [49] E.S. Karp, E.K. Tiburzy, S. Adu-Baker, G.A. Lorigan, The structural properties of the transmembrane segment of the integral membrane protein phospholamban utilizing ^{13}C CP MAS, 2H , and REDOR solid-state NMR spectroscopy, *Biochim. Biophys. Acta* 1758 (2006) 772–780.
- [50] N. Traaseth, R. Verardi, K. Torgersen, C. Karim, D. Thomas, G. Veglia, Spectroscopic validation of the pentameric structure of phospholamban, *Proc. Natl. Acad. Sci. USA* 104 (2007) 14676–14681.
- [51] N. Traaseth, L. Shi, R. Verardi, D. Mullen, G. Barany, G. Veglia, Structure and topology of monomeric phospholamban in lipid membranes determined by a hybrid solution and solid-state NMR approach, *Proc. Natl. Acad. Sci. USA* 106 (2009) 10165–10170.
- [52] E. Georgieva, T. Ramlall, P. Borbat, J. Freed, D. Eliezer, Membrane-bound α -synuclein forms an extended helix: long-distance pulsed ESR measurements using vesicles, bicelles, and rodlike micelles, *J. Am. Chem. Soc.* 130 (2008) 12856–12857.
- [53] J. Wang, S. Kim, F. Kovacs, T. Cross, Structure of the transmembrane region of the M2 protein H(+) channel, *Protein Sci.* 10 (2001) 2241–2250.
- [54] J. Hu, T. Asbury, S. Achuthan, C. Li, R. Bertram, J. Quine, R. Fu, T. Cross, Backbone structure of the amantadine-blocked trans-membrane domain M2 proton channel from influenza A virus, *Biophys. J.* 92 (2007) 4335–4343.
- [55] J.R. Schnell, J.J. Chou, Structure and mechanism of the M2 proton channel of influenza A virus, *Nature* 451 (2008) 591–596.
- [56] S. Cady, K. Schmidt-Rohr, J. Wang, C. Soto, W. Degrad, M. Hong, Structure of the amantadine binding site of influenza M2 proton channels in lipid bilayers, *Nature* 463 (2010) 689–692.
- [57] F. Hu, W. Luo, M. Hong, Mechanisms of proton conduction and gating in influenza M2 proton channels from solid-state NMR, *Science* 330 (2010) 505–508.
- [58] M. Sharma, M. Yi, H. Dong, H. Qin, E. Peterson, D.D. Busath, H.X. Zhou, T.A. Cross, Insight into the mechanism of the influenza A proton channel from a structure in a lipid bilayer, *Science* 330 (2010) 509–512.
- [59] A. Stouffer, R. Acharya, D. Salom, A. Levine, L. Di Costanzo, C. Soto, V. Tereshko, V. Nanda, S. Staybrook, W. DeGrado, Structural basis for the function and inhibition of an influenza virus proton channel, *Nature* 451 (2008) 596–599.
- [60] G.G. Privé, Detergents for the stabilization and crystallization of membrane proteins, *Methods* 41 (2007) 388–397.
- [61] A. Ciulli, G. Williams, A.G. Smith, T.L. Blundell, C. Abell, Probing hot spots at protein-ligand binding sites: a fragment-based approach using biophysical methods, *J. Med. Chem.* 49 (2006) 4992–5000.
- [62] R.D. Krueger-Koplin, P.L. Sorgen, S.T. Krueger-Koplin, I.O. Rivera-Torres, S.M. Cahill, D.B. Hicks, L. Grinius, T.A. Krulwich, M.E. Girvin, An evaluation of detergents for NMR structural studies of membrane proteins, *J. Biomol. NMR* 17 (2004) 43–57.
- [63] A. Lange, K. Giller, S. Hornig, M.-F. Martin-Eauclaire, O. Pongs, S. Becker, M. Baldus, Toxin-induced conformational changes in a potassium channel revealed by solid-state NMR, *Nature* 440 (2006) 959–962.
- [64] F. Aussenac, B. Lavigne, E.J. Dufourc, Toward bicelle stability with ether-linked phospholipids: temperature, composition, and hydration diagrams by 2H and ^{31}P solid-state NMR, *Langmuir* 21 (2005) 7129–7135.
- [65] H. Hauser, Some aspects of the phase behaviour of charged lipids, *Biochim. Biophys. Acta* 772 (1984) 37–50.
- [66] D.H. Jones, K.R. Barber, E.W. VanDerLoo, C.W.M. Grant, Epidermal growth factor receptor transmembrane domain: 2H NMR implications for orientation and motion in a bilayer environment, *Biochemistry* 37 (1998) 16780–16787.
- [67] S.D. Cady, T.V. Mishanina, M. Hong, Structure of amantadine-bound M2 transmembrane peptide of influenza A in lipid bilayers from magic-angle-spinning solid-state NMR: the role of Ser31 in amantadine binding, *J. Mol. Biol.* 385 (2009) 1127–1141.
- [68] S. Hiller, L. Krabben, K.R. Vinothkumar, F. Castellani, B.J. van Rossum, W. Kuhlbrandt, H. Oshkhat, Solid-state magic-angle spinning NMR of outer membrane protein G from *Escherichia coli*, *ChemBiochem* 6 (2005) 1679–1684.
- [69] O.C. Andronesi, S. Becker, K. Seidel, H. Heise, H.S. Young, M. Baldus, Determination of membrane protein structure and dynamics by magic-angle spinning solid-state NMR, *J. Am. Chem. Soc.* 127 (2005) 12965–12974.
- [70] J.-L. Rigaud, D. Lévy, Reconstitution of membrane proteins into liposomes, *Methods Enzymol.* 372 (2003) 65–86.
- [71] J.H. Davis, M. Auger, R.S. Hodges, High resolution 1H nuclear magnetic resonance of a transmembrane peptide, *Biophys. J.* 69 (1995) 1917–1932.
- [72] O. Vinogradova, F.D. Sonnichsen, C.R. Sanders, On choosing a detergent for solution NMR studies of membrane proteins, *J. Biomol. NMR* 4 (1998) 381–386.
- [73] C.R. Sanders, A. Kuhn Hoffmann, D. Gray, M.H. Keyes, C.D. Ellis, French swimwear for membrane proteins, *Chem. Biochem. J.* 5 (2004) 423–426.
- [74] C.R. Sanders, F. Sonnichsen, Solution NMR of membrane proteins: practice and challenges, *Magn. Reson. Chem.* 44 (2006) S24–S40.
- [75] R.C. Page, J.D. Moore, H.B. Nguyen, M. Sharma, R. Chase, F.P. Gao, C.K. Mobley, C.R. Sanders, L. Ma, F.D. Sonnichsen, S. Lee, S.C. Howell, S.J. Opella, T.A. Cross, Comprehensive evaluation of solution nuclear magnetic resonance spectroscopy sample preparation for helical integral membrane proteins, *J. Struct. Funct. Genomics* 7 (2006) 51–64.
- [76] S.F. Poet, M.E. Girvin, Solution NMR of membrane proteins in bilayer mimics: small is beautiful, but sometimes bigger is better, *Biochim. Biophys. Acta* 1768 (2007) 3098–3106.
- [77] T. Raschle, S. Hiller, M. Etzkorn, G. Wagner, Nonmicellar systems for solution NMR spectroscopy of membrane proteins, *Curr. Opin. Struct. Biol.* 20 (2010) 471–479.
- [78] A. Naito, Structure elucidation of membrane-associated peptides and proteins in oriented bilayers by solid-state NMR spectroscopy, *Solid State Nucl. Magn. Reson.* 36 (2009) 67–76.
- [79] A. McDermott, Structure and dynamics of membrane proteins by magic angle spinning solid-state NMR, *Annu. Rev. Biophys.* 38 (2009) 385–403.
- [80] T.A. Egorova-Zachernyuk, J. Hollander, N. Fraser, P. Gast, A.J. Hoff, R. Cogdell, H.J.M. de Groot, M. Baldus, Heteronuclear 2D-correlations in a uniformly ^{13}C , ^{15}N labeled membrane-protein complex at ultra-high magnetic fields, *J. Biomol. NMR* 19 (2001) 243–253.
- [81] W.R. Perkins, S.R. Minchey, P.L. Ahl, A.S. Janoff, The determination of liposome captured volume, *Chem. Phys. Lipids* 64 (1993) 197–217.
- [82] J. Hu, H. Qin, C. Li, M. Sharma, T.A. Cross, F.P. Gao, Structural biology of transmembrane domains: efficient production and characterization of transmembrane peptides by NMR, *Protein Sci.* 16 (2007) 2153–2165.
- [83] D.J. Hirsh, J. Hammer, W.L. Maloy, J. Blazys, J. Schaefer, Secondary structure and location of a magainin analogue in synthetic phospholipid bilayers, *Biochemistry* 35 (1996) 12733–12741.
- [84] K.P. Howard, S.J. Opella, High-resolution solid-state NMR spectra of integral membrane proteins reconstituted into magnetically oriented phospholipid bilayers, *J. Magn. Reson. B* 112 (1996) 91–94.
- [85] M. Ali, M.R.R. De Planque, N. Huyn, N. Manolios, F. Separovic, Biophysical studies of transmembrane peptide derived from the T cell antigen receptor, *Lett. Pept. Sci.* 8 (2002) 227–233.
- [86] M.R.R. De Planque, D.T.S. Rijkers, J.E. Fletcher, R.M.J. Liskamp, F. Separovic, The $\alpha M1$ segment of the nicotinic acetylcholine receptor exhibits conformational flexibility in a membrane environment, *Biochim. Biophys. Acta* 1165 (2004) 40–47.
- [87] R. Mani, M. Tang, X. Wu, J.J. Buffy, A.J. Waring, M.A. Sherman, M. Hong, Membrane-bound dimer structure of a β -hairpin antimicrobial peptide from rotational-echo double-resonance solid-state NMR, *Biochemistry* 45 (2006) 8341–8349.
- [88] I. Marcotte, A. Bélanger, M. Auger, The orientation effect of gramicidin A on bicelles and Eu3+-doped bicelles as studied by solid-state NMR and FTIR spectroscopy, *Chem. Phys. Lipids* 139 (2006) 137–149.
- [89] M.R.R. De Planque, D.T.S. Rijkers, R.M.J. Liskamp, F. Separovic, The $\alpha M1$ transmembrane segment of the nicotinic acetylcholine receptor interacts strongly with model membranes, *Magn. Reson. Chem.* 42 (2004) 148–154.
- [90] K.V. Lakshmi, M. Auger, J. Raap, J. Lugtenburg, R.G. Griffin, J. Herzfeld, Internuclear distance measurement in a reaction intermediate: solid-state carbon-13 NMR rotational resonance determination of the Schiff base configuration in the M photointermediate of bacteriorhodopsin, *J. Am. Chem. Soc.* 115 (1993) 8515–8516.
- [91] F. Castellani, B. van Rossum, A. Diehl, M. Schubert, K. Rehbein, H. Oshkhat, Structure of a protein determined by solid-state magic-angle-spinning NMR spectroscopy, *Nature* 420 (2002) 98–102.

- [92] J. Pauli, B. van Rossum, H. Förster, H.J.M. de Groot, H. Oshkhat, Sample optimization and identification of signal patterns of amino acid side chains in 2D RFDR spectra of the α -spectrin SH3 domain, *J. Magn. Reson.* 143 (2000) 411–416.
- [93] H.L. Frericks, D.H. Zhou, L.L. Yap, R.B. Gennis, C.M. Rienstra, Magic-angle spinning solid-state NMR of a 144 kDa membrane protein complex: *E. coli* cytochrome *bo3* oxidase, *J. Biomol. NMR* 36 (2006) 55–71.
- [94] V.S. Bajaj, M.L. Mak-Jurkaskas, M. Belenky, J. Herzfeld, R.G. Griffin, Functional and shunt states of bacteriorhodopsin resolved by 250 GHz dynamic nuclear polarization-enhanced solid state NMR, *Proc. Natl. Acad. Sci. USA* 106 (2009) 9244–9249.
- [95] A. Abdine, M.A. Verhoeven, D.E. Warschawski, Cell-free expression and labeling strategies for a new decade in solid-state NMR, *New Biotechnol.* 28 (2011) 272–276.
- [96] M. Etzkorn, S. Martell, O.C. Andronesi, K. Seidel, M. Engelhard, M. Baldus, Secondary structure, dynamics, and topology of a seven-helix receptor in native membranes, studied by solid-state NMR spectroscopy, *Angew. Chem. Int. Ed. Engl.* 46 (2007) 459–462.
- [97] M. Bloom, E.E. Burnell, A.L. MacKay, C.P. Nichol, M.I. Valic, G. Weeks, Fatty acyl chain order in lecithin model membranes determined from proton magnetic resonance, *Biochemistry* 17 (1978) 5750–5762.
- [98] W. Hu, N.D. Lazo, T.A. Cross, Tryptophan dynamics and structural refinement in a lipid bilayer environment: solid state NMR of the gramicidin channel, *Biochemistry* 34 (1995) 14138–14146.
- [99] R.R. Ketchum, W. Hu, T.A. Cross, High-resolution conformation of gramicidin A in a lipid bilayer by solid-state NMR, *Science* 261 (1993) 1457–1460.
- [100] S.J. Opella, F.M. Marassi, J.J. Gesell, A.P. Valente, Y. Kim, M. Oblatt-Montal, M. Montal, Structures of the M2 channel-lining segments from nicotinic acetylcholine and NMDA receptors by NMR spectroscopy, *Nat. Struct. Biol.* 6 (1999) 374–379.
- [101] J.M. Pope, L. Walker, B.A. Cornell, F. Separovic, Study of the angular dependence of NMR relaxation times in macroscopically oriented lyotropic liquid lamellar phases, *Mol. Cryst. Liq. Cryst.* 89 (1982) 137–150.
- [102] T.A. Cross, A solid state nuclear magnetic resonance approach for determining the structure of gramicidin A without model fitting, *Biophys. J.* 49 (1986) 124–126.
- [103] C.H. Wu, A. Ramamoorthy, S.J. Opella, High-resolution heteronuclear dipolar solid-state NMR spectroscopy, *J. Magn. Reson.* 109A (1994) 270–272.
- [104] F.M. Marassi, S.J. Opella, A solid-state NMR index of helical membrane protein structure and topology, *J. Magn. Reson.* 144 (2000) 150–155.
- [105] J. Wang, J. Denny, C. Tian, S. Kim, Y. Mo, F. Kovacs, Z. Song, K. Nishimura, Z. Gan, R. Fu, J.R. Quine, T.A. Cross, Imaging membrane protein helical wheels, *J. Magn. Reson.* 144 (2000) 162–167.
- [106] X.-M. Gong, J. Choi, C.M. Franzin, D. Zhai, J.C. Reed, F.M. Marassi, Conformation of membrane-associated proapoptotic bBid, *J. Biol. Chem.* 279 (2004) 28954–28960.
- [107] A.A. Nevzorov, S.J. Opella, A “Magic Sandwich” pulse sequence with reduced offset dependence for high-resolution separated local field spectroscopy, *J. Magn. Reson.* 164 (2003) 182–186.
- [108] U.H.N. Dürr, K. Yamamoto, S.-C. Im, L. Waskell, A. Ramamoorthy, Solid-state NMR reveals structural and dynamical properties of a membrane-anchored electron-carrier protein, cytochrome *b5*, *J. Am. Chem. Soc.* 129 (2007) 6670–6671.
- [109] S.H. Park, A. Mrse, A.A. Nevzorov, M.F. Mesleh, M. Oblatt-Montal, M. Montal, S.J. Opella, Three-dimensional structure of the channel-forming trans-membrane domain of virus protein “u” (Vpu) from HIV-1, *J. Mol. Biol.* 333 (2003) 409–424.
- [110] C.R. Sanders, J.H. Prestegard, Magnetically orientable phospholipid bilayers containing small amounts of a bile salt analogue, CHAPSO, *Biophys. J.* 58 (1990) 447–460.
- [111] C.R. Sanders, J.P. Schwonek, Characterization of magnetically orientable bilayers in mixtures of dihexanoylphosphatidylcholine and dimyristoylphosphatidylcholine by solid-state NMR, *Biochemistry* 31 (1992) 8898–8905.
- [112] R.R. Vold, R.S. Prosser, A.J. Deese, Isotropic solutions of phospholipid bicelles: a new membrane mimetic for high-resolution NMR studies of polypeptides, *J. Biomol. NMR* 9 (1997) 329–335.
- [113] C. Loudet, L. Khemtmourian, F. Aussenac, S. Gineste, M.-F. Achard, E.J. Dufourc, Bicelle membranes and their use for hydrophobic peptide studies by circular dichroism and solid state NMR, *Biochim. Biophys. Acta* 1724 (2005) 315–323.
- [114] M. Triba, M. Zoonens, J.L. Popot, P.F. Devaux, D.E. Warschawski, Reconstitution and alignment by a magnetic field of a β -barrel membrane protein in bicelles, *Eur. Biophys. J.* 35 (2006) 268–275.
- [115] C. McKibbin, N.A. Farmer, C. Jeans, P.J. Reeves, H.G. Khorana, B.A. Wallace, P.C. Edwards, C. Villa, P.J. Booth, Opsin stability and folding: modulation by phospholipid bicelles, *J. Mol. Biol.* 374 (2007) 1319–1332.
- [116] H. Biverstahl, J. Lind, A. Bodor, L. Mäler, Biophysical studies of the membrane location of the voltage-gated sensors in the HsAPK and KvAP K⁺ channels, *Biochim. Biophys. Acta* 1788 (2009) 1976–1986.
- [117] É. Chartrand, A.A. Arnold, A. Gravel, S. Jenna, I. Marcotte, Potential role of the membrane in hERG channel functioning and drug-induced long QT syndrome, *Biochim. Biophys. Acta* 1798 (2010) 1651–1662.
- [118] C.R. Sanders, G.C. Landis, Reconstitution of membrane proteins into lipid-rich bilayered mixed micelles for NMR studies, *Biochemistry* 34 (1995) 4030–4040.
- [119] R.S. Prosser, J.S. Hwang, R.R. Vold, Magnetically aligned phospholipid bilayers with positive ordering: a new model membrane system, *Biophys. J.* 74 (1998) 2405–2418.
- [120] J. Struppe, E.A. Komives, S.S. Taylor, R.R. Vold, ²H NMR studies of a myristoylated peptide in neutral and acidic phospholipid bicelles, *Biochemistry* 37 (1998) 15523–15527.
- [121] K.J. Crowell, P.M. Macdonald, Surface charge response of the phosphatidylcholine head group in bilayered micelles from phosphorus and deuterium nuclear magnetic resonance, *Biochim. Biophys. Acta* 1416 (1999) 21–30.
- [122] J. Struppe, J.A. Whiles, R.R. Vold, Acidic phospholipid bicelles: a versatile model membrane system, *Biophys. J.* 78 (2000) 281–289.
- [123] M.A. Parker, V. King, K.P. Howard, Nuclear magnetic resonance study of doxorubicin binding to cardiolipin containing magnetically oriented phospholipid bilayers, *Biochim. Biophys. Acta* 1514 (2001) 206–216.
- [124] E.K. Tiburu, D.M. Moton, G.A. Lorigan, Development of magnetically aligned phospholipid bilayers in mixtures of palmitoylstearylphosphatidylcholine and dihexanoylphosphatidylcholine by solid-state NMR spectroscopy, *Biochim. Biophys. Acta* 1512 (2001) 206–214.
- [125] I. Marcotte, E.J. Dufourc, M. Ouellet, M. Auger, Interaction of the neuropeptide met-enkephalin with zwitterionic and negatively charged bicelles as viewed by ³¹P and ²H solid-state NMR, *Biophys. J.* 85 (2003) 328–339.
- [126] H. Sasaki, S. Fukuzawa, J. Kikuchi, S. Yokoyama, H. Hirota, K. Tachibana, Cholesterol doping induced enhanced stability of bicelles, *Langmuir* 19 (2003) 9841–9844.
- [127] J.J. Chou, J.L. Baber, A. Bax, Characterization of phospholipid mixed micelles by translational diffusion, *J. Biomol. NMR* 29 (2004) 299–308.
- [128] J.-X. Lu, M.A. Caporini, G.A. Lorigan, The effects of cholesterol on magnetically aligned phospholipid bilayers: a solid-state NMR and EPR spectroscopy study, *J. Magn. Reson.* 168 (2004) 18–30.
- [129] E.K. Tiburu, P.C. Dave, G.A. Lorigan, Solid-state ²H NMR studies of the effects of cholesterol on the acyl chain dynamics of magnetically aligned phospholipid bilayers, *Magn. Reson. Chem.* 42 (2004) 132–138.
- [130] M.N. Triba, P.F. Devaux, D.E. Warschawski, Effects of lipid chain length and unsaturation on bicelles stability. A phosphorus NMR study, *Biophys. J.* 91 (2006) 1357–1367.
- [131] L. Barbosa-Barros, A. de la Maza, C. López-Iglesias, O. López, Ceramide effects in the bicelle structure, *Colloids Surf. A* 317 (2008) 576–584.
- [132] A. Gayen, C. Mukhopadhyay, Evidence for effect of GM1 on opioid peptide conformation: NMR study on leucine enkephalin in ganglioside-containing isotropic phospholipid bicelles, *Langmuir* 24 (2008) 5422–5432.
- [133] T.-L. Lau, A.W. Partridge, M.H. Ginsberg, T.S. Ulmer, Structure of the integrin $\beta 3$ transmembrane segment in phospholipid bicelles and detergent micelles, *Biochemistry* 47 (2008) 4008–4016.
- [134] I. Marcotte, M. Auger, Bicelles as model membranes for solid- and solution-state NMR studies of membrane peptides and proteins, *Concepts Magn. Reson.* 24A (2005) 17–37.
- [135] J.A. Whiles, K.J. Glover, R.R. Vold, E.A. Komives, Methods for studying transmembrane peptides in bicelles: consequences of hydrophobic mismatch and peptide sequence, *J. Magn. Reson.* 158 (2002) 149–156.
- [136] M. Ottiger, A. Bax, Bicelle-based liquid crystals for NMR measurement of dipolar couplings at acidic and basic pH values, *J. Biomol. NMR* 13 (1999) 187–191.
- [137] S.F. Poget, S.M. Cahill, M.E. Girvin, Isotropic bicelles stabilize the functional form of a small multidrug-resistance pump for NMR structural studies, *J. Am. Chem. Soc.* 129 (2007) 2432–2433.
- [138] R.A. Shapiro, A.J. Brindley, R.V. Martin, Thermal stabilization of DMPC/DHPC bicelles by addition of cholesterol sulfate, *J. Am. Chem. Soc.* 132 (2010) 11406–11407.
- [139] P. Ram, J.H. Prestegard, Magnetic field induced ordering of bile salt/phospholipid micelles: new media for NMR structural investigations, *Biochim. Biophys. Acta* 940 (1988) 289–294.
- [140] S.H. Park, S.J. Opella, Triton X-100 as the “short-chain lipid” improves the magnetic alignment and stability of membrane proteins in phosphatidylcholine bilayers for oriented-sample solid-state NMR spectroscopy, *J. Am. Chem. Soc.* 132 (2010) 12552–12553.
- [141] M.N. Triba, D.E. Warschawski, P.F. Devaux, Reinvestigation by phosphorus NMR of lipid distribution in bicelles, *Biophys. J.* 88 (2005) 1887–1901.
- [142] A. Diller, C. Loudet, F. Aussenac, G. Raffard, S. Fournier, M. Laguerre, A. Grélaud, S.J. Opella, E.J. Dufourc, Bicelles: a natural “molecular goniometer” for structural, dynamical and topological studies of molecules in membranes, *Biochimie* 91 (2009) 744–751.
- [143] R.S. Prosser, F. Evancik, J.L. Kiteviski, M.S. Al-Abdul-Wahid, Current applications of bicelles in NMR studies of membrane-associated amphiphiles and proteins, *Biochemistry* 45 (2006) 8453–8465.
- [144] M. Ottiger, A. Bax, Characterization of magnetically oriented phospholipid micelles for measurement of dipolar couplings in macromolecules, *J. Biomol. NMR* 12 (1998) 361–372.
- [145] G. Raffard, S. Steinbrückner, A. Arnold, J.H. Davis, E.J. Dufourc, Temperature-composition diagram of dimyristoylphosphatidylcholine-dicaproylphosphatidylcholine “bicelles” self-orienting in the magnetic field. A solid-state ²H and ³¹P study, *Langmuir* 16 (2000) 7655–7662.
- [146] C.R. Sanders, B.J. Hare, K.P. Howard, J.H. Prestegard, Magnetically-oriented phospholipid micelles as a tool for the study of the membrane-associated molecules, *Prog. Nucl. Magn. Reson. Spectrosc.* 26 (1994) 421–444.
- [147] C.R. Sanders, G.C. Landis, Facile acquisition and assignment of oriented sample NMR spectra for bilayer surface-associated proteins, *J. Am. Chem. Soc.* 116 (1994) 6470–6471.
- [148] A. Arnold, T. Labrot, R. Oda, E.J. Dufourc, Cation modulation of “bicelle” size and magnetic alignment as revealed by solid state NMR and electron microscopy, *Biophys. J.* 82 (2002) 2667–2680.
- [149] J.A. Losonczy, J.H. Prestegard, Nuclear magnetic resonance characterization of the myristoylated, N-terminal fragment of ADP-ribosylation factor 1 in a magnetically oriented membrane array, *Biochemistry* 37 (1998) 706–716.
- [150] C. Sizon, F. Aussenac, A. Grélaud, E.J. Dufourc, NMR methods for studying the structure and dynamics of oncogenic and antihistaminic peptides in biomembranes, *Magn. Reson. Chem.* 42 (2004) 180–186.
- [151] A.A. De Angelis, A.A. Nevzorov, S.H. Park, S.C. Howell, A.A. Mrse, S.J. Opella, High-resolution NMR spectroscopy of membrane proteins in aligned bicelles, *J. Am. Chem. Soc.* 126 (2004) 15340–15341.

- [152] A.A. De Angelis, S.C. Howell, A.A. Nevzorov, S.J. Opella, Structure determination of a membrane protein with two trans-membrane helices in aligned phospholipid bicelles by solid-state NMR spectroscopy, *J. Am. Chem. Soc.* 128 (2006) 12256–12267.
- [153] S.D. Müller, A.A. De Angelis, T.H. Walther, S.L. Grage, C. Lange, S.J. Opella, A.S. Ulrich, Structural characterization of the pore forming protein TatA of the twin-arginine translocase in membranes by solid-state ^{15}N -NMR, *Biochim. Biophys. Acta* 1768 (2007) 3071–3079.
- [154] R. Mahalakshmi, F.M. Marassi, Orientation of the *Escherichia coli* outer membrane protein OmpX in phospholipid bilayer membranes determined by solid-state NMR, *Biochemistry* 47 (2008) 6531–6538.
- [155] A.A. De Angelis, S.J. Opella, Bicelle samples for solid-state NMR of membrane proteins, *Nat. Protoc.* 2 (2007) 2332–2338.
- [156] S.H. Park, S. Prytulla, A.A. DeAngelis, J.M. Brown, H. Kiefer, S.J. Opella, High-resolution NMR spectroscopy of a GPCR in aligned bicelles, *J. Am. Chem. Soc.* 128 (2006) 7402–7403.
- [157] G.E. Fanucci, J.Y. Lee, D.S. Cafiso, Membrane mimetic environments alter the conformation of the outer membrane protein BtuB, *J. Am. Chem. Soc.* 125 (2003) 13932–13933.
- [158] L. Czerski, C.R. Sanders, Functionality of a membrane protein in bicelles, *Anal. Biochem.* 284 (2000) 327–333.
- [159] P.A. Luchette, T.N. Vetman, R.S. Prosser, R.E.W. Hancock, M.-P. Nieh, C.J. Glinka, S. Krueger, J. Katsaras, Morphology of fast-tumbling bicelles: a small angle neutron scattering and NMR study, *Biochim. Biophys. Acta* 1513 (2001) 83–94.
- [160] B.M. Gorzelle, J.K. Nagy, K. Oxenoid, W.L. Lonzer, D.S. Cafiso, C.R. Sanders, Reconstitutive refolding of diacylglycerol kinase, an integral membrane protein, *Biochemistry* 38 (1999) 16373–16382.
- [161] G. Cook, S. Opella, NMR studies of p7 protein from hepatitis C virus, *Eur. Biophys. J.* 39 (2010) 1097–1104.
- [162] J.H. Prestegard, New techniques in structural NMR—anisotropic interactions, *Nat. Struct. Mol. Biol.* 5 (1998) 517–522.
- [163] J.H. Prestegard, C.M. Bougault, A.I. Kishore, Residual dipolar couplings in structure determination of biomolecules, *Chem. Rev.* 104 (2004) 3519–3540.
- [164] R.S. Prosser, S.A. Hunt, J.A. DiNatale, R.R. Vold, Magnetically aligned membrane model systems with positive order parameter: switching the sign of Szz with paramagnetic ions, *J. Am. Chem. Soc.* 118 (1996) 269–270.
- [165] R.S. Prosser, V.B. Volkov, I.V. Shiyankovskaya, Novel chelate-induced magnetic alignment of biological membranes, *Biophys. J.* 75 (1998) 2163–2169.
- [166] C. Loudet, S. Manet, S. Gineste, R. Oda, M.-F. Achard, E.J. Dufourc, Biphenyl bicelle disks align perpendicular to magnetic fields on large temperature scales: a study combining synthesis, solid-state NMR, TEM, and SAXS, *Biophys. J.* 92 (2007) 3949–3959.
- [167] C. Tan, B.M. Fung, G. Cho, Phospholipid bicelles that align with their normals parallel to the magnetic field, *J. Am. Chem. Soc.* 124 (2002) 11827–11832.
- [168] S.H. Park, C. Loudet, F.M. Marassi, E.J. Dufourc, S.J. Opella, Solid-state NMR spectroscopy of a membrane protein in biphenyl phospholipid bicelles with the bilayer normal parallel to the magnetic field, *J. Magn. Reson.* 193 (2008) 133–138.
- [169] C. Glaubitz, A. Watts, Magic angle-oriented sample spinning (MAOSS): a new approach toward biomembrane studies, *J. Magn. Reson.* 130 (1998) 305–316.
- [170] J.J. Lopez, A.J. Mason, C. Kaiser, C. Glaubitz, Separated local field NMR experiments on oriented samples rotating at the magic angle, *J. Biomol. NMR* 37 (2007) 91–111.
- [171] D.A. Middleton, A. Ahmed, C. Glaubitz, A. Watts, REDOR NMR on a hydrophobic peptide in oriented membranes, *J. Magn. Reson.* 147 (2000) 366–370.
- [172] C. Glaubitz, I.J. Burnett, G. Gröbner, A.J. Mason, A. Watts, Deuterium-MAS NMR spectroscopy on oriented membrane proteins: applications to photointermediates of bacteriorhodopsin, *J. Am. Chem. Soc.* 121 (1999) 5787–5794.
- [173] C. Glaubitz, G. Gröbner, A. Watts, Structural and orientational information of the membrane embedded M13 coat protein by ^{13}C -MAS NMR spectroscopy, *Biochim. Biophys. Acta* 1463 (2000) 151–161.
- [174] J. Raap, J. Hollander, T.V. Ovchinnikova, N.V. Swischeva, D. Skladnev, S. Kihne, Trans and surface membrane bound zervamicin IIB: ^{13}C -MAOSS-NMR at high spinning speed, *J. Biomol. NMR* (2006) 285–293.
- [175] C. Sizun, B. Bechinger, Bilayer sample for fast or slow magic angle oriented sample spinning solid-state NMR, *J. Am. Chem. Soc.* 124 (2002) 1146–1147.
- [176] O.C. Andronesi, J.R. Pfeifer, L. Al-Momani, S. Özdirekcan, D.T.S. Rijkers, B. Angerstein, S. Luca, U. Koert, J.A. Killian, M. Baldus, Probing membrane protein orientation and structure using fast magic-angle-spinning solid-state NMR, *J. Biomol. NMR* 30 (2004) 263–265.
- [177] A. Kouzayha, O. Wattraint, C. Sarazin, Interactions of two transmembrane peptides in supported lipid bilayers studied by a ^{31}P and ^{15}N MAOSS NMR strategy, *Biochimie* 91 (2009) 774–778.
- [178] O. Wattraint, A. Arnold, M. Auger, C. Bourdillon, C. Sarazin, Lipid bilayer tethered inside a nanoporous support: a solid-state nuclear magnetic resonance investigation, *Anal. Biochem.* 336 (2005) 253–261.
- [179] O. Wattraint, C. Sarazin, Diffusion measurements of water, ubiquinone and lipid bilayer inside a cylindrical nanoporous support: a stimulated echo pulsed-field gradient MAS-NMR investigation, *Biochim. Biophys. Acta* 1713 (2005) 65–72.
- [180] G. Gröbner, A. Taylor, P.T.F. Williamson, G. Choi, C. Glaubitz, J.A. Watts, W.J. de Grip, A. Watts, Macroscopic orientation of natural and model membranes for structural studies, *Anal. Biochem.* 254 (1997) 132–138.
- [181] M. Billeter, G. Wagner, K. Wüthrich, Solution NMR structure determination of proteins revisited, *J. Biomol. NMR* 42 (2008) 155–158.
- [182] T.L. Religa, R. Sprangers, L.E. Kay, Dynamic regulation of archaeal proteasome gate opening as studied by TROSY NMR, *Science* 328 (2010) 98–102.
- [183] J. Lipfert, L. Columbus, V. Chu, S. Lesley, S. Doniach, Size and shape of detergent micelles determined by small-angle X-ray scattering, *J. Phys. Chem. B* 111 (2007) 12427–12438.
- [184] A. Helenius, K. Simons, Solubilization of membranes by detergents, *Biochim. Biophys. Acta* 415 (1975) 29–79.
- [185] C. Fernandez, C. Hilty, G. Wider, P. Güntert, K. Wüthrich, NMR structure of the integral membrane protein OmpX, *J. Mol. Biol.* 336 (2004) 1211–1221.
- [186] A. Gautier, H. Mott, M. Bostock, J. Kirkpatrick, D. Nietispach, Structure determination of the seven-helix transmembrane receptor sensory rhodopsin II by solution NMR spectroscopy, *Nat. Struct. Mol. Biol.* 17 (2010) 768–774.
- [187] P.M. Hwang, W.-Y. Choy, E.I. Lo, L. Chen, J.D. Forman-Kay, C.R.H. Raetz, G.G. Privé, R.E. Bishop, L.E. Kay, Solution structure and dynamics of the outer membrane enzyme PagP by NMR, *Proc. Natl. Acad. Sci. USA* 99 (2002) 13560–13565.
- [188] K. Duquesne, J.N. Sturgis, Membrane protein solubilization, *Methods Mol. Biol.* 601 (2010) 205–217.
- [189] K.R. MacKenzie, J.H. Prestegard, D.M. Engelman, A transmembrane helix dimer: structure and implications, *Science* 276 (1997) 131–133.
- [190] G. Pages, A. Torres, P. Ju, P. Bansal, P. Alewood, P. Kuchel, J. Vandenberg, Structure of the pore-helix of the hERG K⁺ channel, *Eur. Biophys. J.* 39 (2009) 111–120.
- [191] Y. Gohon, J.-L. Popot, Membrane protein–surfactant complexes, *Curr. Opin. Colloid Interface Sci.* 8 (2003) 15–22.
- [192] A.M. Seddon, P. Curnow, P.J. Booth, Membrane proteins, lipids and detergents: not just a soap opera, *Biochim. Biophys. Acta* 1666 (2004) 105–117.
- [193] Y. Mo, B.-K. Lee, J.F. Ankner, J.M. Becker, W.T. Heller, Detergent-associated solution conformations of helical and β -barrel membrane proteins, *J. Phys. Chem. B* 112 (2008) 13349–13354.
- [194] P.M. Hwang, R.E. Bishop, L.E. Kay, The integral membrane enzyme PagP alternates between two dynamically distinct states, *Proc. Natl. Acad. Sci. USA* 101 (2004) 9618–9623.
- [195] A. Arora, F. Abildgaard, J.H. Bushweller, L.K. Tamm, Structure of outer membrane protein A transmembrane domain by NMR spectroscopy, *Nat. Struct. Mol. Biol.* 8 (2001) 334–338.
- [196] B. Liang, L.K. Tamm, Structure of outer membrane protein G by solution NMR spectroscopy, *Proc. Natl. Acad. Sci. USA* 104 (2007) 16140–16145.
- [197] S. Hiller, R.G. Garces, T.J. Malia, V.Y. Orekhov, M. Colombini, G. Wagner, Solution structure of the integral human membrane protein VDAC-1 in detergent micelles, *Science* 321 (2008) 1206–1210.
- [198] Y. Zhou, T. Cierpicki, R. Jimenez, S. Lukasik, J. Ellena, D.S. Cafiso, H. Kadokura, J. Beckwith, J.H. Bushweller, NMR solution structure of the integral membrane enzyme DsbB: functional insights into DsbB-catalyzed disulfide bond formation, *Mol. Cell* 31 (2008) 896–908.
- [199] W.D. Van Horn, H.-J. Kim, C.D. Ellis, A. Hadziselimovic, E.S. Sulistio, M.D. Karra, C. Tian, F.D. Sönnichsen, C.R. Sanders, Solution nuclear magnetic resonance structure of membrane-integral diacylglycerol kinase, *Science* 324 (2009) 1726–1729.
- [200] K.J. Glover, J.A. Whiles, M.J. Wood, G. Melacini, E.A. Komives, R.R. Vold, Conformational dimorphism and transmembrane orientation of prion protein residues 110–136 in bicelles, *Biochemistry* 40 (2001) 13137–13142.
- [201] M. Lindberg, H. Biverstahl, A. Gräslund, L. Måler, Structure and positioning comparison of two variants of penetratin in two different membrane mimicking systems by NMR, *Eur. J. Biochem.* 270 (2003) 3055–3063.
- [202] E. Bárány-Wallje, A. Andersson, A. Gräslund, L. Måler, NMR solution structure and position of transportin in neutral phospholipid bicelles, *FEBS Lett.* 567 (2004) 265–269.
- [203] I. Marcotte, F. Separovic, M. Auger, S.M. Gagné, A multidimensional ^1H NMR investigation of the conformation of methionine-enkephalin in fast-tumbling bicelles, *Biophys. J.* 86 (2004) 1587–1600.
- [204] L. Khemtémourian, K. Bathany, J.-M. Schmitter, E.J. Dufourc, Fast and quantitative recovery of hydrophobic and amphipathic peptides after incorporation into phospholipid membranes, *Anal. Chem.* 78 (2006) 5348–5353.
- [205] J.A. Whiles, R. Brasseur, K.J. Glover, G. Melacini, E.A. Komives, R.R. Vold, Orientation and effects of mastoparan X on phospholipid bicelles, *Biophys. J.* 80 (2001) 280–293.
- [206] M. Salzmann, K. Pervushin, G. Wider, H. Senn, K. Wüthrich, NMR assignment and secondary structure determination of an octameric 110 kDa protein using TROSY in triple resonance experiments, *J. Am. Chem. Soc.* 122 (2000) 7543–7548.
- [207] T. Nakamura, H. Takahashi, K. Takeuchi, T. Kohno, K. Wakamatsu, I. Shimada, Direct determination of a membrane-peptide interface using the nuclear magnetic resonance cross-saturation method, *Biophys. J.* 89 (2005) 4051–4055.
- [208] T.-L. Lau, C. Kim, M.H. Ginsberg, T.S. Ulmer, The structure of the integrin $\alpha\text{IIb}\beta_3$ transmembrane complex explains integrin transmembrane signalling, *EMBO J.* 28 (2009) 1351–1361.
- [209] E.V. Bocharov, Y.E. Pustovalova, K.V. Pavlov, P.E. Volynsky, M.V. Goncharuk, Y.S. Ermolyuk, D.V. Karpunin, A.A. Schulga, M.P. Kirpichnikov, R.G. Efremov, I.V. Maslennikov, A.S. Arseniev, Unique dimeric structure of Bnip3 transmembrane domain suggests membrane permeabilization as a cell death trigger, *J. Biol. Chem.* 282 (2007) 16256–16266.
- [210] E.V. Bocharov, K.S. Mineev, P.E. Volynsky, Y.S. Ermolyuk, E.N. Tkach, A.G. Sobol, V.V. Chupin, M.P. Kirpichnikov, R.G. Efremov, A.S. Arseniev, Spatial structure of the dimeric transmembrane domain of the growth factor receptor ErbB2 presumably corresponding to the receptor active state, *J. Biol. Chem.* 283 (2008) 6950–6956.
- [211] E.V. Bocharov, M.L. Mayzel, P.E. Volynsky, M.V. Goncharuk, Y.S. Ermolyuk, A.A. Schulga, E.O. Artemenko, R.G. Efremov, A.S. Arseniev, Spatial structure and pH-dependent conformational diversity of dimeric transmembrane domain of the receptor tyrosine kinase EphA1, *J. Biol. Chem.* 283 (2008) 6950–6956.

- [12] R.L. Ong, V.T. Marchesi, J.H. Prestegard, Small unilamellar vesicles containing glycoporphin A. Chemical characterization and proton nuclear magnetic resonance studies, *Biochemistry* 20 (1981) 4283–4292.
- [123] G. Da Costa, L. Mouret, S. Chevanne, E. Le Rumeur, A. Bondon, NMR of molecules interacting with lipids in small unilamellar vesicles, *Eur. Biophys. J.* 36 (2007) 933–942.
- [124] M. Goetz, C. Carloti, F. Bontems, E.J. Dufourc, Evidence for an α -helix \rightarrow π -bulge helicity modulation for the neu/erbB-2 membrane-spanning segment. A ^1H NMR and circular dichroism study, *Biochemistry* 40 (2001) 6534–6540.
- [125] F. Penin, V. Brass, N. Appel, S. Ramboarina, R. Montserret, D. Ficheux, H.E. Blum, R. Bartschlag, D. Moradpour, Structure and function of the membrane anchor domain of hepatitis C virus nonstructural protein 5A, *J. Biol. Chem.* 279 (2004) 40835–40843.
- [126] M.E. Girvin, V.K. Rastogi, F. Abildgaard, J.L. Markley, R.H. Fillingame, Solution structure of the transmembrane H $^{+}$ -transporting subunit c of the F $_1$ F $_0$ ATP synthase, *Biochemistry* 37 (1998) 8817–8824.
- [127] M. Schwaiger, M. Lebendiker, H. Yerushalmi, M. Coles, A. Gröger, C. Schwarz, S. Schuldiner, H. Kessler, NMR investigation of the multidrug transporter EmrE, an integral membrane protein, *Eur. J. Biochem.* 254 (1998) 610–619.
- [128] O.Y. Dmitriev, K. Altendorf, R.H. Fillingame, Subunit a of the *E. coli* ATP synthase: reconstitution and high resolution NMR with protein purified in a mixed polarity solvent, *FEBS Lett.* 556 (2004) 35–38.
- [129] A. Wand, M. Ehrhardt, P. Flynn, High-resolution NMR of encapsulated proteins dissolved in low-viscosity fluids, *Proc. Natl. Acad. Sci. USA* 95 (1998) 15299–15302.
- [120] J.M. Kielec, K.G. Valentine, C.R. Babu, A.J. Wand, Reverse micelles in integral membrane protein structural biology by solution NMR spectroscopy, *Structure* 17 (2009) 345–351.
- [121] K.G. Valentine, R.W. Peterson, J. Saad, M. Summers, X. Xu, J. Ames, A.J. Wand, Reverse micelle encapsulation of membrane-anchored proteins for solution NMR studies, *Structure* 18 (2010) 9–16.
- [122] C. Tribet, R. Audebert, J.-L. Popot, Amphipols: polymers that keep membrane proteins soluble in aqueous solutions, *Proc. Natl. Acad. Sci. USA* 93 (1996) 15047–15050.
- [123] C. Tribet, J. Olive, J.-P. Dubacq, J.-L. Popot, Dimer to monomer transition of the cytochrome b6 f complex: causes and consequences, *J. Biol. Chem.* 272 (1997) 21892–21900.
- [124] J.-L. Popot, Amphipols, nanodiscs, and fluorinated surfactants: three nonconventional approaches to studying membrane proteins in aqueous solutions, *Annu. Rev. Biochem.* 79 (2010) 737–775.
- [125] J.-L. Popot, E.A. Berry, D. Charvolin, C. Creuzenet, C. Ebel, D.M. Engelman, M. Flotenmeyer, F. Giusti, Y. Gohon, Q. Hong, J.H. Lakey, K. Leonard, H.A. Shuman, P. Timmins, D.E. Warschawski, F. Zito, M. Zoonens, B. Pucci, C. Tribet, Amphipols: polymeric surfactants for membrane biology research, *Cell. Mol. Life Sci.* 60 (2003) 1559–1574.
- [126] J.L. Catoire, M. Damian, F. Giusti, A. Martin, C. van Heijenoort, J.-L. Popot, E. Guittet, J.L. Banères, Structure of a GPCR ligand in its receptor-bound state: leukotriene B $_4$ adopts a highly constrained conformation when associated to human BLT $_2$, *J. Am. Chem. Soc.* 132 (2010) 9049–9057.
- [127] J.L. Catoire, M. Zoonens, C. Van Heijenoort, F. Giusti, E. Guittet, J.-L. Popot, Solution NMR mapping of water-accessible residues in the transmembrane β -barrel of OmpX, *Eur. Biophys. J.* 39 (2010) 623–630.
- [128] M. Zoonens, J.L. Catoire, F. Giusti, J.-L. Popot, NMR study of a membrane protein in detergent-free aqueous solution, *Proc. Natl. Acad. Sci. USA* 102 (2005) 8893–8898.
- [129] T. Dahmane, M. Damian, S. Mary, J.-L. Popot, J.L. Banères, Amphipol-assisted in vitro folding of G protein-coupled receptors, *Biochemistry* 48 (2009) 6516–6521.
- [130] T.H. Bayburt, Y.V. Grinkova, S.G. Sligar, Self-assembly of discoidal phospholipid bilayer nanoparticles with membrane scaffold proteins, *Nano Lett.* 2 (2002) 853–856.
- [131] A. Nath, W.M. Atkins, S.G. Sligar, Applications of phospholipid bilayer nanodiscs in the study of membranes and membrane proteins, *Biochemistry* 46 (2007) 2059–2069.
- [132] E.N. Lyukmanova, Z.O. Shenkarev, A.S. Paramonov, A.G. Sobol, T.V. Ovchinnikova, V.V. Chupin, M.P. Kirpichnikov, M.J. Blommers, A.S. Arseniev, Lipid-protein nanoscale bilayers: a versatile medium for NMR investigations of membrane proteins and membrane-active peptides, *J. Am. Chem. Soc.* 130 (2008) 2140–2141.
- [133] J. Borch, T. Hamann, The nanodisc: a novel tool for membrane protein studies, *Biol. Chem.* 390 (2009) 805–814.
- [134] I.G. Denisov, Y.V. Grinkova, A.A. Lazarides, S.G. Sligar, Directed self-assembly of monodisperse phospholipid bilayer nanodiscs with controlled size, *J. Am. Chem. Soc.* 126 (2004) 3477–3487.
- [135] B.A. Chromy, E. Arroyo, C.D. Blanchette, G. Bench, H. Benner, J.A. Cappuccino, M.A. Coleman, P.T. Henderson, A.K. Hinz, E.A. Kuhn, J.B. Pesavento, B.W. Segelke, T.A. Sulchek, T. Tarasow, V.L. Walsworth, P.D. Hoepflich, Different apolipoproteins impact nanolipoprotein particle formation, *J. Am. Chem. Soc.* 129 (2007) 14348–14354.
- [136] M. Nakano, M. Fukuda, T. Kudo, M. Miyazaki, Y. Wada, N. Matsuzaki, H. Endo, T. Handa, Static and dynamic properties of phospholipid bilayer nanodiscs, *J. Am. Chem. Soc.* 131 (2009) 8308–8312.
- [137] T.H. Bayburt, S.G. Sligar, Single-molecule height measurements on microsome cytochrome P450 in nanometer-scale phospholipid bilayer disks, *Proc. Natl. Acad. Sci. USA* 99 (2002) 6725–6730.
- [138] A. Jonas, Reconstitution of high-density lipoproteins, *Methods Enzymol.* 128 (1986) 553–582.
- [139] F. Katzen, J.E. Fletcher, J.-P. Yang, D. Kang, T.C. Peterson, J.A. Cappuccino, C.D. Blanchette, T. Sulchek, B.A. Chromy, P.D. Hoepflich, M.A. Coleman, W. Kudlicki, Insertion of membrane proteins into discoidal membranes using a cell-free protein expression approach, *J. Proteome Res.* 7 (2008) 3535–3542.
- [140] J.M. Glück, M. Wittlich, S. Feuerstein, S. Hoffmann, D. Willbold, B.W. Koenig, Integral membrane proteins in nanodiscs can be studied by solution NMR spectroscopy, *J. Am. Chem. Soc.* 131 (2009) 12060–12061.
- [141] B.J. Baas, I.G. Denisov, S.G. Sligar, Homotropic cooperativity of monomeric cytochrome P450 3A4 in a nanoscale native bilayer environment, *Arch. Biochem. Biophys.* 430 (2004) 218–228.
- [142] H. Duan, N.R. Civjan, S.G. Sligar, M.A. Schuler, Co-incorporation of heterologously expressed *Arabidopsis* cytochrome P450 and P450 reductase into soluble nanoscale lipid bilayers, *Arch. Biochem. Biophys.* 424 (2004) 141–153.
- [143] T.H. Bayburt, S.G. Sligar, Self-assembly of single integral membrane proteins into soluble nanoscale phospholipid bilayers, *Protein Sci.* 12 (2003) 2476–2481.
- [144] A.J. Leitz, T.H. Bayburt, A.N. Barnakov, B.A. Springer, S.G. Sligar, Functional reconstitution of β_2 -adrenergic receptors utilizing self-assembling nanodisc technology, *Biotechniques* 40 (2006) 601–610.
- [145] Z.O. Shenkarev, E.N. Lyukmanova, A.S. Paramonov, L.N. Shingarova, V.V. Chupin, M.P. Kirpichnikov, M.J. Blommers, A.S. Arseniev, Lipid-protein nanodiscs as reference medium in detergent screening for high-resolution NMR studies of integral membrane proteins, *J. Am. Chem. Soc.* 132 (2010) 5628–5629.
- [146] A.Z. Kijac, Y. Li, S.G. Sligar, C.M. Rienstra, Magic-angle spinning solid-state NMR spectroscopy of nanodisc-embedded human CYP3A4, *Biochemistry* 46 (2007) 13696–13703.
- [147] A.I. Smirnov, O.G. Poluektov, Substrate-supported lipid nanotube arrays, *J. Am. Chem. Soc.* 125 (2003) 8434–8435.
- [148] H.C. Gaede, K.M. Luckett, I.V. Polozov, K. Gawrisch, Multinuclear NMR studies of single lipid bilayers supported in cylindrical aluminum oxide nanopores, *Langmuir* 20 (2004) 7711–7719.
- [149] G.A. Lorigan, P.C. Dave, E.K. Tiburu, K. Damodaran, S. Abu-Baker, E.S. Karp, W.J. Gibbons, R.E. Minto, Solid-state NMR spectroscopic studies of an integral membrane protein inserted into aligned phospholipid bilayer nanotube arrays, *J. Am. Chem. Soc.* 126 (2004) 9504–9505.
- [150] O. Wattraint, D.E. Warschawski, C. Sarazin, Tethered or adsorbed supported lipid bilayers in nanotubes characterized by deuterium magic angle spinning NMR spectroscopy, *Langmuir* 21 (2005) 3226–3228.
- [151] E.M. Landau, J.P. Rosenbusch, Lipid cubic phases: a novel concept for the crystallisation of membrane proteins, *Proc. Natl. Acad. Sci. USA* 93 (1996) 14532–14535.
- [152] E. Boyle-Roden, N. Hoefler, K.K. Dey, P.J. Grandinetti, M. Caffrey, High resolution ^1H NMR of a lipid cubic phase using a solution NMR probe, *J. Magn. Reson.* 189 (2007) 13–19.
- [153] S. Fraser, F. Separovic, A. Polyzos, Cubic phases of ternary amphiphile-water systems, *Eur. Biophys. J.* 39 (2009) 83–90.
- [154] J.-P. Doulié, Self-assembly of hollow cones in a bola-amphiphile/hexadecylamine salt solution, *J. Am. Chem. Soc.* 127 (2005) 15694–15695.
- [155] Z. Cheng, G.D. D'Ambruso, C.A. Aspinwall, Stabilized porous phospholipid nanoshells, *Langmuir* 22 (2006) 9507–9511.
- [156] T.A. Cross, S.J. Opella, Structural properties of fd coat protein in sodium dodecyl sulfate micelles, *Biochem. Biophys. Res. Commun.* 92 (1980) 478–484.
- [157] A. Bienvenue, M. Bloom, J.H. Davis, P.F. Devaux, Evidence for protein-associated lipids from deuterium nuclear magnetic resonance studies of rhodopsin-dimyristoylphosphatidylcholine recombinants, *J. Biol. Chem.* 257 (1982) 3032–3038.
- [158] M. Munowitz, W.P. Aue, R.G. Griffin, Two-dimensional separation of dipolar and scaled isotropic chemical shift interactions in magic angle NMR spectra, *J. Chem. Phys.* 77 (1982) 1686–1689.
- [159] T.A. Cross, S.J. Opella, Protein structure by solid state nuclear magnetic resonance: residues 40 to 45 of bacteriophage fd coat protein, *J. Mol. Biol.* 182 (1985) 367–381.
- [160] K. Inomata, A. Ohno, H. Tochio, S. Isogai, T. Tenno, I. Nakase, T. Takeuchi, S. Futaki, Y. Ito, H. Hiroaki, M. Shirakawa, High-resolution multi-dimensional NMR spectroscopy of proteins in human cells, *Nature* 458 (2009) 106–109.
- [161] P. Selenko, D.P. Frueh, S.J. Elsaesser, W. Haas, S.P. Gygi, G. Wagner, In situ observation of protein phosphorylation by high-resolution NMR spectroscopy, *Nat. Struct. Mol. Biol.* 15 (2008) 321–329.
- [162] W.C. McMurray, Phospholipids in subcellular organelles and membranes, in: G.B. Ansell, J.N. Hawthorne, R.M.C. Dawson (Eds.), *Form and Function of Phospholipids*, Elsevier, Amsterdam, 1973, pp. 205–251.
- [163] R. Prasad, Structure and distribution of membrane lipids, in: R. Prasad (Ed.), *Manual on Membrane Lipids*, Springer-Verlag, Berlin, 1996, pp. 1–15.
- [164] L.E. Hernández, D.T. Cooke, Modification of the root plasma membrane lipid composition of cadmium-treated *Pisum sativum*, *J. Exp. Bot.* 48 (1997) 1375–1381.
- [165] M.X. Andersson, J.M. Kjellberg, A.S. Sandelius, Chloroplast biogenesis. Regulation of lipid transport to the thylakoid in chloroplasts isolated from expanding and fully expanded leaves of pea, *Plant Physiol.* 127 (2001) 184–193.
- [166] H. Tatsuzawa, E. Takizawa, M. Wada, Y. Yamamoto, Fatty acid and lipid composition of the acidophilic green alga *Chlamydomonas* sp., *J. Phycol.* 32 (1996) 598–601.
- [167] V.M. Tereshina, A.S. Memorskaya, E.R. Kotlova, E.P. Feofilova, Membrane lipid and cytosol carbohydrate composition in *Aspergillus niger* under heat shock, *Microbiology* 79 (2010) 40–46.
- [168] N.H. Georgopapadakou, B.A. Dix, S.A. Smith, J. Freudenberger, P.T. Funke, Effect of antifungal agents on lipid biosynthesis and membrane integrity in *Candida albicans*, *Antimicrob. Agents Chemother.* 31 (1987) 46–51.
- [169] H. Goldfine, Bacterial membranes and lipid packing theory, *J. Lipid Res.* 25 (1984) 1501–1507.
- [170] S. Clejan, T. Kruhwich, K. Mondrus, D. Seto-Young, Membrane lipid composition of obligately and facultatively alkalophilic strains of *Bacillus* spp., *J. Bacteriol.* 168 (1986) 334–340.

RÉFÉRENCES

- [1] Bagal, S. K., Brown, A. D., Cox, P. J., Omoto, K., Owen, R. M., Pryde, D. C., Sidders, B., Skerratt, S. E., Stevens, E. B., Storer, R. I., and Swain, N. A. (2013) Ion channels as therapeutic targets: a drug discovery perspective, *Journal of medicinal chemistry* 56, 593-624.
- [2] Papazian, D. M., Schwarz, T. L., Tempel, B. L., Jan, Y. N., and Jan, L. Y. (1987) Cloning of genomic and complementary DNA from Shaker, a putative potassium channel gene from *Drosophila*, *Science* 237, 749-753.
- [3] Kaplan, W. D., and Trout, W. E., 3rd. (1969) The behavior of four neurological mutants of *Drosophila*, *Genetics* 61, 399-409.
- [4] Warmke, J. W., and Ganetzky, B. (1994) A family of potassium channel genes related to eag in *Drosophila* and mammals, *Proceedings of the National Academy of Sciences of the United States of America* 91, 3438-3442.
- [5] Sanguinetti, M. C., Jiang, C., Curran, M. E., and Keating, M. T. (1995) A mechanistic link between an inherited and an acquired cardiac arrhythmia: HERG encodes the IKr potassium channel, *Cell* 81, 299-307.
- [6] Pringos, E., Vignes, M., Martinez, J., and Rolland, V. (2011) Peptide neurotoxins that affect voltage-gated calcium channels: a close-up on ω -agatoxins, *Toxins* 3, 17-42.
- [7] Pearlstein, R., Vaz, R., and Rampe, D. (2003) Understanding the structure-activity relationship of the human ether-a-go-go-related gene cardiac K⁺ channel. A model for bad behavior, *Journal of medicinal chemistry* 46, 2017-2022.
- [8] Gutman, G. A., Chandy, K. G., Grissmer, S., Lazdunski, M., McKinnon, D., Pardo, L. A., Robertson, G. A., Rudy, B., Sanguinetti, M. C., Stuhmer, W., and Wang, X. (2005) International union of pharmacology. LIII. Nomenclature and molecular relationships of voltage-gated potassium channels, *Pharmacological reviews* 57, 473-508.
- [9] Sanguinetti, M. C., and Tristani-Firouzi, M. (2006) hERG potassium channels and cardiac arrhythmia, *Nature* 440, 463-469.
- [10] Curran, M. E., Splawski, I., Timothy, K. W., Vincent, G. M., Green, E. D., and Keating, M. T. (1995) A molecular basis for cardiac arrhythmia: HERG mutations cause long QT syndrome, *Cell* 80, 795-803.
- [11] Klabunde, R. (2011) *Cardiovascular physiology concepts*, Wolters Kluwer Health.
- [12] Fermini, B., and Fossa, A. A. (2003) The impact of drug-induced QT interval prolongation on drug discovery and development, *Nature Reviews Drug Discovery* 2, 439-447.

- [13] Splawski, I., Shen, J., Timothy, K. W., Lehmann, M. H., Priori, S., Robinson, J. L., Moss, A. J., Schwartz, P. J., Towbin, J. A., Vincent, G. M., and Keating, M. T. (2000) Spectrum of mutations in long-QT syndrome genes. KVLQT1, HERG, SCN5A, KCNE1, and KCNE2, *Circulation* 102, 1178-1185.
- [14] Kapplinger, J. D., Tester, D. J., Salisbury, B. A., Carr, J. L., Harris-Kerr, C., Pollevick, G. D., Wilde, A. A., and Ackerman, M. J. (2009) Spectrum and prevalence of mutations from the first 2,500 consecutive unrelated patients referred for the FAMILION long QT syndrome genetic test, *Heart Rhythm* 6, 1297-1303.
- [15] Jimenez-Vargas, J. M., Restano-Cassulini, R., and Possani, L. D. (2012) Toxin modulators and blockers of hERG K(+) channels, *Toxicon* 60, 492-501.
- [16] De Bruin, M. L., Pettersson, M., Meyboom, R. H., Hoes, A. W., and Leufkens, H. G. (2005) Anti-HERG activity and the risk of drug-induced arrhythmias and sudden death, *European heart journal* 26, 590-597.
- [17] Priest, B. T., Bell, I. M., and Garcia, M. L. (2008) Role of hERG potassium channel assays in drug development, *Channels (Austin)* 2, 87-93.
- [18] Ray, W. A., Stein, C. M., Daugherty, J. R., Hall, K., Arbogast, P. G., and Griffin, M. R. (2002) COX-2 selective non-steroidal anti-inflammatory drugs and risk of serious coronary heart disease, *Lancet* 360, 1071-1073.
- [19] Aronov, A. M. (2005) Predictive in silico modeling for hERG channel blockers, *Drug discovery today* 10, 149-155.
- [20] Kamiya, K., Niwa, R., Mitcheson, J. S., and Sanguinetti, M. C. (2006) Molecular determinants of hERG channel block, *Molecular pharmacology* 69, 1709-1716.
- [21] Gravel, A. E., Arnold, A. A., Dufourc, E. J., and Marcotte, I. (2013) An NMR investigation of the structure, function and role of the hERG channel selectivity filter in the long QT syndrome, *Biochimica et biophysica acta* 1828, 1494-1502.
- [22] Rajamani, R., Tounge, B. A., Li, J., and Reynolds, C. H. (2005) A two-state homology model of the hERG K⁺ channel: application to ligand binding, *Bioorg. Med. Chem. Lett.* 15, 1737-1741.
- [23] Österberg, F., and Aqvist, J. (2005) Exploring blocker binding to a homology model of the open hERG K⁺ channel using docking and molecular dynamics methods, *FEBS letters* 579, 2939-2944.
- [24] Scholz, E. P., Zitron, E., Kiesecker, C., Thomas, D., Kathöfer, S., Kreuzer, J., Bauer, A., Katus, H. A., Remppis, A., Karle, C. A., and Greten, J. (2007) Orange flavonoid hesperetin modulates cardiac hERG potassium channel via binding to amino acid F656, *Nutrition, Metabolism and Cardiovascular Diseases* 17, 666-675.
- [25] Kelemen, K., Kiesecker, C., Zitron, E., Bauer, A., Scholz, E., Bloehs, R., Thomas, D., Greten, J., Remppis, A., Schoels, W., Katus, H. A., and Karle, C. A. (2007) Green tea flavonoid epigallocatechin-3-gallate (EGCG) inhibits

- cardiac hERG potassium channels, *Biochemical and biophysical research communications* 364, 429-435.
- [26] Zitron, E., Scholz, E., Owen, R. W., Luck, S., Kiesecker, C., Thomas, D., Kathofer, S., Niroomand, F., Kiehn, J., Kreye, V. A., Katus, H. A., Schoels, W., and Karle, C. A. (2005) QTc prolongation by grapefruit juice and its potential pharmacological basis: HERG channel blockade by flavonoids, *Circulation* 111, 835-838.
 - [27] Torres, A. M., Bansal, P., Sunde, M., Clarke, C. E., Bursill, J. A., Smith, D. J., Bauskin, A., Breit, S. N., Campbell, T. J., Alewood, P. F., Kuchel, P. W., and Vandenberg, J. I. (2003) Structure of the hERG K⁺ channel S5P extracellular linker, *Journal of Biological Chemistry* 278, 42136-42148.
 - [28] Hu, Y.-T., Hu, J., Li, T., Wei, J.-J., Feng, J., Du, Y.-M., Cao, Z.-J., Li, W.-X., and Wu, Y.-L. (2014) Open conformation of hERG channel turrets revealed by a specific scorpion toxin BmKKx2, *Cell & Bioscience* 4, 18-18.
 - [29] Doyle, D. A., Cabral, J. M., Pfuetzner, R. A., Kuo, A., Gulbis, J. M., Cohen, S. L., Chait, B. T., and MacKinnon, R. (1998) The structure of the potassium channel: molecular basis of K⁺ conduction and selectivity, *Science* 280, 69-77.
 - [30] Petrecca, K., Atanasiu, R., Akhavan, A., and Shrier, A. (1999) N-linked glycosylation sites determine hERG channel surface membrane expression, *Journal of Physiology* 515 (Pt 1), 41-48.
 - [31] Zhang, D. Y., Wang, Y., Lau, C. P., Tse, H. F., and Li, G. R. (2008) Both EGFR kinase and Src-related tyrosine kinases regulate human ether-a-go-go-related gene potassium channels, *Cellular signalling* 20, 1815-1821.
 - [32] Gong, Q., Anderson, C. L., January, C. T., and Zhou, Z. (2002) Role of glycosylation in cell surface expression and stability of HERG potassium channels, *American Journal of Physiology - Heart and Circulatory Physiology* 283, H77-H84.
 - [33] Long, S. B., Campbell, E. B., and MacKinnon, R. (2005) Crystal structure of a mammalian voltage-dependent Shaker family K⁺ channel, *Science* 309, 897-903.
 - [34] Long, S. B., Campbell, E. B., and MacKinnon, R. (2005) Voltage sensor of Kv1.2: structural basis of electromechanical coupling, *Science* 309, 903-908.
 - [35] Jiang, Y., Lee, A., Chen, J., Cadene, M., Chait, B. T., and MacKinnon, R. (2002) Crystal structure and mechanism of a calcium-gated potassium channel, *Nature* 417, 515-522.
 - [36] Jiang, Y., Lee, A., Chen, J., Cadene, M., Chait, B. T., and MacKinnon, R. (2002) The open pore conformation of potassium channels, *Nature* 417, 523-526.
 - [37] Morais Cabral, J. H., Lee, A., Cohen, S. L., Chait, B. T., Li, M., and MacKinnon, R. (1998) Crystal structure and functional analysis of the hERG potassium channel N terminus: a eukaryotic PAS domain, *Cell* 95, 649-655.
 - [38] Li, Q., Gayen, S., Chen, A. S., Huang, Q., Raida, M., and Kang, C. (2010) NMR solution structure of the N-terminal domain of hERG and its interaction with

- the S4-S5 linker, *Biochemical and biophysical research communications* 403, 126-132.
- [39] Ng, C. A., Hunter, M. J., Perry, M. D., Mobli, M., Ke, Y., Kuchel, P. W., King, G. F., Stock, D., and Vandenberg, J. I. (2011) The N-terminal tail of hERG contains an amphipathic alpha-helix that regulates channel deactivation, *PLoS One* 6, e16191.
- [40] Muskett, F. W., and Mitcheson, J. S. (2011) Resonance assignment and secondary structure prediction of the N-terminal domain of hERG (Kv11.1), *Biomolecular NMR assignments* 5, 15-17.
- [41] Liu, J., Jiang, M., and Tseng, G.-N. (2002) Structural and functional role of the extracellular S5-P linker in the hERG potassium channel, *The Journal of general physiology* 120, 723-737.
- [42] Hattab, G., Warschawski, D. E., Moncoq, K., and Miroux, B. (2015) Escherichia coli as host for membrane protein structure determination: a global analysis, *Scientific reports* 5, 12097.
- [43] Berman, H. M., Westbrook, J., Feng, Z., Gilliland, G., Bhat, T. N., Weissig, H., Shindyalov, I. N., and Bourne, P. E. (2000) The Protein Data Bank, *Nucleic Acids Research* 28, 235-242.
- [44] Krogh, A., Larsson, B., von Heijne, G., and Sonnhammer, E. L. (2001) Predicting transmembrane protein topology with a hidden Markov model: application to complete genomes, *Journal of molecular biology* 305, 567-580.
- [45] Lehnert, U., Xia, Y., Royce, T. E., Goh, C. S., Liu, Y., Senes, A., Yu, H., Zhang, Z. L., Engelman, D. M., and Gerstein, M. (2004) Computational analysis of membrane proteins: genomic occurrence, structure prediction and helix interactions, *Quarterly reviews of biophysics* 37, 121-146.
- [46] Ju, P., Pages, G., Riek, R. P., Chen, P. C., Torres, A. M., Bansal, P. S., Kuyucak, S., Kuchel, P. W., and Vandenberg, J. I. (2009) The pore domain outer helix contributes to both activation and inactivation of the hERG K⁺ channel, *Journal of Biological Chemistry* 284, 1000-1008.
- [47] Jiang, M., Zhang, M., Maslennikov, I. V., Liu, J., Wu, D.-M., Korolkova, Y. V., Arseniev, A. S., Grishin, E. V., and Tseng, G.-N. (2005) Dynamic conformational changes of extracellular S5-P linkers in the hERG channel, *Journal of Physiology* 569, 75-89.
- [48] Bax, A., and Davis, D. G. (1985) MLEV-17-based two-dimensional homonuclear magnetization transfer spectroscopy, *Journal of Magnetic Resonance* 65, 355-360.
- [49] Jeener, J., Meier, B. H., Bachmann, P., and Ernst, R. R. (1979) Investigation of exchange processes by two-dimensional NMR spectroscopy, *The Journal of Chemical Physics* 71, 4546-4553.
- [50] Rance, M., Sorensen, O. W., Bodenhausen, G., Wagner, G., Ernst, R. R., and Wuthrich, K. (1983) Improved spectral resolution in cosy 1H NMR spectra of

- proteins via double quantum filtering, *Biochemical and biophysical research communications* 117, 479-485.
- [51] Bernèche, S., and Roux, B. (2002) The ionization state and the conformation of Glu-71 in the KcsA K⁺ channel, *Biophysical journal* 82, 772-780.
 - [52] Sansom, M. S. P., Shrivastava, I. H., Bright, J. N., Tate, J., Capener, C. E., and Biggin, P. C. (2002) Potassium channels: structures, models, simulations, *Biochimica et biophysica acta* 1565, 294-307.
 - [53] Shrivastava, I. H., Tieleman, D. P., Biggin, P. C., and Sansom, M. S. P. (2002) K⁺ versus Na⁺ ions in a K channel selectivity filter: A simulation study, *Biophysical journal* 83, 633-645.
 - [54] Domene, C., Klein, M. L., Branduardi, D., Gervasio, F. L., and Parrinello, M. (2008) Conformational changes and gating at the selectivity filter of potassium channels, *Journal of the American Chemical Society* 130, 9474-9480.
 - [55] Zhou, Y., Morais-Cabral, J. H., Kaufman, A., and MacKinnon, R. (2001) Chemistry of ion coordination and hydration revealed by a K⁺ channel-Fab complex at 2.0 Å resolution, *Nature* 414, 43-48.
 - [56] Bernèche, S., and Roux, B. (2000) Molecular dynamics of the KcsA K⁺ channel in a bilayer membrane, *Biophysical journal* 78, 2900-2917.
 - [57] Ng, C. A., Perry, M. D., Tan, P. S., Hill, A. P., Kuchel, P. W., and Vandenberg, J. I. (2012) The S4-S5 linker acts as a signal integrator for HERG K⁺ channel activation and deactivation gating, *PLoS One* 7, e31640.
 - [58] Long, S. B., Tao, X., Campbell, E. B., and MacKinnon, R. (2007) Atomic structure of a voltage-dependent K⁺ channel in a lipid membrane-like environment, *Nature* 450, 376-382.
 - [59] Ferrer, T., Rupp, J., Piper, D. R., and Tristani-Firouzi, M. (2006) The S4-S5 linker directly couples voltage sensor movement to the activation gate in the human ether-a'-go-go-related gene (hERG) K⁺ channel, *Journal of Biological Chemistry* 281, 12858-12864.
 - [60] Labro, A. J., Raes, A. L., Grottesi, A., Van Hoorick, D., Sansom, M. S., and Snyders, D. J. (2008) Kv channel gating requires a compatible S4-S5 linker and bottom part of S6, constrained by non-interacting residues, *The Journal of general physiology* 132, 667-680.
 - [61] Smith, G. A., Tsui, H. W., Newell, E. W., Jiang, X., Zhu, X. P., Tsui, F. W., and Schlichter, L. C. (2002) Functional up-regulation of hERG K⁺ channels in neoplastic hematopoietic cells, *Journal of Biological Chemistry* 277, 18528-18534.
 - [62] Piper, D. R., Varghese, A., Sanguinetti, M. C., and Tristani-Firouzi, M. (2003) Gating currents associated with intramembrane charge displacement in hERG potassium channels, *Proceedings of the National Academy of Sciences of the United States of America* 100, 10534-10539.

- [63] Stuhmer, W., Conti, F., Suzuki, H., Wang, X. D., Noda, M., Yahagi, N., Kubo, H., and Numa, S. (1989) Structural parts involved in activation and inactivation of the sodium channel, *Nature* 339, 597-603.
- [64] Perozo, E., Papazian, D. M., Stefani, E., and Bezanilla, F. (1992) Gating currents in Shaker K⁺ channels. Implications for activation and inactivation models, *Biophysical journal* 62, 160-168; discussion 169-171.
- [65] Stefani, E., Toro, L., Perozo, E., and Bezanilla, F. (1994) Gating of Shaker K⁺ channels: I. Ionic and gating currents, *Biophysical journal* 66, 996-1010.
- [66] Sanguinetti, M. C., and Xu, Q. P. (1999) Mutations of the S4-S5 linker alter activation properties of hERG potassium channels expressed in *Xenopus* oocytes, *Journal of Physiology* 514 (Pt 3), 667-675.
- [67] Tristani-Firouzi, M., Chen, J., and Sanguinetti, M. C. (2002) Interactions between S4-S5 linker and S6 transmembrane domain modulate gating of hERG K⁺ channels, *Journal of Biological Chemistry* 277, 18994-19000.
- [68] Piper, D. R., Hinz, W. A., Tallurri, C. K., Sanguinetti, M. C., and Tristani-Firouzi, M. (2005) Regional specificity of human ether-a'-go-go-related gene channel activation and inactivation gating, *Journal of Biological Chemistry* 280, 7206-7217.
- [69] van Slyke, A. C., Rezazadeh, S., Snopkowski, M., Shi, P., Allard, C. R., and Claydon, T. W. (2010) Mutations within the S4-S5 linker alter voltage sensor constraints in hERG K⁺ channels, *Biophysical journal* 99, 2841-2852.
- [70] Alonso-Ron, C., de la Pena, P., Miranda, P., Dominguez, P., and Barros, F. (2008) Thermodynamic and kinetic properties of amino-terminal and S4-S5 loop HERG channel mutants under steady-state conditions, *Biophysical journal* 94, 3893-3911.
- [71] de la Pena, P., Alonso-Ron, C., Machin, A., Fernandez-Trillo, J., Carretero, L., Dominguez, P., and Barros, F. (2011) Demonstration of physical proximity between the N terminus and the S4-S5 linker of the human ether-a-go-go-related gene (hERG) potassium channel, *Journal of Biological Chemistry* 286, 19065-19075.
- [72] Post, J. A., Verkleij, A. J., and Langer, G. A. (1995) Organization and function of sarcolemmal phospholipids in control and ischemic/reperfused cardiomyocytes, *Journal of Molecular and Cellular Cardiology* 27, 749-760.
- [73] Owens, K., Pang, D. C., and Weglicki, W. B. (1979) Production of lysophospholipids and free fatty acids by a sarcolemmal fraction from canine myocardium, *Biochemical and biophysical research communications* 89, 368-373.
- [74] Panagia, V., Lamers, J. M., Singal, P. K., and Dhalla, N. S. (1982) Ca²⁺- and Mg²⁺- dependent ATPase activities in the deoxycholate-treated rat heart sarcolemma, *International Journal of Biochemistry* 14, 387-397.
- [75] Philipson, K. D., Bers, D. M., and Nishimoto, A. Y. (1980) The role of phospholipids in the Ca²⁺ binding of isolated cardiac sarcolemma, *Journal of Molecular and Cellular Cardiology* 12, 1159-1173.

- [76] Post, J. A., Langer, G. A., Op den Kamp, J. A., and Verkleij, A. J. (1988) Phospholipid asymmetry in cardiac sarcolemma. Analysis of intact cells and 'gas-dissected' membranes, *Biochimica et biophysica acta* 943, 256-266.
- [77] Tibbits, G. F., Sasaki, M., Ikeda, M., Shimada, K., Tsuruhara, T., and Nagatomo, T. (1981) Characterization of rat myocardial sarcolemma, *Journal of Molecular and Cellular Cardiology* 13, 1051-1061.
- [78] Vasdev, S. C., Biro, G. P., Narbaitz, R., and Kako, K. J. (1980) Membrane changes induced by early myocardial ischemia in the dog, *Canadian Journal of Biochemistry* 58, 1112-1119.
- [79] Weglicki, W. B., Owens, K., Kennett, F. F., Kessner, A., Harris, L., and Wise, R. M. (1980) Preparation and properties of highly enriched cardiac sarcolemma from isolated adult myocytes, *Journal of Biological Chemistry* 255, 3605-3609.
- [80] Bouvrais, H. (2012) Chapter one - bending rigidities of lipid bilayers: their determination and main inputs in biophysical studies, In *Advances in Planar Lipid Bilayers and Liposomes* (Aleš, I., Ed.), pp 1-75, Academic Press.
- [81] Mouritsen, O. G. (2004) *Life - As a matter of fat: the emerging science of lipidomics*, Springer Berlin Heidelberg.
- [82] Jouhet, J. (2013) Importance of the hexagonal lipid phase in biological membrane organization, *Frontiers in Plant Science* 4, 494.
- [83] Vist, M. R., and Davis, J. H. (1990) Phase equilibria of cholesterol/dipalmitoylphosphatidylcholine mixtures: deuterium nuclear magnetic resonance and differential scanning calorimetry, *Biochemistry* 29, 451-464.
- [84] Lorin, A., Flore, C., Thomas, A., and Brasseur, R. (2004) *Les liposomes : description, fabrication et applications*, Vol. 8, Faculté universitaire des sciences agronomiques, Gembloux, BELGIQUE.
- [85] Mayer, M., and Meyer, B. (1999) Characterization of ligand binding by saturation transfer difference NMR spectroscopy, *Angewandte Chemie International Edition* 38, 1784-1788.
- [86] Bernchou, U., Midtby, H., Ipsen, J. H., and Simonsen, A. C. (2011) Correlation between the ripple phase and stripe domains in membranes, *Biochimica et Biophysica Acta (BBA) - Biomembranes* 1808, 2849-2858.
- [87] Pabst, G., Danner, S., Karmakar, S., Deutsch, G., and Raghunathan, V. A. (2007) On the propensity of phosphatidylglycerols to form interdigitated phases, *Biophysical Journal* 93, 513-525.
- [88] Hansen, P. L., Miao, L., and Ipsen, J. H. (1998) Fluid lipid bilayers: intermonolayer coupling and its thermodynamic manifestations, *Physical Review E - Statistical Physics, Plasmas, Fluids, and Related Interdisciplinary Topics* 58, 2311-2324.
- [89] Miao, L., Hansen, P. L., and Ipsen, J. H. (1998) Fluid lipid-bilayer membranes: some basic physical mechanisms for lateral self-organization, In *Dynamical Networks in Physics and Biology: At the Frontier of Physics and Biology* Les

- Houches Workshop, March 17–21, 1997* (Beysens, D. A., and Forgacs, G., Eds.), pp 237-248, Springer Berlin Heidelberg, Berlin, Heidelberg.
- [90] Warschawski, D. E., Arnold, A. A., Beaugrand, M., Gravel, A., Chartrand, É., and Marcotte, I. (2011) Choosing membrane mimetics for NMR structural studies of transmembrane proteins, *Biochimica et Biophysica Acta (BBA) - Biomembranes* 1808, 1957-1974.
 - [91] Czerski, L., and Sanders, C. R. (2000) Functionality of a membrane protein in bicelles, *Analytical Biochemistry* 284, 327-333.
 - [92] van Swaay, D., and deMello, A. (2013) Microfluidic methods for forming liposomes, *Lab on a Chip* 13, 752-767.
 - [93] Lin, C.-M., Li, C.-S., Sheng, Y.-J., Wu, D. T., and Tsao, H.-K. (2012) Size-dependent properties of small unilamellar vesicles formed by model lipids, *Langmuir* 28, 689-700.
 - [94] Da Costa, G., Mouret, L., Chevance, S., Le Rumeur, E., and Bondon, A. (2007) NMR of molecules interacting with lipids in small unilamellar vesicles, *European Biophysics Journal* 36, 933-942.
 - [95] Morales-Pennington, N. F., Wu, J., Farkas, E. R., Goh, S. L., Konyakhina, T. M., Zheng, J. Y., Webb, W. W., and Feigenson, G. W. (2010) GUV preparation and imaging: minimizing artifacts, *Biochimica et biophysica acta* 1798, 1324-1332.
 - [96] Sanders, C. R., 2nd, and Schwonek, J. P. (1992) Characterization of magnetically orientable bilayers in mixtures of dihexanoylphosphatidylcholine and dimyristoylphosphatidylcholine by solid-state NMR, *Biochemistry* 31, 8898-8905.
 - [97] Sanders, C. R., and Prestegard, J. H. (1990) Magnetically orientable phospholipid bilayers containing small amounts of a bile salt analogue, CHAPSO, *Biophysical journal* 58, 447-460.
 - [98] Ram, P., and Prestegard, J. H. (1988) Magnetic field induced ordering of bile salt/phospholipid micelles: new media for NMR structural investigations, *Biochimica et biophysica acta* 940, 289-294.
 - [99] Park, S. H., and Opella, S. J. (2010) Triton X-100 as the "short-chain lipid" improves the magnetic alignment and stability of membrane proteins in phosphatidylcholine bilayers for oriented-sample solid-state NMR spectroscopy, *Journal of the American Chemical Society* 132, 12552-12553.
 - [100] Otten, D., Lobbecke, L., and Beyer, K. (1995) Stages of the bilayer-micelle transition in the system phosphatidylcholine-C12E8 as studied by deuterium- and phosphorous-NMR, light scattering, and calorimetry, *Biophysical journal* 68, 584-597.
 - [101] Marcotte, I., and Auger, M. (2005) Bicelles as model membranes for solid-and solution-state NMR studies of membrane peptides and proteins, *Concepts in Magnetic Resonance Part A: Bridging Education and Research* 24, 17-35.

- [102] Mahalakshmi, R., and Marassi, F. M. (2008) Orientation of the Escherichia coli outer membrane protein OmpX in phospholipid bilayer membranes determined by solid-State NMR, *Biochemistry* 47, 6531-6538.
- [103] Marassi, F. M., and Opella, S. J. (2003) Simultaneous assignment and structure determination of a membrane protein from NMR orientational restraints, *Protein Science* 12, 403-411.
- [104] Triba, M. N., Warschawski, D. E., and Devaux, P. F. (2005) Reinvestigation by phosphorus NMR of lipid distribution in bicelles, *Biophysical journal* 88, 1887-1901.
- [105] Diller, A., Loudet, C., Aussenac, F., Raffard, G., Fournier, S., Laguerre, M., Grelard, A., Opella, S. J., Marassi, F. M., and Dufourc, E. J. (2009) Bicelles: A natural 'molecular goniometer' for structural, dynamical and topological studies of molecules in membranes, *Biochimie* 91, 744-751.
- [106] Bortolus, M., De Zotti, M., Formaggio, F., and Maniero, A. L. (2013) Alamethicin in bicelles: orientation, aggregation, and bilayer modification as a function of peptide concentration, *Biochimica et biophysica acta* 1828, 2620-2627.
- [107] Bertelsen, K., Vad, B., Nielsen, E. H., Hansen, S. K., Skrydstrup, T., Otzen, D. E., Vosegaard, T., and Nielsen, N. C. (2011) Long-term-stable ether-lipid vs conventional ester-lipid bicelles in oriented solid-state NMR: altered structural information in studies of antimicrobial peptides, *The Journal of Physical Chemistry B* 115, 1767-1774.
- [108] Dürr, U. H. N., Soong, R., and Ramamoorthy, A. (2013) When detergent meets bilayer: Birth and coming of age of lipid bicelles, *Progress in Nuclear Magnetic Resonance Spectroscopy* 69, 1-22.
- [109] Sanders, C. R., Hare, B. J., Howard, K. P., and Prestegard, J. H. (1994) Magnetically-oriented phospholipid micelles as a tool for the study of membrane-associated molecules, *Progress in Nuclear Magnetic Resonance Spectroscopy* 26, 421-444.
- [110] Sanders, C. R., and Landis, G. C. (1994) Facile acquisition and assignment of oriented sample NMR spectra for bilayer surface-associated proteins, *Journal of the American Chemical Society* 116, 6470-6471.
- [111] Yamamoto, K., Soong, R., and Ramamoorthy, A. (2009) Comprehensive analysis of Lipid dynamics variation with lipid composition and hydration of bicelles using nuclear magnetic resonance (NMR) spectroscopy, *Langmuir* 25, 7010-7018.
- [112] Katsaras, J., Harroun, T. A., Pencer, J., and Nieh, M. P. (2005) "Bicellar" lipid mixtures as used in biochemical and biophysical studies, *Die Naturwissenschaften* 92, 355-366.
- [113] Yamamoto, K., Percy, P., and Ramamoorthy, A. (2014) Bicelles exhibiting magnetic alignment for a broader range of temperatures: a solid-state NMR study, *Langmuir* 30, 1622-1629.

- [114] Nieh, M. P., Raghunathan, V. A., Glinka, C. J., Harroun, T. A., Pabst, G., and Katsaras, J. (2004) Magnetically alignable phase of phospholipid "bicelle" mixtures is a chiral nematic made up of wormlike micelles, *Langmuir* 20, 7893-7897.
- [115] Harroun, T. A., Koslowsky, M., Nieh, M. P., de Lannoy, C. F., Raghunathan, V. A., and Katsaras, J. (2005) Comprehensive examination of mesophases formed by DMPC and DHPC mixtures, *Langmuir* 21, 5356-5361.
- [116] van Dam, L., Karlsson, G., and Edwards, K. (2004) Direct observation and characterization of DMPC/DHPC aggregates under conditions relevant for biological solution NMR, *Biochimica et biophysica acta* 1664, 241-256.
- [117] Sandre, O., Menager, C., Prost, J., Cabuil, V., Bacri, J. C., and Cebers, A. (2000) Shape transitions of giant liposomes induced by an anisotropic spontaneous curvature, *Physical Reviews E Statistical Physics, Plasmas, Fluids, and Related Interdisciplinary Topics* 62, 3865-3870.
- [118] Loudet, C., Diller, A., Grelard, A., Oda, R., and Dufourc, E. J. (2010) Biphenyl phosphatidylcholine: a promoter of liposome deformation and bicelle collective orientation by magnetic fields, *Progress in lipid research* 49, 289-297.
- [119] Macomber, R. S. (1998) *A complete introduction to modern NMR spectroscopy*, Wiley.
- [120] Levitt, M. H. (2008) *Spin dynamics: basics of nuclear magnetic resonance*, 2nd ed., John Wiley & Sons, Chichester.
- [121] Marcotte, I. (2016) Notes de cours, CHI-7180: Méthodes d'analyses spectroscopiques avancées, Université du Québec à Montréal (UQAM).
- [122] King, R. W., and Williams, K. R. (1989) Topics in chemical instrumentation: The fourier transform in chemistry - Part 2. Nuclear magnetic resonance: the single pulse experiment, *Journal of Chemical Education* 66, A243-A248.
- [123] Seelig, J. (1978) ³¹P Nuclear magnetic resonance and the head group structure of phospholipids in membranes, *Biochimica et biophysica acta* 515, 105-140.
- [124] Smith, I. C. P., and Ekiel, I. H. (1984) Phosphorus-31 NMR of phospholipids in membranes, In *Phosphorus-31 NMR: Principles and Applications* (Gorenstein, Ed.), pp 447-475, Academic Press Inc., London.
- [125] Kim, Y., and Prestegard, J. H. (1990) Refinement of the NMR structures for acyl carrier protein with scalar coupling data, *Proteins* 8, 377-385.
- [126] Brändén, C. I., and Tooze, J. (1999) *Introduction to Protein Structure*, Garland Pub.
- [127] Kleckner, I. R., and Foster, M. P. (2011) An introduction to NMR-based approaches for measuring protein dynamics, *Biochimica et biophysica acta* 1814, 942-968.
- [128] Berger, S., and Braun, S. (2004) *200 and More NMR Experiments*, Wiley.
- [129] Guntert, P. (1998) Structure calculation of biological macromolecules from NMR data, *Quarterly reviews of biophysics* 31, 145-237.

- [130] Bothner-By, A. A., Stephens, R. L., Lee, J., Warren, C. D., and Jeanloz, R. W. (1984) Structure determination of a tetrasaccharide: transient nuclear Overhauser effects in the rotating frame, *Journal of the American Chemical Society* 106, 811-813.
- [131] Wu, D. H., Chen, A. D., and Johnson, C. S. (1995) An improved diffusion-ordered spectroscopy experiment incorporating bipolar-gradient pulses, *Journal of Magnetic Resonance A* 115, 260-264.
- [132] Altieri, A. S., Hinton, D. P., and Byrd, R. A. (1995) Association of biomolecular systems via pulsed field gradient NMR self-diffusion measurements, *Journal of the American Chemical Society* 117, 7566-7567.
- [133] Wang, J., Schnell, J. R., and Chou, J. J. (2004) Amantadine partition and localization in phospholipid membrane: a solution NMR study, *Biochemical and biophysical research communications* 324, 212-217.
- [134] Meyer, B., and Peters, T. (2003) NMR spectroscopy techniques for screening and identifying ligand binding to protein receptors, *Angewandte Chemie International Edition* 42, 864-890.
- [135] Mayer, M., and Meyer, B. (2001) Group epitope mapping by saturation transfer difference NMR to identify segments of a ligand in direct contact with a protein receptor, *Journal of the American Chemical Society* 123, 6108-6117.
- [136] Strandberg, E., and Ulrich, A. S. (2004) NMR methods for studying membrane-active antimicrobial peptides, *Concepts in Magnetic Resonance Part A* 23A, 89-120.
- [137] Rance, M., and Byrd, R. A. (1983) Obtaining high-fidelity spin-12 powder spectra in anisotropic media: Phase-cycled Hahn echo spectroscopy, *Journal of Magnetic Resonance* 52, 221-240.
- [138] Dubinnyi, M. A., Lesovoy, D. M., Dubovskii, P. V., Chupin, V. V., and Arseniev, A. S. (2006) Modeling of ³¹P-NMR spectra of magnetically oriented phospholipid liposomes: a new analytical solution, *Solid state nuclear magnetic resonance* 29, 305-311.
- [139] Guard-Friar, D., Chen, C. H., and Engle, A. S. (1985) Deuterium isotope effect on the stability of molecules: phospholipids, *The Journal of Physical Chemistry* 89, 1810-1813.
- [140] Davis, J. H., Jeffrey, K. R., Bloom, M., Valic, M. I., and Higgs, T. P. (1976) Quadrupolar echo deutron magnetic resonance spectroscopy in ordered hydrocarbon chains, *Chemical Physics Letters* 42, 390-394.
- [141] Seelig, J. (1977) Deuterium magnetic resonance: theory and application to lipid membranes, *Quarterly reviews of biophysics* 10, 353-418.
- [142] Seelig, J., and Seelig, A. (1980) Lipid conformation in model membranes and biological membranes, *Quarterly reviews of biophysics* 13, 19-61.
- [143] Sakurai, I., Kawamura, Y., Ikegami, A., and Iwayanagi, S. (1980) Magneto-orientation of lecithin crystals, *Proceedings of the National Academy of Sciences of the United States of America* 77, 7232-7236.

- [144] Sanders, C. R., 2nd, Schaff, J. E., and Prestegard, J. H. (1993) Orientational behavior of phosphatidylcholine bilayers in the presence of aromatic amphiphiles and a magnetic field, *Biophysical journal* 64, 1069-1080.
- [145] Triba, M. N., Zoonens, M., Popot, J. L., Devaux, P. F., and Warschawski, D. E. (2006) Reconstitution and alignment by a magnetic field of a beta-barrel membrane protein in bicelles, *European Biophysics Journal* 35, 268-275.
- [146] Prosser, R. S., Hunt, S. A., DiNatale, J. A., and Void, R. R. (1996) Magnetically aligned membrane model systems with positive order parameter: Switching the sign of S= with paramagnetic ions, *Journal of the American Chemical Society* 118, 269-270.
- [147] Prosser, R. S., Volkov, V. B., and Shiyanovskaya, I. V. (1998) Solid-state NMR studies of magnetically aligned phospholipid membranes: taming lanthanides for membrane protein studies, *Biochemistry and Cell Biology* 76, 443-451.
- [148] Shah, R. R. (2005) Drug-induced QT interval prolongation - regulatory guidance and perspectives on hERG channel studies, In *The hERG cardiac potassium channel: structure, function, and long QT syndrome* (Chadwick, D. J., and Goode, J., Eds.), pp 251-285, John Wiley & Sons Ltd, Chichester.
- [149] Mason, P. K., and Mounsey, J. P. (2007) Drug-induced long QT syndrome: molecular mechanisms for congenital and acquired QT prolongation, *Drug discovery today* 4, 159-163.
- [150] Noskov, S. Y., Berneche, S., and Roux, B. (2004) Control of ion selectivity in potassium channels by electrostatic and dynamic properties of carbonyl ligands, *Nature* 431, 830-834.
- [151] Wang, J., Myers, C. D., and Robertson, G. A. (2000) Dynamic control of deactivation gating by a soluble amino-terminal domain in HERG K⁺ channels, *The Journal of general physiology* 115, 749-758.
- [152] Zhang, M., Liu, J., and Tseng, G.-N. (2004) Gating charges in the activation and inactivation processes of the hERG channel, *The Journal of general physiology* 124, 703-718.
- [153] Tseng, G.-N., Sonawane, K. D., Korolkova, Y. V., Zhang, M., Liu, J., Grishin, E. V., and Guy, H. R. (2007) Probing the outer mouth structure of the hERG channel with peptide toxin footprinting and molecular modeling, *Biophysical journal* 92, 3524-3540.
- [154] Chartrand, É., Arnold, A. A., Gravel, A., Jenna, S., and Marcotte, I. (2010) Potential role of the membrane in hERG channel functioning and drug-induced long QT syndrome, *Biochimica et biophysica acta* 1798, 1651-1662.
- [155] Ng, C., Torres, A., Pagès, G., Kuchel, P., and Vandenberg, J. (2012) Insights into hERG K⁺ channel structure and function from NMR studies, *European Biophysics Journal* 42, 71-79.
- [156] Pardo-Lopez, L., Zhang, M., Liu, J., Jiang, M., Possani, L. D., and Tseng, G.-N. (2002) Mapping the binding site of a human *ether-a-gogo*-related gene-

- specific peptide toxin (ErgTx) to the channel's outer vestibule, *Journal of Biological Chemistry* 277, 16403-16411.
- [157] Guidoni, L., and Carloni, P. (2002) Potassium permeation through the KcsA channel: a density functional study, *Biochimica et biophysica acta* 1563, 1-6.
- [158] Miloshevsky, G. V., and Jordan, P. C. (2008) Conformational changes in the selectivity filter of the open-state KcsA channel: an energy minimization study, *Biophysical journal* 95, 3239-3251.
- [159] Gayen, S., Li, Q., and Kang, C. (2012) The solution structure of the S4-S5 linker of the hERG potassium channel, *Journal of Peptide Science* 18, 140-145.
- [160] Unnerst  le, S., Madani, F., Gr  slund, A., and M  ler, L. (2012) Membrane-perturbing properties of two Arg-rich Paddle domains from voltage-gated sensors in the KvAP and HsapBK K⁺ channels, *Biochemistry* 51, 3982-3992.
- [161] Gill, A., Flaim, S. F., Damiano, B. P., Sit, S. P., and Brannan, M. D. (1992) Pharmacology of bepridil, *American Journal of Cardiology* 69, 11D-16D.
- [162] Prystowsky, E. N. (1992) Effects of bepridil on cardiac electrophysiologic properties, *American Journal of Cardiology* 69, 63D-67D.
- [163] Gilbert, J. D., Cahill, S. A., McCartney, D. G., Lukas, A., and Gross, G. J. (2000) Predictors of torsades de pointes in rabbit ventricles perfused with sedating and nonsedating histamine H1-receptor antagonists, *Canadian Journal of Physiology and Pharmacology* 78, 407-414.
- [164] Zareba, W., Moss, A. J., Rosero, S. Z., Hajj-Ali, R., Konecki, J., and Andrews, M. (1997) Electrocardiographic findings in patients with diphenhydramine overdose, *American Journal of Cardiology* 80, 1168-1173.
- [165] Mitcheson, J. S., Chen, J., Lin, M., Culberson, C., and Sanguinetti, M. C. (2000) A structural basis for drug-induced long QT syndrome, *Proceedings of the National Academy of Sciences of the United States of America* 97, 12329-12333.
- [166] Milnes, J. T., Crociani, O., Arcangeli, A., Hancox, J. C., and Witchel, H. J. (2003) Blockade of HERG potassium currents by floxamine: incomplete attenuation by S6 mutations F656 or Y652, *British Journal of Pharmacology* 139, 887-898.
- [167] Pardo-Lopez, L., Garc  a-Valdez, J., Gurrola, G. B., Robertson, G. A., and Possani, L. D. (2002) Mapping the receptor site for ergotoxin, a specific blocker of ERG channels, *FEBS letters* 510, 45-49.
- [168] Carfagna, M. A., and Muhoberac, B. B. (1993) Interaction of tricyclic drug analogs with synaptic plasma membranes: structure-mechanism relationships in inhibition of neuronal Na⁺/K⁺-ATPase activity, *Molecular pharmacology* 44, 129-141.
- [169] van Beek, J. D. (2007) matNMR: A flexible toolbox for processing, analyzing and visualizing magnetic resonance data in Matlab  , *Journal of Magnetic Resonance* 187, 19-26.

- [170] Delaglio, F., Grzesiek, S., Vuister, G. W., Zhu, G., Pfeifer, J., and Bax, A. (1995) NMRPipe: a multidimensional spectral processing system based on UNIX pipes, *Journal of Biomolecular NMR* 6, 277-293.
- [171] Johnson, B. A., and Blevins, R. A. (1994) NMRView: a computer program for the visualization and analysis of NMR data, *Journal of Biomolecular NMR* 4, 603-614.
- [172] Pearlstein, R., Vaz, R., and Rampe, D. (2003) Understanding the structure-activity relationship of the human ether-a-gogo-related gene cardiac K⁺ channel. A model for bad behavior., *Journal of medicinal chemistry* 46, 2017-2022.
- [173] Davis, J. H. (1983) The description of membrane lipid conformation, order and dynamics by 2H-NMR, *Biochimica et Biophysica Acta (BBA) - Reviews on Biomembranes* 737, 117-171.
- [174] Burnell, E. E., Cullis, P. R., and De Kruijff, B. (1980) Effects of tumbling and lateral diffusion on phosphatidylcholine model membrane ³¹P-NMR lineshapes, *Biochimica et biophysica acta* 603, 63-69.
- [175] Binder, H., and Zschörnig, O. (2002) The effect of metal cations on the phase behavior and hydration characteristics of phospholipid membranes, *Chemistry and physics of lipids* 115, 39-61.
- [176] Gurtovenko, A. A., and Vattulainen, I. (2008) Effect of NaCl and KCl on phosphatidylcholine and phosphatidylethanolamine lipid membranes: insight from atomic-scale simulations for understanding salt-induced effects in the plasma membrane, *The Journal of Physical Chemistry B* 112, 1953-1962.
- [177] Roux, M., and Bloom, M. (1990) Ca²⁺, Mg²⁺, Li⁺, Na⁺, and K⁺ distributions in the headgroup region of binary membranes of phosphatidylcholine and phosphatidylserine as seen by deuterium NMR, *Biochemistry* 29, 7077-7089.
- [178] Lind, J., Graslund, A., and Maler, L. (2006) Membrane interactions of dynorphins, *Biochemistry* 45, 15931-15940.
- [179] Joshi, U. M., Kodavanti, P. R. S., Coudert, B., Dwyer, T. M., and Mehendale, H. M. (1988) Types of interaction of amphiphilic drugs with phospholipid vesicles, *Journal of Pharmacology and Experimental Therapeutics* 246, 150-157.
- [180] Mitcheson, J. S. (2003) Drug binding to hERG channels: evidence for a 'non-aromatic' binding site for fluvoxamine, *British Journal of Pharmacology* 139, 883-884.
- [181] Jo, S.-H., Hong, H.-K., Chong, S. H., Lee, H. S., and Choe, H. (2009) H1 antihistamine drug promethazine directly blocks hERG K⁺ channel, *Pharmacological research* 60, 429-437.
- [182] Dolainsky, C., Möps, A., and Bayerl, T. M. (1993) Transverse relaxation in supported and nonsupported phospholipids model membranes and the influence of ultraslow motions: a ³¹P-NMR study, *The Journal of Chemical Physics* 98, 1712-1720.

- [183] Dufourc, E. J., Smith, I. C. P., and Jarrell, H. C. (1984) Interaction of amphotericin B with membrane lipids as viewed by ^2H -NMR, *Biochimica et biophysica acta* 778, 435-442.
- [184] Bernèche, S., and Roux, B. (2005) A gate in the selectivity filter of potassium channels, *Structure (London, England : 1993)* 13, 591-600.
- [185] Yohannan, S., Hu, Y., and Zhou, Y. (2007) Crystallographic study of the tetrabutylammonium block to the KcsA K^+ channel, *Journal of molecular biology* 366, 806-814.
- [186] Capener, C. E., Proks, P., Ashcroft, F. M., and Sansom, M. S. P. (2003) Filter flexibility in a mammalian K^+ channel: models and simulations of Kir6.2 mutants, *Biophysical journal* 84, 2345-2356.
- [187] Woosley, R. L. (1996) Cardiac actions of antihistamines, *Annual Reviews of Pharmacology and Toxicology* 36, 233-252.
- [188] Taglialatela, M., Pannaccione, A., Castaldo, P., Giorgio, G., Zhou, Z., January, C. T., Genovese, A., Marone, G., and Annunziato, L. (1998) Molecular basis for the lack of hERG K^+ channel block-related cardiotoxicity by the H1 receptor blocker cetirizine compared with other second-generation antihistamines, *Molecular pharmacology* 54, 113-121.
- [189] Hoffmann, P., and Warner, B. (2006) Are hERG channel inhibition and QT interval prolongation all there is in drug-induced torsadogenesis? A review of emerging trends, *Journal of Pharmacological Toxicology Methods* 53, 87-105.
- [190] van Balen, G. P., Caron, G., Ermondi, G., Pagliara, A., Grandi, T., Bouchard, G., Fruttero, R., Carrupt, P. A., and Testa, B. (2001) Lipophilicity behaviour of the zwitterionic antihistamine cetirizine in phosphatidylcholine liposomes/water systems, *Pharmacological research* 18, 694-701.
- [191] Marcotte, I., Separovic, F., Auger, M., and Gagné, S. M. (2004) A multidimensional ^1H NMR investigation of the conformation of methionine-enkephalin in fast-tumbling bicelles, *Biophysical journal* 86, 1587-1600.
- [192] Cafiso, D. S. (1998) Dipole potentials and spontaneous curvature: membrane properties that could mediate anesthesia, *Toxicology Letters* 100-101, 431-439.
- [193] Mouritsen, O. G., and Jorgensen, K. (1998) A new look at lipid-membrane structure in relation to drug research, *Pharmaceutical Research* 15, 1507-1519.
- [194] Schmidt, D., and MacKinnon, R. (2008) Voltage-dependent K^+ channel gating and voltage sensor toxin sensitivity depend on the mechanical state of the lipid membrane, *Proceedings of the National Academy of Sciences of the United States of America* 105, 19276-19281.
- [195] Klabunde, R. E. (2012) *Cardiovascular physiology concepts*, 2nd ed., Lippincott Williams & Wilkins/Wolters Kluwer, Baltimore, MD.
- [196] Grant, A. O. (2009) Cardiac ion channels, *Circulation: arrhythmia and electrophysiology* 2, 185-194.

- [197] Trudeau, M. C., Warmke, J. W., Ganetzky, B., and Robertson, G. A. (1995) HERG, a human inward rectifier in the voltage-gated potassium channel family, *Science* 269, 92-95.
- [198] Smith, P. L., Baukrowitz, T., and Yellen, G. (1996) The inward rectification mechanism of the hERG cardiac potassium channel, *Nature* 379, 833-836.
- [199] Vandenberg, J. I., Perry, M. D., Perrin, M. J., Mann, S. A., Ke, Y., and Hill, A. P. (2012) HERG K(+) channels: structure, function, and clinical significance, *Physiological Reviews* 92, 1393-1478.
- [200] Lu, Y., Mahaut-Smith, M. P., Varghese, A., Huang, C. L., Kemp, P. R., and Vandenberg, J. I. (2001) Effects of premature stimulation on HERG K(+) channels, *Journal of Physiology* 537, 843-851.
- [201] Smith, P. L., and Yellen, G. (2002) Fast and slow voltage sensor movements in hERG potassium channels, *The Journal of general physiology* 119, 275-293.
- [202] Lorinczi, E., Gomez-Posada, J. C., de la Pena, P., Tomczak, A. P., Fernandez-Trillo, J., Leipscher, U., Stuhmer, W., Barros, F., and Pardo, L. A. (2015) Voltage-dependent gating of KCNH potassium channels lacking a covalent link between voltage-sensing and pore domains, *Nature communications* 6, 6672.
- [203] Nolandt, O. V., Walther, T. H., Grage, S. L., and Ulrich, A. S. (2012) Magnetically oriented dodecylphosphocholine bicelles for solid-state NMR structure analysis, *Biochimica et biophysica acta* 1818, 1142-1147.
- [204] Perry, M. D., Ng, C. A., Phan, K., David, E., Steer, K., Hunter, M. J., Mann, S. A., Imtiaz, M., Hill, A. P., Ke, Y., and Vandenberg, J. I. (2016) Rescue of protein expression defects may not be enough to abolish the pro-arrhythmic phenotype of long QT type 2 mutations, *Journal of Physiology*.
- [205] Liu, S., Rasmusson, R. L., Campbell, D. L., Wang, S., and Strauss, H. C. (1996) Activation and inactivation kinetics of an E-4031-sensitive current from single ferret atrial myocytes, *Biophysical journal* 70, 2704-2715.
- [206] Ng, C. A., Phan, K., Hill, A. P., Vandenberg, J. I., and Perry, M. D. (2014) Multiple interactions between cytoplasmic domains regulate slow deactivation of Kv11.1 channels, *Journal of Biological Chemistry* 289, 25822-25832.
- [207] Ng, C. A., Ke, Y., Perry, M. D., Tan, P. S., Hill, A. P., and Vandenberg, J. I. (2013) C-Terminal beta9-strand of the cyclic nucleotide-binding homology domain stabilizes activated states of Kv11.1 channels, *PLoS One* 8, e77032.
- [208] Tan, P. S., Perry, M. D., Ng, C. A., Vandenberg, J. I., and Hill, A. P. (2012) Voltage-sensing domain mode shift is coupled to the activation gate by the N-terminal tail of hERG channels, *The Journal of general physiology* 140, 293-306.
- [209] Serrano, L., Bycroft, M., and Fersht, A. R. (1991) Aromatic-aromatic interactions and protein stability. Investigation by double-mutant cycles, *Journal of molecular biology* 218, 465-475.

- [210] Horovitz, A., Serrano, L., Avron, B., Bycroft, M., and Fersht, A. R. (1990) Strength and co-operativity of contributions of surface salt bridges to protein stability, *Journal of molecular biology* 216, 1031-1044.
- [211] Waldburger, C. D., Schildbach, J. F., and Sauer, R. T. (1995) Are buried salt bridges important for protein stability and conformational specificity?, *Nature Structural & Molecular Biology* 2, 122-128.
- [212] Marqusee, S., and Sauer, R. T. (1994) Contributions of a hydrogen bond/salt bridge network to the stability of secondary and tertiary structure in lambda repressor, *Protein Science* 3, 2217-2225.
- [213] Tissot, A. C., Vuilleumier, S., and Fersht, A. R. (1996) Importance of two buried salt bridges in the stability and folding pathway of barnase, *Biochemistry* 35, 6786-6794.
- [214] Loewenthal, R., Sancho, J., and Fersht, A. R. (1992) Histidine-aromatic interactions in barnase. Elevation of histidine pKa and contribution to protein stability, *Journal of molecular biology* 224, 759-770.
- [215] Guex, N., and Peitsch, M. C. (1997) SWISS-MODEL and the Swiss-PdbViewer: An environment for comparative protein modeling, *Electrophoresis*, 2714-2723.
- [216] Bordoli, L., Kiefer, F., Arnold, K., Benkert, P., Battey, J., and Schwede, T. (2009) Protein structure homology modeling using SWISS-MODEL workspace, *Nature protocols* 4, 1-13.
- [217] Arnold, K., Bordoli, L., Kopp, J., and Schwede, T. (2006) The SWISS-MODEL Workspace: A web-based environment for protein structure homology modelling, *Bioinformatics* 22, 195-201.
- [218] Zubcevic, L., Herzik, M. A., Jr., Chung, B. C., Liu, Z., Lander, G. C., and Lee, S. Y. (2016) Cryo-electron microscopy structure of the TRPV2 ion channel, *Nature Structural & Molecular Biology* 23, 180-186.
- [219] Cao, E., Liao, M., Cheng, Y., and Julius, D. (2013) TRPV1 structures in distinct conformations reveal activation mechanisms, *Nature* 504, 113-118.
- [220] Zalk, R., Clarke, O. B., des Georges, A., Grassucci, R. A., Reiken, S., Mancina, F., Hendrickson, W. A., Frank, J., and Marks, A. R. (2015) Structure of a mammalian ryanodine receptor, *Nature* 517, 44-49.
- [221] Zhang, X., Ren, W., DeCaen, P., Yan, C., Tao, X., Tang, L., Wang, J., Hasegawa, K., Kumasaka, T., He, J., Wang, J., Clapham, D. E., and Yan, N. (2012) Crystal structure of an orthologue of the NaChBac voltage-gated sodium channel, *Nature* 486, 130-134.
- [222] Payandeh, J., Scheuer, T., Zheng, N., and Catterall, W. A. (2011) The crystal structure of a voltage-gated sodium channel, *Nature* 475, 353-358.
- [223] Howard, K. P., and Opella, S. J. (1996) High-resolution solid-state NMR spectra of integral membrane proteins reconstituted into magnetically oriented phospholipid bilayers, *Journal of magnetic resonance. Series B* 112, 91-94.

- [224] Poget, S. F., and Girvin, M. E. (2007) Solution NMR of membrane proteins in bilayer mimics: small is beautiful, but sometimes bigger is better, *Biochimica et biophysica acta* 1768, 3098-3106.
- [225] Sanders, C. R., and Sonnichsen, F. (2006) Solution NMR of membrane proteins: practice and challenges, *Magnetic resonance in chemistry : MRC 44 Spec No*, S24-40.
- [226] Krueger-Koplin, R. D., Sorgen, P. L., Krueger-Koplin, S. T., Rivera-Torres, I. O., Cahill, S. M., Hicks, D. B., Grinius, L., Krulwich, T. A., and Girvin, M. E. (2004) An evaluation of detergents for NMR structural studies of membrane proteins, *Journal of Biomolecular NMR* 28, 43-57.
- [227] Miyanoshita, M., Hashida, C., Ikeda, S., and Gohtani, S. (2011) Development of low-energy methods for preparing food Nano-emulsions, *Journal of oleo science* 60, 355-362.
- [228] Lallbeeharry, P., Tian, Y., Fu, N., Wu, W. D., Woo, M. W., Selomulya, C., and Chen, X. D. (2014) Effects of ionic and nonionic surfactants on milk shell wettability during co-spray-drying of whole milk particles, *Journal of dairy science* 97, 5303-5314.
- [229] Liu, L., Qi, W., Schwartz, D. K., Randolph, T. W., and Carpenter, J. F. (2013) The effects of excipients on protein aggregation during agitation: an interfacial shear rheology study, *Journal of pharmaceutical sciences* 102, 2460-2470.
- [230] Zhao, L. X., Liu, A. C., Yu, S. W., Wang, Z. X., Lin, X. Q., Zhai, G. X., and Zhang, Q. Z. (2013) The permeability of puerarin loaded poly(butylcyanoacrylate) nanoparticles coated with polysorbate 80 on the blood-brain barrier and its protective effect against cerebral ischemia/reperfusion injury, *Biological and Pharmaceutical Bulletin* 36, 1263-1270.
- [231] Bhowal, S., Priyanka, B. S., and Rastogi, N. K. (2014) Mixed reverse micelles facilitated downstream processing of lipase involving water-oil-water liquid emulsion membrane, *Biotechnology progress* 30, 1084-1092.
- [232] Chachra, D., Coote, J. G., Parton, R., and Jand, S. K. (2011) Haemolytic and cytotoxic activities of the Tween 80-extracted putative haemolysin of *Pasteurella multocida* B:2, *Veterinary microbiology* 150, 331-337.
- [233] Rajan, R., Jose, S., Mukund, V. P. B., and Vasudevan, D. T. (2011) Transferosomes - A vesicular transdermal delivery system for enhanced drug permeation, *Journal of Advanced Pharmaceutical Technology & Research* 2, 138-143.
- [234] Oh, Y. K., Kim, M. Y., Shin, J. Y., Kim, T. W., Yun, M. O., Yang, S. J., Choi, S. S., Jung, W. W., Kim, J. A., and Choi, H. G. (2006) Skin permeation of retinol in Tween 20-based deformable liposomes: in-vitro evaluation in human skin and keratinocyte models, *Journal of Pharmacy and Pharmacology* 58, 161-166.

- [235] Barbosa, R. M., Severino, P., Preté, P. S. C., and Santana, M. H. A. (2016) Influence of different surfactants on the physicochemical properties of elastic liposomes, *Pharmaceutical Development and Technology*, 1-10.
- [236] Speyer, J. B., Sripada, P. K., Das Gupta, S. K., Shipley, G. G., and Griffin, R. G. (1987) Magnetic orientation of sphingomyelin-lecithin bilayers, *Biophysical journal* 51, 687-691.
- [237] Bitbol, M., Dempsey, C., Watts, A., and Devaux, P. F. (1989) Weak interaction of spectrin with phosphatidylcholine-phosphatidylserine multilayers: A ²H and ³¹P NMR study, *FEBS letters* 244, 217-222.
- [238] Jansson, M., Thurmond, R. L., Trouard, T. P., and Brown, M. F. (1990) Magnetic alignment and orientational order of dipalmitoylphosphatidylcholine bilayers containing palmitoylsphosphatidylcholine, *Chemistry and physics of lipids* 54, 157-170.
- [239] Picard, F., Paquet, M. J., Levesque, J., Belanger, A., and Auger, M. (1999) ³¹P NMR first spectral moment study of the partial magnetic orientation of phospholipid membranes, *Biophysical journal* 77, 888-902.
- [240] Marsh, D. (2013) *Handbook of Lipid Bilayers, Second Edition*, 2 ed., Taylor & Francis.
- [241] Brauner, J. W., and Mendelsohn, R. (1986) A comparison of differential scanning calorimetric and Fourier transform infrared spectroscopic determination of mixing behavior in binary phospholipid systems, *Biochimica et biophysica acta* 861, 16-24.
- [242] Pott, T., and Dufourc, E. J. (1995) Action of melittin on the DPPC-cholesterol liquid-ordered phase: a solid state ²H-and ³¹P-NMR study, *Biophysical journal* 68, 965-977.
- [243] Marcotte, I., Ouellet, M., and Auger, M. (2004) Insights on the interaction of met-enkephalin with negatively charged membranes: an infrared and solid-state NMR spectroscopic study, *Chemistry and physics of lipids* 127, 175-187.
- [244] Seddon, A. M., Curnow, P., and Booth, P. J. (2004) Membrane proteins, lipids and detergents: not just a soap opera, *Biochimica et biophysica acta* 1666, 105-117.
- [245] Goni, F. M., Urbaneja, M. A., Arrondo, J. L., Alonso, A., Durrani, A. A., and Chapman, D. (1986) The interaction of phosphatidylcholine bilayers with Triton X-100, *European Journal of Biochemistry* 160, 659-665.
- [246] Lee, D. C., Durrani, A. A., and Chapman, D. (1984) A difference infrared spectroscopic study of gramicidin A, alamethicin and bacteriorhodopsin in perdeuterated dimyristoylphosphatidylcholine, *Biochimica et biophysica acta* 769, 49-56.
- [247] Laroche, G., Carrier, D., and Pezolet, M. (1988) Study of the effect of poly(L-lysine) on phosphatidic acid and phosphatidylcholine/phosphatidic acid bilayers by Raman spectroscopy, *Biochemistry* 27, 6220-6228.
- [248] van der Crujisen, E. A., Nand, D., Weingarh, M., Prokofyev, A., Hornig, S., Cukkemane, A. A., Bonvin, A. M., Becker, S., Hulse, R. E., Perozo, E.,

- Pongs, O., and Baldus, M. (2013) Importance of lipid-pore loop interface for potassium channel structure and function, *Proceedings of the National Academy of Sciences of the United States of America* 110, 13008-13013.
- [249] Weingarh, M., Prokofyev, A., van der Crujisen, E. A. W., Nand, D., Bonvin, A. M. J. J., Pongs, O., and Baldus, M. (2013) Structural determinants of specific lipid binding to potassium channels, *Journal of the American Chemical Society* 135, 3983-3988.
- [250] Xu, Y., Ramu, Y., and Lu, Z. (2008) Removal of phospho-head groups of membrane lipids immobilizes voltage sensors of K(+) channels, *Nature* 451, 826-829.
- [251] Sargent, D. F., and Schwyzer, R. (1986) Membrane lipid phase as catalyst for peptide-receptor interactions, *Proceedings of the National Academy of Sciences of the United States of America* 83, 5774-5778.
- [252] Bazzoni, G., and Rasia, M. (1998) Effects of an amphipathic drug on the rheological properties of the cell membrane, *Blood Cells, Molecules, and Diseases* 24, 552-559.
- [253] Wee, C. L., Bemporad, D., Sands, Z. A., Gavaghan, D., and Sansom, M. S. P. (2006) SGTx1, a Kv channel gating-modifier toxin, binds to the interfacial region of lipid bilayers, *Biophysical journal* 92, L07-L09.
- [254] Ng, C. A., Gravel, A. E., Perry, M. D., Arnold, A. A., Marcotte, I., and Vandenberg, J. I. (2016) Tyrosine residues from the S4-S5 linker of Kv11.1 channels are critical for slow deactivation, *Journal of Biological Chemistry*.
- [255] Vestergaard, M., Kraft, J. F., Vosegaard, T., Thøgersen, L., and Schiøtt, B. (2015) Bicelles and other membrane mimics: comparison of structure, properties, and dynamics from MD simulations, *The Journal of Physical Chemistry B* 119, 15831-15843.
- [256] Bodor, A., Kövér, K. E., and Mäler, L. (2015) Membrane interactions in small fast-tumbling bicelles as studied by ³¹P NMR, *Biochimica et Biophysica Acta (BBA) - Biomembranes* 1848, 760-766.
- [257] Raschi, E., Vasina, V., Poluzzi, E., and De Ponti, F. (2008) The hERG K⁺ channel: target and antitarget strategies in drug development, *Pharmacological research* 57, 181-195.
- [258] Witchel, H. J. (2011) Drug-induced hERG block and long QT syndrome, *Cardiovascular Therapy* 29, 251-259.
- [259] Li, C., and Liu, M. (2013) Protein dynamics in living cells studied by in-cell NMR spectroscopy, *FEBS letters* 587, 1008-1011.
- [260] Warnet, X. L., Laadhari, M., Arnold, A. A., Marcotte, I., and Warschawski, D. E. (2016) A (2)H magic-angle spinning solid-state NMR characterisation of lipid membranes in intact bacteria, *Biochimica et biophysica acta* 1858, 146-152.
- [261] Tardy-Laporte, C., Arnold, A. A., Genard, B., Gastineau, R., Morancais, M., Mouget, J. L., Tremblay, R., and Marcotte, I. (2013) A (2)H solid-state NMR

- study of the effect of antimicrobial agents on intact *Escherichia coli* without mutating, *Biochimica et biophysica acta* 1828, 614-622.
- [262] Renault, M., Tommassen-van Boxtel, R., Bos, M. P., Post, J. A., Tommassen, J., and Baldus, M. (2012) Cellular solid-state nuclear magnetic resonance spectroscopy, *Proceedings of the National Academy of Sciences of the United States of America* 109, 4863-4868.
- [263] Wang, S., Munro, R. A., Shi, L., Kawamura, I., Okitsu, T., Wada, A., Kim, S.-Y., Jung, K.-H., Brown, L. S., and Ladizhansky, V. (2013) Solid-state NMR spectroscopy structure determination of a lipid-embedded heptahelical membrane protein, *Nature Methods* 10, 1007-1012.
- [264] Zoonens, M., and Miroux, B. (2010) Expression of membrane proteins at the *Escherichia coli* membrane for structural studies, *Methods in Molecular Biology* 601, 49-66.
- [265] Kang, C., and Li, Q. (2011) Solution NMR study of integral membrane proteins, *Current Opinions in Chemical Biology* 15, 560-569.
- [266] Whiles, J. A., Deems, R., Vold, R. R., and Dennis, E. A. (2002) Bicelles in structure-function studies of membrane-associated proteins, *Bioorganic chemistry* 30, 431-442.
- [267] van Meer, G., Voelker, D. R., and Feigenson, G. W. (2008) Membrane lipids: where they are and how they behave, *Nature Reviews Molecular Cell Biology* 9, 112-124.
- [268] Killian, J. A. (1998) Hydrophobic mismatch between proteins and lipids in membranes, *Biochimica et biophysica acta* 1376, 401-415.
- [269] Webb, R. J., East, J. M., Sharma, R. P., and Lee, A. G. (1998) Hydrophobic mismatch and the incorporation of peptides into lipid bilayers: a possible mechanism for retention in the golgi, *Biochemistry* 37, 673-679.
- [270] Bretscher, M. S., and Munro, S. (1993) Cholesterol and the Golgi apparatus, *Science* 261, 1280-1281.
- [271] Park, S. H., De Angelis, A. A., Nevzorov, A. A., Wu, C. H., and Opella, S. J. (2006) Three-dimensional structure of the transmembrane domain of Vpu from HIV-1 in aligned phospholipid bicelles, *Biophysical journal* 91, 3032-3042.
- [272] Dvinskikh, S. V., Dürr, U. H. N., Yamamoto, K., and Ramamoorthy, A. (2007) High-resolution 2D NMR spectroscopy of bicelles to measure the membrane interaction of ligands, *Journal of the American Chemical Society* 129, 794-802.
- [273] Luckey, M. (2008) *Membrane structural biology: with biochemical and biophysical foundations*, Cambridge University Press, New York.
- [274] Cevc, G., Gebauer, D., Stieber, J., Schätzlein, A., and Blume, G. (1998) Ultraflexible vesicles, Transfersomes, have an extremely low pore penetration resistance and transport therapeutic amounts of insulin across the intact mammalian skin, *Biochimica et Biophysica Acta (BBA) - Biomembranes* 1368, 201-215.

- [275] Romero, E. L., and Morilla, M. J. (2013) Highly deformable and highly fluid vesicles as potential drug delivery systems: theoretical and practical considerations, *International Journal of Nanomedicine* 8, 3171-3186.
- [276] Derome, A. E., and Bowden, S. (1991) Low-temperature solid-state NMR of proteins, *Chemical Reviews* 91, 1307-1320.
- [277] McNamara, R., Wu, C. H., and Opella, S. J. (1992) Instrumental techniques for low-temperature solid-state NMR studies of peptides and proteins, *Journal of Magnetic Resonance* (1969) 100, 559-566.
- [278] MacKenzie, K. R., Prestegard, J. H., and Engelman, D. M. (1997) A transmembrane helix dimer: structure and implications, *Science* 276, 131-133.
- [279] Van Horn, W. D., Kim, H. J., Ellis, C. D., Hadziselimovic, A., Sulistijo, E. S., Karra, M. D., Tian, C., Sonnichsen, F. D., and Sanders, C. R. (2009) Solution nuclear magnetic resonance structure of membrane-integral diacylglycerol kinase, *Science* 324, 1726-1729.
- [280] Ketchum, R., Hu, W., and Cross, T. (1993) High-resolution conformation of gramicidin A in a lipid bilayer by solid-state NMR, *Science* 261, 1457-1460.
- [281] Cross, T. A., and Opella, S. J. (1980) Structural properties of fd coat protein in sodium dodecyl sulfate micelles, *Biochemical and biophysical research communications* 92, 478-484.
- [282] Bienvenue, A., Bloom, M., Davis, J. H., and Devaux, P. F. (1982) Evidence for protein-associated lipids from deuterium nuclear magnetic resonance studies of rhodopsin-dimyristoylphosphatidylcholine recombinants, *Journal of Biological Chemistry* 257, 3032-3038.
- [283] Bianchi, L., Wible, B., Arcangeli, A., Taglialatela, M., Morra, F., Castaldo, P., Crociani, O., Rosati, B., Faravelli, L., Olivotto, M., and Wanke, E. (1998) herg encodes a K⁺ current highly conserved in tumors of different histogenesis: a selective advantage for cancer cells?, *Cancer research* 58, 815-822.
- [284] Cherubini, A., Taddei, G. L., Crociani, O., Paglierani, M., Buccoliero, A. M., Fontana, L., Noci, I., Borri, P., Borrani, E., Giachi, M., Becchetti, A., Rosati, B., Wanke, E., Olivotto, M., and Arcangeli, A. (2000) HERG potassium channels are more frequently expressed in human endometrial cancer as compared to non-cancerous endometrium, *British journal of cancer* 83, 1722-1729.
- [285] Pillozzi, S., Brizzi, M. F., Balzi, M., Crociani, O., Cherubini, A., Guasti, L., Bartolozzi, B., Becchetti, A., Wanke, E., Bernabei, P. A., Olivotto, M., Pegoraro, L., and Arcangeli, A. (2002) HERG potassium channels are constitutively expressed in primary human acute myeloid leukemias and regulate cell proliferation of normal and leukemic hemopoietic progenitors, *Leukemia* 16, 1791-1798.
- [286] Wang, H., Zhang, Y., Cao, L., Han, H., Wang, J., Yang, B., Nattel, S., and Wang, Z. (2002) HERG K⁺ channel, a regulator of tumor cell apoptosis and proliferation, *Cancer research* 62, 4843-4848.

- [287] Afrasiabi, E., Hietamaki, M., Viitanen, T., Sukumaran, P., Bergelin, N., and Tornquist, K. (2010) Expression and significance of HERG (KCNH2) potassium channels in the regulation of MDA-MB-435S melanoma cell proliferation and migration, *Cellular signalling* 22, 57-64.
- [288] Asher, V., Warren, A., Shaw, R., Sowter, H., Bali, A., and Khan, R. (2011) The role of Eag and HERG channels in cell proliferation and apoptotic cell death in SK-OV-3 ovarian cancer cell line, *Cancer cell international* 11, 6.
- [289] Wang, Z. (2004) Roles of K⁺ channels in regulating tumour cell proliferation and apoptosis, *Pflugers Archiv : European journal of physiology* 448, 274-286.
- [290] Pardo, L. A., del Camino, D., Sanchez, A., Alves, F., Bruggemann, A., Beckh, S., and Stuhmer, W. (1999) Oncogenic potential of EAG K(+) channels, *European Molecular Biology Organization Journal* 18, 5540-5547.
- [291] Lastraioli, E., Guasti, L., Crociani, O., Polvani, S., Hofmann, G., Witchel, H., Bencini, L., Calistri, M., Messerini, L., Scatizzi, M., Moretti, R., Wanke, E., Olivotto, M., Mugnai, G., and Arcangeli, A. (2004) herg1 gene and HERG1 protein are overexpressed in colorectal cancers and regulate cell invasion of tumor cells, *Cancer research* 64, 606-611.
- [292] Fontana, L., D'Amico, M., Crociani, O., Biagiotti, T., Solazzo, M., Rosati, B., Arcangeli, A., Wanke, E., and Olivotto, M. (2001) Long-term modulation of HERG channel gating in hypoxia, *Biochemical and biophysical research communications* 286, 857-862.
- [293] Masi, A., Becchetti, A., Restano-Cassulini, R., Polvani, S., Hofmann, G., Buccoliero, A. M., Paglierani, M., Pollo, B., Taddei, G. L., Gallina, P., Di Lorenzo, N., Franceschetti, S., Wanke, E., and Arcangeli, A. (2005) hERG1 channels are overexpressed in glioblastoma multiforme and modulate VEGF secretion in glioblastoma cell lines, *British journal of cancer* 93, 781-792.
- [294] Garcia-Quiroz, J., and Camacho, J. (2011) Astemizole: an old anti-histamine as a new promising anti-cancer drug, *Anticancer Agents in Medicinal Chemistry* 11, 307-314.